CRANFIELD UNIVERSITY

E.N. SMITH

OPTIMAL HANDLING CHARACTERISTICS FOR ELECTRIC VEHICLES WITH TORQUE VECTORING

SCHOOL OF AEROSPACE, TRANSPORT AND MANUFACTURING
Advanced Vehicle Engineering Centre

PhD
Academic Year: 2016–2017

Supervisor: Dr. E. Velenis & Dr. D. Cao
August 2017

CRANFIELD UNIVERSITY

SCHOOL OF AEROSPACE, TRANSPORT AND MANUFACTURING
Advanced Vehicle Engineering Centre

PhD

Academic Year: 2016–2017

E.N. SMITH

Optimal handling characteristics for Electric Vehicles with Torque Vectoring

Supervisor: Dr. E. Velenis & Dr. D. Cao
August 2017

Abstract

Torque vectoring by virtue of independent electric motors is the focus of an increasing number of studies as electric vehicles gain prominence as the chosen direction for the automotive industry. Building on active yaw control systems developed over the past decades, torque vectoring benefits from the high-responsiveness and controllability of the electric motor actuator. Furthermore, and especially in the case of vehicles equipped with one independent motor per wheel, the overall performance envelope of the vehicle is significantly improved, as well as the ability to actively shape the vehicle handling.

Much attention has been focussed on controller development and control allocation aspects of torque vectoring controllers, but little on the appropriate yaw rate reference. Optimal control studies have been successfully used to mimic the expert driver in both minimum-time circuit racing and high-sideslip rally driving, and can offer insight into how to optimally tune active chassis control systems, such as torque vectoring yaw control.

The main aim of this thesis was to investigate the optimal handling characteristics of an electric vehicle with four independent electric motors at the limits of performance.

A TV controller was first developed for a prototype sportscar with 4 independent motors, employing a model-based design process that encompassed real-time software in the loop testing. Real-world track testing demonstrated the controller was able to successfully modify the handling characteristic of the vehicle in both understeer and oversteer directions, achieving good controller performance in steady-state and transient manoeuvres.

The limit performance of the TV-controlled vehicle was subsequently investigated in the simulation domain. Numerical techniques were used to solve optimal control problems for a single-track vehicle model with linear tyres and an external yaw moment term representing the overall yaw moment arising from the difference in torques at each wheel. For a U-turn manoeuvre, it was shown that torque vectoring significantly lowers manoeuvre time in comparison with the vehicle without TV active, and that modifying the passive understeer gradient does not affect manoeuvre time. The system dynamics were reformulated to include a feedback torque vectoring controller. The target yaw rate reference was varied and it was found that the manoeuvre time was highly sensitive to the yaw rate reference. For minimising laptime, the target understeer gradient should be set to the passive understeer gradient value. The methodology was repeated for a higher fidelity model including nonlinear tyres and lateral load transfer, and found that when the torque vectoring controller was included in the system dynamics, the manoeuvre time showed

little sensitivity to the target understeer gradient.

Following the contradictory results of the optimal control problems, the vehicle models were investigated next. Time optimal yaw rate gain surfaces were generated from further minimum-time optimal control problems. Open-loop manoeuvres investigating effects of tyre model, lateral load transfer and torque vectoring generation mechanism found that tyre modelling was the dominant differentiator and tyre nonlinearity is an essential modelling consideration.

Optimal control techniques have been used for high sideslip manoeuvring for conventional vehicles but no studies have explored the effects of torque vectoring on agility. In the final chapter, an aggressive turn-around manoeuvre was simulated and it was found that torque vectoring can significantly increase agility and reduce the space taken for an aggressive turn-around manoeuvre. Reducing yaw inertia increased agility, as well as increasing longitudinal slips limits. A critique of agility metrics in this context was given.

Keywords

optimal control; vehicle handling; torque vectoring; minimum-time; agility

Contents

List of Figures

List of Tables

Nomenclature

Quantity	Description
α	angle of the vehicle relative to the road centreline
β	sideslip angle at CM
χ	relative yaw angle
δ	steering angle of the front wheels
δ_{dyn}	dynamic steer wheel angle
δ_{kin}	kinematic steering angle of the front wheels
$\dot{\psi}$	yaw rate
$\dot{\psi}_{err}$	yaw rate error
$\dot{\psi}_{ref}$	yaw rate reference
$\dot{\psi}_{ref}^{SS}$	yaw rate steady-state value
ℓ_F, ℓ_R	distance of the CM to the front and rear axle
η_F	front tyre cornering coefficient
η_R	rear tyre cornering coefficient
γ	proportion of total torque applied at the front axle
κ	instantaneous path curvature of the vehicle trajectory
μ_{max}	tyre-road friction coefficient
ω_{ij}	wheel angular speed
ψ	vehicle heading angle at CM
ρ_{air}	air density
σ	tyre relaxation length
σ_{ijk}	tyre slips
θ_R	heading relative to origin
a_x, a_y	longitudinal and lateral accelerations at CM
B	Magic Formula stiffness factor
C	Magic Formula shape factor

C_d	aerodynamic drag coefficient
C_F	front tyre cornering stiffness
C_R	rear tyre cornering stiffness
D	Magic Formula peak value
f_{ijk}	tyre forces at the contact patch
F_x	longitudinal force demand
g	gravitational acceleration constant
h	height of the CM
I	integral gain (PID)
I_w	moment of inertia of wheel about axis of rotation
I_z	moment of inertia about the vertical axis
J_y	lateral jerk
K	understeer gradient
K_{AW}	anti-windup gain
K_{nat}^{SS}	natural steady-state understeer gradient
K_{tar}	target understeer gradient
L	wheelbase
m	vehicle mass
$M_{z,req}$	yaw moment request
M_z	Yaw moment
P	Power
R	instantaneous path radius
r	wheel radius
R_0	kinematic path radius
s	position of the vehicle along the road centreline
s_{ijk}	theoretical slip quantity for tyre
s_{ijx} and s_{ijy}	theoretical longitudinal and lateral slips
s_n	lateral position relative to the road centreline
s_t	tangent to the road centreline at point s
t	elapsed time
$T_{ij,req}$	final wheel torque requests
T_{ij}	drive/brake torque applied on each wheel
T_x	Longitudinal torque demand
T_s	sample time

t_z	effective suspension time constant
V	vector velocity
V_x	longitudinal velocity
w	vehicle track width
x_R	global coordinates on two nominal orthogonal axes relative to an origin
y_R	global coordinates on two nominal orthogonal axes relative to an origin
z	z-transform

List of Abbreviations

SATM	School of Aerospace, Technology and Manufacturing
SEEA	School of Energy, Environment and Agrifoods
TV	Torque Vectoring
4EM	Four Electric Motor
4EM	Four Electric Motor
4WD	Four Wheel Drive
ABS	Anti-Lock Braking System
BEV	Battery Electric Vehicle
CAN	Controller Area Network
CM	Centre of Mass
DiL	Driver in the Loop
DOF	Degree Of Freedom
DYC	Direct Yaw Control
EV	Electric Vehicle
F-R	Front-to-Rear
FWD	Front Wheel Drive
JLR	Jaguar Land Rover
HiL	Hardware in the Loop

IVCS	Integrated Vehicle Control Structure
KKT	Karush-Kuhn-Tucker (conditions)
LQR	Linear Quadratic Regulator
MF	Magic Formula
MiL	Model in the Loop
MPC	Model Predictive Control
NLP	Nonlinear Programming
NS	Neutral Steer
OCP	Optimal Control Problem
OEM	Original Equipment Manufacturer
PID	Proportional Integral Derivative (Control)
RWD	Rear Wheel Drive
SiL	Software in the Loop
SL	Straight line
SQP	Sequential Quadratic Programming
SNOPT	Sparse Nonlinear Optimiser
S-O	Subjective-Objective
TV	Torque Vectoring
VDC	Vehicle Dynamics Control

Acknowledgements

My soul, give praise to the Lord;
I will praise the Lord all my days,
make music to my God while I live.
Put no trust in princes,
in mortal men in whom there is no help.
Take their breath, they return to clay
and their plans that day come to nothing.
He is happy who is helped by Jacob's God,
whose hope is in the Lord his God,
who alone made the heavens and earth,
the seas and all they contain.
-Psalm 146: 1-6

Four years can feel like both a very short and a very long time. For those reading this who are embarking on doctoral study, I would like to encourage you that, whilst everyone's experience is different, if you surround yourself with good people, do some work every day (except Sundays) and do one thing at a time, you will get to the end successfully. And do not be afraid to ask questions and look stupid.

And with that said, I would like to do my best to acknowledge some of the countless people who have touched my life and made this possible. My parents, Berenice and Stephen Smith have instilled in me, like their parents before them, the values of hard work and discipline. I will be forever grateful to them for pushing me to be my best throughout school, and to live a balanced life at university, and for all the support through the uncertain times of young adulthood. My sister, Lucinda Smith and my brother, Benjamin Smith, make my life a joy and I am very proud of them both, the love and laughter has kept me going. I am so thankful for Rebecca Short. She is an unrelenting source of happiness and love, not to mention a gifted proof-reader. Without her, the final lap of the phD would have felt more like scaling a cliff face rather than merely conquering a Munro. To my very good friends, Gregory Jackson, John Howard and fr Bruno Clifton: you were my rocks. Thank you for the light relief, the good conversation, the prayers and the pints. fr Robert Gay, Dom Anslem Brumwell, Dom David Foster, fr Lawrence Lew, fr Tim Calvert and Calum MacKellar your strong example and guidance have encouraged me in my faith and guided me along the better way.

Dr Efstathios Velenis, my supervisor, thank you for your patience, warmth and example. You have had a greater impact on my life than you know. I am indebted to Dr Dongpu Cao for his incisive manuscript editing and pragmatism. I would particularly like to thank the anonymous reviewers at Vehicle System Dynamics whose comments through the journal submission process led to some important breakthroughs in understanding. Thank you, too, John Whitehead, for your guidance at imporant points along the journey. Chris Jeffs, thank you for letting me play in your workshop all those summers ago - look where it got me.

To all the Autolads, thank you. Room F5 has been a wonderful brotherhood. With special mention to Deepak, Sofian and Karsten, Davide, Siampis, Stergios and Ganesh, and Marcin. I am also indebted to Tony Tremlett for his guidance. To the postdocs and

staff in AVEC, it has been a pleasure to have worked alongside you and to profit from your teaching; thank you specially to Dr Daniel Auger, Dr Stefano Longo and Dr Amir Soltani.

To Mario, Gregg and Manlio, thank you for your friendship and fellowship and the adventure of CCS, and Fr Ken Bowen, too. You are all fine gentlemen. For a home away from home, Dr Josephine Tew and Richard Halliburton.

In the wider expanses of my life, I would like to thank all my friends at the Alliance of Pro-Life Students for keeping me sane, especially Eve Farren, Maria Stopyra, Phil Campbell and Alithea Williams, Niall O'Coinleain and James Tranter.

And to my good friends who I do not see as often as I would like but who nonetheless have given me great strength and joy over the past decade, I'm glad you're you! Bianca Hilado, Jordan Scott, Laura Lynch, Andrew Latham, Chris Oldroyd, Isabel Fawcett, Laura Back, Daniel Rathbone, Andy Houlihan, Paul Heron, Ben Norman, Anna McConnell, Paul Rickard, Patrick Leahy and especially the inimitable Madeline McNamara.

I feel ridiculously fortunate to have been able to indulge my passion for learning and fast cars for the past four years, with the generous support of the Engineering and Physical Sciences Research Council Industrial Cooperative Awards in Science & Technology studentship and sponsor Jaguar Land Rover under Grant EP/K504324/1. With humble thanks to my industrial supervisor at JLR, Mark McNally, and Prof. Francis Assadian, who made it all possible.

Edward Neville Smith. Wednesday 13th December 2018.

Ad maiorem Dei gloriam

Chapter 1

Introduction & Literature Review

The purpose of this chapter is firstly to briefly introduce the relevant theory and knowledge that underpins the work of this thesis and secondly to assess the state of knowledge in the pertinent areas.

1.1 Introduction & Motivation

A chief concern of vehicle dynamics engineers is to deliver good handling, for subjective enjoyment as well as safety.

To engineer a vehicle with good handling is a non-trivial task. Firstly, it presumes the knowledge of what constitutes 'good handling', assuming this is a concept that can be quantified. Secondly, it requires the scientific understanding and tools to achieve this definition over the full range of vehicle operation. A definition of vehicle handling is therefore required. It is concerned with the lateral and yaw responses of the vehicle to steering and throttle/brake control inputs.

Non-specialist motoring enthusiasts will be familiar with the terms 'understeer' and

'oversteer'; these and others will be expanded in §1.2.1 but for now, it is sufficient to state that a well-balanced vehicle in the realm of passenger vehicles is one which offers a prompt response to turn-in that is predictable at a large range of speeds and a stability at high speeds and control effort in all cases should be kept to a minimum [1].

Historically, vehicles of purely mechanical composition without modern electronic augmentation have been tuned to achieve the desired handling by passive means; choosing architectural parameters such as wheelbase, track width, centre of mass (CM) position, and front and rear roll centres. Of vital importance are the relative tyre stiffnesses between front and rear axles. The choice of suspension philosophy and wheel orientation in terms of camber and toe-in and caster angles also play a role. These 'basics' remain important, however, 'active chassis control' systems have enabled a more flexible and complex tuning of the vehicle handling characteristics 'on-the-fly' and by means of new actuators, such as the electric motor.

The effects of making passive adjustments has its limitations. Handling characteristics are heavily affected by dynamic lateral and longitudinal load transfers, weight distribution (fuel and passenger), and tyre pressure. In addition, there will be variations between individual vehicles coming off a production line and each vehicle's characteristics will change as components wear and are replaced. The other disadvantage of passive handling tuning is that it is a highly subjective endeavour and one setting will not please every driver.

The other major factor that affects handling design and development is the compromise required to achieve stability; this has traditionally implied the requirement for an understeering vehicle such that a critical speed at which the vehicle becomes unstable is avoided. This requirement comes at the expense of responsiveness.

The engineer must also consider the driver skill level when designing the handling characteristics. The average driver has a lower bandwidth of steering input than an expert

driver, for example, and will prefer to drive the vehicle in the linear range of operation. This means that the full performance envelope of the vehicle cannot be exploited.

The full performance envelope of the vehicle can be extended by semi-active and active systems, even when piloted by an average driver. The performance envelope of the driver-vehicle system may be smaller than the full potential of the vehicle; the degree to which this is true is dependent on the driver and the control system philosophy chosen and its optimisation.

Early active control systems included Anti-lock Braking Systems (ABS), active steer, Electronic Stability Control (ESC), and active/semi-active differential technology. Of particular interest are the active control systems. Active chassis control systems allow the engineer to actively modify the handling behaviour of the vehicle to achieve not only a more stable vehicle for the passenger, but also improve the responsiveness. These systems control the yaw dynamics of the vehicle and have historically been developed primarily for maintaining stability and controllability in the form first of active steering systems and later of ESC systems that apply brake pressure on individual corners of the car to adjust the path.

In the early 90s, actively-controlled rear-wheel-steer (RWS) systems were investigated to augment driver-controlled front-wheel steer (also referred to as all-wheel-steer (AWS). Despite showing promise, these systems exhibit a reduction in closed-loop control stability in limit-handling conditions [1] [23].

Yaw rate control in limit-handling situations was dramatically increased by the development of ESC in 1995 [2]. The ESC system allowed individual wheels to be braked in order to correct terminal understeer or oversteer, and reduced traffic casualties dramatically by allowing non-expert drivers to control the vehicle on their intended path to avoid

[1] Limit-handling definition: where one tyre or more is close to peak friction use or the entire vehicle is at the lateral acceleration limit

collisions [27]. The disadvantage of this system is the consequential reduction in vehicle speed and that braking is highly energy-dissipative and hence only suitable for emergency conditions. Indeed, in some scenarios, reducing speed can exacerbate the danger, as in motorway obstacle avoidance.

Passive, semi-active and active differential systems have been developed that tune the handling response across a larger area of the operation of the vehicle. For everyday driving scenarios, sub-limit [2], differential technology was developed to allow a modest biasing of torque from faster- to slower-rotating wheels to modify understeer/oversteer behaviour. The biasing was achieved using 'Limited Slip Differentials' (LSD) and Electronic-limited Slip Differentials (ELSD). More advanced torque biasing/vectoring differentials were developed that allowed torque to be distributed at will, not only from faster-rotating to slower-rotating wheels. However, the major disadvantage to these systems is that they can only effect change during positive acceleration. Latterly, some advanced differential systems have been developed to vector torque to the faster-rotating wheel, allowing a degree of authority over the handling characteristics.

At the time of writing, the automotive industry is undergoing a revolution- electrification. With drive and brake torque now provided by fast-responding electric motor-generators, a new freedom has been granted engineers to deliver torque in a continuously variable and flexible manner to the wheels.

Torque vectoring (TV), the system by which torque is delivered to each wheel according to a particular control law, is a powerful tool to allow active modification of the vehicle handling. With electric motors, the continuous, instant operation in both drive and brake modes delivers the ability to vector torque at will, even when no acceleration demand is present. This requires at least two motors on one axle, although the configuration with greatest potential to improve handling consists of having one motor per wheel.

[2] operating below the peak tyre friction

Four-wheel TV for passenger vehicles is not a reality at present due to limitations on packaging and cost, however, advances in battery technology and government policy phasing out conventionally-powered vehicles in the next few decades points to a future where four-wheel torque vectoring is commercially viable.

Motorsport is a key arena in which passenger vehicle manufacturers boost their marketing profile and, in the case of high-end motorsport, develop new technologies. For electric vehicle development, the nascent FIA Formula E (FE) championship was created with the specific aim of accelerating electric vehicle technological development [3] . Currently in its third season, the interest in team buy-in of factory OEM teams is high, with Mercedes, Porshe, BMW and Audi investing in factory teams and Ferrari likely to join with one of their brands [4]. Not only does competition accelerate engineering development and technical learning, but it necessitates the maximum performance of the vehicle to be extracted in order to win.

TV is, at present, not permitted in Formula E, Formula 1 or the World Endurance Championships, despite cutting edge electric and hybrid-electric powertrains. However, it is highly feasible that they could be permitted in the near future, with FE releasing a new vehicle in 2018/19 season and Formula 1 discussing the strategy of the sport from 2020, with new ownership from late 2016 . Roborace, an autonomous racing car championship which will act as a support race for FE from late 2017, possesses a very powerful 4-wheel torque vectoring powertrain [5].

However, TV is not of interest only for the future of motorsport or for current-day sublimit passenger vehicle operation, but investigation of the vehicle dynamics at the limit of adhesion and a greater understanding of the controls required to achieve this is of vital importance in developing active control systems that are able to manoeuvre the vehicle in the nonlinear and even unstable regions of the performance envelope to enhance safety for passenger vehicles. This is especially important for the future development of

autonomous electric vehicle control strategies.

With the considerably-expanded vehicle manoeuvring envelope in terms of yaw moment and lateral acceleration capability accessible through torque vectoring, it is important to determine the optimal handling characteristics of the actively-controlled vehicle in order to extract the maximum performance. Up until now, much research has been conducted into aspects of the TV system, but very little work has been undertaken to optimise the yaw rate reference for the TV system. The yaw rate reference is the high-level motion objective that essentially prescribes the desired vehicle path, and ultimately dictates the usage of the available handling performance. It is therefore of fundamental importance in realising the potential of a TV system.

This thesis sets out to explore and analyse the optimal handling characteristics for electric vehicles with TV, with an emphasis on maximising performance.

This chapter presents a review of the attempts to define and capture vehicle handling behaviour, touching on classical vehicle handling stability analysis and subjective driver requirements. A review of the literature concerning active yaw control systems and the state-of-the-art TV control systems is undertaken. Particular attention is paid to the yaw rate reference for such systems. The literature review concludes with a survey of the application of nonlinear optimal control theory for vehicle dynamics studies. A separate but related review which draws upon all these subject areas is not presented in this chapter but presented within chapter 7 with an emphasis on agile manoeuvring.

Section §1.3 sets out the aim and objectives for this research.

1.2 Literature Review

1.2.1 Classical vehicle handling & stability

This section gives a brief overview of the relevant theory behind the study of vehicle handling and stability. For more in depth treatment of the subject, the reader is directed towards [6–8]. The theory is placed within the context of the practicalities of the handling development process of a new vehicle by an automotive OEM.

Handling Development Process

For an automotive OEM, such as Jaguar Land Rover, the past decades have seen a shift in the emphasis of vehicle development. Vehicles have become far more complex as increasingly sophisticated active systems are implemented on the vehicle to the extent that the contemporary vehicle dynamicist requires a good knowledge of mechatronic engineering.

The increase in vehicle complexity has been accompanied by the increasing power of computers and simulation. Traditionally, the handling development process is time-intensive and highly manual, making use of experienced test drivers and engineers. Increasing investment is made into computer simulation and modelling. However, testing of prototype vehicles to determine suitability for sign-off for production and the marketplace remains a core aspect of the process. The tests for assessing prototypes sit somewhere on the scale of chance and design, where results in the form of subjective ratings of handling quality are described in a common language within a development community, typically unique to each manufacturer or even department [9].

Focus is divided between vehicle handling responsiveness and vehicle stability; the objective of the former is to create a vehicle that satisfies a range of subjective criteria that is desired by the consumer; the objective of the latter is to make vehicles safe over

the full range of operation. A compromise between these two objectives is necessary and a balance must be found. Vehicle path, yaw rate and lateral acceleration are related to handling responsiveness and sideslip and roll angles to directional stability [10] .

The vehicle handling requirement varies depending on vehicle class and brand. The handling characteristics of a certain brand are a large part of its appeal: the so-called 'DNA'. Prototype vehicles are evaluated on dedicated test facilities, typically including a steering pad, general durability circuit, closed handling circuit, ride and handling circuit and a high speed oval circuit.

Rauh [11] describes the virtual development process for vehicle handling, outlining various models and evaluation procedures, highlighting the advantages of modern simulation giving a common stock to relatively easily cooperate over a number of vehicle dynamics disciplines. Simulation has the advantage of repeatability and the ability to isolate certain effects. Simulation models are required to have modularity, flexibility and robustness and must be able to allow systems to be optimised within realistic time periods; in the case of Hardware-in-the-Loop (HiL) simulation, calculations must be completed in real-time. The computational burden is dependent on the control system. For an Electric Power-Assisted Steering (EPAS) system, for example, the high-level controller should run at 3Hz in order to be greater than the steering input ability of an advanced driver [89]. Further, the low-level controllers of the electric motors for the EPAS system must be higher than the high-level value. Taking into account the control transfer function for a DC motor raises the control system bandwidth requirement to 16Hz [89].

The vehicle model fidelity is an important consideration and should be appropriate for the level of investigation: a bicycle model may be suitable for parameter sensitivity studies, which a 3D functional model based on physical properties of individual components may be a requirement for simulating ride comfort or crash tests.

Vehicle handling target attributes should be developed, iterated, optimised in the sim-

ulation environment, with prototype vehicles required only to validate the concept and make final tuning adjustments.

Objective testing including closed-loop driver control is difficult [11]. Driver-in-the-Loop (DIL) simulation may be used for subjective evaluation, whose relevance is determined by how well the haptic responses are imitated, while HiL is now commonplace for rapid development iteration of the electronic control unit (ECU) before testing in the real vehicle.

Handling

The shift towards the simulation domain in vehicle handling development necessitates an ability to define characteristics objectively, together with some kind of understanding of the subjective perception of changes in handling character.

A pithy definition of vehicle handling is difficult to express. Essentially, it is concerned with the response of the vehicle in terms of yaw rate and lateral motion to control inputs from the driver [10]. For passenger vehicles and track motorsports, motion can be assumed to be predominantly constrained to a two-dimensional horizontal plane. Pitch and heave dynamics are coupled effects that arise from driver inputs indirectly. Indeed, lateral motion originates as a secondary effect from yawing motion induced by steering inputs at the front tyres. Yaw plane dynamics are, therefore, most important to consider.

The single-track 'bicycle' model of the vehicle allows an understanding of the fundamentals of vehicle handling to be developed, without complication by secondary detail. A constant forward speed is assumed, leaving the two degrees of freedom (DOF) of lateral and yawing motions. Roll motion is neglected along with lateral load transfer [12]. To describe the behaviour of the vehicle in response to steering inputs or external force disturbances, the single-track vehicle model is instrumental.

The single track dynamic equations of motion can be exploited in steady-state form to extract the yaw rate gain:

$$\frac{\dot{\psi}_{SS}}{\delta} = \frac{V}{l + V^2 K}, \tag{1.1}$$

where V is the forward speed of the vehicle, l is the length and K is the understeer gradient, defined as:

$$K = \frac{m(bC_R - aC_F)}{lC_F C_R} \tag{1.2}$$

where a and b are the distances from the CM to the front and rear axles respectively, l is the wheelbase, C_F and C_R are the front and rear tyre cornering stiffnesses. The yaw rate gain response gives indications of the *understeer* or *oversteer* characteristic of the vehicle. Understeer/oversteer is the core concept for vehicle handling dynamics. An alternative formulation of the steady-state yaw rate response is the path curvature response, which gives a more intuitive understanding of the handling behaviour:

$$\frac{\rho_{SS}}{\delta} = \frac{1}{l + u^2 K}, \tag{1.3}$$

where ρ_{SS} is the steady-state path curvature.

The $bC_R - aC_F$ term in K is the 'stability margin' and determines its sign. When $K = 0$, the curvature response is equal to the pure kinematic steering geometry. When $K > 0$, the vehicle takes a wider path than the neutral steer. This response is always stable and the reason for understeer being designed into passenger vehicles. When $K < 0$, the vehicle is oversteering and takes a path tighter than the neutral steer response. At a 'critical' speed, the yaw damping becomes insufficient and the vehicle becomes unstable. [8]. These conditions are shown in Figure 1.1. Commonly, steady-state understeer behaviour is determined from steady-state steer pad tests, which are open-loop manoeuvres. Either

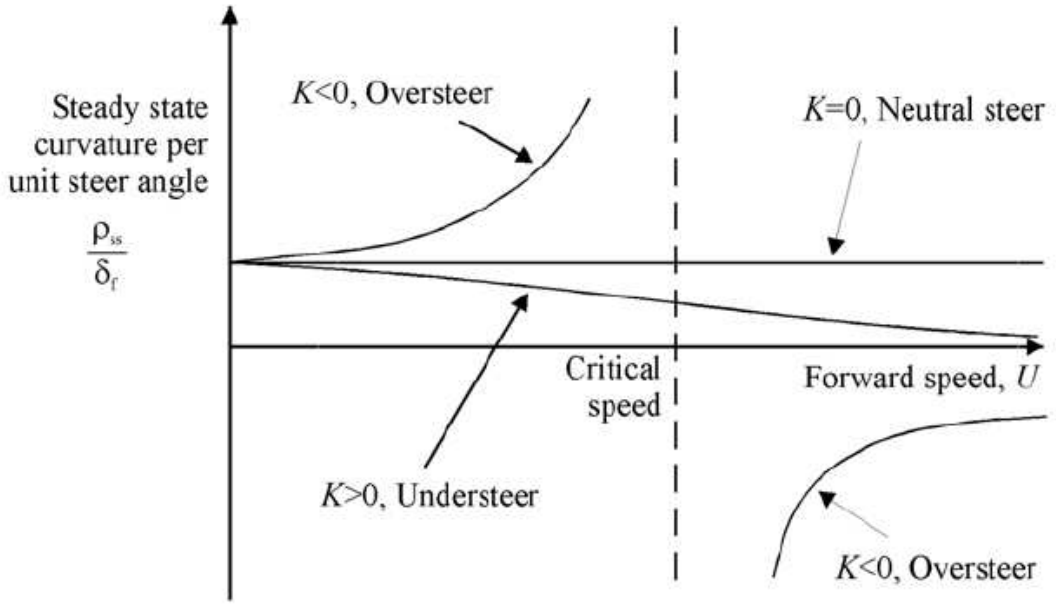

Figure 1.1: Curvature response for understeer, oversteer and netural steer vehicles (after [12])

the driver sets a constant steer angle and the path radius is recorded at incremented speeds, or a constant radius is followed by the driver by adjusting the steering angle for a range of speeds.

An alternative and equally intuitive way to understand understeer/oversteer is known as the Olley definition [8]. On the application of an external force at the CM, the understeer car will turn in the direction of the applied force (for zero steering angle); whilst the oversteer car will turn *towards* the applied force. A neutral steer car will continue without changing path.

Whilst attempts to capture new ways of expressing handling response objectively e.g. [13], the steady-state definitions remain standard practice. The understeer angle, defined as the difference between the front and rear slip angles (α_f and α_f, respectively), is useful for capturing handling balance in steady state and transient conditions:

$$K_{UA} = \alpha_f - \alpha_r. \tag{1.4}$$

The physical meaning for understeer is that the front tyres need to develop more slip angle than the rears to turn on the same path as the neutral steer, while the oversteering vehicle develops greater slip angles at the rear than the front in order to follow the same path as the neutral steer vehicle.

Subjective handling requirements The subjective 'feel' of the vehicle is important, and whilst every driver is unique, it is possible to make broad statements on general requirements. According to [12] two fundamental quantities are considered important influences on subjective perception: yaw rate relates to what the driver sees; lateral acceleration to what the driver feels.

Both contribute to the perception of responsiveness, which refers to the vehicles sen-

sitivity to driver control inputs. The yaw rate and lateral acceleration response should correlate predictably to the driver input and the progression should be smooth as the limit is approached [1, 14]. According to [15], transient behaviour is very important for a drivers subjective assessment. Drivers prefer a fast-responding front axle to a lateral demand, whilst the rear remains 'planted', resulting in a yawing motion that pivots around the rear axle, not the CM.

In general, responses should not overshoot excessively, as this feels imprecise or instable, and should be smooth [15]. A rapid settling time is desirable [14]. Additionally, oscillations after the initial steer input should be minimal in roll, yaw, pitch and heave modes.

Stability and Controllability

Quantitative definition A vehicle is defined as stable if sufficient restoring moments and forces exist to regain equilibrium following a disturbance [12]. Controllability refers to the degree of response of the vehicle dynamics to control inputs.

If the steering input to the bicycle model equations is set to zero, the transient response to small disturbances can be analysed via Eigenvalue analysis. Controllability is related to sideslip angle. Figure 1.2 shows the the 'β- method' developed by [16] which plots the variation of yaw moment with sideslip and steering angle, and at different levels of longitudinal acceleration. As the sideslip angle of the vehicle increases, the yaw moment gain decreases and the vehicle become much harder to control, since the yaw moment and therefore yaw rate of the vehicle are almost insensitive in changes in steering angle [2]. The β- method neglects dynamics, so a β- phase plane method was suggested by Inagaki et al. [17] that plots sideslip angle against sideslip rate. This allows information about sideslip damping and natural frequency to be given and allows control action to be

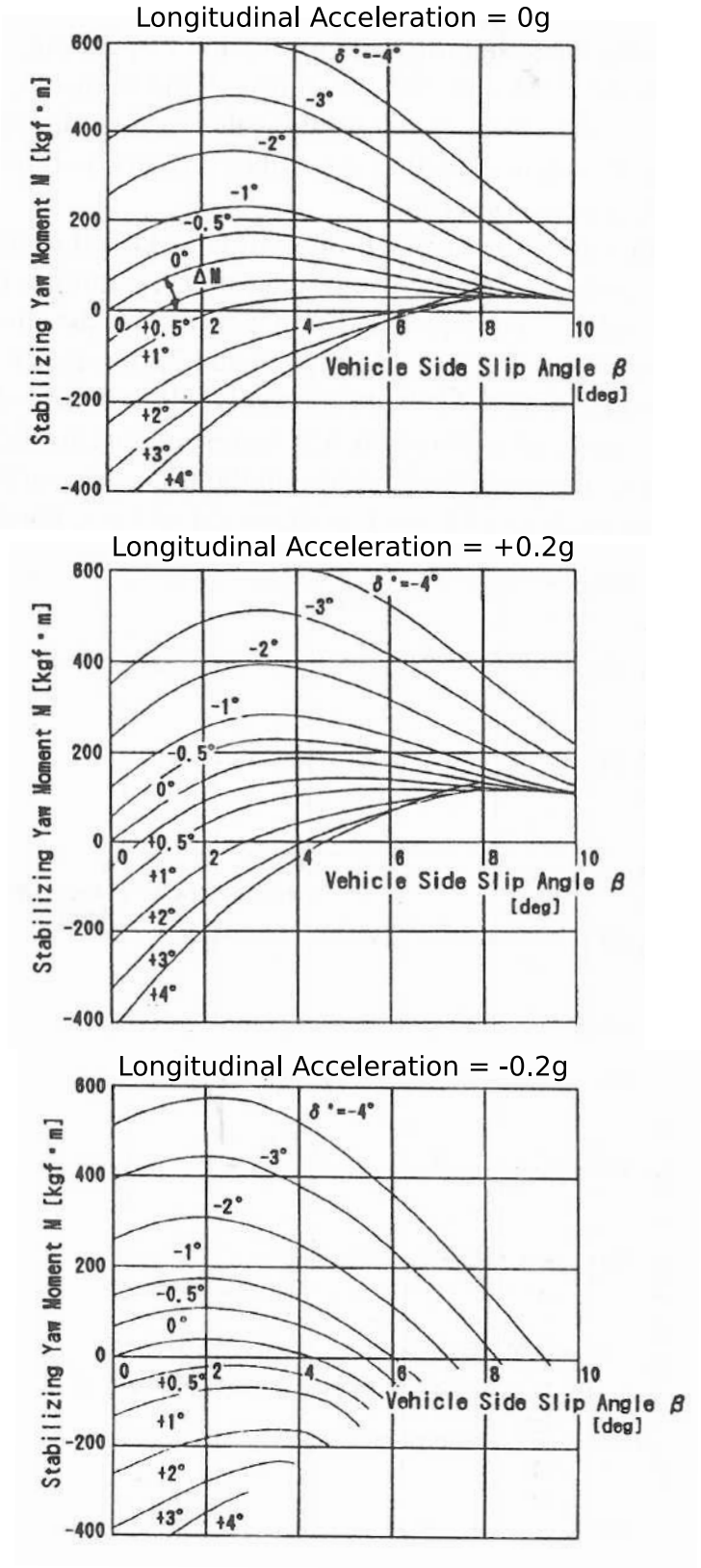

Figure 1.2: 'β- method' analysis of stabilising yaw moment available at various steering angles and different levels of longitudinal acceleration (from [16])

determined based on whether in the stable or unstable region.

Qualitative requirements The 'friction ellipse' is a concept that refers to the combinations of lateral and longitudinal tyre forces that are possible at given operating conditions, for example, of normal load [8]. The friction ellipse dictates the overall forces available from the tyres; an increase in lateral demand will reduce the available longitudinal force and vice versa. Longitudinal weight transfer under acceleration or braking modifies the traction force available on the front or rear axle and therefore the lateral force capability for scenarios with acceleration and braking in a turn. The relative load transfer effects front-rear and left-right will affect the path following ability of the car and will result in understeer or oversteer behaviour. Sharp [9] explains that decoupling of vehicle longitudinal and lateral response makes driving easier but notes that this coupling can be used by an expert driver to induce a lateral response of the vehicle to longitudinal control of the rear tyres via the throttle in RWD (Rear Wheel Drive) or 4WD (Four Wheel Drive) vehicles (c.f. rally driving). It will be shown later that active control of coupled lateral and longitudinal control can be used to extend the performance of the vehicle while keeping the driving task simple.

Subjective-objective Correlation

Vehicle handling evaluation is a popular theme in automotive engineering: there is a desire for designers to understand what parameters contribute to handling characteristics; test drivers wish to know what the reason is for a vehicle feeling better or worse. It is relatively easy to quantify an improvement in limit handling performance. However, it is much less clear what constitutes a performance improvement under normal driving conditions [18]. Inevitably, this latter goal involves a strong element of subjective assessment and interpretation [19]. Sharp [9] concluded after noting that an improved objective spec-

ification of vehicle dynamics based on high subjective rating was needed that the prize for fully extending predictive capabilities, extending into proper quality judgements is great. That is to say, the vehicle development process can be shortened if simulation can accurately predict the subjective rating of an objective change in advance of physical testing. Manning and Crolla [19] conducted an extensive review of sixty-eight papers in the field of lateral handling control, noting that it is difficult to map the control objectives (such as yaw rate, sideslip angle) to high-level subjective criteria (e.g. predictable, stable). However, with all the attempts at correlation [20–22], there is not enough data for the results to be considered statistically reliable, especially considering the extensive averaging that is required for analysis. Collecting sufficient quantities of reliable data, especially subjective ratings, is a significant challenge.

Summary To summarise, vehicle handling DNA is extremely important to automotive OEMs, especially premium brands, and therefore the development of modern active handling control systems requires an understanding of traditional concepts such as understeer and oversteer but also how to use these concepts in the simulation environment. Increasing emphasis on vehicle handling development in the simulation environment saves time and reduces costs, but there needs to be a way to map objective measures to the subjective feeling of drivers. Whilst studies have tried to correlate these, there is insufficient data for it to be reliable. The subjective feeling of the driver is outside the scope of this thesis in a formal way. However, since active yaw control targets are set subjectively, the work in this thesis attempts to understand in greater depth the effect of the subjective choice of handling behaviour on the objective response and performance of the vehicle.

1.2.2 Handling & stability control Systems

The previous subsection gave a general introduction to handling. The focus of this section is the active control of handling of the more classical type, encompassing active steer and yaw control by brake.

Dixon [23] undertook a literature review of FWS, RWS and AWS active yaw control systems, which were common in the 1990s. DYC-by-brake was a superior system in terms of ease of direct control of forces, an insensitivity to sideslip angle on the effectiveness of control, greater robustness and effectiveness at the limit. Its greatest drawback, however, was the brake actuator's effect on vehicle speed and significant energy consumption. According to Dixon [23], DYC-by-brake had advantages over 2WS and 4WS in that there is little sensitivity in ability to change yaw acceleration with respect to torque inputs with changes in sideslip. The direct control of forces is an advantage for DYC, despite being limited by load transfers and at the expense of a much greater energy consumption.

Mirzaei [24] executes a general strategy on DYC control using analytic LQ optimal control. The optimal control cost function trades off yaw rate and sideslip errors and usage of DYC- external yaw moment. A 2DOF single track model enriched with a M_z term was used for control law development and simulations run using an 8DOF model including roll DOF. Mirzaei found that for a J-turn manoeuvre, yaw moment could be dramatically reduced with acceptable trade-off in yaw rate tracking. Since this study was for limit conditions considering DYC-by-brake, the results are acceptable when stability is the main concern. For continuously activation DYC in the case of TV, the tracking errors would not be acceptable.

Rubin [25] formulates an MPC controller using an LPV single-track vehicle model for a yaw stability controller for a vehicle with an Active Limited-Slip Differential. Yaw rate and sideslip following is good for a step-steer in simulation with a 10DOF model with

nonlinear tyres and tyre relaxation features. Closed-loop double-lane change on packed snow ($\mu = 0.4$) is performed without loss of control and with tighter path following and fewer oscillations than a sliding mode reference controller. Torque control inputs are of high frequency, as no torque rate constraints are considered; there is no mention of the computation time.

Front-rear torque vectoring Piyabongkarn et. al. [26] investigate the effect of combinations of front-rear and left-right torque biasing for a 4WD SUV on handling. A centre coupler modulates torque front-rear and a Electronic-Limited Slip Differential (ELSD) on the rear axle controls torque bias, with the possibility only of biasing torque from faster to slower rotating wheel- which allows only relative understeer to be induced. Single-track bicycle model analysis in steady-state coupled with a Dugoff tyre model shows that longitudinal force distribution with front bias induces understeer. A CarSim simulation demonstrated greater effect from left-right bias than front-rear for a step-steer on-throttle manoeuvre for both low and high mu surfaces. The effect is greater on low-mu for left-right torque bias but front-rear has less effect on low-mu (smaller acceleration). Off-throttle allows torque bias only from left-right ELSD. In experimental testing, a T-junction launching on full-throttle is improved with the front-rear torque vectoring.

In an article [27], Piyabongkarn et. al. describe various types of active driveline torque management (ADTM) systems, from ELSDs, to torque vectoring differentials by means of one or two clutches. The following summarises the key information from the article. Electronic Stability Control (ESC) was introduced first on the 1995 Mercedes E-Class and was used for limit handling conditions as a safety device by activating the appropriate brake to modify the path of the vehicle. It typically has an activation time of < 50ms and is integrated with ABS and traction control (TC) systems. The introduction of ESC (now mandatory) has led to a drastic reduction in serious accidents and fatalities. Modification of handling in sub-limit conditions, however, is also of interest for “fun-

to-drive", and a more consistent vehicle behaviour in the presence of load transfer effects and other nonlinearities. ADTM systems seek to transfer torque from front to rear and left to right. Front-rear varying torque split has been achieved in the Nissan CUE-X, ET-S, Haldex LSC, BMW xDrive and Bosch CCC. For left-right torque biasing using a limited slip differential, which transfers torque from the faster rotating outer wheel to the inner wheel, has been implemented by Eata, GKN TMD and others. Electronic limited-slip differentials allows the torque to be modulated continuously and actively. A step further are Honda's SH-AWD, a system by Ricardo and Mitsubishi's SAYC. These devices allow torque to be transferred whichever direction required by use of one or more clutches in parallel with the main differential. These torque vectoring differentials are powerful in their ability to correct oversteer situations, as demonstrated on a T-junction pull-away on low-μ surfaces, and in better path following and stability in lane-changes. Their major limitation, however, is that acceleration demand from the driver is necessary for the system to operate.

1.2.3 Torque vectoring in Electric Vehicles

Torque vectoring for electric vehicles has been given increasing research attention over the past decade and especially in the last 5 years. This section first introduces the fundamentals of the concept and the core vehicle dynamics theory, before introducing the standard TV control system with a brief section reviewing the literature in each area of development. The yaw rate reference is presented separately in section §1.2.4 in more detail.

Fundamentals and Vehicle Dynamics performance

Torque vectoring yaw moment arises from the torque difference between the tracks of the vehicle, while secondary effects arise from coupling of longitudinal and lateral tyre forces. In the seminal work investigating direct yaw control (DYC), Shibatahata et. al. [16] show that DYC, the same mechanism exploited by torque vectoring, increases the limit lateral force of the vehicle. They also showed, via the β- method, that DYC is able to overcome load transfer effects to comparable with the steady-state performance (top plot in Figure 1.2). This was for a vehicle with transverse distribution of drive/brake forces across the rear axle only. For torque vectoring, [28] show for a vehicle with torque vectoring across the rear axle, performance is limited under braking, where at a certain level of sideslip, TV vectoring is unable to fully compensate for load transfer effects and will not deliver the desired steady-state performance.

Horiuchi [29] later showed through determination of yaw rate - lateral velocity 'controllability regions' that DYC increases the operating range over which the vehicle is controllable, later extending the work to evaluate the performance of different feedforward control laws of DYC performance [30].

TV Control Systems

It has been shown in the literature that DYC increases the vehicle handling envelope; this section will turn to presenting the state-of-the-art in torque vectoring control systems that show even greater benefit. Crolla and Cao [10], warn, however, that "Despite the significant volume of theoretical studies of TV on vehicle handling control, there is no widely accepted design methodology of how to exploit it to improve vehicle handling and stability significantly". Torque vectoring control systems have the high-level objective of following one or more motion reference signal inputs, achieved by the control and

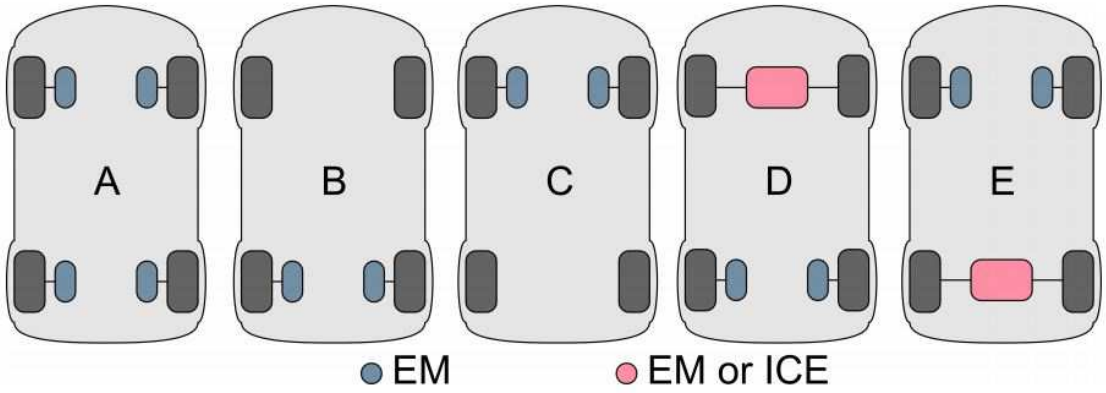

Figure 1.3: EV/HEV topologies (from [31])

modulation of the torques of the electric motor actuators. Electric motors as actuators are ideal for control systems, due to their high responsiveness, precise controllability and instant torque delivery.

There are a variety of torque vectoring vehicle topologies, with different combinations of electric motors [32]. Figure 1.3 shows a variety of layouts for EVs/HEVs. [31] compared the topology performance in steady-state and transient manoeuvres against their corresponding passive layouts (for an understeering vehicle only), finding that: the four electric motor (layout A) delivered the greatest performance; followed by rear independent drive (layout B), which has improved steady-state performance but lacked damping in transients; front independent (layout C) performed almost to the level of A; while D and E were the best solutions for modifying ICE vehicles.

When two electric motors (EM) power the same axle, there is a only one way to command a yaw moment; through the torque difference between the actuators [33], whereas when four EMs are adopted, there is redundancy in the system: over actuation. This means that the torques demanded from each EM can be combined in numerous combinations to achieve the same yaw moment at the vehicle CM. Therefore a more sophisticated strategy for the distribution of torques between the actuators is required.

Torque vectoring control systems can be broadly categorised into two main architectures: model predictive control or hierarchical.

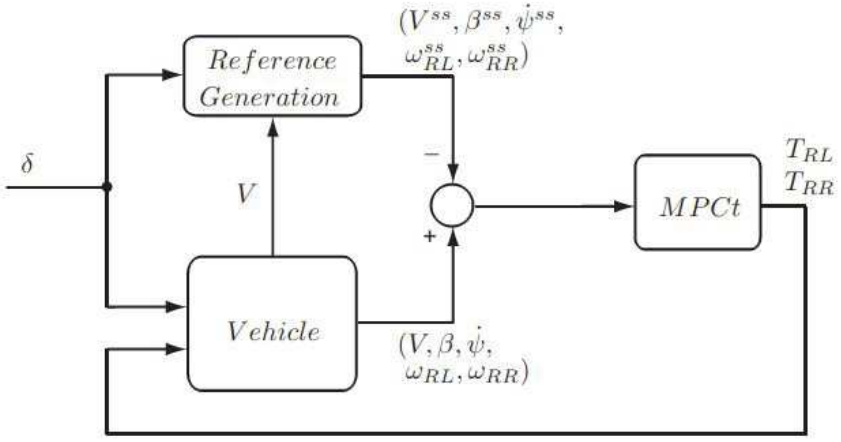

Figure 1.4: Model Predicitve Control architecture for RWD TV (after [34]

Model Predictive Control Control architectures using Model Predictive Control (MPC) are becoming increasingly popular as computing power and knowledge in this area grows. The MPC-based TV control systems take high-level motion reference signal inputs and calculate the wheel torques required to follow the reference, solving optimal control problems in real time, subject to constraints and a particular objective function. The architecture is shown in Figure 1.4.

Siampis et. al. [34] used an MPC controller to stabilise a vehicle at high lateral acceleration using rear-axle transverse TV. The MPC controller model is a 7DOF planar model with Pacejka tyres and lateral load transfer; trialled with and without wheel spin dynamics. Constraints ensured the vehicle is maintained in a stable region in comparison with an LQR controller and solved is real-time. They concluded that the slip input model is sufficient and the MPC strategy is robust.

Bächle et. al. [35] implemented an MPC control structure for a 4WTV to allocate both longitudinal force and yaw moment, delivering good performance in a double-lane

change in the CarMaker high fidelity simulation package. The MPC was formulated with wheel torque, desired wheel torque and slip ratio for each corner and the objective function included hard constraints on torques and soft constraints on slips. It delivered an impressive performance in CarMaker for a lane change on high friction and under heavy braking, keeping slips below 0.1, while closely following the reference.

To conclude, MPC is useful for control allocation considering constraints and an objective in real-time, however it does not eliminate the need for a control allocation, controller and reference; it simply is a means of solving the problem on-line, which inevitably pays a price in terms of computational burden and complexity.

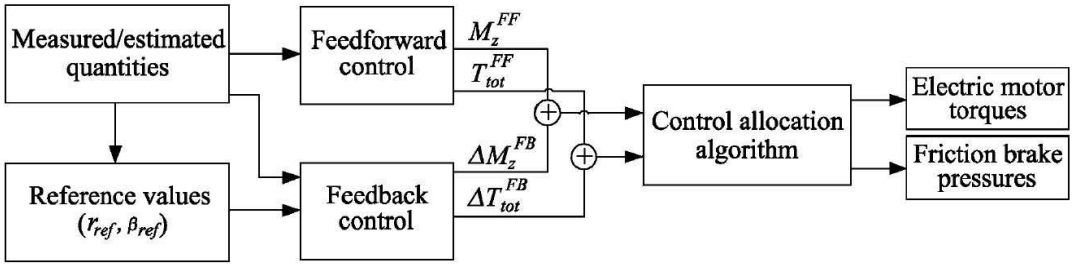

Figure 1.5: Hierarchical torque vectoring control system (in [36], after [37]

Hierarchical torque vectoring controllers The hierarchical torque vectoring control system follows the general form shown in Figure 1.5, comprising reference generator, controller and control allocation. Low-level control of motor torques for slip control systems [38], for example, are outwith the scope of this survey.

Controller reference Torque vectoring control systems take as reference signals any number of yaw rate, sideslip and velocity. Most use yaw rate (explored in more depth in §1.2.4), to achieve a desired handling response, with sideslip used to keep the vehicle in the stable operating window. A triplet reference of yaw rate, sideslip and velocity is used

by [34] with rear axle TV.

Controller As shown in the diagram, the controller may be composed of feedforward and feedback elements. Using both feedforward and feedback control helps to prevent controller saturation, to improve tracking and is also of benefit to control high order dynamics with limited controller bandwidth.

Feedforward control is used in [32]. A quasi-steady vehicle model is used to determine the yaw moments required to follow a set of yaw rate references, such that a look-up table can be used for the desired feedforward control, depending on the selected reference. Feedforward elements were also employed by [39] in the form of the single-track vehicle model transfer function to output a yaw rate signal to be combined with the feedback error.

Feedback control forms the basic strategy in torque vectoring control systems, although a great variety of control philosophies are employed. Control design is not a focus of this thesis, so if suffices to give a brief overview. PID controllers are adopted by [40, 41], the tuning of which is conducted in the simulation environment using first a single-track vehicle model, then higher-order models before finally a genetic optimisation algorithm was employed to fine-tune the desired response. [42] also use a PID controller for a rear-axle TV system. A Linear Quadratic Regulator is used for understeer mitigation via rear-wheel TV in [34], while a Linear Parameter Varying controller is adopted by [43] and [24]. [40] and [25] choose sliding mode controllers. [44] compare conventional and adaptive PID and two second-order sliding mode controllers. It was found that the PID controllers achieved very good steady-state and transient vehicle performance while the strengths of the sliding mode controllers lay in robustness in the presence of vehicle parameter variation.

Control allocation is required for two or more motors, with many possibilities for three or more actuators when redundancy allows for secondary objectives to be considered after the demanded yaw moment is satisfied by the appropriate distribution of longitudinal tyre forces. Determining the control allocation for over-actuated vehicles can be computationally demanding when considering modelling nonlinearities. Accordingly, an offline optimisation scheme is employed in [45], with the objective of minimising time for a 4 independent motor EV; the results of optimal control problems revealed that a control allocation proportional to the normal load on the tyre should be employed. This strategy is relatively simple to use online, but other secondary objectives prove more difficult.

Other research considering a 4 independent motor EV [36,46] use an offline optimisation-based approach to determine the control allocation for a range of objective functions, including electric power minimisation and tyre slip minimisation. A quasi-static vehicle model was used to reduce computation complexity.

In subsequent research, De Castro et. al. [33] developed a real-time approach, using a full nonlinear tyre friction model but using convex approximations to the actuator physical limits, and then solved an optimal control problem using fast quadratic programming solvers, with the objective of minimising tyre friction usage.

Torque vectoring studies

The previous section gave an overview of the torque vectoring control system. In this section, some case studies are described in more depth.

Yu et. al. [47] develop an integrated yaw and stability control system for enhancement of handling in the stable region and for controllability near the limits of stability. Phase-plane analysis of sideslip against sideslip rate is used to determine the stability limits at which the side-slip stability control should be smoothly activated. An LQR con-

troller is implemented with adaptive gains based on online cornering stiffness estimation. Control allocation between the 4 electric motors is achieved by means of a quadratic program that minimised yaw rate error and energy usage simultaneously. A single-track vehicle model with nonlinear tyres is used for phase-plane analysis; steady-state linear single track model for the yaw rate reference. The integrated strategy is a good approach. However, by restricting vehicle operation to the stable region, advanced manoeuvrability available when operated in the unstable region is missed.

Kaiser et. al. [43] developed an LPV controller for yaw rate and longitudinal speed control for a FWD vehicle with left-right TV capability on the front axle. The control strategy considered torque and power limits and motor slew rate limits. The LPV controller was developed considering a nonlinear single-track model (including longitudinal dynamics) with linear tyres, which trades off yaw rate and v_x following considering slip targets of $\lambda = 0.1$. Gain scheduling was devised through a "parameter space" approach and has integrated anti-wind-up features. The controller was validated using a 14DOF vehicle model including spin dynamics and vertical displacement. A manoeuvre considering lateral and longitudinal dynamics separately and then combined was run using two different versions of the controller, trading off yaw rate-following or speed-following. Good performance was achieved, whilst respecting constraints. The controller model is valid for $\lambda < 0.1$ and $\alpha < 0.08$rads. Electric machines limits were: $\dot{T} = 1000$Nm/s; $T_{max} = 775$Nm;$P_{max} = 20$kW.

De Novellis et. al. [41] compared PID and sliding mode yaw rate controllers for yaw control for TV, including feedforward components derived from a QSS vehicle model. Evaluation in CarMaker concluded that a PID controller was a good solution for feedback control, feedforward control was useful for achieving steady-state yaw rate target, and inclusion of a 1st order delay on the yaw rate reference was good practice. The feedforward component was a lookup table of yaw moment generated from a linearised QSS model

with yaw, sideslip and roll rates set to zero, given the current operating state and piecewise yaw rate reference. The PID gains were tuned using the Frechet method and stability analysed using phase-plane techniques. The vehilce response was analysed in time- and frequency- domains and for robustness in mass, friction and tyre variation in CarMaker. PID, adaptive PID, suboptimal SM and twisting SM controller were compared. It was found that feedfoward was necessary for good PID tracking but was not as effective in the presence of disturbances. SM was a better strategy for following references for longitudinal acceleration variation but exhibited undesirable oscillations. A PID with gains scheduled as a function of speed was good but not useful for ramp steer manoeuvres.

Gruber et. al. [48] conducted an analysis of 4-wheel TV controller for energy efficiency for control allocation and understeer characteristic. The objectives were to minimise power losses in both these components and it was assumed that power loss in the drivetrain due to slip loss is a significant factor. Small steer angles and basic geometry were assumed and only steady-state tests conducted. For the control allocation, power losses were measured on the demonstrator vehicle on a rolling road. Handling was evaluated on a skid pad using constant steer tests. A 4% improvement in energy savings during cornering conditions was reported compared to a fixed 50:50 control allocation. The optimal understeer characteristic for energy efficiency was close to neutral steer for the demonstrator vehicle, which corresponded to an 11% reduction in input power.

De Novellis et. al. [40] described a yaw rate controller with sideslip regulation system for the E-VECTOORC vehicle with left-right TV over the front axle. Controller tuning was conducted in simulation before experimental testing, delivering very good agreement between simulation and experimental results. The study objectives were to analyse the performance improvement (handling), to demonstrate the offline-determined yaw moment feedforward component and to demonstrate the PID tuning with particle swarm optimisation. The PID gains were tuned using traditional linear system loop-shaping

techniques, then refined using particle swarm optimisation and finally in CarMaker with a high-fidelity model. Feedforward terms from QSS simulation were included in a lookup table, and are yaw rate reference-dependent. An impressive level of agreement was found between simulation and experimental data.

Siampis et. al. [34] used an MPC controller to stabilise a vehicle at high lateral acceleration using rear-axle transverse TV, with velocity regulated to a feasible value. The understeer target was set to neutral steer using the standard bicycle model expression. The MPC controller model used was a 7DOF planar model with Pacejka tyres and lateral load transfer; trialled with and without wheel spin dynamics. Constraints ensured the vehicle was maintained in the stable region in comparison with an LQR controller and solved in real-time. An MPC formulation with slip inputs (no wheel spin dynamics) used sliding mode control to find the required torques and the study concluded that the slip input model was sufficient for good control and that MPC was robust to a certain level of uncertainty.

Bächle et. al. [35] implemented an MPC control structure for a 4WTV to allocate both longitudinal force and yaw moment, completing a successful double lane change in CarMaker. The yaw rate reference utilised the single-track model augmented with a direct yaw moment term in transfer function form. The control allocation model used a four-wheel model with nonlinear tyres. A MPC controller was formulated with wheel torque, desired wheel torque and slip ratio for each corner, while the cost function included hard constraints on torques and soft constraints on slips.

1.2.4 Yaw rate reference

The previous section introduced TV control systems. TV control systems, and their predecessor DYC systems both require yaw rate references, which is the focus of this section. In the following section, a review of optimal control techniques for vehicle dynamics ap-

plications are introduced.

The selection of a control system reference (or set point) is an important element in extracting the full potential from the active system. Dixon [23] investigated the influence of sideslip target on vehicles with active handling systems and notes that control strategy components and their combination is important for overall system performance "The target or reference of a controller refers to the manner in which the controller strives to get the vehicle to behave. Target plus control strategy is important for overall performance. Likewise, the "choice of target influences the difficulty of the control task and the performance of the choice of target influence difficulty of control task and performance of control structure with alternative targets rarely discussed."

While Dixon has investigated the effect of sideslip reference on performance, a similar investigation has not been pursued for yaw rate reference for active handling control systems. Horiuchi [29, 30] investigated the closed-loop control performance of DYC, 2WS and AWS handling control systems using optimal control in terms of controllability to compare against their theoretical potential. However, the active control systems under investigation used only feedforward control laws to calculate active steering/yaw moment control inputs rather than feedback control seeking to follow a yaw rate reference value.

TV systems typically follow a yaw rate reference, achieved by tuning of a controller and a subsequent Control Allocation (CA) for torque arbitration between individual wheels. Advanced techniques using mathematical analysis and simulation tools have been used to optimise both controller [34, 40, 43] and CA [36, 40, 45] performance, yet very little rigorous work has been undertaken into research of the optimal yaw rate reference. It has been shown that TV extends the maximum cornering force by superior distribution of yaw moment, making better use of friction availability and hence the vehicle performance envelope is increased with individually-controllable electric motors [10, 49]. It has now become more important to optimise the reference such that the full performance potential

of the driver-vehicle system can be realised.

The goals when designing the yaw rate reference are often highly subjective, but objective criteria have been produced. In general, an understeering vehicle is desired for the following reasons: control theory and physiology predict that human drivers find an oversteering vehicle difficult to operate; the closed-loop stability of an oversteer car becomes unstable at the critical speed; taking into account modelling and experimental errors requires a conservative approach and therefore understeer is required [1].

In addition to the open-loop stability of an understeer car, however, it is important that the subjective desires of the driver are taken into account. A great deal of work has been undertaken into understanding the correlation between objective metrics and subjective assessment in the hope of understanding how to design a handling response that is satisfying to the driver that largely eliminates the need for time-consuming and costly iterative vehicle testing. Additionally, the variability in subjective assessment between drivers presents a problem [20, 50]. The advantage of TV systems is that any yaw rate reference could be selected at the touch of a button, customisable to the driver.

In addition to stability and subjective preference, average drivers also require a consistency of response at all levels of lateral acceleration (linear response). Further objective criteria include, clearly, that the reference is feasible and that the reference is bounded to a safe margin (if an oversteer behaviour is selected for some or all of the range of operation).

The yaw rate references that appear in the literature include: steady-state linear bicycle model; a piecewise linear-exponential expression and a dynamic linear bicycle model.

Steady-state linear bicycle model

A common approach is to set the reference target from the steady-state solution of the classical linear-tyre bicycle vehicle model and choosing a desirable value for the understeer gradient, K [25, 42, 43, 51, 52]. The steady-state equation for yaw-rate (equation 1.5 and the expression for understeer gradient (equation 1.6) may be combined to arrive at an expression for desired yaw-rate in terms of steering angle, vehicle speed and vehicle dynamic parameters [53].

$$\dot{\psi}_{ref} = \frac{V}{R} = \frac{V}{l + V^2.K}\delta \tag{1.5}$$

$$K = \frac{m(\ell_R C_R - \ell_F C_F)}{L C_F C_R} \tag{1.6}$$

where $\dot{\psi}_{ref}$ is the target yaw rate, V_x is the longitudinal velocity, R is the instantaneous path radius ℓ_F and ℓ_R are the distances from the centre of mass (CM) to the front and rear axles respectively, L is the wheelbase, m is the vehicle mass, C_F and C_R are the front and rear tyre cornering stiffnesses.

The majority of yaw rate references have been derived from the steady-state single-track linear-tyre equations, modifying the handling for stability (understeer) or responsiveness /agility /'fun-to-drive' (oversteer) by selecting an appropriate target understeer gradient, K_{tar} [25, 42, 43, 51, 52]. This is a linear relation when expressed on the 'handling diagram' of dynamic steer wheel angle, δ_{dyn}, against lateral acceleration, a_y (where $\delta_{dyn} = \delta - \delta_{kin}$; δ_{dyn} and δ_{kin} [8] are the dynamic and kinematic steer angles), the gradient of which is determined by the understeer gradient. Ni and Hu [54] varied K_{tar} as a function of speed to achieve a tight turn radius at low speeds and a stable character at

high speed.

A bounding of yaw-rate to:

$$|\dot{\psi}_{ref}| \leq \mu g / V_x \tag{1.7}$$

is common in the literature [2,25,42,53,55–58]. [42] allows a higher bound by multiplying the right hand side of the equation by a constant greater than 1 to induce a controlled drift.

Piecewise linear-exponential expression

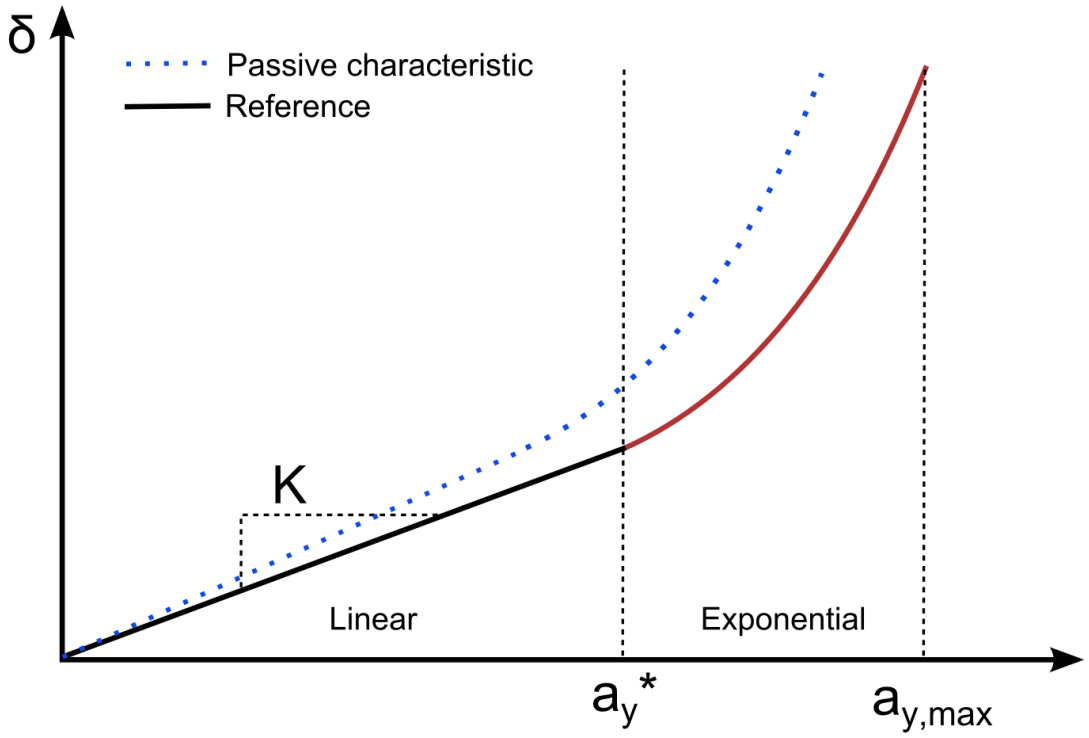

Figure 1.6: Yaw rate Reference (Piecewise)

A Piecewise linear-exponentional reference is used in the E-VECTOORC project [40].

$$\dot{\psi}_{ref} = \frac{V_x}{R} = \frac{V_x}{l + V_x^2.K}\delta \tag{1.8}$$

$$K = \frac{m(bC_R - aC_F)}{lC_FC_R} \tag{1.9}$$

$$\dot{\psi}_{ref} = \frac{a_y}{V}, \tag{1.10}$$

$$\text{where: } a_y = \{\frac{\delta_{dyn}}{K}, \text{ if } \delta_{dyn} < a_y^*K \tag{1.11}$$

$$a_{y,max} + (a_y^* - a_{y,max})e^{\frac{a_y^*K - \delta_{dyn}}{(a_{y,max} - a_y^*)K}} \tag{1.12}$$

$$\text{if } \delta_{dyn} \geq a_y^*K\}. \tag{1.13}$$

where $\dot{\psi}_{ref}$ is the target yaw rate, V_x is the longitudinal velocity, R is the instantaneous path radius a and b are the distances from the CM to the front and rear axles respectively, l is the wheelbase, C_F and C_R are the front and rear tyre cornering stiffnesses. $\delta_{dyn} = \delta - \delta_{kin}$ where δ_{dyn} and δ_{kin} are the dynamic and kinematic steer angles.

The available friction and longitudinal acceleration determine the maximum lateral acceleration possible, and, according to a parameter, a_y^*: the proportion of $a_{y,max}$ over which the $\delta - a_y$ plot becomes nonlinear. [36] In reality, the handling diagram exhibits highly nonlinear behaviour towards the limit lateral acceleration due to tyre nonlinearities [16]. This was considered by Canale et al. [56] to calculate achievable limits for yaw rate as a function of both steering angle and velocity ($\dot{\psi}_{ref} = f(\delta, V)$) by steady-state analysis considering a single-track model with nonlinear tyres, taking into account a direct yaw moment term to represent an active rear differential. A reference is then chosen heuristically between the limits, ensuring a smooth transition between linear and nonlinear regions. For an EV with left-right TV across the front axle, De Novellis et. al. and Pennycott et. al. [40, 59] adopted the approach in [56], with yaw rate reference set heuris-

tically such that the linear region is extended, lateral acceleration boundary maximised, and responsiveness is increased in the linear region of the handling diagram. A subjective improvement in 'fun-to-drive' was reported for a yaw rate reference with a value of K_{tar} in the linear region set lower than the value for the vehicle without TV active.

Canale et al. [56] calculate reference by means of steady-state bicycle model equations, taking into account a yaw moment applied by an active differential and nonlinear magic formula tyre model. Achievable limits of the handling diagram (Figure 1.7a) are calculated for a range of constant speeds by varying manipulatable variables (for the non-DYC case). The reference may then be chosen within the achievable limits according to some criteria (Fig. 1.7a) and subject to a maximum lateral acceleration $a_{y,max} \leq 0.85\mu$ [53]. The yaw-rate reference is then calculated using $\dot{\psi}_{ref} = \frac{a_y}{V}$. A static map was then built up as a function of speed and steering angle, $\dot{\psi}_{ref} = f(\delta, V)$.

Wheals et. al. [60] constructed a similar map ($\dot{\psi}_{ref} = f(\delta, V)$) by interrogation of a high-fidelity model at steady-state with equal wheel torques applied and noted significant differences to the single-track model attributed to roll and nonlinear tyres but do not make use of it in the controller. However, they implemented a simpler linearised two-track model considering nonlinear tyres and aerodynamic forces in which sideslip and velocity derivatives were decoupled and the reference set presuming zero sideslip and no longitudinal acceleration ($a_y = \left(\dot{\beta} + \dot{\psi}\right) V$). No evaluation of the reference was made

Dynamic linear bicycle model

A first-order delay to account for the yaw inertia of the vehicle was incorporated by [60–62] however Bünte et. al. [39] proposed a yaw rate reference considering fully-dynamic elements, combining steady-state and lateral dynamics transfer functions from the single-

track model, tuned heuristically to modify the transient response.

Bunte et. al. [39] propose a yaw rate reference target that is a significant departure from the rest of the literature. The reference is a combination of transfer functions of a static term derived from the standard steady-state bicycle model expression (the understeer gradient is given the equivalent term of "self-steer" gradient) and a dynamic term, as shown in figure 1.8. The dynamic behaviour of $\dot{\psi}_{ref}$ is given by the linear filter, with steady-state gain of unity.

$$\Gamma_{\delta_f \to \dot{\psi}_{ref}}(s) = \frac{G_{\delta_f \to \dot{\psi}_{ref}}(s)}{G_{\delta_f \to \dot{\psi}_{ref}}(0)} \tag{1.14}$$

$G_{\delta_f \to \dot{\psi}_{ref}}$ is a modified transfer function of the single-track dynamics of the passive vehicle, where

$$G_{\delta_f \to \psi_{ref}}(s) = \frac{\dot{\psi}_{STM}(s)}{\delta_f(s)} \tag{1.15}$$

Both the physical parameters (such as rotational inertia) and speed-dependent parameters can be modified to give the desired response. The transfer function is given as follows:

$$G_{\delta_f \to \psi_{ref}}(s) = \frac{\lambda_K K(\upsilon)(1 + \frac{T(\upsilon)s}{\lambda_Z \lambda_s})}{1 + 2(1 - \lambda_D(1 - D(\upsilon)))\frac{s}{\lambda_s \omega_D(\upsilon)}(\frac{s}{\lambda_s \omega_D(\upsilon)})^2} \tag{1.16}$$

The parameters λ_D, λ_Z, λ_s and λ_K are tuned using a GUI by the control engineer and modify the damping ratio, the significance of the transfer function zero, time scaling and the steady-state gain respectively. In other sources, a less sophisticated dynamic term has been incorporated into the reference by means of a first-order delay to account for the yaw inertia of the vehicle [61]. Thus this reference strategy is the most advanced found

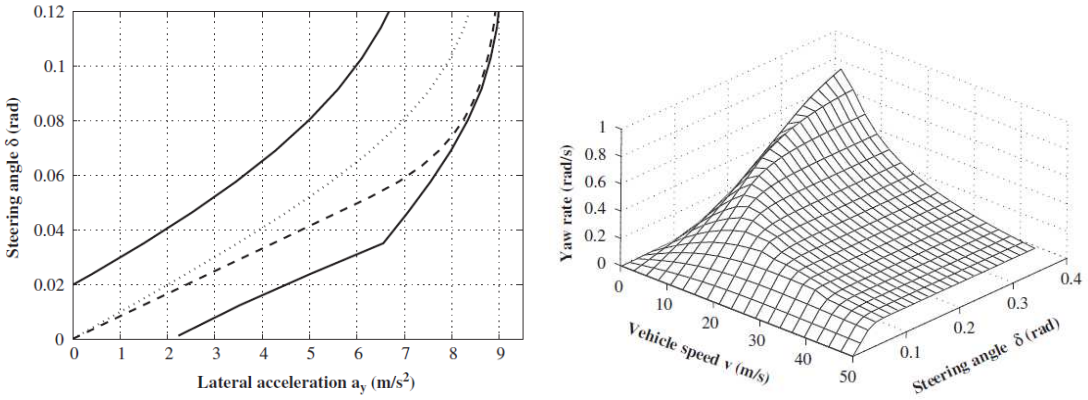

Figure 1.7: Yaw rate reference from [56] calculated using bicycle-model steady-state equations and an imposed yaw moment(a) Understeer characteristics and limits calculated for 80kph. Solid lines indicate achievable limits; dotted is the vehicle response without DYC active; dashed is the chosen reference (b) yaw-rate reference static map as a function of speed and steering angle (after [56])

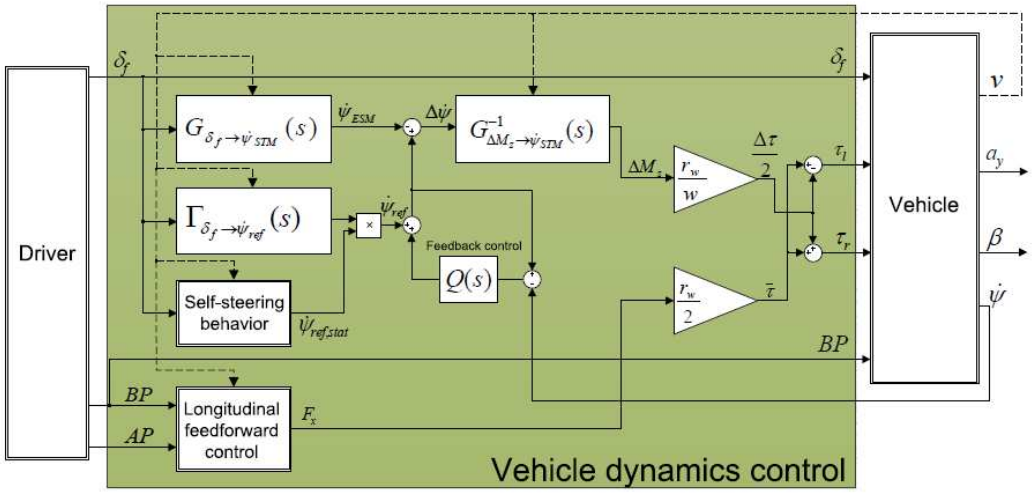

Figure 1.8: TV control structure including bicycle model with static and dynamic reference components (after [39])

in the literature, as it combines both steady-state and dynamic feedforward elements. The approach makes use both of a mathematical approach and the subjective judgement of the control engineer.

The standard method for generating the yaw rate reference, then, is by parameterising the steady-state linear single-track model. A heuristic approach is used to select the desired target understeer gradient. Non-heuristic, optimality-based approaches to various vehicle dynamics studies have been explored for open-loop manoeuvring in the context of time minimisation [63–66] with EV topologies considered in [36, 45, 62]. The inclusion of vehicle handling control systems in optimal control was undertaken in [29, 30] but only considering feedforward control laws.

Objective assessment of yaw rate reference

Only two studies, to the author's knowledge, have attempted to analyse the performance of the yaw rate reference objectively, both of which undertake an analysis based on energy efficiency.

[46] analysed the impact of reference understeer characteristics on the input power of electric drivetrains; finding that reducing the degree of understeer under acceleration can improve energy consumption by up to 6%. This was performed using quasi-static vehicle models and optimisation.

Gruber et. al. [48] conduct an analysis of 4-wheel TV control for energy efficiency for control allocation and understeer characteristic via real-world testing. The objectives were to minimise power losses in both these components. It was assumed that power loss in the drivetrain due to slip loss is a significant factor. Small steer angles and basic geometry were assumed and only steady-state tests conducted. For the control allocation, power losses were measured on the demonstrator vehicle on a rolling road. Handling

was evaluated on a skid pad using constant steer tests. A 4% improvement in energy savings during cornering conditions was reported from a fixed 50:50 control allocation. The optimal understeer characteristic for energy efficiency was close to neutral steer for the demonstrator vehicle, which corresponds to an 11% reduction in input power.

These studies use steady/quasi-steady assumptions and the objective of minimising energy usage; a transient analysis and the use of closed-loop manoeuvring remains absent from the literature, as well as an assessment of the effect of reference on outright performance.

Yaw rate reference conclusions

The steady-state linear bicycle model is the standard reference due to its simplicity and in general is subjectively tuned via one parameter: the target understeer gradient. In recent work, this reference has been extended to include a nonlinear component; the limits for which have been calculated using modelling but the chosen reference is subjectively drawn within those limits.

Despite some research into selecting yaw rate reference based on maximising energy efficiency, there have, however, been no attempts to determine or compare the relative performance of yaw rate reference for maximising performance, nor transient, closed-loop manoeuvring. In addition, whilst limits for the yaw rate reference have been determined by modelling, this did not consider a vehicle equipped with active control via yaw control moment.

1.2.5 Optimal Control for vehicle dynamics problems

Vehicle system behaviour is highly complex and nonlinear, with numerous combinations of control actions possible to achieve a desired objective. With conflicting objectives

for different aspects of vehicle performance, compromises must be found to adequately satisfy as many as possible simultaneously, and over the full range of dynamic scenarios. Optimal control theory allows the control action required to achieve a certain objective, given a system with actuation and control and a definition of the system limits to be computed [67]. In vehicle engineering, applications include: active suspension design; worst-case manoeuvring (attempting to find the worst possible disturbance input to give maximum destabilisation); driver and vehicle control; state estimation; obstacle/collision avoidance; integrated motion control; enginer air-fuel ratio control; transmission clutch torque control; minimum-time manoeuvring [67].

Direct optimisation online can be challenging (for example, when based on discontinuous motor efficiency data), although Quadratic Programming (using the active set method) may be practically implemented online in some cases. However, higher-order polynomials with the presence of multiple local minima would be computationally demanding and impractical, according to [68]. By performing optimisation offline, more computationally-demanding, higher-fidelity nonlinear models may be used which would be too complex to process in real-time. For problems that seek to find an optimal control trajectory for a vehicle navigating a track (i.e. solving over a distance-history), it is not possible to solve this in real-time without *a priori* knowledge of the road boundaries and tyre-road friction coefficient.

Research that has used optimal control theory to analyse vehicle dynamic behaviour can be categorised into the following: minimum time parameter studies; minimum time active/semi-active control studies; expert driver mimicry (high-sideslip); vehicle model fidelity considerations; optimal control solution considerations.

Minimum time parameter studies

Research that employs optimal control for vehicle dynamics studies has in large part been used to investigate the control of vehicles at the limit of adhesion, expressed in the form of minimum-time manoeuvring problems. The nonlinear optimal control solution gives an ideal driver behaviour (no mistakes, limit operation, full preview of future conditions)– which is not possible with a causal driver model, racing-line following [69], or model predictive control [70].

Hendrikx [71] developed an OCP solution using nonlinear 4-wheel vehicle model and tyres and investigated the controls for double lane change for various vehicle power layouts (FWD/RWD). A change of independent variable to distance travelled to facilitate the use of implementing affine road boundary constraints.

Subsequently, a Formula 1 car was modelled with the objective of minimising lap time [72], investigating the effect of yaw inertia on lap time and racing line [73]. The advantage of nonlinear optimal control over the quasi-steady-state simulations prevalent at the time is that the racing line was not set in advance but was determined as part of the optimisation problem.

Recent work in analysis of F1 behaviour has investigated the effects of parameters on behaviour [74] and [63]. [63] investigate the sensitivity of laptime to centre of mass position, centre of aerodynamic pressure, roll balance and differential fluid viscosity. Wheel dynamics were neglected, however, suspension dynamics, effects of fuel loads and aerodynamic drag and downforce coefficients as a function of front and rear ride heights, roll, pitch, yaw and steering angles were included. A planar track model is considered. The same authors' later related work [74] introduces a three-dimensional track to investigate the effect of road camber and gradient in addition to yaw plane curvature. Using the optimal control technique to emulate the racing driver also allows information to help the

driver maximise vehicle performance to be found. Tremlett and Limebeer [75] continue the previous work with the same vehicle model and optimal control formulation with the exception of a realistic abrasive tyre wear model fitted to data, with tyre wear a function of frictional power and surface temperature. The cost function was modified to minimise lap time while minimising tyre wear. The results gave insight to driving technique that could be adopted by the real driver to minimise tyre wear in racing. Furthermore, the technique was applied to inform differential parameter settings to reduce wear.

Lot and Dal Bianco [76] developed a vehicle model to capture the dynamics of a racing kart, including the significance of the compliance of the chassis in the absence of any suspension and wheel lifting, which was successfully verified against professional kart driver data.

Recent work by the same researchers [77] use optimal control to optimise the design of an electric racing motorbike, including gear ratio, battery pack capacity and number of electric motors, reducing laptime by 6% of the baseline. This demonstrates how optimal control can be used in the development of vehicles, not just for set-up changes or racing emulation.

Tremlett [78] investigated effect of open-, closed- and limited-slip differentials on minimum time circuit dynamics. A full 4-wheel vehicle model with nonlinear tyres was considered and an indirect optimisation technique employed.

Minimum time with active/semi-active control

With modern advanced vehicles, the optimal control technique has been extended to not only correctly mimic the professional driver, but to gain insight into how to maximise the performance of control passive, semi-active or active systems given a certain objective. Whilst the output from these studies gives control trajectories that are not based on a

control law, they lend insight into the development of such a law.

In [64, 78], Tremlett et. al. investigated the ideal torque bias trajectories for a RWD racing saloon car during a lane change manoeuvre to gain insight for the set-up of a limited-slip differential (LSD). It was found that the LSD was advantageous by permitting a increased peak yaw rate, enabling faster turning. The results could be used for settings of a passive torque or speed-sensing LSD or for a semi-active device algorithm. It was noted that including a dynamic model was important for capturing the phases where the LSD gained an advantage.

A number of studies in recent years have used numerical optimal control in a similar manner for gaining insight into the ideal operation of vehicle systems for increasing performance. A series of papers investigated the optimal controls for pre-2013 Formula 1 cars, while the later research considered the complex powertrain of the 2013-era cars that feature energy recovery systems (ERSs), kinetic and heat energy, and electric motor deployment alongside the internal combustion engine [79]. More complex aerodynamic maps were also employed, but the suspension system was again neglected. A 'bang-bang' strategy was found for electric motor deployment, while the energy recovery strategy was more complex. These insights are then used to program the control logic of the F1 cars.

The control logic for complex F1 race cars is, in a sense, more straightforward than for passenger vehicles, in that the sequence of controls required to navigate a lap of a specific race circuit is known to a high degree of certainty and is repeated every lap, with factors such as fuel mass reduction and tyre degradation allowed for. For passenger vehicles, driver intention and prediction is much more difficult to ascertain. Assuming no knowledge of the route, road conditions or imminent corner/straight characteristics, the task of, for instance, actively-controlled handling relies solely on pre-programmed settings, sensed or estimated vehicle states and the driver control inputs. From this information, the correct control of the active device is determined.

Little research has been conducted in the field of optimal control of electric vehicles using optimal control techniques for vehicle dynamics studies. An important contribution that considers an electric vehicle with four-independent motors is [45]. The researchers developed a realisable causal control allocation scheme that distributed wheel torques according to normal load on the wheel. The first step was to generate the optimal trajectories, allowing the individual wheel torques to be controlled independently as control inputs, along with the steering angle. This was conducted for a U-turn manoeuvre with the objective of minimising time. The causal control allocation cannot rely on minimum time, as this relies on full manoeuvre preview, so an allocation rule was developed based on vehicle accelerations (since normal loads are related to accelerations through load transfer effects). This remains the only optimal control study to the author's knowledge that implements torque vectoring in an offline nonlinear optimal control setting.

Expert driver mimicry

While minimum-time manoeuvring studies use the optimal control technique to 'drive the car', the optimal controls are straightforward to understand intuitively, as well as the objective of the driver. The circuit race driver attempts to minimise time by simultaneously minimising corner curvature and maximising vehicle speed as he progresses around the track.

In the rally-driving context, the overall goal of minimising time from point A to point B is essentially the same as circuit racing. However, the way to achieve minimum time over the full course is less intuitive. Research has been undertaken in this context to mimic the professional rally driver successfully.

Velenis & Tsiotras [80] compare, for a 90° corner, the behaviour of a vehicle when the objective of minimising time of travel, and the objective of maximising exit velocity

are used. A single-track vehicle with nonlinear tyres and suspension is used within an optimal control problem that constrains straight-line running at manoeuvre entry and a defined initial speed. The track layout is a 5m straight followed by a constant radius bend of $R = 9$m and a track width of only 2m. The effect of load transfer is explored by changing the vehicle CM height. Optimal control problem inputs are the front and rear torques and the steering input. Maximum exit velocity exhibits an initial counter-steer to the outside of the track before accelerating close to the inside edge of the track. The minimum-time solution, on the other hand, uses all the available space in the road. Eliminating load transfer allows marginally more rear tyre friction ot be used.

Velenis, Tsiotras & Lu [65] reproduce a rally trailbraking (TB) techniques collected from experimental data using numerical optimisation tecniques. Control input patterns are observed and then the optimisation problem simplified by re-casting as a parameter-optimisation and results are validated using CarSim high-fidelity commercial package. The objective is to learn from expert drivers for the eventual programming of a controller for chassis control for safety. A low-order single-track model enriched with front and rear torque inputs and Pacejka tyres was used and a U-turn manoeuvre formulated on a low- mu surface ($\mu = 0.5$). A static map was used for normal load transfer. Boundary conditions were important for re-creating the manoeuvre: maximising exit speed whilst minimising total manoeuvre time was key. Parameter optimisation of throttle and steering inputs gave similar results to continuous-control authority.

Tavernini et. al. [66] investigate the optimality of limit handling techniques through the use of nonlinear optimal control. Low-slip cornering on dry and wet paved road and high-slip on dirt and gravel. The effect of transmission layout (FWD, RWD and AWD) is also investigated. A single-track vehicle model enriched with Pacejka nonlinear tyres with longitudinal and lateral coupling is used. Longitudinal load transfer is by quasi-static approximation, with suspension dynamics emulated by a simple first-order delay on the

normal loads. Lateral and longitudinal tyre force relaxation are included using first-order delays by including these as states in the optimisation problem. Wheel spin dynamics are included. Road boundaries are included by transformation of state and control differential equations into an independent variable of elapsed distance. Constraints are imposed on the steering angle, steering bandwidth (to model a perfect human driver), torque rate and total engine power. An indirect numerical optimisation technique is employed with equations generated using a symbolic algebra package [81]. The constraints are included in the cost function by means of penalty functions and Lagrange multipliers. Manoeuvre is 180° turn of $R = 10$m and 10m road width. Turn is surrounded by two 30m straights. Initial conditions enforce straight-line running and an initial speed of 55kph, starting in the centre of the road. Straight line running is also enforced at the end of the manoeuvre. The objective function seeks to minimise time of travel.

Four different tyre configurations are used: high-grip, peak force at low slip; low-grip, peak force at low slip; mid-grip peak force at high slip; low-grip with extreme high slip peak. These represent dry paved, wet paved, gravel and dirt, respectively. The key finding is that the value of slip at which peak tyre force is generated is the central factor in the drifting characteristic, *not* the peak friction itself. For low-grip, high-slip-peak-μ, minimum-time manoeuvring is the high-drift, slow-in, fast out characteristic.

1.2.6 Literature Review Conclusions

Torque vectoring is gaining wide-spread acceptance as a desirable system for changing vehicle handling characteristics. Four-wheel torque vectoring is not currently feasible on passenger cars, but is likely to become so in the future, and, in a shorter time-frame in electric motor racing such as Formula E and Roborace. The findings in the literature review can be summarised as follows.

- Developing vehicles with good handling is a non-trivial task that requires knowledge of objective measures of handling, namely the concept of understeer, and an understanding of the subjective requirements of the driver. The task is non-trivial and is increasingly performed in the simulation environment. The trade-off between handling and stability is also of importance.
- Electric vehicles offer the ability to substantially expand the vehicle handling envelope through torque vectoring, and to actively shape the vehicle handling dynamics. Torque vectoring with four independent electric motors offers the greatest benefit.
- Most torque vectoring control systems adopt a hierarchical approach consisting of yaw rate reference, controller and control allocation. A great deal of attention has been paid to research into feedback controllers, with some investigation into feedforward control. Similarly, a significant amount of work has been expended on the control allocation development
- Yaw rate reference is predominantly the steady-state bicycle model, parametrised by understeer gradient characteristic. This has been extended in recent studies with a nonlinear component at high lateral accelerations. A handful of studies have implemented the dynamic bicycle model. Only two attempts have been made to evaluate the yaw rate reference in terms of some objective performance metric, but both consider only steady/quasi-steady open-loop manoeuvring.
- Optimal control has been successfully used to mimic expert drivers in both circuit racing and rally-driving. Some studies have additionally used the technique to develop active control strategies for e.g. semi-active differentials. Only one study has investigated an electric vehicle with torque vectoring.
- A variety of different vehicle models have been adopted for optimal control use. Successful results have been claimed for a single-track vehicle models and double-

track. All have included longitudinal load transfer and nonlinear tyre models. Differences occur in the modelling of suspension dynamics, aerodynamic forces and the modelling of wheel spin dynamics.

1.3 Aim & Objectives

The fundamental aim of this thesis is to investigate optimal handling for an electric vehicle with torque vectoring. The objectives are to:

1. Develop and test a TV control system with the capability of controlling the yaw rate of a high-performance sports vehicle with four independent electric motors with torque vectoring capability. Make use of model-based design and real-time Software-in-the-loop testing before proof on the real vehicle.

2. Investigate the optimal handling characteristics of the same vehicle topology when seeking to minimise manoeuvre time. Determine the mechanisms that torque vectoring employs to increase performance. Determine the sensitivity of the minimum time performance to the yaw rate reference, when the TV controller is incorporated into the problem.

3. Investigate the effect of the vehicle model fidelity on the optimal handling characteristics for minimum-time manoeuvring and explain the difference between results.

4. Investigate the optimal controls required to conduct highly agile manoeuvres with torque vectoring and the sensitivity of such controls to vehicle parameters and control bounds.

For objective 1, model-based design will be used, before real-time software-in-the-loop and real-car testing. Software-in-the-loop testing offers the advantage of proving the control system on the prototype ECU in real-time to identify and fix bugs and to fine-tune the system before the time-consuming and expensive real-car testing. The remaining objectives use numerical optimal control techniques.

1.4 Thesis structure

The thesis is subdivided into three parts.

In part I, 'Modelling and Torque vectoring topology', chapter 2 introduces the vehicle models used in the optimal control studies, while chapter 3 introduces the torque vectoring control system that forms the platform for this research, describing its development and eventual live testing on vehicles.

Part II, 'Time-optimal handling characteristics' investigates the optimal handling characteristics of the torque vectored vehicle when manoeuvring in minimum time. Chapters 4 and 5 present the results of optimal control problems solved considering the two different vehicle models, while chapter 6 examines the differences between the model results in depth.

Finally, part III 'Optimal Agile Manoeuvring' extends the optimal control method to investigate torque vectoring controls when highly agile behaviour is required.

Part I

Modelling and Torque vectoring

Control System

Chapter 2

Vehicle Models

2.1 Introduction

Vehicle models are central to every aspect of work addressed in this thesis. Since the focus is on active handling control, vehicle models that capture realistic handling behaviour are important. It is preferable to keep the vehicle model as simple as possible whilst capturing the dominant effects, to ensure equations can be solved in a reasonable time frame and to keep the analysis simple.

Velenis et. al. [65] succeeded in implementing a single-track vehicle model using optimal control, with nonlinear tyres to re-produce similar characteristics to those logged by an expert driver in a rally-driving trail braking scenario, neglecting lateral load transfer but including longitudinal dynamics. Front and rear wheel dynamics were included. Excellent agreement with experimental data was shown. Tavernini et. al. [66, 82] used the same model but with additions of an approximation to suspension dynamics through a first-order delay on the normal loads. Both studies demonstrate that it is possible to accurately capture rally-like manoeuvres without a two-track model.

Research into the optimal control of a Formula 1 car, on the other hand, used a much more complex four-wheel model with lateral and longitudinal load transfers, downforce and drag aerodynamics [63, 74, 79]. Wheel dynamics were neglected, however, with the justification that their variation was of much greater magnitude than the yaw dynamics.

A relatively recent study investigated the effect of order of modelling on optimal control results, for a GT class sports car on the Adria race circuit [83]. Parametric analysis of CM location and suspension stiffness was also undertaken. A 14 DOF model including wheel spin and vertical motion, a 10 DOF version that neglected wheel hop and a 7DOF model that removed suspension motion completely were examined, finding that whilst the 14 and 10 DOF models gave similar results, there was a loss in fidelity when suspension dynamics removed.

Two vehicle models are used in this thesis. The motivation behind this is twofold: i) to gain experience using numerical optimal control techniques before adding complexity and ii) to investigate the level of modelling fidelity on the optimal handling balance.

Firstly, a new variation on the traditional bicycle model is developed. Longitudinal dynamics are included, as this has been demonstrated to be important for handling in scenarios involving combined braking and accelerating [65]. To model torque vectoring, an additional component is included in the yaw dynamics equation. Secondly, a more detailed 7DOF two-track model is presented which employs a nonlinear combined-slip model.

A significant part of this thesis investigates the differences between the models, which leads to conclusions about what the necessary aspects to accurately model handling dynamics for EVs with torque vectoring capability are.

2.2 3DOF Single-track model

This section sets out the vehicle model required for the optimal control problem formulation in chapter 4.

2.2.1 Single-Track Vehicle Model

This study uses a three degree of freedom (DOF) single-track dynamic model with linear tyres (equations (2.1-2.3)), parameterised to represent a high-performance EV with an electric motor powering each wheel independently (Table 2.1). In the context of minimum-time manoeuvring considered in this study, acceleration/deceleration is of fundamental importance, hence longitudinal dynamics are included in contrast to the the standard two DOF single-track model. Lateral load transfer is neglected, along with roll and pitch dynamics. Retarding torque is provided exclusively by regenerative braking; no friction brakes are modelled.

$$m\dot{V}_x = m\left(a_x + V_y\dot{\psi}\right) \tag{2.1}$$

$$m\dot{V}_y = -\frac{(C_f + C_r)}{V_x}V_y + \left(-mV_x + \frac{(-l_fC_f + l_rC_r)}{V_x}\right)\dot{\psi} + C_f\delta \tag{2.2}$$

$$I_z\ddot{\psi} = -\frac{(l_fC_f - l_rC_r)}{V_x}V_y - \frac{(l_f^2C_f + l_r^2C_r)}{V_x}\dot{\psi} + l_fC_f\delta + M_z \tag{2.3}$$

where a_x is the longitudinal acceleration, considered as an input to the system, m is the vehicle mass; $\dot{\psi}$ is the yaw rate; I_z is the yaw moment of inertia about the vertical axis; l_f and l_r are the distances of the front and rear axles to the centre of gravity (CM); C_f and C_r and the front and rear tyre cornering stiffnesses; V_x and V_y are the longitudinal and lateral vehicle velocities respectively. To emulate left-right torque vectoring, a direct yaw moment, M_z, is included in the yaw acceleration equation (2.3), a full explanation of

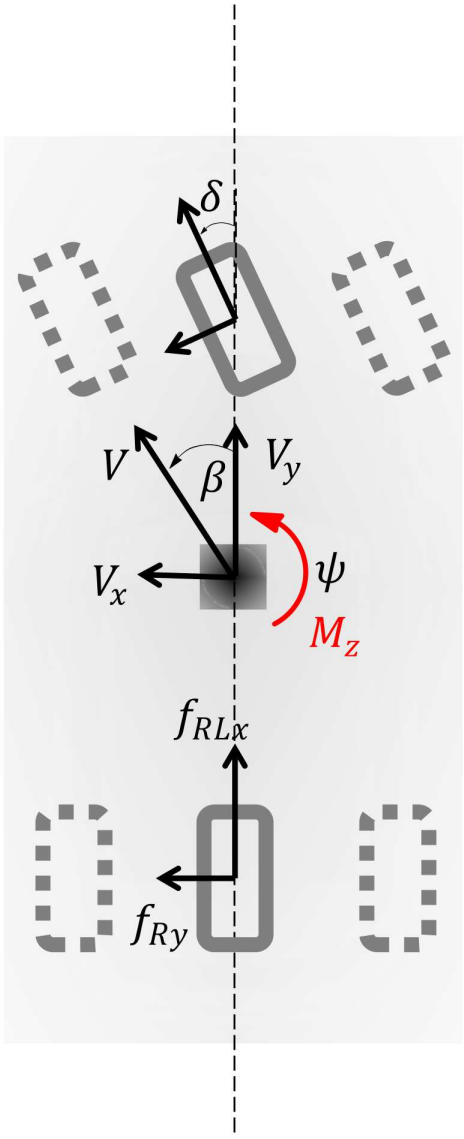

Figure 2.1: Single-track vehicle model

Symbol	Name	Unit	Value
m	mass	kg	1137
L	wheelbase	m	2.5
w	track width	m	1.374
h	height of CM	m	0.317
ℓ_f	distance of CM to front axle	m	1.18
ℓ_r	distance of CM to rear axle	m	1.313
I_z	yaw moment of inertia	kgm^2	1174
μ_{max}	tyre-road friction coefficient	-	1
R_w	wheel radius	m	0.298
n_δ	rack ratio	-	16
η_f	front tyre cornering coefficient[a]	rad^{-1}	24
η_r	rear tyre cornering coefficient[a]	rad^{-1}	30
B_f	front Pacejka stiffness factor[a]	-	16.4
B_r	rear Pacejka stiffness factor[a]	-	20.7
C	Pacejka shape factor	-	1.46
D	Pacejka peak factor	-	1
T_{max}	motor torque limit	Nm	685
P_{max}	motor power limit	kW	90

Table 2.1: Vehicle Parameters for 3DOF and 7DOF models

which may be found in chapter 6. [24] uses a similar external yaw moment term.

2.2.2 Linear Tyre Model

A linear tyre model with cornering stiffness dependent on normal load is used (Figure 2.4), considering a quasi-steady-state approximation to normal load:

$$
\begin{aligned}
F_{yj} &= -C_j \alpha_j, \\
\text{where:} \qquad C_j &= \eta_j F_{zj}, \\
\alpha_f &= \frac{V_y + l_f \dot{\psi}}{V_x} - \delta, \\
\alpha_r &= \frac{V_y - l_r \dot{\psi}}{V_x}, \\
\text{and:} \qquad F_{zf} &= \frac{mgl_r}{L} - \frac{h}{L} m a_x; \\
F_{zr} &= \frac{mgl_f}{L} + \frac{h}{L} m a_x.
\end{aligned}
$$

For each $j \in [f,r]$, η_j is the tyre cornering coefficient, α_j is the tyre slip angle, F_{zj} is the axle normal load and F_{yj} is the axle lateral force on front and rear. g is the gravitational acceleration constant, L is the wheelbase, h is the height of the CM. The natural, steady-state understeer gradient of the vehicle without TV active is defined as [6]:

$$
K_{nat}^{SS} = \left(\frac{1}{\eta_f} - \frac{1}{\eta_r} \right) / g, \tag{2.4}
$$

and modified by selecting cornering coefficient values η_f and η_r, assuming that the cornering coefficient is constant.

2.2.3 Limit friction circle

Longitudinal and lateral forces are coupled and saturated at the limit by friction circle constraints and front and rear:

$$\left(\frac{F_{xj}}{F_j}\right)^2 + \left(\frac{F_{yj}}{F_j}\right)^2 \leq \mu_{max}^2, \tag{2.5}$$

$$\text{where} \qquad F_j = \mu_{max} F_{zj}, \tag{2.6}$$

where μ_{max} is the tyre-road friction coefficient.

2.3 7DOF Four wheel model

2.3.1 7DOF Vehicle Model

A 7DOF, two-track vehicle model is employed with nonlinear tyres (Fig. 2.2), including a quasi-static representation of longitudinal and lateral load transfers. Roll and pitch dynamics are neglected. Retarding torque is provided exclusively by regenerative braking. In a similar manner to [65, 66], aerodynamic forces and rolling resistance are neglected since the manoeuvres under consideration are of moderate speed. In the following, $i = \{F,R\}$ (front, right), $j = \{L,R\}$ (left, right), $k = \{x,y,z\}$. x, y and z denote the longitudinal, lateral and vertical directions respectively. Quantities without subscript k denote resultants. The equations of motion for the 7DOF vehicle model (Fig. 2.2) are:

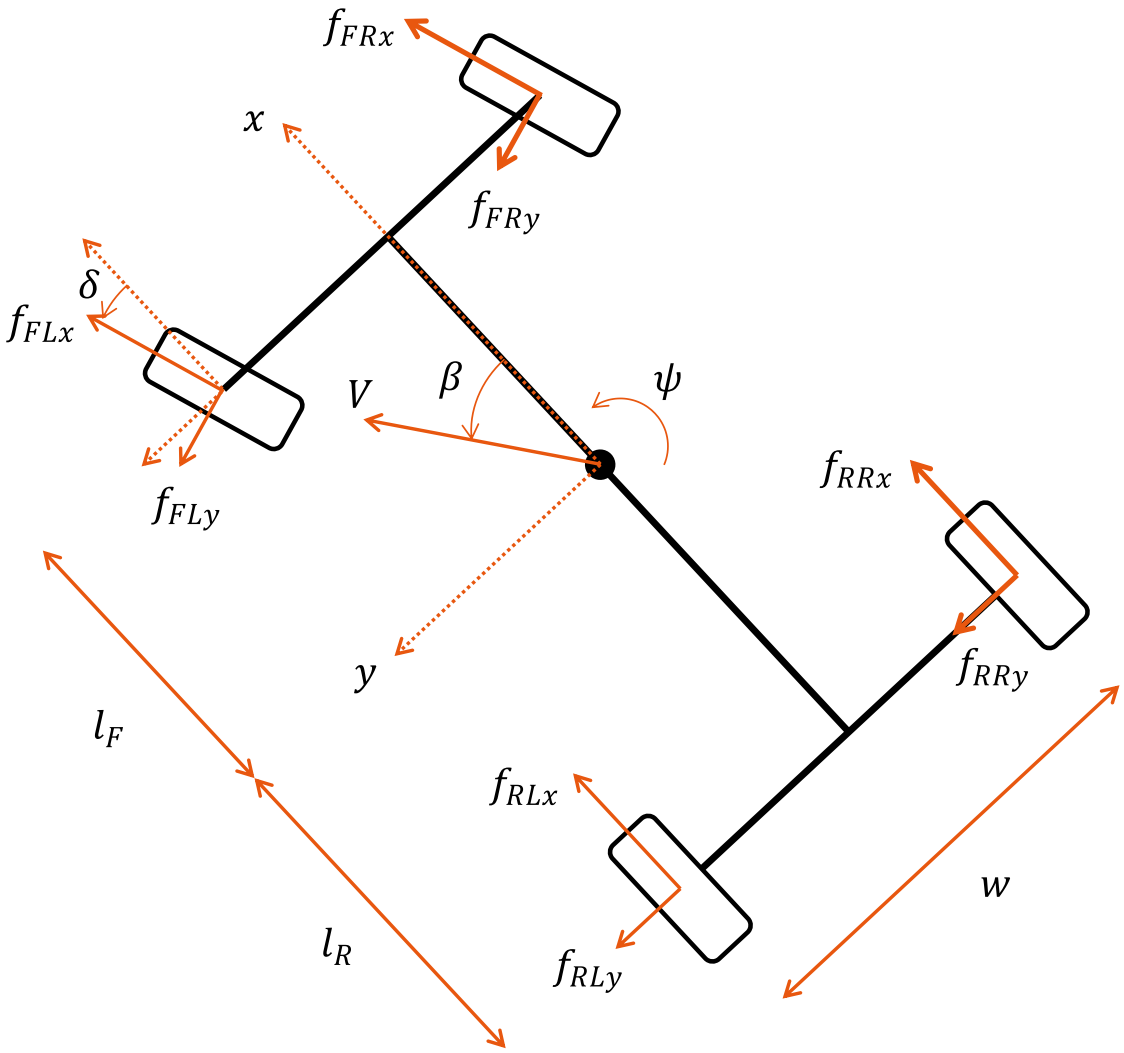

Figure 2.2: 7DOF planar vehicle model

$$\begin{aligned}
\dot{V} &= \frac{1}{m}\left[(f_{FLx}+f_{FRx})\cos(\delta-\beta)-(f_{FLy}+f_{FRy})\sin(\delta-\beta)\right. && (2.7)\\
&+ \left.(f_{RLx}+f_{RRx})\cos\beta+(f_{RLy}+f_{RRy})\sin\beta\right],\\
\dot{\beta} &= \frac{1}{mV}\left[(f_{FLx}+f_{FRx})\sin(\delta-\beta)+(f_{FLy}+f_{FRy})\cos(\delta-\beta)\right. && (2.8)\\
&- \left.(f_{RLx}+f_{RRx})\sin\beta+(f_{RLy}+f_{RRy})\cos\beta\right]-\dot{\psi},\\
\ddot{\psi} &= \frac{1}{I_z}\left[\ell_F\left\{(f_{FLy}+f_{FRy})\cos\delta+(f_{FLx}+f_{FRx})\sin\delta\right\}-\ell_R\,(f_{RLy}+f_{RRy})\right. && (2.9)\\
&+ w/2\,(f_{FLy}\sin\delta-f_{FLx}\cos\delta-f_{RLx})\\
&+ \left.w/2\,(f_{FRx}\cos\delta-f_{FRy}\sin\delta+f_{RRx})\right]\\
\dot{\omega}_{ij} &= \frac{1}{I_w}\left[T_{ij}-f_{ijx}r\right], && (2.10)
\end{aligned}$$

where: m is the vehicle mass; I_z is the moment of inertia about the vertical axis; V is the vehicle velocity at the center of mass (CM); β is the vehicle sideslip angle at the CM; $\dot{\psi}$ is the yaw-rate. The moment of inertia of each wheel about its axis of rotation is I_w; the wheel radius is r; the wheel angular speeds are ω_{ij}; the steering angle is δ; the drive/brake torque applied on each wheel is T_{ij}. Tyre forces are denoted by f_{ijk}. The parameters ℓ_F, ℓ_R determine the location of the CM with respect to the center of each wheel; w is the track width.

2.3.2 Nonlinear Tyre Model

The tyres are modelled using the simplified Pacejka Magic Formula (MF) [84], as shown in Figure 2.3. A comparison of the linear and nonlinear tyre models used in this thesis is shown in Figure 2.4, highlighting the equal stiffness at zero slip angle.

The tyre model originates from thesis research [85] undertaken on the same test vehicle used herein, which will be introduced in more detail in chapter 3. In [85], Ewin developed a vehicle model from standard Dymola libraries, with a MF 5.2 model param-

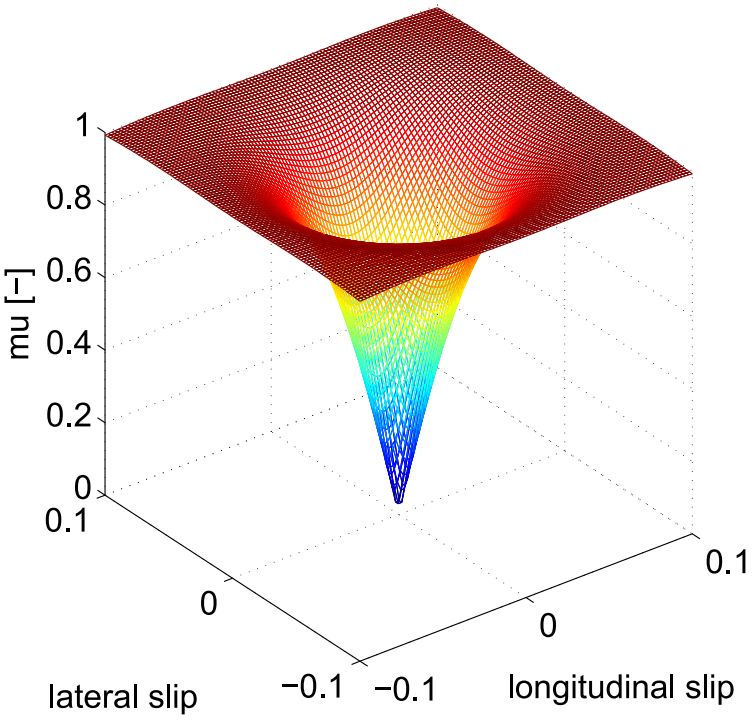

Figure 2.3: Nonlinear tyre model

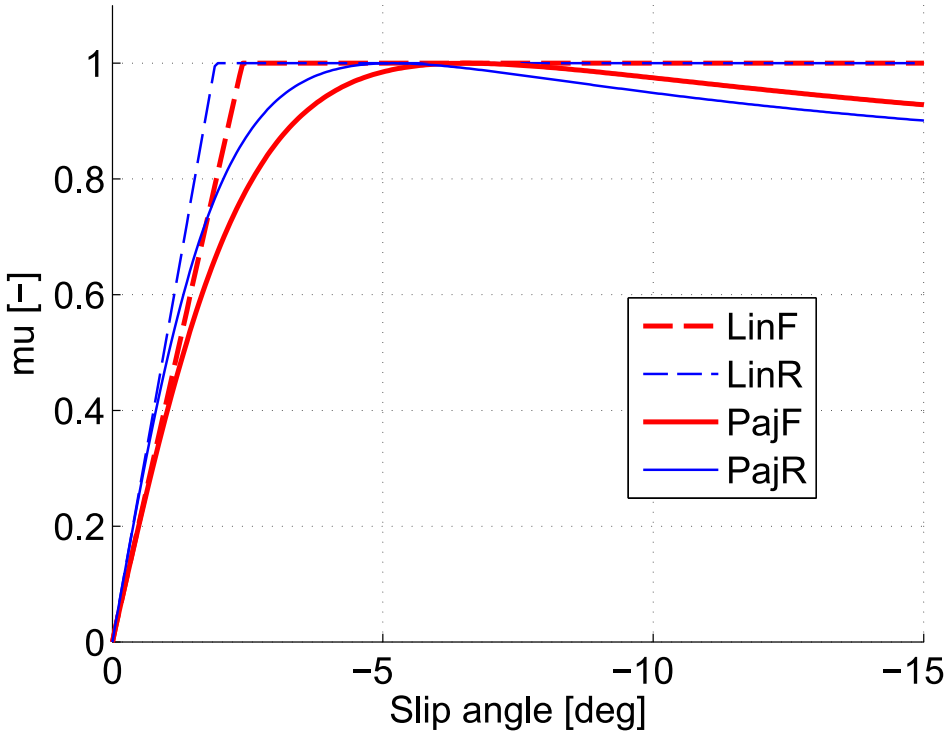

Figure 2.4: Comparison of linear and nonlinear tyre models (pure lateral slip condition)

eterised for the mass and geometry of the 205/55 R17 Bridgestone Potenza RE50 tyres used by the test vehicle. Two MF parameters were adjusted to match the understeer gradient in the linear region of the handling diagram measured from experimental data of a constant radius test: the rear lateral cornering stiffness and the peak grip coefficient. The vehicle model mass, inertia, centre of mass, driveline inertia and rolling resistance were calibrated and validated against test data, which gives confidence in the validity of the tyre model parameterisation. Ewin's MF 5.2 model [85] was simplified by [86] by taking an average of the lateral and longitudinal characterisitcs to achieve an isotropic behaviour. The resulting simplified curve captures the dominant shape of the MF 5.2 curve, whilst requiring only three parameters (2.24) and is adopted in this work. The simplified MF requires tyre slip as inputs. The longitudinal slip, κ_{ij}, and slip angle, α_{ij}, the 'practical' slip quantities [84], are defined:

$$\kappa_{ij} = \frac{\omega_{ij} r_{ij} - V_{ijx}}{V_{ijx}}, \tag{2.11}$$

$$\tan \alpha_{ij} = \frac{V_{ijy}}{V_{ijx}}, \tag{2.12}$$

where V_{ijk} are the vehicle velocities in the tyre frame of reference at the wheel contact patch.

The velocities are defined as follows:

$$
\begin{aligned}
V_{FLx} &= V\cos(\delta-\beta)-\dot{\psi}\ell_{FL}\sin(\gamma_{FL}-\delta), && (2.13)\\
V_{FLy} &= -V\sin(\delta-\beta)+\dot{\psi}\ell_{FL}\cos(\gamma_{FL}-\delta), && (2.14)\\
V_{FRx} &= V\cos(\delta-\beta)+\dot{\psi}\ell_{FR}\sin(\gamma_{FR}+\delta), && (2.15)\\
V_{FRy} &= -V\sin(\delta-\beta)+\dot{\psi}\ell_{FR}\cos(\gamma_{FR}+\delta), && (2.16)\\
V_{RLx} &= V\cos(\beta)-\dot{\psi}\ell_{RL}\sin(\gamma_{RL}), && (2.17)\\
V_{RLy} &= -V\sin(\beta)-\dot{\psi}\ell_{RL}\cos(\gamma_{RL}), && (2.18)\\
V_{RRx} &= V\cos(\beta)+\dot{\psi}\ell_{RR}\sin(\gamma_{RR}), && (2.19)\\
V_{RRy} &= -V\sin(\beta)-\dot{\psi}\ell_{RR}\cos(\gamma_{RR}, && (2.20)
\end{aligned}
$$

where $\ell_{ij}=\sqrt{\ell_i^2+(\frac{w}{2})^2}$, $\gamma_{ij}=\tan^{-1}\frac{\frac{w}{2}}{\ell_i}$.

The MF requires a quantity that combines longitudinal slip and lateral slip angles into a 'theoretical' slip for each of the longitudinal and lateral directions that facilitates coupling between longitudinal and lateral forces in the model explicitly. They are defined:

$$
\begin{aligned}
s_{ijx} &= \frac{V_{ijx}-\omega_{ij}r_{ij}}{|\omega_{ij}r_{ij}|}, && (2.21)\\
s_{ijy} &= \frac{V_{ijy}}{|\omega_{ij}r_{ij}|}=(1+s_{ijx})\frac{V_{ijy}}{|V_{ijx}|}, && (2.22)
\end{aligned}
$$

and the resultant:

$$
s_{ij}=\sqrt{s_{ijx}^2+s_{ijy}^2}. \qquad (2.23)
$$

Wheel velocities and slip definitions

Assuming tyre friction force is linearly dependent on the tyre normal force, and isotropic tyre force characteristics:

$$\mu_{ij}(|s_{ij}|) = \text{MF}(|s_{ij}|) = D\sin(C\text{atan}(B_i s_{ij})), \quad \text{where: } |s_{ij}| = \sqrt{s_{ijx}^2 + s_{ijy}^2}, \tag{2.24}$$

where $|s_{ij}|$ is the resultant tyre slip magnitude, and s_{ijx} and s_{ijy} are the theoretical longitudinal and lateral slips, respectively [84]; μ_{ij} is the total tyre force coefficient; B_i, C, D are the MF coefficients. The coefficients are shown in table 2.1. Tyre force components are given by:

$$|f_{ij}| = \sqrt{f_{ijx}^2 + f_{ijy}^2}, \quad \text{where: } f_{ijk}/f_{ijz} = \mu_{ijk} = -\frac{s_{ijk}}{|s_{ij}|}\mu_{ij}(|s_{ij}|), \tag{2.25}$$

where μ_{ijk} are the tyre force coefficients for tyre ij in longitudinal or lateral directions ($k = \{x, y\}$). Similarly, s_{ijk} is the theoretical slip quantity for tyre ij in the $k = \{x, y\}$ directions.

A quasi-static representation is used to determine the normal loads on each wheel, f_{ijz}, adopted from [87] and re-presented here, by neglecting pitch, roll and vertical translation—considering only the static weight distribution and weight transfers generated by lateral and longitudinal accelerations. The normal loads on each wheel are given by:

$$\begin{aligned} f_{FLz} &= f_{FLz}^0 - \Delta f_L^x - \Delta f_F^y, \qquad f_{FRz} = f_{FRz}^0 - \Delta f_R^x + \Delta f_F^y, \\ f_{RLz} &= f_{RLz}^0 + \Delta f_L^x - \Delta f_R^y, \qquad f_{RRz} = f_{RRz}^0 + \Delta f_R^x + \Delta f_R^y, \end{aligned} \tag{2.26}$$

where the static normal loads are:

$$f^0_{FLz} = f^0_{FRz} = \frac{mg\ell_R}{2(\ell_F + \ell_R)}, \qquad (2.27)$$
$$f^0_{RLz} = f^0_{RRz} = \frac{mg\ell_F}{2(\ell_F + \ell_R)}.$$

Changes in normal load arising due to lateral acceleration across the front and rear axles are given by:

$$\Delta f^y_F = \frac{mh\ell_R}{w(\ell_F + \ell_R)} a_y, \qquad \Delta f^y_R = \frac{mh\ell_F}{w(\ell_F + \ell_R)} a_y, \qquad (2.28)$$

while the changes due to longitudinal acceleration on the left and right tracks (assuming left and right tracks are equal) are given by:

$$\Delta f^x_L = \Delta f^x_R = \frac{mh}{2(\ell_F + \ell_R)} a_x. \qquad (2.29)$$

Chapter 3

Torque Vectoring Control System

3.1 Introduction

In chapter 2, the vehicle models used in this work were described. The work presented in chapters 4 and 5 exploits a torque vectoring controller to evaluate the yaw rate reference's contribution to the overall performance. A torque vectoring control system is developed for real-world application in this section, the successful results of which give confidence that the theoretical results developed in the later optimal control chapters are translatable to the real-world, based on a comprehensively tested platform.

The TV controller was developed as part of the £16m Jaguar Land Rover $Evoque_e$ project in collaboration with Cranfield University and numerous academic and industrial partners. In particular, the focus in Work Package 2 of the project was to '*deliver driver-demanded acceleration and handling*'. The author's contribution to the project was to develop a yaw rate control system to exploit the torque vectoring potential of one of the fully-electric development vehicles.

In this chapter, the TV controller is developed through a process of model-based de-

sign, starting with desktop Model-in-the-Loop (MiL) simulation, before progressing to real-time testing with Software-in-the-Loop (SiL) and, finally, vehicle testing. The test vehicle topology is first presented, followed by an overview of the control system architecture, a description of the model-based design stages and then a detailed presentation of the controller components. Real-time Software-in-the-Loop testing and real-world vehicle test results conclude the chapter.

3.2 Controller Overview

3.2.1 4WD electric vehicle topology

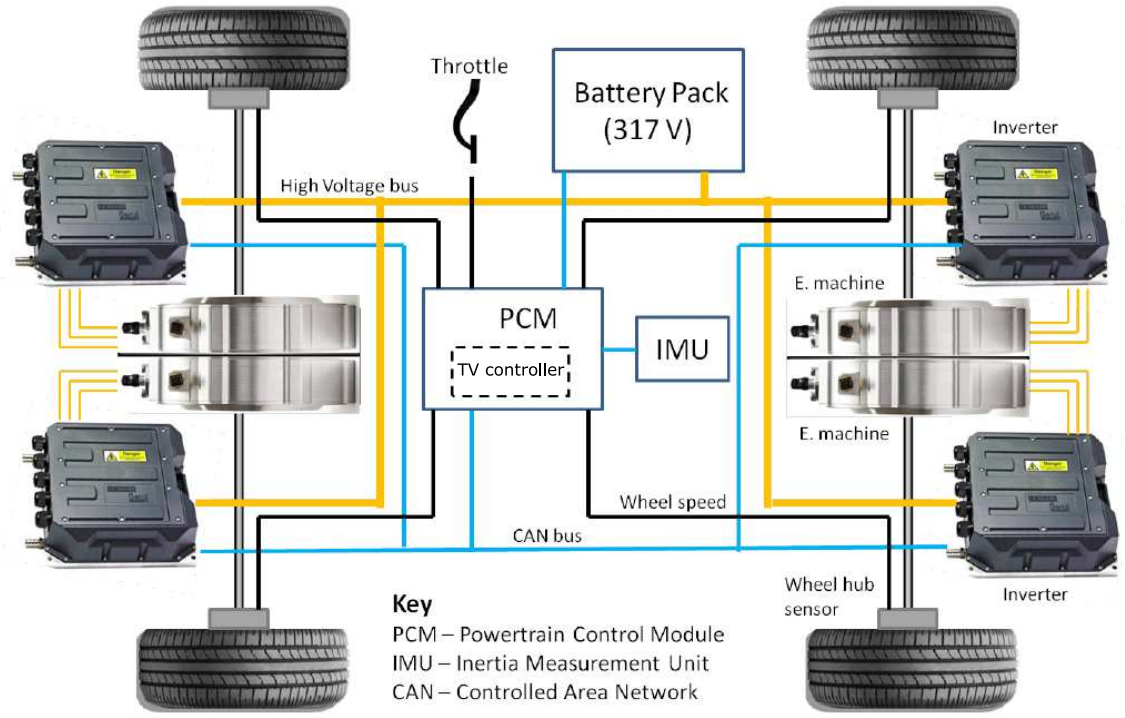

Figure 3.1: Delta Motorsport E4 Coupe 4 independent motor topology (adapted from [85])

The Delta Motorsport E4 is a high-performance sportscar equipped with 4 inboard

electric machines (YASA 750) that power each wheel independently. The topology is shown in Figure 3.1. The electric machines are under the authority of motor controllers, which accept torque demand inputs from the Powertrain Control Module (PCM), via a CAN bus, and return motor current and rotor velocity [85]. As a prototype vehicle, the Delta E4 coupe lends itself well to a rapid control prototyping (RCP) process, since it makes use of a real-time prototyping system instead of a dedicated ECU. It is on this that the torque vectoring control system is tested.

3.2.2 Control Structure Overview

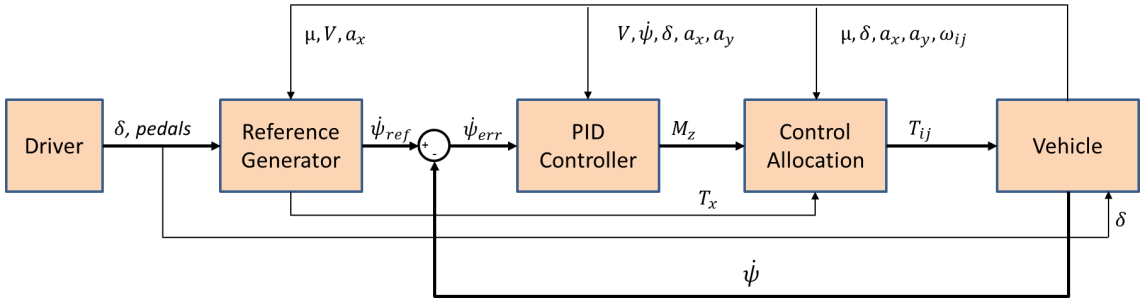

Figure 3.2: TV control structure showing principal components and signals

A feedback TV controller for the Delta E4 was developed for active yaw control using a hierarchical control structure, shown in Figure 3.2. First driver inputs and vehicle states are fed to the Reference Generator block which determines the desired yaw rate. A PID controller outputs a yaw moment request, M_z, which is converted to final wheel torque requests, T_{ij}. The torque requests are passed to the actuator controllers and hence the motors. Vehicle dynamic states are fed back to reference generator, PID controller, control allocation; and to the driver, through his senses.

3.2.3 Controller Development Process

The torque vectoring controller was developed using model-based design [88]. Model-based design places a greater emphasis of vehicle development on simulation, which offers advantages in terms of greater rate of development, reduced cost and repeatability. The development process chosen for this project is shown in Figure 3.3, and broken down into 3 stages:

(a) **Model-in-the-Loop**

Model-in-the-Loop (MiL) development was conducted on desktop computers to develop and debug the controller functionality. To enable the controlled vehicle handling to be assessed using a high-fidelity vehicle model, the controller was developed in the Simulink environment, in co-simulation with IPG's commercial high-fidelity vehicle modelling package, CarMaker. CarMaker offers the additional advantages of 3D graphical visualisation and data viewer built-in.

For MiL, the control inputs may be determined by the IPG Driver model, open-loop commands specified by the engineer, or by using gaming controllers and wheels/pedals. Specifying steering and throttle/brake commands as a function of time or distance permit open-loop control inputs to be repeated identically and therefore the impact of controller changes to be isolated. Using a driver model allows for closed-loop manoeuvres such as navigating U-turn bends or performing double-lane change manoeuvres to be assessed. Despite excellent documentation, the operation of a package such as IPG Driver still remains to a certain extent a "black box" for commercial reasons. Using gaming controllers to perform more complex closed-loop manoeuvre simulations is particularly effective for exposing any unexpected behaviour that is not captured in the specific manoeuvres tested previously, and is an important step before taking the controller to the next prototyping step. Gaming controller testing is limited

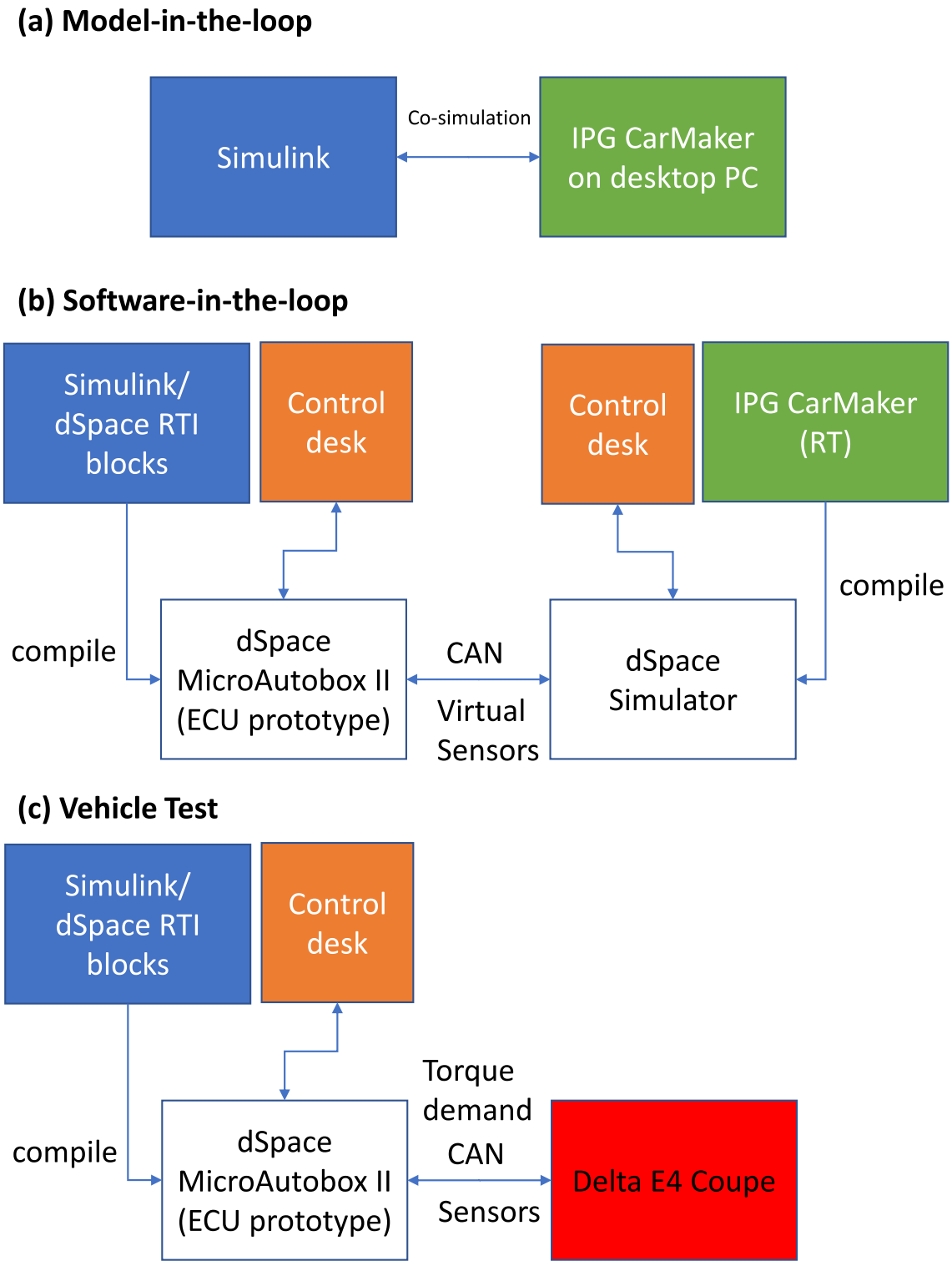

Figure 3.3: Controller development process: (a) Model-in-the-Loop (MiL); (b) Software-in-the-loop (SiL); (c) Vehicle testing

by the graphics hardware and ability to solve the simulation in real-time or better. The former proved problematic but was resolved to some extent by running the graphics at lower resolution and frame rate. Furthermore, precision in controlling the vehicle was not required; simply the ability to expose un-tested behaviour through 'free' control inputs and perform a general sense-check.

Converting the original control design from continuous- to discrete-time ready for real-time execution was performed at this stage to allow rapid development and debugging. Additionally, artifical noise was added to the controller signals and delays imposed on the signals to simulate real-world features encountered with physical sensor signals transported via CAN.

(b) **Real-time Software-in-the-Loop**

Real-time testing was carried out in advance of installing the controller on the Delta vehicle in a Software-in-the-Loop set-up in order to check operation of the controller in real-time operation, including CAN communication and to develop test manoeuvres that could be run feasibly during the vehicle test with given knowledge of the proving ground layout and space availability. Steady-turn and step-steer manoeuvres were carried out using the Delta vehicle model in CarMaker.

Figure 3.3(b), the SiL set-up consists of a dSpace MicroAutobox II (MABx) real-time system in place of an ECU, communicating with a dSpace Simulator via CAN. The TV controller is compiled using dSpace RTI blocks and flashed onto the MABx. The plant model, running in CarMaker, is hosted on a dedicated dSpace Simulator. dSpace Control Desk instances allow the TV controller parameters to be adjusted on the fly and the vehicle plant model throttle/brake and steering inputs to be manually controlled, if required.

(c) **Real-Time Vehicle Test**

Vehicle testing was carried out with the same TV controller proven in the SiL tests. The arrangement is shown in Figure 3.3 (c). The prototype controller is carried over from SiL testing, however it now sits within Delta Motorsport's PCM. Torque demand signals are relayed via CAN to the four independent motors on the E4 vehicle. A 'System Protection' layer sits at the lowest level to limit torque demands from the TV controller to respect power limitations of the battery and electric machines [85].

3.3 Torque vectoring controller detail

3.3.1 IVCS: Integrated Vehicle Control Structure

A centralised 'Integrated Vehicle Control Structure' (IVCS) [89] was adopted that allows multiple Vehicle Dynamics Control (VDC) systems to be coordinated together, reducing complexity. This approach is also used for over-actuated vehicles in some recent work in the literature [57, 59]. As the torque vectoring controller was just one of a number of vehicle dynamics control systems developed as part of Work Package 2 of the *Evoque_e* project, it was decided to implement it within the IVCS. The IVCS is a hierarchical structure composed of Supervisory Control, High Level Control and Low Level Control blocks, as shown in Figure 3.4.

3.3.2 Supervisory Control

The Supervisory Control level is concerned with determining driver intent from inputs, and determining the vehicle motion reference values, in the case of this controller, yaw rate. The level consists of Estimation, Reference Generator and Decision blocks, as shown in figure 3.5. The Estimation block contains estimation algorithms (or, simply, constants)

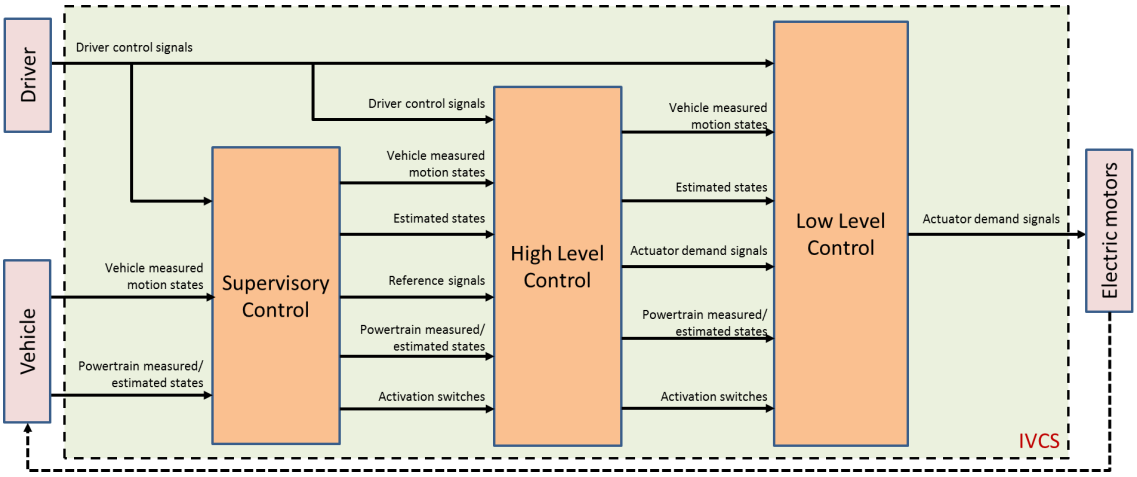

Figure 3.4: Integrated Vehicle Control Structure hierarchical elements

for parameters including tyre-road friction coefficient, μ, vehicle speed, slip and longitudinal forces. μ is simply set as a constant value and all other quantities required for the controller are measured or estimated prior to delivery into the IVCS. Parallel studies in the Work Package developed μ estimation algorithms that could be introduced to the IVCS following validation [90]

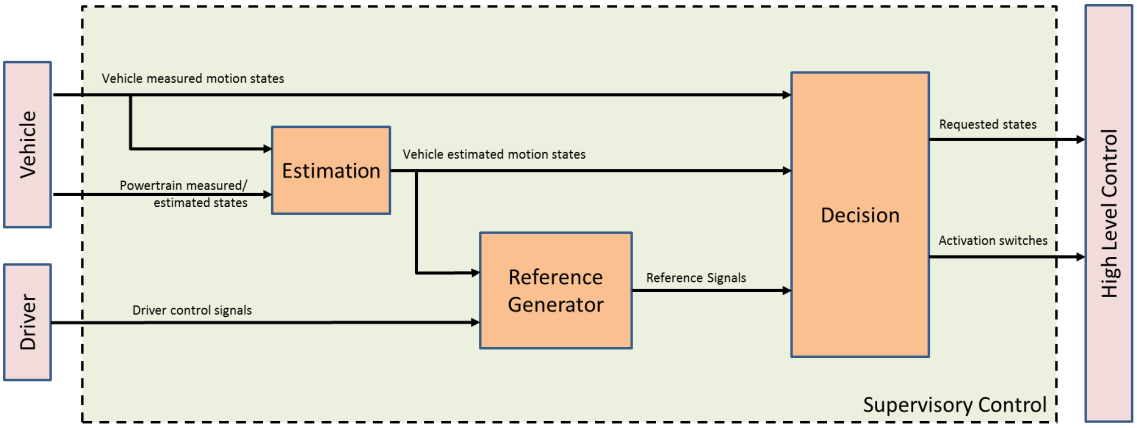

Figure 3.5: Supervisory Control level, showing Estimation, Reference Generator and Decision blocks

Reference Generator

The Reference Generator outputs the reference yaw rate for the controller to follow. The reference strategy may be switched between the piecewise reference adopted from [36,40] and a look-up table-based reference: for example the yaw rate gain surfaces in §6.2. The piecewise reference is composed of a linear and exponential part, as shown in Figure 1.6 in §1.2.4.

With reference to Figure 3.6, the reference generator takes as inputs μ, a_x, V, δ and the desired understeer gradient for the linear reference. The available friction and longitudinal acceleration determine the maximum lateral acceleration possible, and, according to a parameter, a_y^*: the proportion of $a_{y,max}$ over which the $\delta - a_y$ plot becomes nonlinear. A first order delay is applied to the steer input such that the reference is achievable while taking into account the yaw inertia of the vehicle. The time constant is $\tau = 0.09$s, tuned heuristically. The time-optimal reference only requires speed and lateral acceleration as inputs; the resulting yaw-rate gain value, $\dot{\psi}/\delta$, from the look up table is multiplied by steer angle to give the yaw-rate reference. The reference is saturated to a maximum absolute value according to the friction level (1.7).

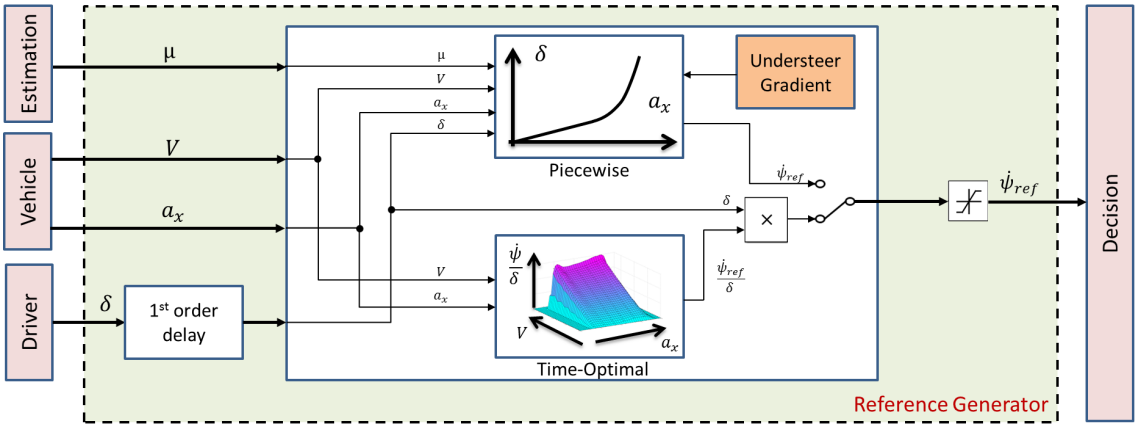

Figure 3.6: Reference Generator featuring a switchable reference strategy, yaw dynamic delay and yaw-rate saturation

Decision Block

The Decision Block is where information derived from comparison of desired and actual motion variables is gathered to be passed down to lower levels of the IVCS architecture. In this case, the yaw-rate error is calculated to be passed to the PID controller, where $\dot{\psi}_{err} = \dot{\psi}_{ref} - \dot{\psi}_{actual}$. A torque vectoring activation switch is also located in this block.

In addition to yaw rate, longitudinal torque demand is another reference to be followed. Longitudinal torque demand is set according to a pedal position-torque map outside the IVCS and passes without alteration through the Supervisory Control block to the Control Allocation block. The proportion of the total torque demanded from each wheel is determined by the Control Allocation feedforward logic rather than a feedback controller, so is not considered a control variable as such.

3.3.3 High Level Control

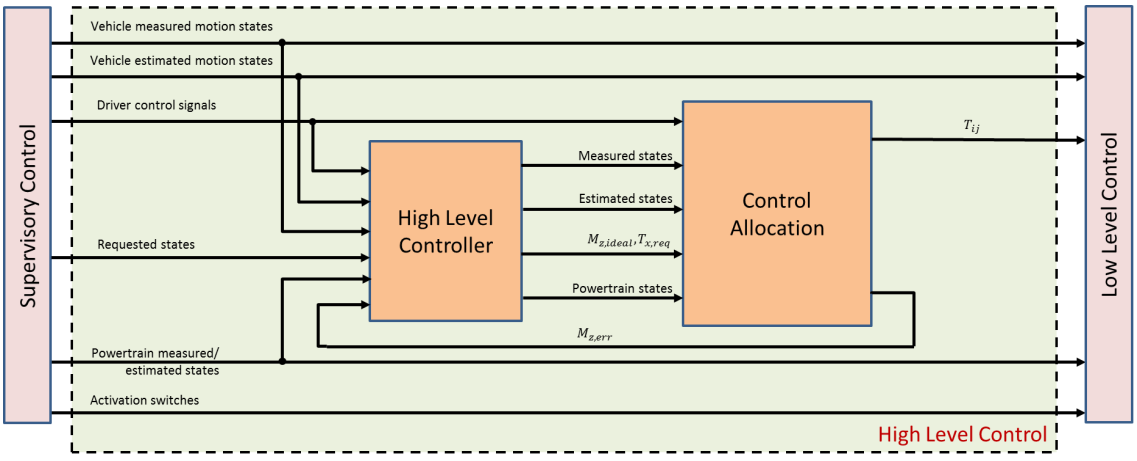

Figure 3.7: High Level Control layer, incorporating High Level Controller (PID) and Control Allocation blocks for the appropriate distribution of torques

The High Level Control layer (Fig. 3.7) is concerned with determining the control action required to deliver the desired motion determined in the Supervisory layer [89].

In this case, the High Level Controller converts yaw rate error into a yaw moment demand, which is then passed to the Control Allocation, where the individual wheel torques required to deliver the yaw moment and longitudinal torque demands are calculated.

High Level Controller

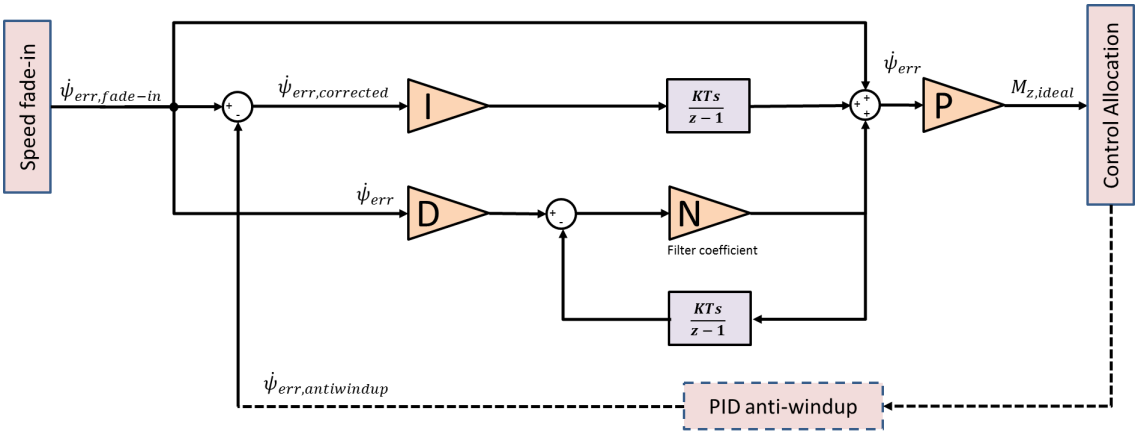

Figure 3.8: PID schematic. Dashed elements are shown in more detail in figure 3.9

The High Level Controller block consists of a PID controller comprising anti-windup and reset features (shown in fig. 3.8, further detail in figure 3.9).

A classical PID formulation is used, including a filter on the derivative term to reduce noise [91]. The PID formulation (equation 3.1) is arranged, with the proportional gain multiplying the sum of all of the actions. The controller must be converted into the z-domain in order to function in the discrete-time environment required for real-time implementation (3.2).

$$M_{z,req,ideal}(s) = P\left[1 + I\left(\frac{1}{s}\right) + D\left(\frac{Ns}{s+N}\right)\right]\dot{\psi}_{err} \tag{3.1}$$

$$M_{z,req,ideal}(z) = P\left[1 + I\left(\frac{T_s}{z-1}\right) + D\left(\frac{N}{1+N\left(\frac{T_s}{z-1}\right)}\right)\right]\dot{\psi}_{err} \tag{3.2}$$

where: $M_{z,req,ideal}$ is the ideal requested yaw moment, not considering actuator saturation or friction limits; $\dot{\psi}_{err}$ is the yaw-rate error; P, I, D, N are the proportional, integral, derivative gains and filter coefficient respectively; T_s is the sampling time.

Integral anti-windup was a necessary addition to the PID functionality, to account for motor torque and power limits, in addition to friction limits which restrict the yaw moment that the vehicle is capable of achieving. When the yaw moment is saturated, the closed-loop controller essentially becomes open-loop; the integrated error continues to grow without check, and hence also the yaw moment demand, $M_{z,req,ideal}$, as no action is possible to reduce the error [92]. Anti-windup negates further integral action when saturation occurs. In the solution used in this project, shown in Figure 3.9, a reduction in the yaw-rate error, $\dot{\psi}_{err,AW}$, to be subtracted from the yaw-rate error fed to the integral term is calculated by taking the difference ($M_{z,req,err}$) between the ideal yaw moment request, $M_{z,req,ideal}$ (output by the PID) and actual yaw moment request, $M_{z,req,actual}$, (output from the Torque Allocation block, considering friction and motor limits), multiplied by a gain. The resulting formulation is as follows:

$$M_{z,req,ideal}(z) = P\left[\left(1 + I\left(\frac{T_s}{z-1}\right) + D\left(\frac{N}{1+N\left(\frac{T_s}{z-1}\right)}\right)\right)\dot{\psi}_{err} - I\left(\frac{T_s}{z-1}\right)\dot{\psi}_{err,AW}\right] \tag{3.3}$$

where $\dot{\psi}_{err,AW} = K_{AW} M_{z,req,err}$, and K_{AW} is the anti-windup gain. In addition, a fade-in feature is included, designed to progressively introduce torque vectoring as a function of vehicle speed (Fig. 3.10). A simple ramp look-up table outputs a multiplier for the yaw rate error rising from 0 at an initial fade-in speed to 1 at a higher speed determined by the initial fade-in speed and a desired speed interval over which to reach full TV. These were

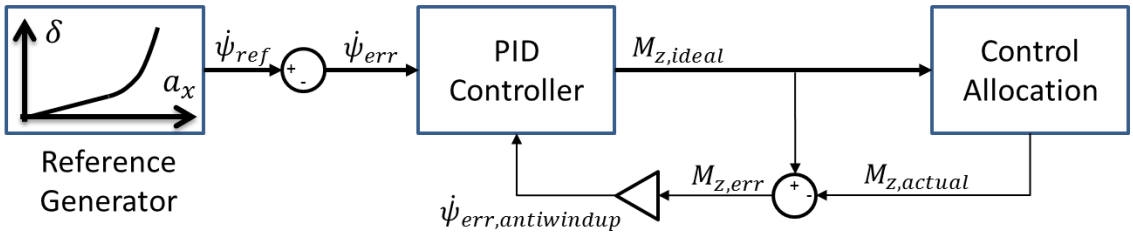

Figure 3.9: PID anti-windup, omitting parts of the full TV control structure (Fig. 3.2) for clarity

set to 5 and 2kph respectively. During shakedown testing, this narrow interval was not found to present any problems.

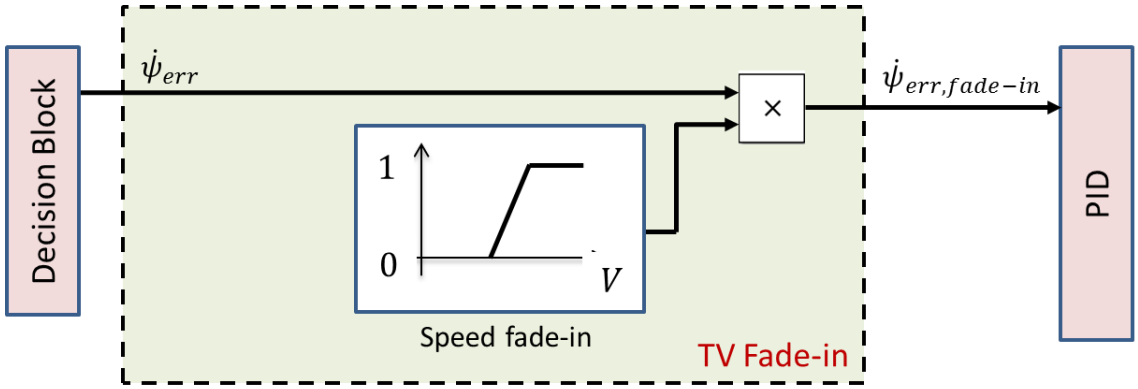

Figure 3.10: Speed-dependent fade-in of torque vectoring

Control Allocation

The control allocation block defines the torque split strategy. There are two strategies. A fixed torque allocation, distributing torques equally between the wheels is used when torque vectoring is turned off.

The requested yaw moment, M_z, is generated by the combination of wheel torques via the control allocation. After the overall difference in torque between the left and right tracks is calculated, the approach distributes torques front-rear by allocating wheel torques in proportion to the normal load on the axle, since this was found to be the opti-

mal distribution in the literature for minimum-time manoeuvring [45, 59] and in general permits a higher cornering force [16]. The following approach is simplified from [93].

First, torque limits are calculated for each wheel: the minimum of motor and friction limits. The summation of the front and rear limits determines the left- and right-track limits. The achievable overall longitudinal torque, T_x, is converted to longitudinal force, F_x. The torque that must be supplied by each track are given by the following equations:

$$T_L = \frac{r}{t_w}(wF_x - M_z), \tag{3.4}$$

$$T_R = \frac{r}{t_w}(wF_x + M_z), \tag{3.5}$$

$$\tag{3.6}$$

where T_L and T_R are the longitudinal torques to be supplied by the left and right tracks of the vehicle, respectively and w is the track width. The track torques are split front-rear according to the proportion of normal load on each wheel:

$$T_{FL} = T_L\frac{f_{FLz}}{(f_{FLz}+f_{RLz})}, \qquad T_{FR} = T_R\frac{f_{FRz}}{(f_{FRz}+f_{RRz})}, \tag{3.7}$$

$$T_{RL} = T_L\frac{f_{RLz}}{(f_{FLz}+f_{RLz})}, \qquad T_{RR} = T_R\frac{f_{RRz}}{(f_{FRz}+f_{RRz})}. \tag{3.8}$$

$$\tag{3.9}$$

Thus, the overall torque demand, T_x, from the driver, and the yaw moment demand from the PID-controller, M_z, are converted into the torques at each wheel, while considering motor and friction limits.

A final check is conducted to determine whether there is any spare capacity at any corner. If so, the front-rear split is redistributed [93]. The individual wheel torque demands are sent to the Low Level Control and finally to the actuator controllers. The difference

between the ideal yaw-moment demand and the actual yaw-moment demand achievable is computed and fed back to the PID anti-windup function.

3.4 Practical considerations

Running a controller in real-time and the real world require some practical modifications. Instrumentation practicalities were simulated at the MiL stage to ensure robust performance of the controller in their presence. Signal delays (to emulate the CAN) and signal noise were introduced. When carried to the SiL, simulated CAN delays were removed since a physical CAN is present on the SiL setup. The major modification required for simulation on the SiL was to convert the controller to run in discrete-time. Conversion of the PID controller into discrete-time formulation has already been mentioned. Initial PID tuning was carried out using a combination of classical tuning rules-of-thumb, bicycle plant model transfer function frequency analysis and MATLAB's built-in PID tuner. There was a significant discrepancy between the tuning for the bicycle plant model and the high-fidelity model response to a step-steer in CarMaker, so final modifications were performed manually in CarMaker using trial-and-error.

Additional considerations already mentioned include PID anti-windup, TV speed fade-in and the inclusion of a first order lag on the yaw rate reference.

3.5 Real-Time Software-in-the-Loop Testing

Real-time testing was carried out in advance of installing the controller on the Delta vehicle in order to a) check operation of the controller in real-time operation, including CAN signalling and b) develop test manoeuvres. Steady-turn and step-steer manoeuvres were

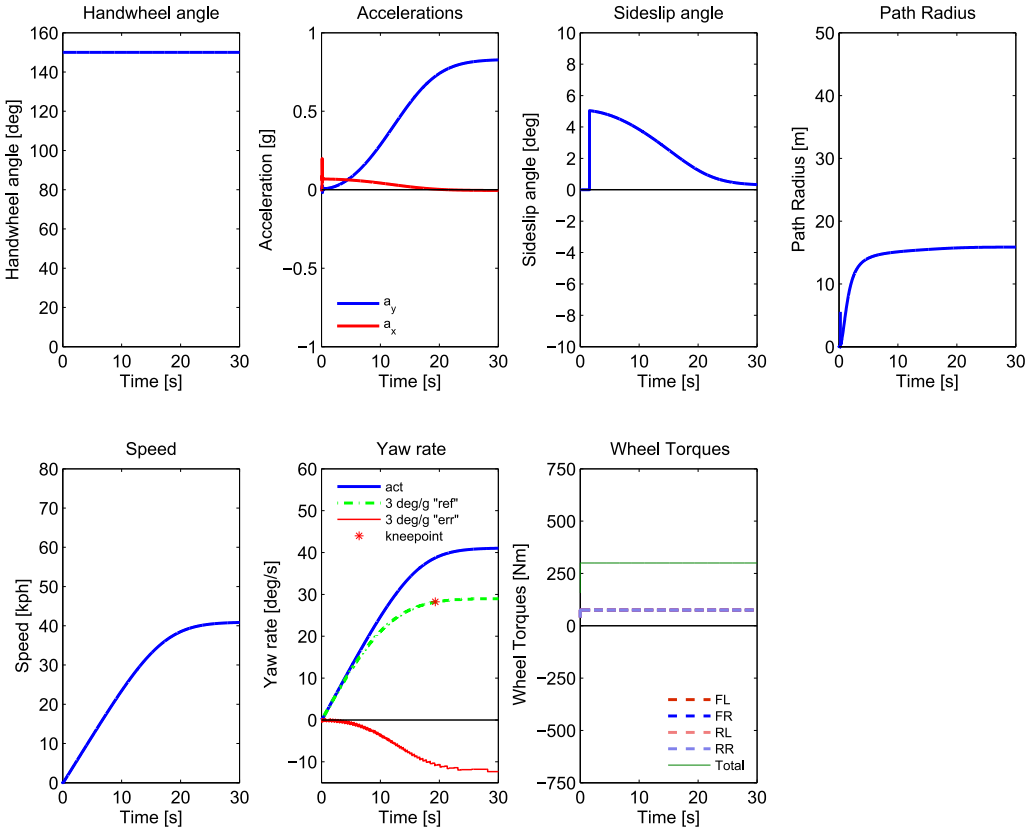

Figure 3.11: Real-time test results with TV inactive, left steady-turn with slowly increasing velocity and handwheel angle of 150°. Target understeer gradient of $+3°/g$ (inactive) plotted for comparison.

carried out using the Delta vehicle model in CarMaker.

3.5.1 Steady-turn

The steady-turn manoeuvre was modelled on the British Standard BS ISO 4138 [94] and consisted of a constant handwheel angle of 150°, starting from stationary and slowly increasing velocity at very low longitudinal acceleration. The longitudinal acceleration was achieved by specifying a constant longitudinal torque request of 350Nm. This quasi-steady-state approximation of the steady-turn was chosen because it is more repeatable by the driver, as the handwheel angle is constant and multiple data points are collected as numerous speeds are recorded per manoeuvre.

Figure 3.11 shows the response with TV inactive, with an inactive yaw rate 'reference' plotted to compare the handling characteristics. Figure 3.12 shows the vehicle response for an target understeer gradient of +3deg/g for a steady left turn. The left wheel torques are greater than the right, generating an anti-clockwise moment with a peak of $\sim -2200Nm$ in an opposite sense to the turn in order to cause the vehicle to achieve the +3deg/g target. The magnitude of the control yaw moment developed from the torque difference between the motors increases as lateral acceleration builds, reaching a peak at about 15s. This is due to the slope of the reference in the linear range of the piecewise expression demanding an ever-decreasing yaw rate compared to the vehicle with TV inactive as lateral acceleration increases. As both the reference and TV-inactive response become nonlinear, the 'error' between the two becomes near constant, and so the yaw moment also (compare yaw rate '3deg/g "err" in Fig.3.11 with Yaw Moment plot in Fig. 3.12. The transition between linear and nonlinear region of the reference ($0.6a^*_{y,max}$) is denoted by a red star in the yaw rate plot.

The longitudinal acceleration tends to zero at 20s, as the tractive and dissipative forces

reach equilibrium. The yaw rate builds to $\sim 33°$/s, with the path radius increasing up to $\sim 20m$ from the kinematic radius, following the reference very closely. The path radius is calculated from the relation $R = \frac{V^2}{a_y \cos\beta - a_x \sin\beta}$, where V is vehicle speed vector, a_y is the lateral acceleration, a_x is the longitudinal acceleration, β is the sideslip angle. Note that torque vectoring only begins when the vehicle speed reaches 5kph, according to the fade-in feature discussed in section 3.3.3.

Figure 3.13 shows the vehicle response for an target understeer gradient of $-3°$/g for a steady left turn. In this case, the right wheel torques are greater than the left, generating a clockwise, positive peak yaw moment of $\sim$ 2200Nm applied to the vehicle in the same sense of the turn. Interestingly, the initial response between 2 and $7s$ requires a negative, understeer moment, indicating that the behaviour of the TV-inactive vehicle exhibits a greater degree of understeer than the reference for this period. This phenomenon is difficult to explain, however it may be a result of the ramp feature of the speed fade-in not delivering the full torque immediately, or perhaps a latency in delivery of the commanded torque. Nevertheless, the resulting yaw rate behaviour follows the reference closely, with a yaw rate of $45°$/s and a path radius of $14m$, $7m$ lower than for the understeer behaviour. This is a fairly extreme oversteer target and the vehicle reaches a terminal speed of $40kph$ after only about $20s$; the speed builds at a lower rate for the understeer target.

3.5.2 Step-steer

Step-steer manoeuvers were performed with a left step handwheel input of $150°$ at an initial speed of $60kph$. Figure 3.14 shows that for the target understeer gradient of $+5°$/g, initial spikes of torque are required to provide the instant turn-in immediately following the step input, building a peak of lateral acceleration very quickly ($\sim 0.2s$), and a negative, anti-clockwise yaw moment applied in the opposite sense of the turn. The automated

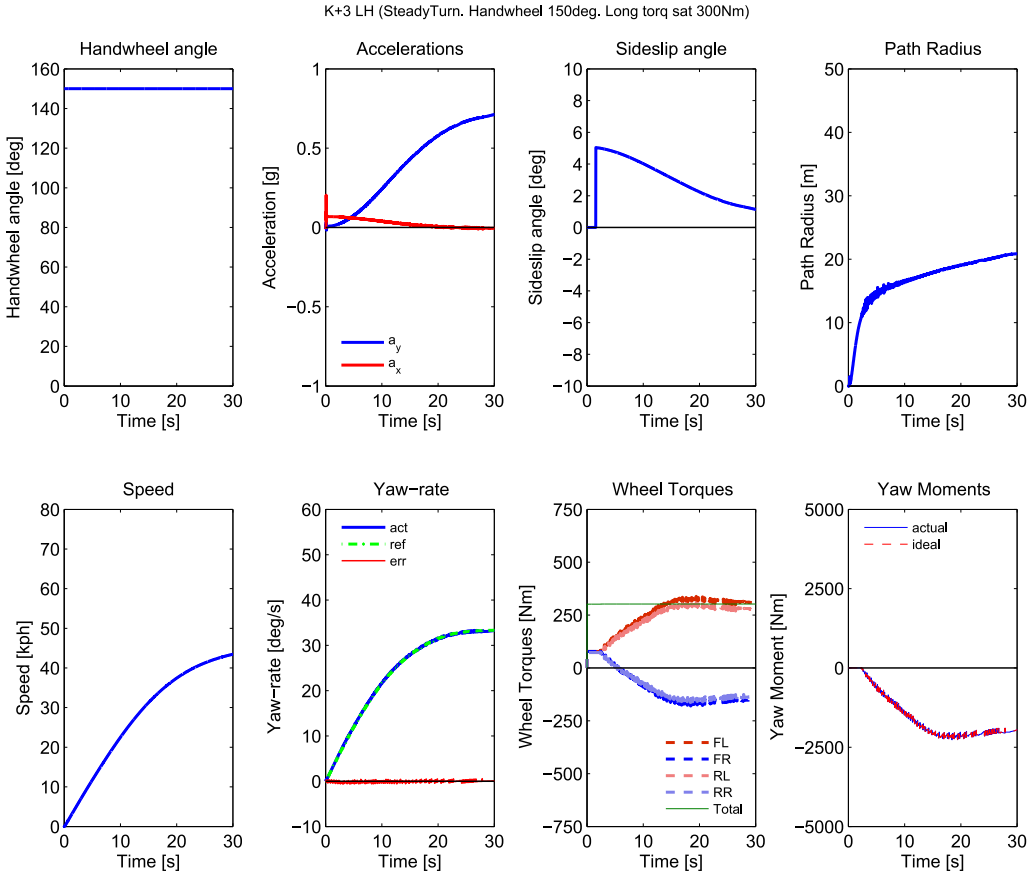

Figure 3.12: Real-time SiL test results for TV, left steady-turn with slowly increasing velocity and handwheel angle of 150°. Target understeer gradient of $+3°/g$.

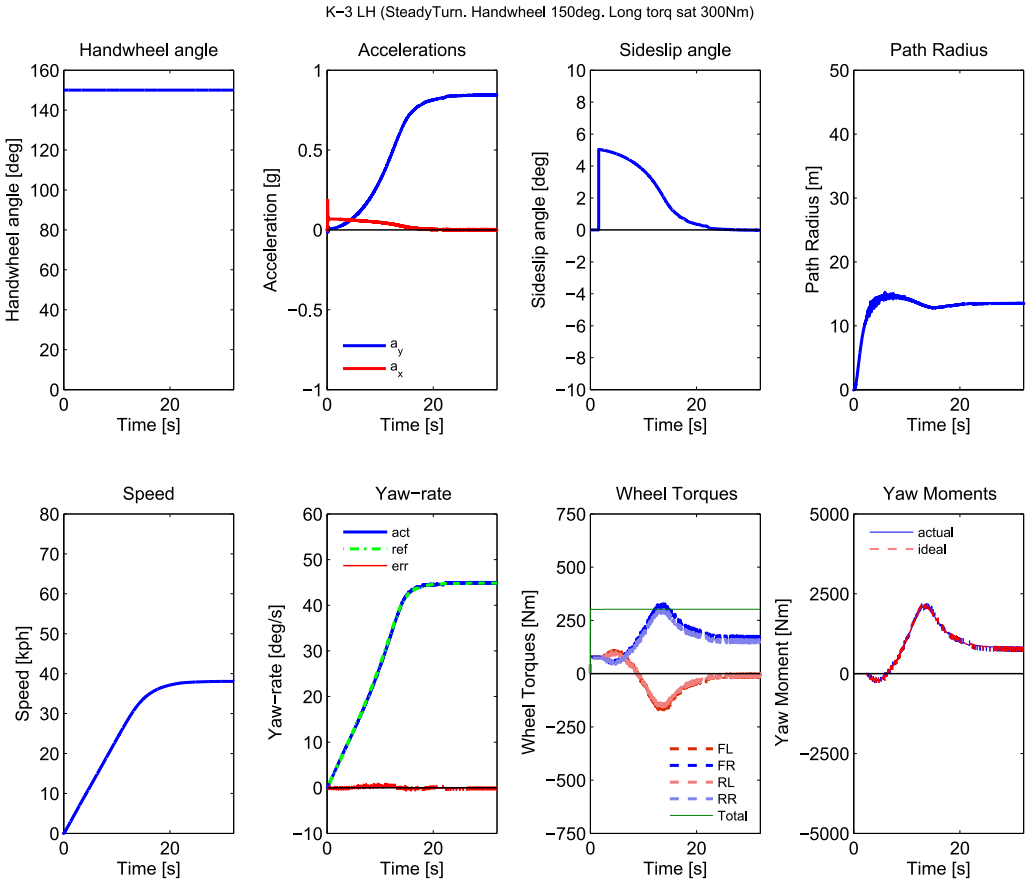

Figure 3.13: Real-time SiL test results for TV, left steady-turn with slowly increasing velocity and handwheel angle of 150°. Target understeer gradient of $-3°/g$.

driver seeks to maintain a speed of 60kph, in order that left and right torques might increase after the step input. The path radius after the initial transient response is around $32m$, compared to just over $25m$ for the oversteer target of $-3°$/g shown in figure 3.15. The yaw rate leads the reference by $\sim 0.05s$ at the initial step, due to the first-order delay on the reference (section 3.3.2). The yaw rate overshoots the steady-state reference by an acceptable amount but settles rapidly to the final value.

For the oversteer case, there is an initial oversteer yaw moment since the yaw rate is not sufficient to meet the target; once the yaw rate overshoots the reference, an understeer moment is required to control the behaviour of the car. It can be seen from the sideslip angle trace that this oversteer reference is too aggressive, as the sideslip angle does not stabilise after the step input but continues to grow. A target of $-1°$/g was also tried (not shown) and results in a stable response which is a more conservative target for the vehicle test. This controller is designed for continuously adjusting the vehicle handling; an additional stability controller could be implemented to ensure safety for a production vehicle when operating above a certain sideslip/sideslip rate threshold.

3.5.3 Real-time SiL Testing Conclusions

Real-time testing has shown that the TV system is delivering a desired performance in a real-time environment. For both tests, parameters such as handwheel angle, longitudinal acceleration (steady) and initial speed (step) were tuned to give desirable and acceptable results for translation into the real-world tests. The configuration of the steady-state test is satisfactory in terms of simplicity for the driver, repeatability, and provision of sufficient data per run and can be performed within the steerpad limits available. Likewise, the step-steer test is simple to perform for the driver and various targets have been tried such that the vehicle remains within the limits of stability for the oversteer case.

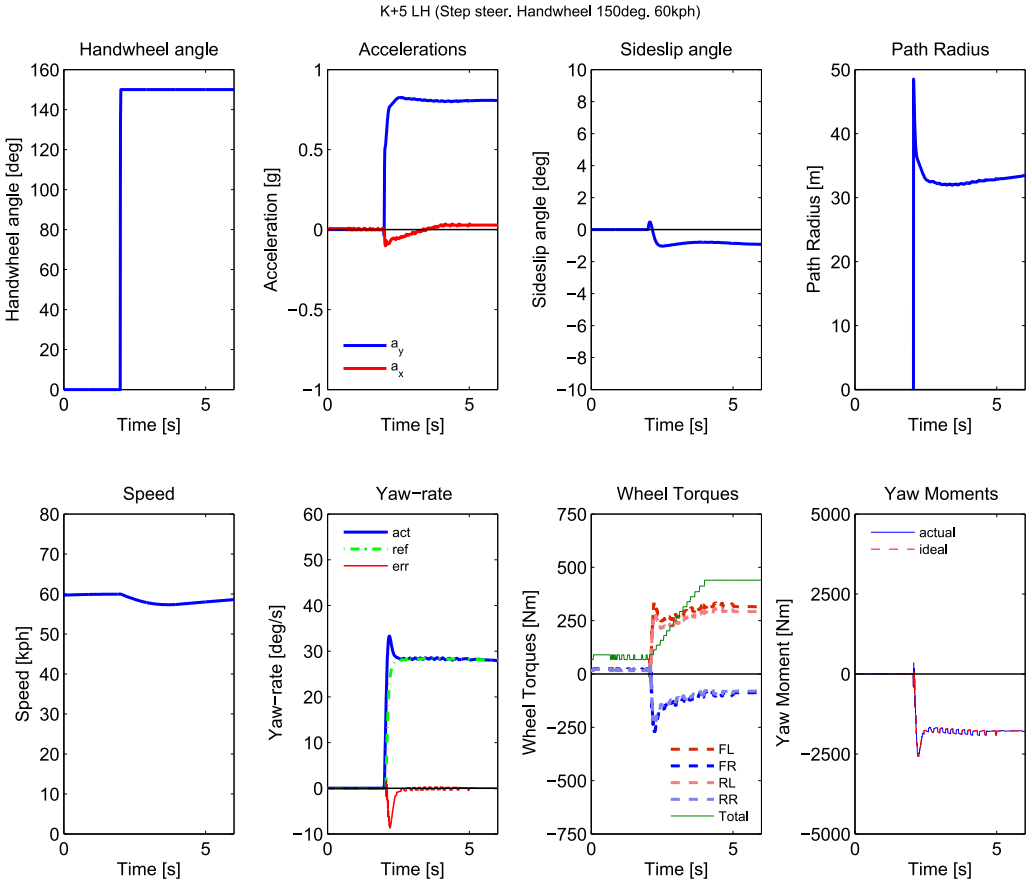

Figure 3.14: Real-time SiL test results for TV, left step steer turn at 60kph initial speed and handwheel angle of 150°. Target understeer gradient of +5°/g.

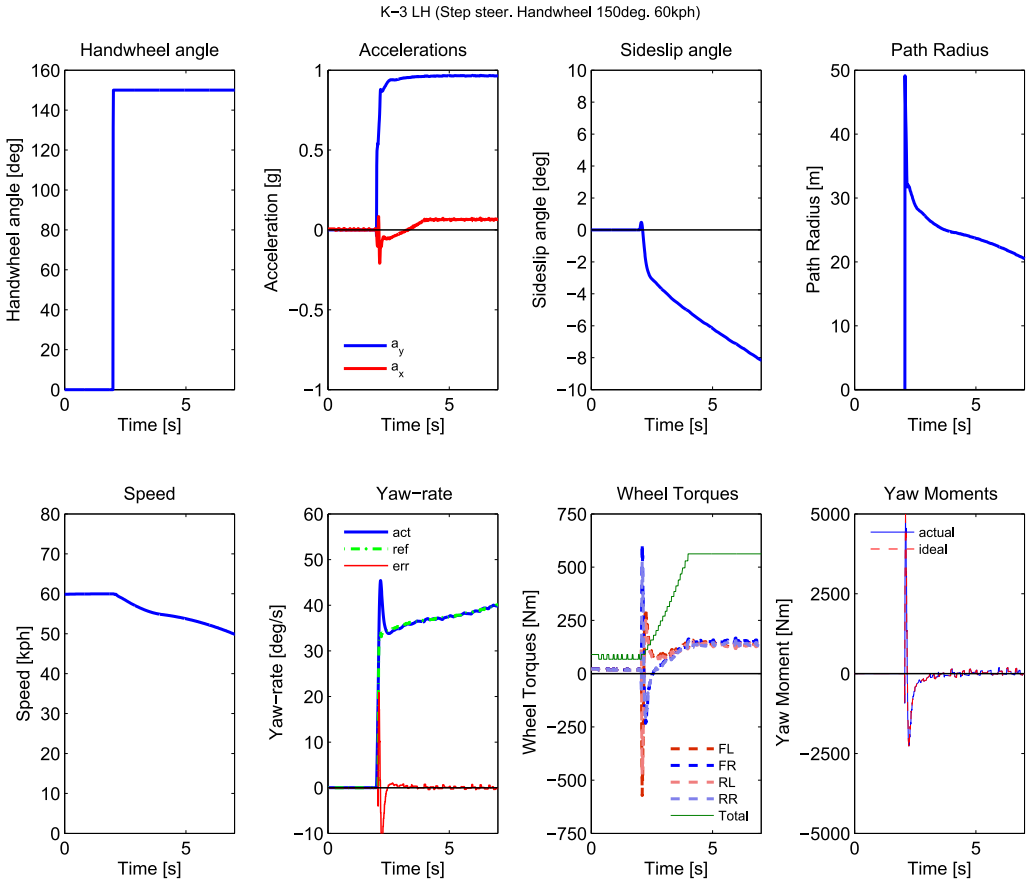

Figure 3.15: Real-time SiL results for TV, left step steer turn at 60kph initial speed and handwheel angle of 150°. Target understeer gradient of $-3°$/g.

3.6 Delta Motorsport E4 Vehicle Test

Real-time SiL testing proved the control system could perform well in standard handling tests in real-time with the presence of simulated noise and signal delays, considering a high-fidelity vehicle model. The next stage was to prove the controller on the Delta Motorsport E4 test vehicle - with the additional challenges of real signal noise, disturbances from the road friction conditions and surface roughness and unevenness, and the unmodelled vehicle characteristics such as steering and suspension compliance, uneven weight distribution and, of course, complex tyre force characteristics. Furthermore, the controller must interact with the vehicle's other control systems. Testing was performed on the high friction asphalt surface at Jaguar Land Rover test facilities at Gaydon, UK. Steady-turn tests were conducted on the 30m-radius skid pad and step-steer manoeuvres on the North bend test area.

3.6.1 Steady-turn

Steady-turns were performed as described in the real-time testing section (3.5), with some small adaptations. The handwheel angle was set to 130°, as this corresponded to the simplest angle for the test driver to maintain reliably, without access to a steering robot. A torque saturation limit was set such that the test driver could fully depress the throttle pedal and still request a small, exact longitudinal torque to ensure quasi-

Figure 3.16: Systems and software check in Delta vehicle

steady conditions. This was set to $300Nm$ to give a good compromise between practical test time and steady-state conditions. A range of target understeer gradients were conducted: $K \in [+5, 0, -0.5, -1, -3]^\circ$/g. It was found that the -1 and -3°/g demanded yaw moments were restricted by the 'system protection layer' of the control logic in the Delta Motorsport layer of the controller, so only $+5$ and -0.5°/g target results are presented in the following.

To give an overview, Figure 3.17a shows that the turning radius ratio, R/R_0 (where $R_0 = L/\delta_{kin}$) for the understeer reference increases with lateral acceleration, while the oversteer reference decreases, demonstrating that the controller is performing generally as expected. At low lateral acceleration ($\sim 0.05\text{ms}^{-2}$), the vehicle with TV inactive exhibits a higher turning radius ratio than both TV-controlled set-ups. Figure 3.17b shows plots of the manoeuvres in the global X-Y coordinates and clearly demonstrates that, with reference to the TV-inactive vehicle, a tighter turn radius is possible for an oversteer target, whilst a greater turn radius is navigated when following an understeer reference. Figure 3.18 shows the skid pad results for the vehicle with TV inactive. It is important to note that the handwheel angle was maintained near-constant by the driver for most of the manoeuvre ($\pm 2^\circ$, signal with Butterworth low-pass filter applied, red). Secondly, the measured yaw rate is noisy in comparison to the yaw rate reference, giving rise to a noisy yaw rate error as the input signal to the controller. The wheel torques are equal, as expected, and total torque demand is saturated at $300Nm$ in order to achieve quasi-static conditions. The noise of the torques is at a low, acceptable level of amplitude $\sim$ 10Nm.

Figure 3.19 shows the steer pad results for $K = +5^\circ$/g. The yaw rate tracks the reference closely, with the greatest contribution to the control effort coming from the integral term. Constant radius tests (maintained by varying handwheel angle) conducted indicate that the steady-state understeer gradient of the vehicle with TV inactive is approximately

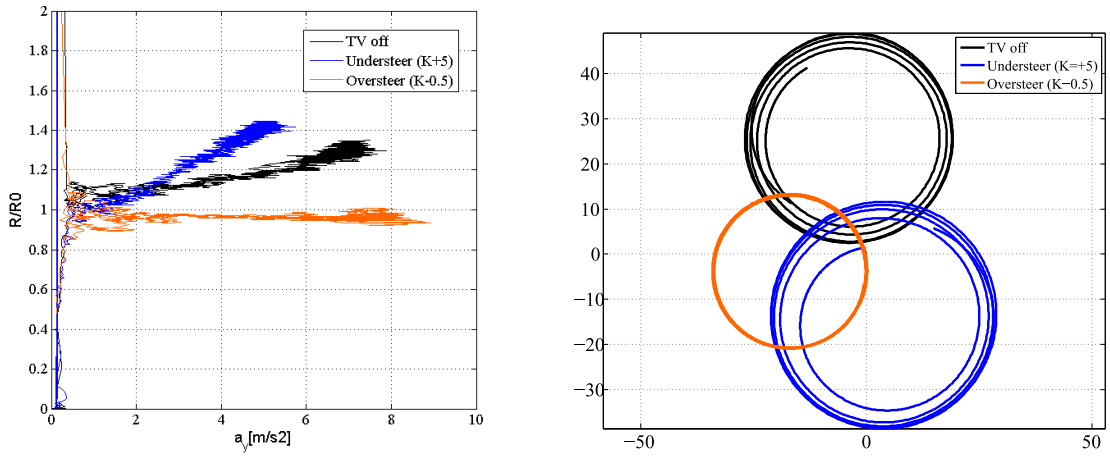

Figure 3.17: (a) Skid pad test results from experimental tests of the four individual motor demonstrator vehicle showing turning radius ratio, R/R_0, as a function of lateral acceleration for: TV inactive; TV active with understeer gradient of $+5°$/g; TV active with understeer gradient of $-0.5°$/g. (b) visualisation of skid pad turning radius in global X-Y coordinate frame

1.75°/g. Theoretically, therefore, an understeer moment is required to actively push the vehicle behaviour to $+5°$/g. For this left-turn manoeuvre, an understeer yaw-moment is negative, and for speeds above $\sim 20kph$ (time $> 17s$). There is, however, a positive moment acting in the *same* sense of the turn at low speed, indicating that the behaviour of the vehicle when TV is inactive exhibits a high level of understeer at very low speed. This result is not visible in the real-time test results (Fig. 3.12) so it must be concluded that there is some aspect of the vehicle behaviour that is not being faithfully captured by the CarMaker model. This observation is corroborated in [85]. Nevertheless, the yaw rate reference is closely tracked.

Figure 3.20 shows the skid pad results for $K = -0.5°$/g. Once again, the yaw rate reference is followed. A yaw moment in the same sense of the turn is required to achieve the oversteer behaviour and this is delivered in a consistent manner, with the right torques greater than left, building with lateral acceleration as the vehicle speed increases. As the limit of adhesion is reached, the yaw rate becomes very noisy. From experience riding

on board the vehicle, this was due to the rear end repeatedly sliding and then regaining traction. The surface of the skid pad was slightly sloped, with a fairly irregular surface curvature and with varying μ between different age asphalt patches. Hence the friction ellipse is constantly changing according to friction level and weight transfers. This could explain the rear sliding, since as the rear tyres operate around the peak friction point, friction level decreases as the slip varies below and above the peak point. Tuning the filter on the derivative signal or reverting to PI control could be a solution to reduce sensitivity to the yaw rate noise.

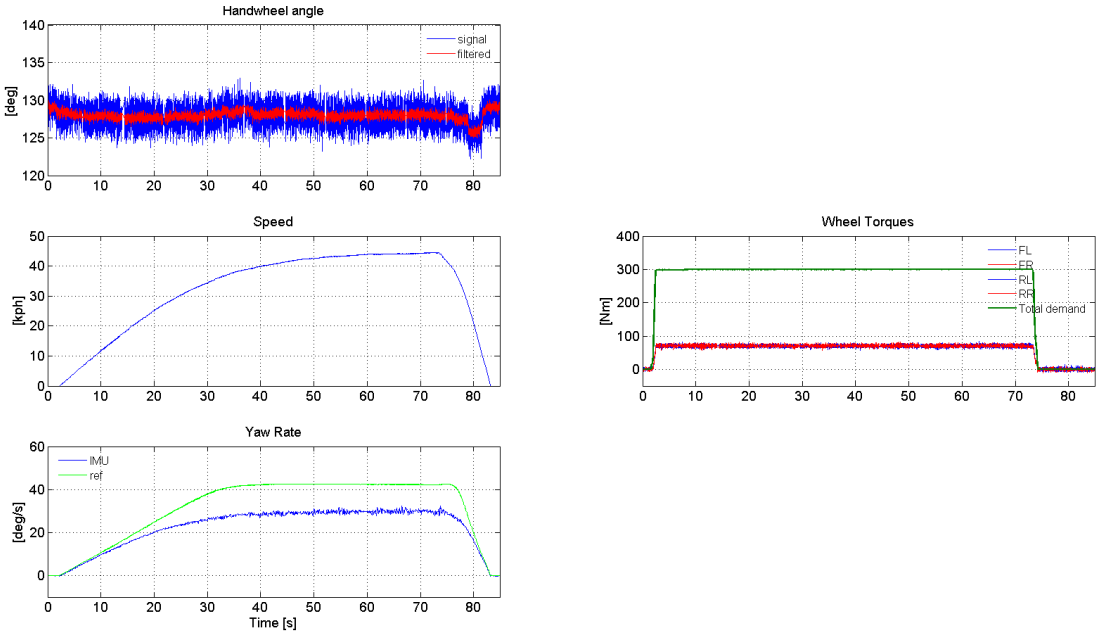

Figure 3.18: High-μ test results for response with TV inactive, left steady-turn with slowly increasing velocity and nominal handwheel angle of 130°.

3.6.2 Step-steer

Step-steer manoeuvres were performed as described in the real-time testing section (3.5), and modified to give a handwheel angle step of 130°, and an initial vehicle speed of

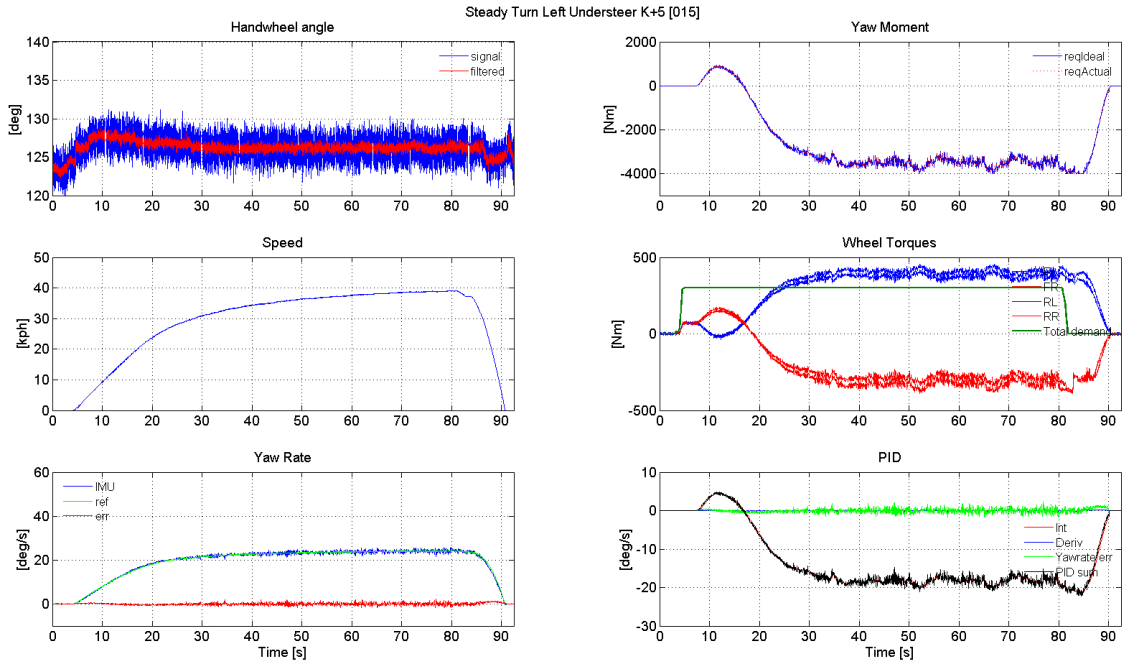

Figure 3.19: High-μ test results for TV, left steady-turn with slowly increasing velocity and nominal handwheel angle of 130°. Target understeer gradient of $+5°/g$.

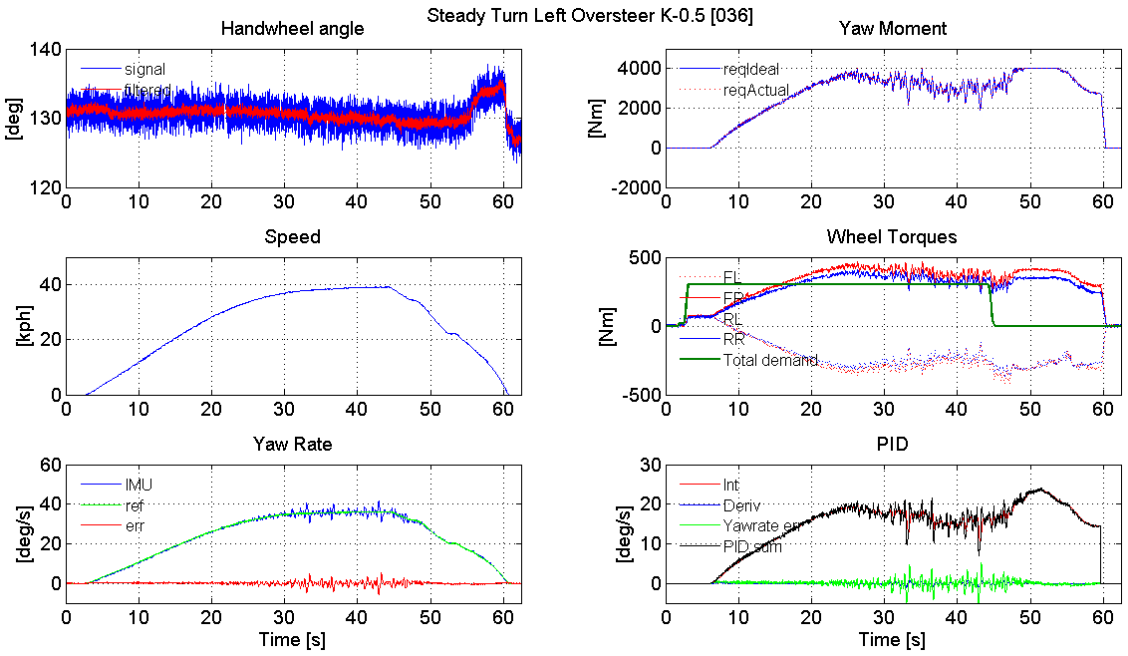

Figure 3.20: High-μ test results for TV, left steady-turn with slowly increasing velocity and nominal handwheel angle of 130°. Target understeer gradient of $-0.5°/g$.

$40kph$, achieved by activation of a cruise control system in the Delta controller.

Figure 3.21 below shows the TV-inactive vehicle response to a right step-steer. The controller was run "in the background", with understeer target of 1.75°/g. The actual yaw rate is within $\sim 2°$/s of this "reference".

Figure 3.22 shows a right step-steer for $K = +5°$/g. Firstly, it can be noted that the yaw rate reference clearly leads the yaw rate during the initial step input. From a controller perspective, the vehicle is "understeering" the reference, and therefore an oversteer yaw moment (negative) is required initially to chase the reference. Once the step has been applied, there is an acceptable overshoot of yaw rate as the controller reverses the yaw moment to an anti-sense, understeer, value (positive) required to push the handling to deliver a greater understeer characteristic than the vehicle with TV inactive. The results are slightly affected by the Delta 'system protection layer' imposing a yaw moment rate limit. This is especially evident between 10.5 and $11.8s$, where yaw moment has a constant gradient, and is responsible for limiting the speed at which the PID is able to reduce the yaw rate overshoot to the steady-state value. In order to account for this, a yaw moment limit could be calculated at every time step, since it is constant in discrete-time operation. This could be incorporated in the Control Allocation block in addition to the motor torque and power limit and the friction limitation on achievable yaw moment, and hence considered by the anti-windup feature.

Figure 3.23 shows a right step-steer for $K = -0.5°$/g. Once again, the yaw rate lags the reference. The delay is $0.2s$, which is likely imperceptible to the average driver. Recall that the yaw rate reference is subject to a first-order delay (applied to the steering angle signal): the time constant of this delay needs to be increased for this frequency of input to achieve a match. A more dynamic adjustment could be made by implementing

a frequency-dependent delay (e.g. based on the yaw rate gain transfer function for the TV-inactive vehicle [39]). For this understeer case, there is no overshoot of yaw rate and it follows the reference well after the step input.

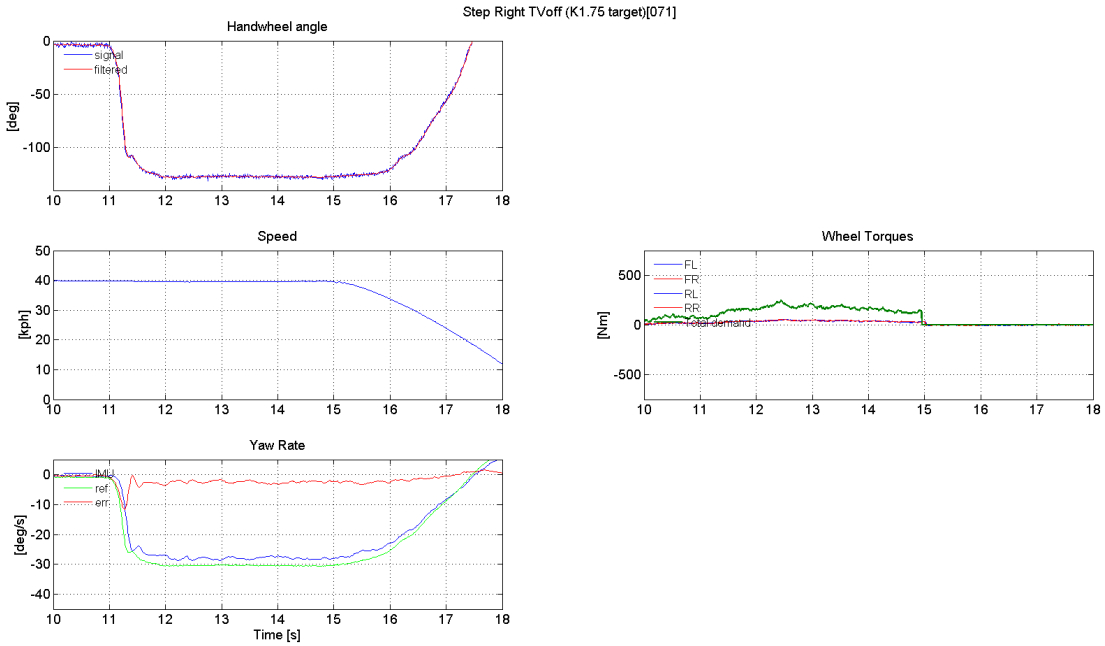

Figure 3.21: High-μ test results for the TV-inactive response, right step-steer at initial velocity of 40kph and handwheel angle input of 130°.

3.7 Vehicle Test Conclusions

Overall the real-world vehicle testing has shown that the control system is able to significantly modify the handling characteristics according to a desired target. The system may now be further developed in the simulation environment with the knowledge that results will transfer well to real-world application. In particular we may conclude that the controller:

- is able to successfully modify the handling characteristic to target understeer gra-

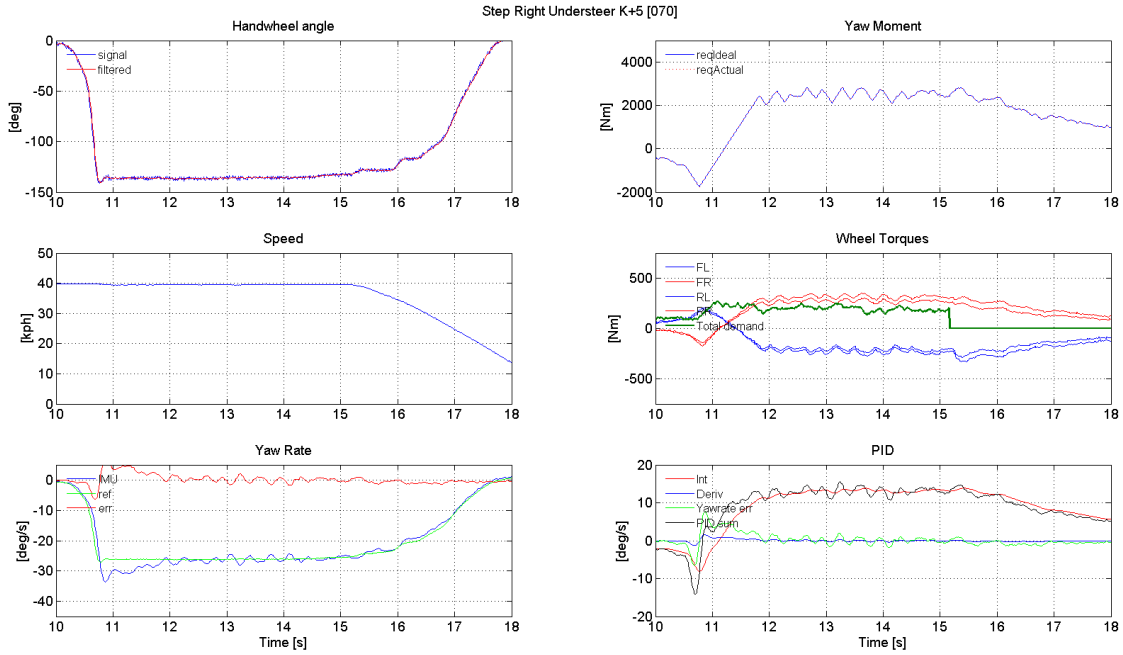

Figure 3.22: High-μ test results for TV, right step-steer at initial velocity of 40kph and handwheel angle input of 130°. Target understeer gradient of +5°/g.

dients significantly far from the behaviour with TV inactive in both understeer and oversteer directions;

- is able to follow the reference in both steady-state and transient manoeuvres;
- gives acceptable transient response and steady-state tracking;
- can be incorporated successfully into a real-time environment and perform using measured signals over a CAN system.

The following improvements may be considered for fine-tuning the controller:

- more advanced PID tuning for enhanced noise rejection and a reduced overshoot (consider gain scheduling);
- a first-order delay that includes a varying time-constant on the yaw rate reference;

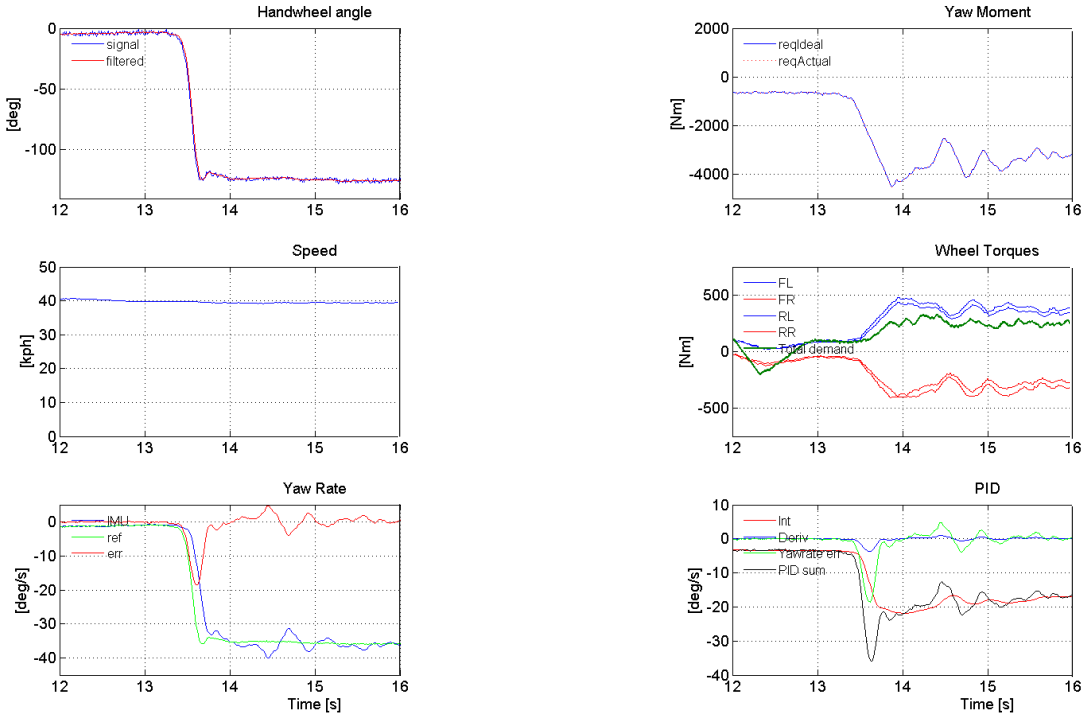

Figure 3.23: High-μ test results for TV, right step-steer at initial velocity of 40kph and handwheel angle input of 130°. Target understeer gradient of -0.5°/g.

- considering ‘system protection’ constraints in the reference generation/torque allocation blocks.

Acknowledgements. The work carried out in this section was a collaborative project. The following contributions are acknowledged. The yaw controller presented in this section was initially developed by Cyril Claret in the Model-in-the-Loop environment [93]. This was the starting point from which the author formed it into the heirarchical structure mandated by the IVCS (Drs. Amir Soltani [89], Davide Tavernini) and performed all the work of converting the system for testing in the real-time environment and real-world testing. Real-time SiL testing was conducted with the help of Drs. Davide Tavernini, Amir Soltani and Efstathios Siampis. Real-world testing involved the interfacing of the Cranfield-designed control system with the Delta Motorsport system, which was a collaboration between the author, Nathan Ewin and Davide Tavernini.

Part II

Time-optimal handling characteristics

Chapter 4

Time-optimal handling: 3DOF Vehicle model

In this second part of the thesis, the focus is on analysis of vehicle handling characteristics at the limits of performance: minimum-time manoeuvring. Since minimum-time manoeuvring is the objective and the optimal controls to achieve these are calculated, the analysis in this part of the thesis is called 'time-optimal'. Two distinct objectives are pursued: the first investigates the effect of variation of the passive handling of the vehicle on the torque-vectored active response; the second investigates the effect of the target understeer gradient on the controlled response of the torque-vectored vehicle. In this chapter 4, optimal control problems are formulated and solved to address these objectives, considering the 3DOF single-track vehicle model presented in §2.2. In chapter 5, an identical methodology is followed considering the 7DOF 4 wheel model. The commonalities and contradictions of the results from each model are explored in detail in chapter 6.

4.1 Introduction

The previous chapter introduced the torque vectoring control system that was developed and tested for real-time implementation. With confidence that the topology under consideration is able to actively modify the handling balance in the real-world, further investigation can be carried out in the simulation domain.

The focus of this chapter is to investigate the time-optimal handling characteristics of torque vectoring. That is to say, minimum-time manoeuvring.

Minimum-time manoeuvring is traditionally the realm of competitive motorsports. Motorsport is a key arena in which passenger vehicle manufacturers boost their marketing profile and, in the case of high-end motorsport, develop new technologies. For electric vehicle development, the nascent FIA Formula E championship was created with the specific aim of accelerating electric vehicle technological development [3] . Currently in its third season, the interest in team buy-in of factory OEM teams is high, with Mercedes, Porshe, BMW and Audi investing in factory teams and Ferrari likely to join with one of their brands [4]. Not only does competition accelerate engineering development and technical learning, but it necessitates the maximum performance of the vehicle to be extracted in order to win.

Torque vectoring is, at present, not permitted in Formula E, Formula 1 or the World Endurance Championships, despite cutting edge electric and hybrid-electric powertrains. However, it is highly feasible that they could be permitted in the near future, with FE releasing a new vehicle in 2018/19 season and Formula 1 discussing the strategy of the sport from 2020, with new ownership from late 2016 . Roborace, an autonomous racing car championship which will act as a support race for FE from late 2017, possesses a very powerful 4-wheel torque vectoring powertrain [5].

However, minimum-time manoeuvring is not only of interest for the motorsport ap-

plication. Investigation of the vehicle dynamics at the limit of adhesion and a greater understanding of the controls required to achieve this is of vital importance in developing active control systems that are able to manoeuvre the vehicle in the nonlinear and even unstable regions of the performance envelope to enhance safety for passenger vehicles. This is especially important for the future development of autonomous electric vehicle control strategies.

With the considerably-expanded vehicle manoeuvring envelope in terms of yaw moment and lateral acceleration capability accessible through torque vectoring, it is important to determine the optimal handling characteristics of the actively-controlled vehicle in order to extract the maximum performance and hence minimise time.

In this chapter, the aim is to investigate the optimal controls and resulting state trajectories that manoeuvre that vehicle in minimum-time. Specifically, the objectives are to:

- investigate the effect of TV active against TV inactive;
- investigate the effect of natural handling characteristics on controlled response
- determine the effect of target understeer gradient on closed-loop TV response.

The 3DOF single-track vehicle model in §2.2 is employed. The numerical nonlinear optimal control technique is the method that forms the basis of the analysis in this chapter, since it allows the optimal use of the vehicle controls to be determined, emulating an ideal driver. An overview of the theory of the numerical optimisation method and its use in the solution of optimal control problems are given in the following section, §4.2.

4.2 Theory: solution of an optimal control problem

The purpose of this section is not to give a complete treatment of the theory required for the solution of an optimal control problem; this is available in a range of excellent texts [95–97], to which the author defers. The purpose, however, is to give a sufficient 'map' of the various aspects required to solve an optimal control problem and the different approaches and practical considerations that were relevant in choosing an approach for this work.

An complementary section to this theory resides in Appendix A, which collates practical notes on the 'rules of thumb' that the author has refined during the course of the doctoral research useful in the solution of the optimal control problems detailed in this thesis.

4.2.1 The Optimal Control Problem

A general optimal control problem (OCP) is solved by finding continuous control inputs that, considering constraints on controls and states, forces the states of a nonlinear system to minimise an objective function defined over a certain interval and for the final state. The solution is iteratively improved by modifying the controls until the objective function becomes stationary (i.e. when the derivatives of the controls are zero).

The plant model, constraints and objective must be mathematically defined. Diehl and Gros [97] put it simply as the optimal choice of inputs for a dynamic system. There are different classes of dynamic systems, but in the case of vehicle dynamics, the behaviour is described by deterministic differential equation models.

Problem description

Starting with the end in mind, the optimal control problem is to find the controls, **u**, and corresponding states, **x**; initial and final time that minimises the objective function:

$$f(x) = \phi[\mathbf{x}(t_0, t_f)] + \int_{t_0}^{t_f} L[\mathbf{x}(t), \mathbf{u}(t)], \tag{4.1}$$

where 0 and f subscripts denote initial and final values, ϕ denotes the Mayer term and L denotes the Lagrange integral term. This is subject to the dynamic constraint defined by the (vehicle) equations of motion:

$$\dot{\mathbf{x}} = \mathbf{f}[\mathbf{x}(t), \mathbf{u}(t)], \tag{4.2}$$

equality and inequality path constraints:

$$\mathbf{p}[\mathbf{x}(t), \mathbf{u}(t)] = 0, \qquad \mathbf{g}[\mathbf{x}(t), \mathbf{u}(t)] \leq 0, \tag{4.3}$$

and subject to initial and final boundary conditions:

$$\mathbf{x}(t_0) = \mathbf{x}_0, \qquad \mathbf{x}(t_f) = \mathbf{x}_f. \tag{4.4}$$

Optimality conditions

In order to find the solution to the OCP, the minimum of the objective function must be found. There exist optimality conditions that determine whether the minimum has been found [96].

Adopting the notation used in [95], from which the following is summarised, $f(\mathbf{x})$ is

the function that it to be minimised:

$$minf(\mathbf{x}). \tag{4.5}$$

There are two optimality conditions: *necessary and sufficient*, such that a point x^*, is proved to be a solution to (4.5). For unconstrained optimisation, the necessary conditions are that $\nabla f(x^*) = 0$ and $\nabla^2 f(x^*)$ is positive semidefinite. The sufficient conditions state that for the point x^* where $\nabla f(x^*) = 0$ and $\nabla^2 f(x^*)$ is positive definite, the point is a strong local minimiser of f [95]. $\nabla f(x)$ and $\nabla^2 f(x)$ are known as the Jacobian and Hessian matrices.

For constrained optimisation, the Lagrangian is introduced, which is an augmented version of the cost function:

$$L(\mathbf{x},\lambda) = f(\mathbf{x}) = f(\mathbf{x}) - \lambda^T c(\mathbf{x}) = f(\mathbf{x}) - \sum_{i=1}^{m} \lambda_i c_i(\mathbf{x}), \tag{4.6}$$

where λ is an vector of m Lagrange multipliers and $c(\mathbf{x})$ is a constraint function [96]. Optimality conditions include the augmented cost $L(\mathbf{x},\lambda)$ in place of $f(\mathbf{x})$, such that the necessary conditions become:

$$\nabla_x L(\mathbf{x}^*,\lambda^*) = 0, \tag{4.7}$$

$$\nabla_\lambda L(\mathbf{x}^*,\lambda^*) = 0, \tag{4.8}$$

$$\tag{4.9}$$

However, whilst these determine the zero curvature of the augmented cost, they do not

specify the nature, for which the Hessian of the Lagrangian must be defined:

$$\mathbf{H}_L = \nabla^2_{xx} L = \nabla^2_{xx} F - \sum_{i=1}^{m} \lambda_i \nabla^2_{xx} c_i(\mathbf{x}). \tag{4.10}$$

The sufficient condition is that

$$\mathbf{v}^T \mathbf{H}_L \mathbf{v} \geq 0, \tag{4.11}$$

for the vector $\mathbf{v}$ in the constraint tangent space [96]. In comparison to the unconstrained case, the curvature of the objective function need be positive only in the direction of the constrained space. The concept of the 'feasible set' needs to be introduced to expand this definition to inequality constraints, on which more can be read in [96].

4.2.2 Numerical methods

The optimal control problem may be solved using numerical methods. The numerical optimisation method hinges on the ability to solve difficult problems by decomposition into a series of simple subproblems that are easier to solve [96].

Indirect vs Direct

The optimal control problem may be solved in two ways. The *indirect* approach seeks to find the solution to the first-order necessary conditions while the *direct method* sets out to solve the optimal control problem itself [98].

Indirect Indirect optimisation forms a 2-point boundary-value problem, where state equations with initial conditions are solved forwards in time and co-state equations with final conditions are solved backwards in time, assuming a known control history (this is

the implicit approach [98]). The solution is iteratively improved by modifying the controls until the necessary conditions are satisfied. This requires information about the first and second derivatives, which is computationally demanding [67]. MBSymba [81] is a software package that was developed to ease the process of calculating equations of motion and derivatives for vehicle dynamics problems using symbolic mathematics tools, which has helped overcome this difficulty e.g. [66, 76, 83].

Direct Direct optimisation takes the 'first discretise, then optimise' approach [97]. This approach transcribes the continuous OCP into a finite-dimensional nonlinear programming problem (NLP), which is then solved with a NLP solver. The states and controls are discretised onto the finite-dimension grid, after which a continuous control history may be constructed by interpolation. Equality constraints are introduced to ensure continuity at the nodes between the grid. Integrals are replaced by approximations.The problem becomes finite and controls that minimise the objective function at the grid points, considering constraints is to be found. Satisfaction of the Karush-Kuhn-Tucker (KKT) conditions (detailed in [95]) and the Lagrangian (combination of the objective function and constraint equations) exhibiting positive curvature in feasible directions guarantees an optimal solution [67].

Unfortunately, it results in a parameter optimisation problem composed of a very large number of variables (although sparsity can be leveraged) [97] and the solution is only an approximation to the solution of the original continuous problem.

The advantage to the direct approach is that it is simpler to implement and more robust. Gradient information is also not essential. It facilitates the use of state-of-the-art methods for NLP solution, and is able to treat inequality constraints and multi-point constraints in an easier way.

Comparison Recent studies have employed both approaches successfully for vehicle dynamics studies, which implies that either approach could be adopted, depending on the experience and skills of the engineer. Since there was no established optimal control working practice in the Advanced Vehicle Engineering Centre at Cranfield University, a direct optimisation approach was adopted for the work during this thesis, because it offers a more accessible start to the inexperienced.

With regards to the relative performance of indirect and direct methods, a recent conference presentation has directly compared the two [99]. They implement the direct method using GPOPS-II [100] in conjunction with IPOPT solver [101] and compare it against the PINS-Xoptima approach [102]. Three optimal control problems were compared: minimum-time to roll of a motorcycle; track curvature reconstruction; lap-time minimisation of a vehicle. It was found that both approaches give the same results in practical terms. GPOPS-II is generally slower than PINS. The robustness in the presence of noise on the initial guess did not show any particular trend. Finally, GPOPS-II gives a result that is able to approach the constraints more closely by virtue of the barrier-method employed by IPOPT.

Scaling

The performance of an algorithm for solving optimal control problems can be highly dependent on the formulation; if changes in states in a given direction result in a greater degree of variation in f, the objective function, than another direction, the problem is poorly scaled and will make finding a solution more difficult [95]. Difference in rates of processes in physical systems are a cause of poor scaling and must be modified to improve scaling. Steepest descent algorithms are sensitive to scaling while those based on Newton's method are not [95].

The optimal control problem must be preconditioned to improve the performance of the optimisation algorithm [96]. Decision variables must be as equally-weighted as possible to minimise errors in determination of the search direction to improve rate of convergence. Scaling the state matrix to improve conditioning is performed to ensure all decision variables are $\mathscr{O}(1)$. The scaling scheme used in this work is detailed in Appendix A.7.

4.2.3 Nonlinear Programming

A nonlinear programming problem seeks to find a finite number of variables to minimise an objective function without violation of constraints.

Sequential Quadratic Programming (SQP) is a method for the solution of direct optimisation problems. SQP starts with an approximation, or "guess", of the optimal controls. The objective and constraint functions are expanded using the Taylor series about the control guess, but limited such that the new approximations to the objective function is quadratic and the constraints linear. This quadratic subproblem (a nonlinear programming problem, or NLP) is solved to find a set of controls that gives a solution close to the optimum. Thus a series of quadratic subproblems are solved, with a line-search method used to rapidly seek the optimum. Another globalization mechanism for refining the quadratic subproblem is the trust-region method [95, 103].

SNOPT [104] (Sparse Nonlinear Optimiser) is a popular solver for SQPs (especially trajectory optimisation in aerospace), utilising a quasi-Newton approximation to the Hessian of the Lagrangian, as finding derivatives symbolically is highly computationally demanding. It can cope with thousands of constraints and up to ~ 2000 degrees of freedom.

An alternative method are the interior-point solvers (e.g. IPOPT [101]), used in [36, 45]. The advantage of the IPOPT solver is evident in the manner in which it handles con-

straints. The log-barrier method approximates hard constraints with a soft-constraining penalty function that tends to infinity as the constraint approaches. As the problem converges to the solution, a parameter, τ, is reduced, such that the log-barrier approaches the hard constraint that it approximates progressively more closely [97]. SNOPT is adopted for chapters 4 and 5.

GPOPS-II Software *GPOPS − II* software is used to solve the optimisation problems in this thesis. It is based in MATLAB, and utilises the direct method [100]. The continuous-time-optimal control problem is converted to a large sparse NLP using the Legendre-Gauss-Radau quadrature orthogonal collocation method for the mesh definition. Quasi-Newton (first derivative) or Newton (second derivative) NLP solvers can be employed for NLP solution (SNOPT and IPOPT, respectively). All derivatives can be approximated using sparse finite-differencing of the optimal control problem functions, or derivative equations can be supplied directly. It assumes all functions have continuous first and second derivatives [100]. *GPOPS − II* uses *hp*-adaptive Gaussian quadrature collocation that allows both the number of mesh intervals and degree of approximating polynomial within each mesh interval to be varied depending on required accuracy, which significantly increases efficiency [100].

A description of the optimal control problem is supplied by the user. The problem properties are found and state, control, time and parameter dependencies of the control problem functions are determined. The NLP is scaled and then the OCP transcribed into a large sparse NLP. The NLP is solved on an initial mesh before being reverse transcribed and the error in the discrete approximation estimated. If the user-defined error tolerance is not met, a new mesh is determined and the same procedure repeated, if is met, the solution is found.

4.3 Application: Minimum-time optimal control

This section describes the mathematical formulation of the optimal control problem to simulate the expert driver manoeuvring the TV vehicle around a track section in minimum time.

4.3.1 Control Configurations

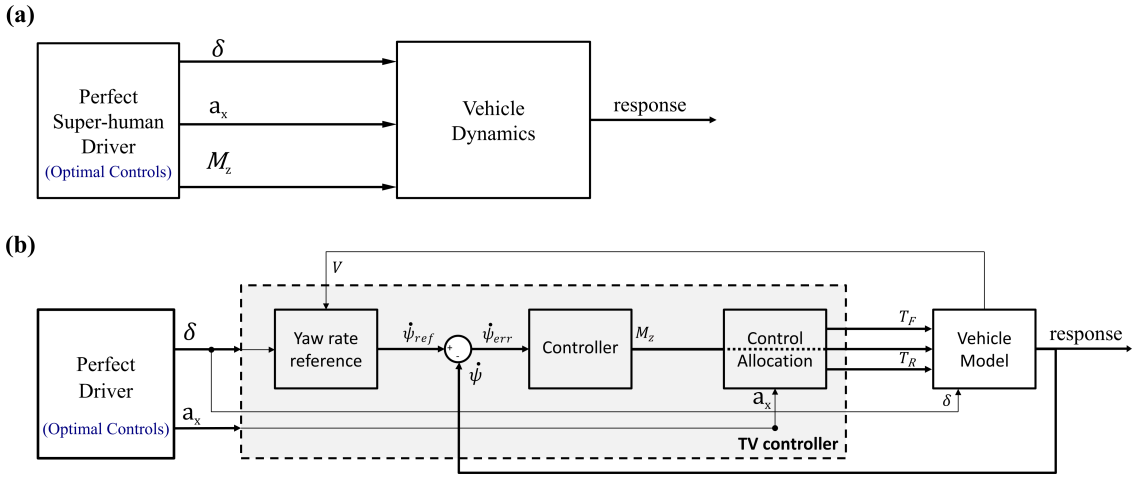

Figure 4.1: In the open-loop OCP formulation (a), the control inputs are steering rate, acceleration demand and direct yaw moment, M_z. In the closed-loop OCP (b), the control inputs to be optimised are steering rate and acceleration demand. The front and rear longitudinal forces are determined by the control allocation; the direct yaw moment, M_z, by the Controller which follows a yaw rate reference corresponding to the desired handling behaviour.

To meet the objectives stated at the beginning of the chapter of generating baseline optimal trajectories, assessing passive charactistics on controlled behaviour, and evaluating the effect of modifying the yaw rate reference of the TV controller, two OCP formulations are required. Figure 4.1(a) shows the open-loop *control method* [29, 30] from which the maximum theoretical performance potential of the vehicle with TV may be ascertained– by determining the optimal control inputs that must be applied to the vehicle *directly*. The

efficient cause[1] of this control is a 'perfect', 'super-human' driver. 'Perfect', defined as the ability to operate the vehicle at the limit of adhesion at every instant without making errors. 'Super-human', since he has direct authority over individual wheel torques (T_{ij} in (4.38)). This formulation is used to generate the baseline optimal trajectories for TV in §4.4.1, and to analyse the effect of passive handling balance on controlled response in §4.4.3.

Figure 4.1(b) shows the closed-loop *control algorithm* formulation [29, 30]. Perfect open-loop control is a-causal and hence only of theoretical interest; a causal active yaw control system is required to determine the torques applied at each wheel to follow the desired high-level motion objectives; in this case yaw rate, $\dot{\psi}$, and total longitudinal torque demand, T_x. The specific component of interest for this research is the yaw rate reference and by incorporating a closed-loop controller into the system dynamics of the OCP, the performance of the reference may be evaluated (§4.5). To evaluate the reference, a 'perfect' driver is once again required but merely a 'human' one, with authority over only longitudinal torque demand and steering, not individual axle torques/forces which are now outputs of the control allocation. Further detail is given in §4.5.

4.3.2 Mathematical Formulation

To find the optimal controls and corresponding vehicle states required to achieve a specified manoeuvre in minimum-time, optimal control problems are mathematically formulated as follows. Consider a dynamic system in the general state-space form:

$$\dot{\mathbf{x}} = \mathbf{f}[\mathbf{x}(t), \mathbf{u}(t)], \tag{4.12}$$

where $\mathbf{x}$ and $\mathbf{u}$ are state and control vectors respectively and t is the elapsed time.

[1] Aristotle. Physics, 195a

The state and control vectors for the vehicle model configurations are

$$\mathbf{x} = \{V_x, V_y, \dot{\psi}, x_R, y_R, \theta_R, s_n, \chi, \delta, t\}^T, \tag{4.13}$$

$$\mathbf{u} = \{a_x, M_z, \dot{\delta}\}^T, \tag{4.14}$$

with the equations of motion (2.1-2.3) for the 3DOF vehicle model in §2.2.

Although the objective is to minimise time, a change of the independent variable is performed. Elapsed time, t, is transformed to distance travelled along the road centreline, s, such that the formulation must now be expressed with respect to s (see Figure 4.2). Two related coordinates are required to map differential equations from time to distance: lateral position relative to the road centreline, s_n, and the angle of the vehicle relative to the road centreline, χ [63, 105], explained in more detail in the next subsection. This change of coordinate reference frame from vehicle-centred to road-centred 'curvilinear coordinates' is made to ensure affine road boundary constraints.

Thus the dynamic system in (4.12) becomes:

$$\dot{\mathbf{x}}(\mathbf{s}) = \mathbf{f}[\mathbf{x}(s), \mathbf{u}(s)]; \tag{4.15}$$

The OCP now seeks to find the control vector sequence to minimise the cost function:

$$J = \phi[\mathbf{x}(s_0, s_f)] + \int_{s_0}^{s_f} L[\mathbf{x}(s), \mathbf{u}(s)], \tag{4.16}$$

subject to initial and final conditions:

$$\mathbf{x}(s_0) = \mathbf{x}_0, \qquad \mathbf{x}(s_f) = \mathbf{x}_f, \tag{4.17}$$

and equality and inequality constraints:

$$\mathbf{p}[\mathbf{x}(s),\mathbf{u}(s)] = 0, \qquad \mathbf{g}[\mathbf{x}(s),\mathbf{u}(s)] \leq 0, \tag{4.18}$$

where 0 and f subscripts denote initial and final values, ϕ denotes the Mayer term and L denotes the Lagrange integral term.

In the current study the cost function is represented only by the Lagrange integral term to minimise time to complete the manoeuvre, mapping dynamic equations from the independent variable of time to distance along the road centreline:

$$J(t) = \int_{t_0}^{t_f} dt \qquad \mapsto \qquad J(s) = \int_{s_0}^{s_f} \frac{1}{\dot{s}}\, ds \tag{4.19}$$

It is assumed that the driver is capable of instantaneously switching between accelerator and brake. Additional constraints include steering rate bandwidth limited to $1Hz$ [106, 107] and motor power and motor torque limited by a power curve:

$$|\dot{\delta}| \leq \dot{\delta}_{max} \qquad |F_{xj}|V_x \leq 2P_{max} \qquad |T_{xj}| \leq 2T_{max} \qquad |s_n| \leq s_{n,max} \tag{4.20}$$

where P_{max}, T_{max} denote the maximum power and torque of the individual motors respectively (one per wheel), and $s_{n,max}$ is the half-width of the road.

The boundary conditions required to keep the vehicle within the road boundary, and to start the manoeuvre in a straight line with no yaw rate or lateral velocity are given in Table 4.1.

$\mathbf{x}$	$\mathbf{x}_0$	$\mathbf{x}_f$
s	0	s_f
Vx	free[b]	free
Vy	0	free
$\dot{\psi}$	0	free
s_n	free	free
χ	0	free
x_R	free	free
y_R	free	free
θ_R	$\frac{\pi}{2}$	free
$\dot{\delta}$	free	free

Table 4.1: Boundary conditions

Control Allocation

Longitudinal tyre forces are determined from the longitudinal acceleration demand, a_x distributed between front and rear axles according to two Control Allocation strategies. A 50:50 static distribution is used for the vehicle without TV control:

$$F_{xj} = \frac{ma_x}{2}, \tag{4.21}$$

where F_{xj} is the longitindal force on the j axle. For TV, front-rear torque vectoring is modelled by distributing torques front-rear by a CA that allocates longitudinal forces in proportion to the normal load on the axle (hereafter referred to as *CA* F_z), found to be the optimal distribution in [45]:

$$F_{xj} = ma_x \frac{F_{zj}}{F_{zf} + F_{zr}}. \tag{4.22}$$

Neglecting wheel spin axis rotational inertia, wheel torques become:

$$T_{xj} = F_{xj} R_w, \tag{4.23}$$

where R_w is the rolling radius of the tyres.

Curvilinear coordinate frame

The change of variables to curvilinear coordinates is standard practice for similar minimum-time studies e.g. [66, 74, 108]. The curvilinear coordinate frame is shown in Figure 4.2, and time derivatives are defined as:

$$\dot{s} = \frac{(V_x cos\chi - V_y sin\chi)}{1 - s_n \kappa_R}, \qquad \dot{s}_n = V_x sin\chi - V_y cos\chi, \qquad \dot{\chi} = \dot{\psi} - \kappa_R \dot{s}, \tag{4.24}$$

$$\text{where } V_x = V cos\beta, \qquad V_y = V sin\beta, \tag{4.25}$$

and V is the vehicle speed, κ_R is the instantaneous path curvature of the road centreline, $\dot{\psi}$ is the vehicle yaw rate and β is the sideslip angle at the CM. In Figure 4.2, s_t, denotes the tangent to the road centreline at point s. Equations of motion (general equation 4.15)

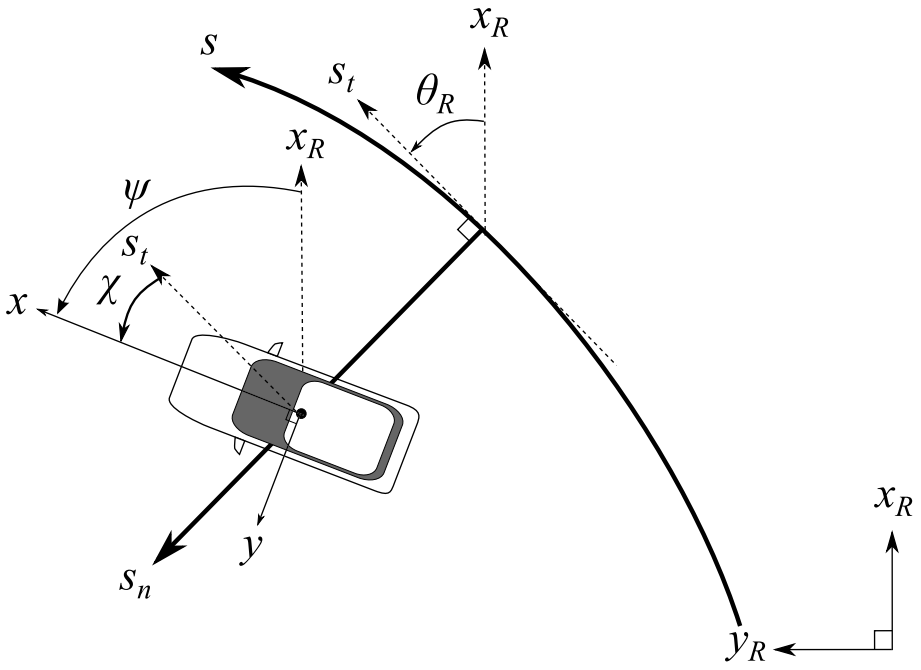

Figure 4.2: Curvilinear coordinate definition; independent variable, s, distance travelled along road centreline

and curvilinear coordinates (4.24) are transformed from a time-base to a distance-base as follows:

$$\frac{d\zeta}{ds} = \zeta' = \frac{d\zeta}{dt}\frac{dt}{ds} = \dot{\zeta}\dot{s}^{-1} \tag{4.26}$$

where ζ is any state. Control-related state distance derivatives, δ and t, are calculated:

$$\frac{d\delta}{ds} = \delta' = \frac{\delta}{dt}\frac{dt}{ds} = \dot{\delta}\dot{s}^{-1}, \tag{4.27}$$

$$\frac{dt}{ds} = t' = \dot{s}^{-1}. \tag{4.28}$$

Distance derivatives of the global coordinates of the road centreline are given as:

$$x'_R = \cos\theta_R, \qquad y'_R = \sin\theta_R, \qquad \theta'_R = \kappa_R, \tag{4.29}$$

where x_R, y_R are the global coordinates on two nominal orthogonal axes relative to an origin and θ_R is the heading relative to that origin.

4.4 Results: Open-loop control method

In this section, the absolute potential of the TV system is determined. This is the *open-loop control method* described in §4.3.1 (and Fig. 4.1(a)). This will allow the torque vectoring performance to be compared against the vehicle where TV is inactive in §4.4.1. It will also allow analysis of what effect the passive, steady-state understeer gradient has on the controlled response in §4.4.3.

A U-turn manoeuvre (Figure 4.3) with $R = 35$m is navigated. In general terms, the vehicle enters the manoeuvre on the right at high speed in a straight line, exerting maximum braking torque. As the speed reduces and the road curvature increases, braking

is reduced, steering is gradually applied until the maximum curvature point is reached and the vehicle has moved to the inside road boundary. After this midpoint (where lateral acceleration is maximal), torque is gradually applied, steering is reduced to zero as high-speed, straight-line running is approached and the vehicle returns to the outside road boundary.

4.4.1 Torque Vectoring active vs. inactive

The optimal control problems for TV active vs. TV inactive set-ups are presented for comparison in this section. The *TV* set-up is formulated as in 4.3.2, with cost function (4.16). The vehicle with TV inactive is optimised in two configurations: the first with 50:50 control allocation (recall (4.21)), hereafter referred to as '*NoTV* 50*:*50'); the second with control allocation proportional to normal load (recall (4.22) for front-rear TV), hereafter referred to as '*NoTV* F_z'). Whilst *CA* F_z may be considered an 'active' distribution, the purpose was to use a control allocation that was common to both TV-active and TV inactive configurations so that the contribution from the direct yaw moment in the TV case may be isolated for comparison. The optimally-controlled *TV* vehicle emulates left-right TV capability by direct yaw moment, M_z.

Thus three open-loop control method optimisations are now presented for comparison. With torque vectoring capability, the manoeuvre time (8.827s) is 0.374s (to 3 significant figures) faster than *NoTV* 50*:*50 (9.201s). This is a significant benefit for just one corner and when extrapolated over a whole lap of 10-15 turns, would give a benefit of the order of $\sim 3-4$s, which is considerable in the racing context. In this analysis, two plots will be examined.

First, Figure 4.4 overlays states, controls and calculated quantities for all optimisations. A dynamic scenario is considered, yet the steady-state understeer gradient calcu-

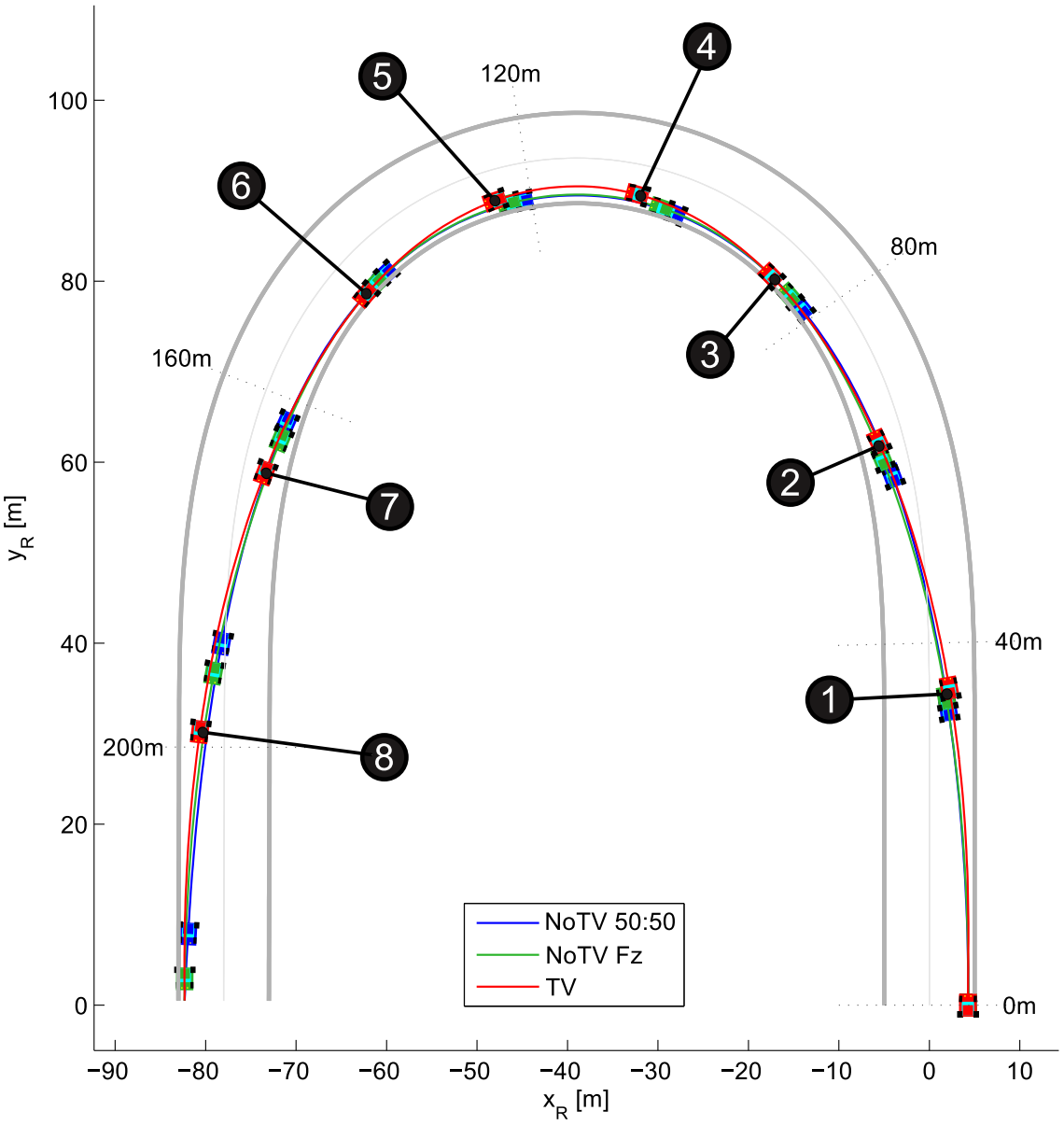

Figure 4.3: Path trajectory comparison for: TV inactive (50:50 torque distribution); TV inactive (torque distribution in proportion to normal load); optimal TV active.

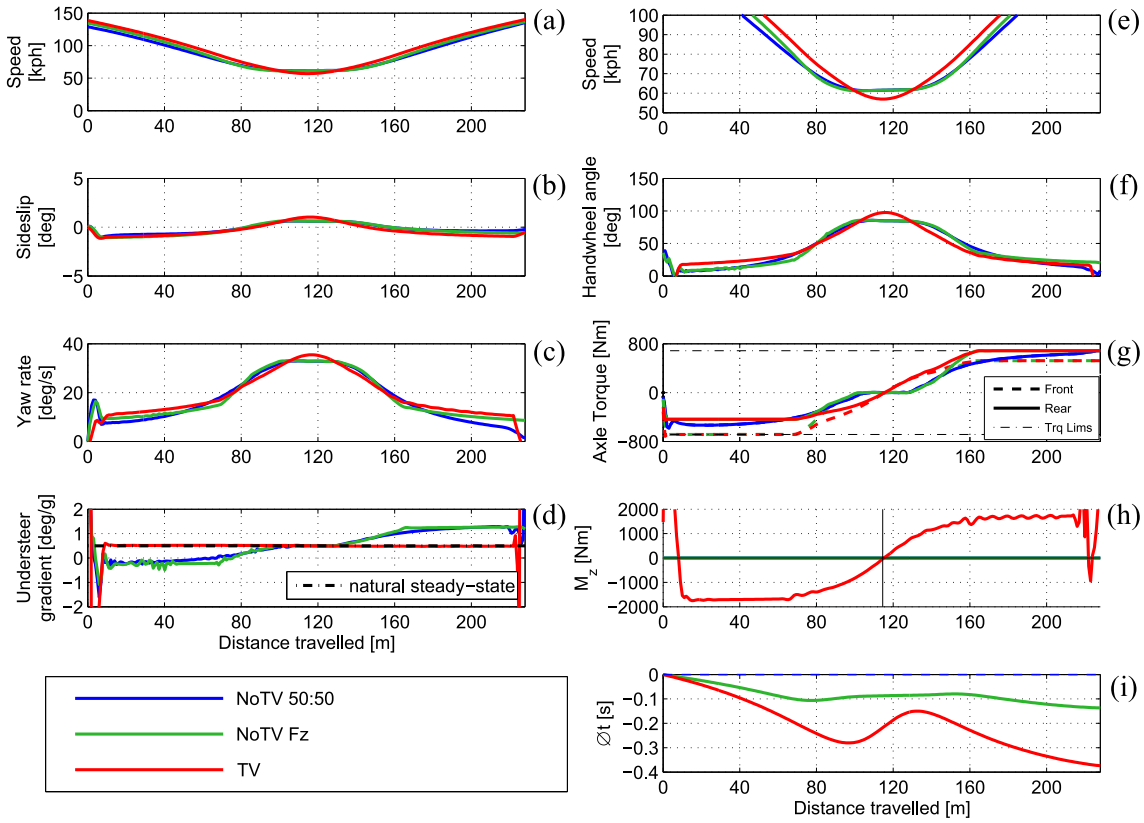

Figure 4.4: States and controls trajectory comparison for: TV inactive (50:50 torque distribution); TV inactive (torque distribution in proportion to normal load); optimal TV active.

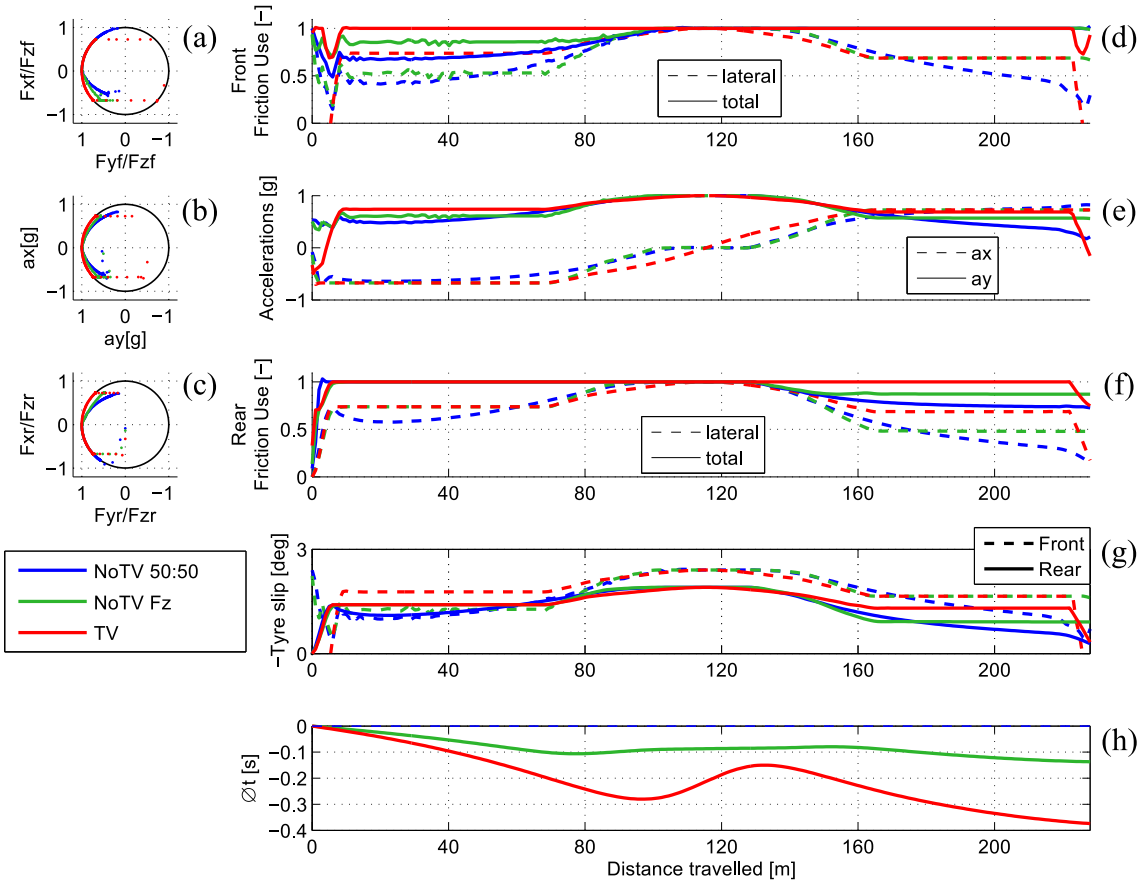

Figure 4.5: Friction utilisation comparison for: TV inactive (50:50 torque distribution); TV inactive (torque distribution in proportion to normal load); optimal TV active

lated at every instant is still useful in giving an indication of vehicle handling behaviour, defined as follows [6]:

$$K_{inst}^{SS} = \frac{\frac{V\delta}{\dot{\psi}} - L}{V^2}. \tag{4.30}$$

K_{inst}^{SS} is plotted in Figure 4.4(d). Further insight is drawn from plots of friction utilisation, as shown in Figure 4.5, for each tyre separately. Friction utilisation is defined as the lateral, longitudinal or resultant force divided by the total force available on the wheel:

$$\mu_{ij} = \frac{F_{ij}}{\mu_{max} F_{iz}}, \tag{4.31}$$

where $i \in [F,R]$; $j \in [x,y]$ and μ_{max} is the tyre-road friction coefficient. Also plotted in Figure 4.5 are CM accelerations and tyre slip angles (the negative of the slip angles are plotted for clarity).

With reference to Figures 4.4(a) and 5(g), looking first of all at the vector velocity and torque traces, it is clear that *TV* is able to sustain a greater level of total drive/brake torque and hence can both start and exit the manoeuvre at higher speeds.

There is an interesting difference in path trajectory at the midpoint (Fig. 4.3): the vehicles with TV inactive take a tighter line, hugging the inside edge of the track for $80 < s < 130$m, whilst *TV* takes more of a 'double apex', reaching a point of maximum path curvature ($\max(\kappa_{path})$, at point of minimum speed, V_{min}) at $s = 0.5 s_f$. *TV* has a lower V_{min} (see larger scale in Figure 4.4(e)), since in effect its maximum path curvature, κ_{path}, is greater than the TV-inactive paths: $V_{min} \approx \sqrt{\frac{a_{centripetal}}{\max(\kappa_{path})}}$. The TV-inactive vehicles are able to maintain higher speed over $90 < s < 120$m and thus gain time back during this portion of the manoeuvre. With reference to Figure 4.4(c), yaw rate is increased gradually with respect to s for *TV*, since the path curvature increases more gradually also. The TV-inactive vehicles exhibit steady-state behaviour here, maintaining constant yaw, sideslip

and vehicle speed. The *TV* vehicle is able to accelerate and brake much more aggressively than the TV-inactive, which is forced to coast during the constant radius section.

NoTV F_z, with 9.064s manoeuvre time, is 0.137s (3 s.f.) faster than *NoTV* 50:50, attributable to the superior CA. *NoTV* F_z is 0.237s (3 s.f.) slower than *TV* and this time difference directly attributable to left-right torque vectoring (emulated by M_z).

It is clear that *NoTV* F_z is able to use more friction at the front under braking than *NoTV* 50:50 (Fig. 4.5(d)) and more friction at the rear under acceleration (Fig. 4.5(f)). This is because it considers load transfer effects and hence can sustain greater longitudinal acceleration (Fig. 4.5(c)). Hence all time is gained by *NoTV* F_z over *NoTV* 50:50 when acceleration is non-zero (Fig. 4.5(h) green line).

K_{inst}^{SS} is plotted in Figure 4.4(d): the key finding is that *TV* is able to achieve the natural steady-state understeer gradient, K_{nat}^{SS} (2.4), throughout the manoeuvre whereas the TV-inactive vehicle handling exhibits oversteer relative to K_{nat}^{SS} under braking and understeer relative to K_{nat}^{SS} during acceleration, an effect well-known due to longitudinal load transfer effects [65, 109, 110]. It is interesting to note that yaw rate and handwheel angle have a strong impact on the magnitude of the understeer gradient, despite seemingly small differences of only a few degrees. The greatest difference between *TV* and TV-inactive understeer gradient is at highest longitudinal accelerations of the order 0.5deg/g.

Examination of slip angles in Figure 4.5(g) is another useful tool for understanding the dynamic handling balance, since understeer gradient is related to slip angles from the steady-state single-track definition [6]:

$$K_{inst}^{SS} = (\alpha_f - \alpha_r)/a_y. \tag{4.32}$$

Referring to Figures 4.5(f) and 4.5(g), under braking the vehicles with TV inactive have a reduced rear lateral friction capability due to longitudinal load transfer and therefore

friction use is saturated at the rear. Assuming the lateral acceleration trajectory is common to both scenarios, when α_r is increased and α_f reduced, an oversteer balance relative to K_{nat}^{SS}(0.5deg/g) results. The opposite is true during acceleration. M_z, shown in Figure 4.4(h), is stabilising under braking and destabilising during acceleration in order to counteract load transfer effects and achieve a constant K_{inst}^{SS} equal to K_{nat}^{SS}. Figure 4.6 shows

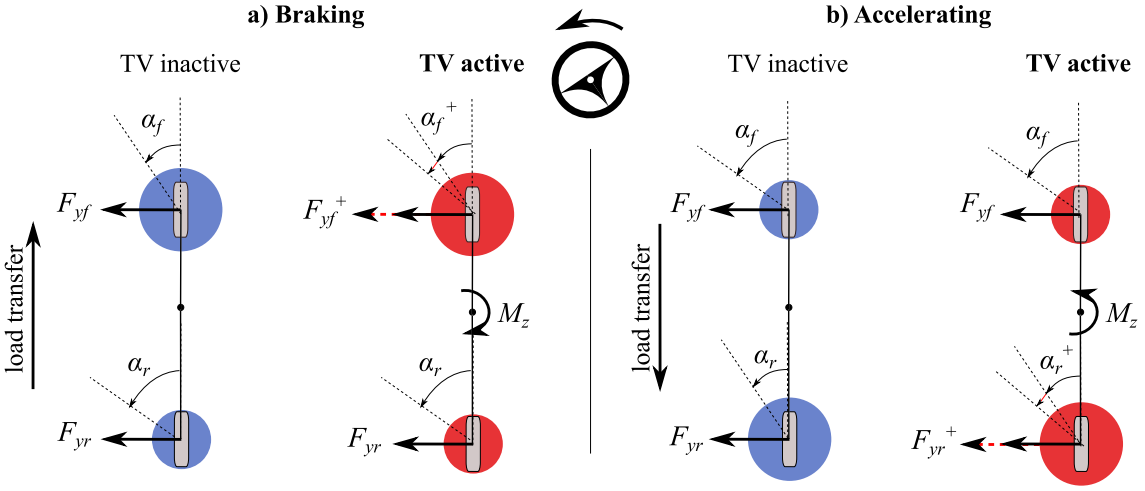

Figure 4.6: Analysis: TV yaw moment effect on lateral force potential and slip angles and therefore understeer gradient for a left turn. Red arrows indicate additional lateral force and associated slip angle that TV is able to generate. Circles indicate friction levels available due to load transfer.

how yaw moment effects lateral force and slip angle for the left turn. Under braking (Fig. 4.6(a)), stabilising M_z is applied clockwise for TV, such that larger lateral force from the front tyres can be applied in the direction of the turn to maintain yaw dynamic equilibrium. As a result, Figures 4.5(g), (d), (f) and Figure 4.4(d) respectively show larger front slip angles are developed, tyre friction availability maximised, and K_{inst}^{SS} exhibits a greater degree of understeer for TV with respect to both TV-inactive cases. Figure 4.6(b) shows the acceleration case. Figure 4.5(g) shows that the TV-inactive vehicles develops larger slip angles at the front than rear due to load transfer (understeer relative to K_{nat}^{SS}). *TV*, in contrast, is able to develop greater slip angle at the rear than TV-inactive to balance the

destabilising yaw moment and hence make full use of the friction available, counteracting the tendency to understeer. *NoTV* F_z is able to maintain a slightly greater difference between front and rear slip angles than *NoTV* 50:50 but not to the same degree as *TV*.

Inspection of Figure 4.4(h) shows that magnitude of yaw moment is proportional to a_x. This trend of direct yaw control effecting a stabilising yaw moment under deceleration and a destabilising yaw moment under acceleration is confirmed by findings for a similar electric vehicle topology analysed in [45], and a brake torque vectoring differential study for a RWD conventionally-powered touring car in research by Tremlett et. al. [64,78,111] and Kaspar et. al. [112]. De Novellis et. al. [36] describe a similar finding for this yaw moment trend when a yaw rate reference independent of longitudinal acceleration is used. In the seminal work of Shibahata et. al. [16], it was demonstrated using the β-method, that for a 6DOF vehicle model with nonlinear tyres and direct yaw control on the rear axles, adverse effects of longitudinal (and lateral) load transfer effects could be overcome.

4.4.2 Effect of yaw moment constraint

In the previous subsection, it was assumed that yaw moment could be applied without restriction. This section explores the influence of constraints on yaw moment on the open-loop *control method* results. The OCPs were rerun with two additional path constraints:

$$M_z \leq M_{z,max}, M_z \geq M_{z,min}. \tag{4.33}$$

Limits of yaw moment, $M_{z,max}$ and $M_{z,min}$ were calculated as follows. The philosophy adopted prioritises driver acceleration (longitudinal demand) over delivery of yaw moment [93]. First, the limits on longitudinal torque that can be applied on each 'track' are

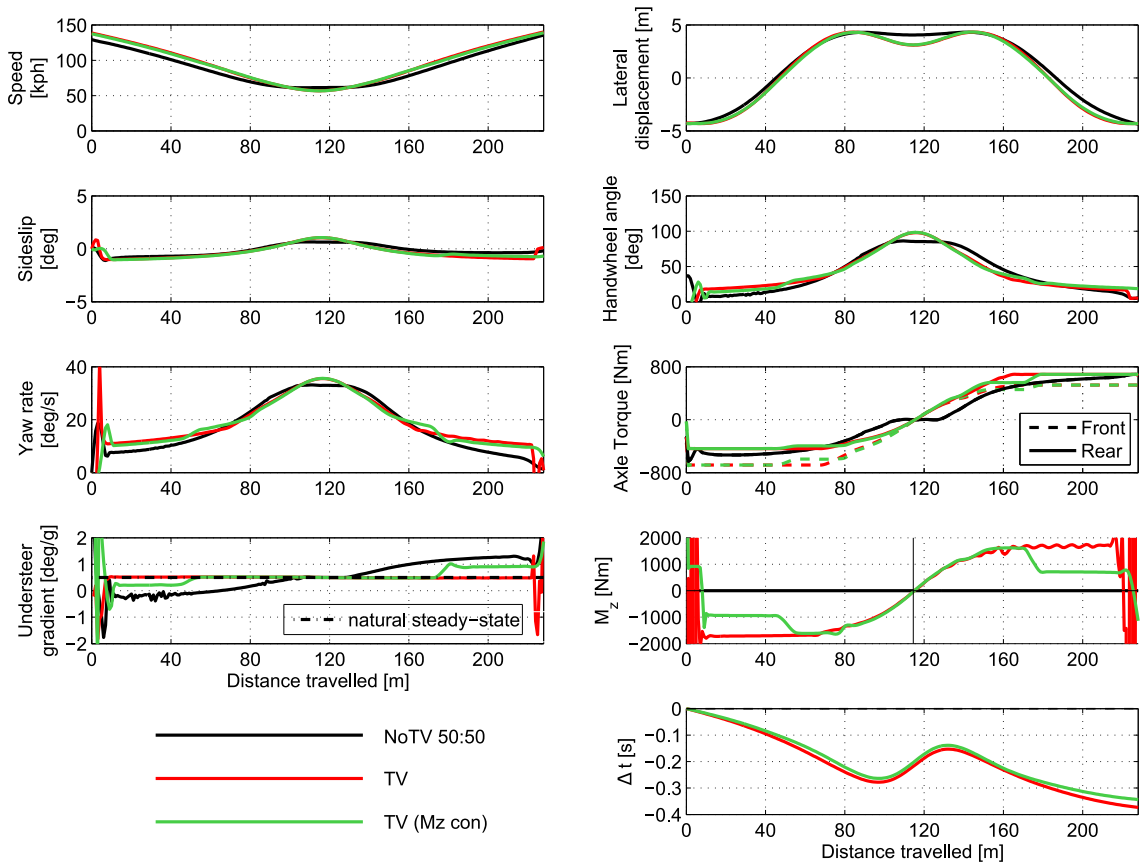

Figure 4.7: Comparison of TV-inactive, TV and TV including constraints on yaw moment control input

calculated (these are identical, since there is only one track):

$$T_{i,max} = min\left(T_{i,friction}, T_{i,torque}, T_{i,power}\right) \tag{4.34}$$

where $T_{i,friction}$, $T_{i,torque}$, $T_{i,power}$ are...$T_{i,min} = -T_{i,max}$, $i = [l,r]$.

$$M_{z,max} = \frac{w}{2}\left(\frac{T_{r,max}}{R_w} - \frac{T_{l,min}}{R_w} - sgn(F_x)F_x\right) \tag{4.35}$$

$$M_{z,min} = \frac{w}{2}\left(\frac{T_{r,min}}{R_w} - \frac{T_{l,max}}{R_w} + sgn(F_x)F_x\right) \tag{4.36}$$

where F_x is the longitudinal force demand (4.22).

Including yaw moment constraints in addition gives results shown in Figure 4.7. For the majority of braking into the turn and acceleration out, K^{SS}_{ref} is able to be maintained. The main observation is that $0 < s < 50$m, and $170 < s < s_f$m, yaw moment is limited due to motor torque limits (as full torque is demanded at these points). The understeer gradient shows a similar shape to *NoTV 50:50* but to a milder extent; the effect on manoeuvre time is a small proportion of the benefit of *TV* over *NoTV 50:50*.

There are in fact two points during the manoeuvre where yaw rate is actually *higher* when yaw moment constraints are considered, where $s \in [50,75]$m and $s \in [150,175]$m. In the first of these periods, the 'driver' eases off maximum braking torque earlier, allowing a greater yaw moment earlier.

4.4.3 Effect of passive handling characteristic

It has been demonstrated that *TV* is 0.374s faster than *NoTV* 50:50, for a passive steady-state understeer gradient $K^{SS}_{pas} = 0.5°$/g.

Since TV extends the performance envelope of the vehicle by the correct distribution

Parameter	Unit	Values								
K_{pas}^{SS}	°/g	-2.0	-1.5	-1.0	-0.5	0.0	0.5	1.0	1.5	2.0
η_f	rad^{-1}	24	24	24	24	24	24	24	24	24
η_r	rad^{-1}	13	15	17	20	24	30	41	63	142
B_f	-	16.4	16.4	16.4	16.4	16.4	16.4	16.4	16.4	16.4
B_r	-	8.9	10.1	11.7	13.6	16.4	20.7	28.0	43.6	97.5

Table 4.2: Tyre parameters for modifying passive steady-state understeer gradient

of tyre forces, the pertinent question is whether there is a certain K_{pas}^{SS} for which tyre force distribution by TV gives the greatest performance envelope and therefore delivers a faster manoeuvre time. To answer this question, optimal control problems (with TV active) are formulated and solved for a range of passive understeer characteristics. This is achieved by modifying tyre parameters.

Optimisations were run for TV and *NoTV* 50:50 for $K_{pas}^{SS} = \{-2.0 : 0.5 : 2.0\}$ by altering front and rear cornering coefficient values η_f and η_r and corresponding values of front and rear Pacejka stiffness factors B_f and B_r according to table 4.2 (assuming that the cornering coefficient is constant), where:

$$\eta_f = B_f CD \qquad \eta_r = B_r CD. \tag{4.37}$$

The range in the understeer direction ranges from sports cars (typically neutral steer) to representative of passenger road cars. In the oversteer direction, the values are intended as a theoretical investigation, as these values are not in the intended design range of real vehicles. Nevertheless, poor maintenance of correct tyre pressures, unevenly-laiden vehicles and possibly other mechanical wear could result in negative understeer gradient vehicles in everyday life. Table 4.3 shows the manoeuvre time and final time difference, Δt_f, with respect to the baseline natural balance, $K_{nat}^{SS} = 0.5$deg/g. With reference to Table

4.3, Δt_f for *NoTV* 50:50 sit within $-0.008/+0.004$s (3s.f.) relative to the baseline natural balance, $K_{nat}^{SS} = 0.5$deg/g; the greater the balance from the baseline, the greater Δt_f, with the trend of oversteer faster than understeer. The same trend is true for *TV* but within a tolerance half an order of magnitude smaller (± 0.001s (3s.f.)), too small to reliably differentiate between vehicle dynamics behaviour and OCP phenomena such as discretisation or mesh errors. Figure 4.8 shows states, controls and calculated quantities for the *TV* case and Figure 4.9 shows corresponding friction utilisation and tyre slip angles. Friction is fully used in all cases (Fig. 4.9(d) and (f)). Figure 4.8(d) shows that *TV* K_{inst}^{SS} follows K_{nat}^{SS} closely for every case.

Remark 1 *Focusing only on the TV results, the main differentiator between the optimisations is the sideslip angle; there is a clear trend from nose-out sideslip to increasing tail-out sideslip as* K_{nat}^{SS} *progresses from* $+2.0$ *to* -2.0*deg/g (Fig. 4.8(c)). This effect is complemented by handwheel angle, which is increased with natural understeer gradient, whilst* M_z *shows little variation. This is an important result since it demonstrates that the control yaw moment (vehicle authority) is used to counteract the load transfer effects on understeer gradient, whilst the steering angle (driver control authority) is used to 'fine-tune' the handling response to achieve understeer/oversteer.*

It must be reiterated that the open-loop set-up with M_z directly applied is unrealisable in the real world for reasons noted in section 4.3.1; nonetheless it demonstrates what the open-loop control method must do to achieve optimality in terms of time minimisation.

Natural handling balance	K_{nat}^{SS} (°/g)	NoTV 50:50 Time (s)	NoTV 50:50 Δt_f [a] (s)	TV Time (s)	TV Δt_f [a] (s)
Baseline - 2.5°/g	-2.0	9.193	-0.008	8.8261	-0.0008
Baseline - 2.0°/g	-1.5	9.194	-0.007	8.8263	-0.0006
Baseline - 1.5°/g	-1.0	9.196	-0.005	8.8266	-0.0003
Baseline - 1.0°/g	-0.5	9.197	-0.004	8.8267	-0.0002
Baseline - 0.5°/g	+0.0	9.199	-0.003	8.8266	-0.0003
Baseline Balance	+0.5	9.201	+0.000	8.8269	+0.0000
Baseline + 0.5°/g	+1.0	9.202	+0.001	8.8273	+0.0004
Baseline + 1.0°/g	+1.5	9.204	+0.003	8.8289	+0.0020
Baseline + 1.5°/g	+2.0	9.206	+0.005	8.8279	+0.0010

Table 4.3: Effect of passive handling characteristic
[a]Time difference with respect to open-loop baseline $K_{nat}^{SS} = 0.5$°/g.

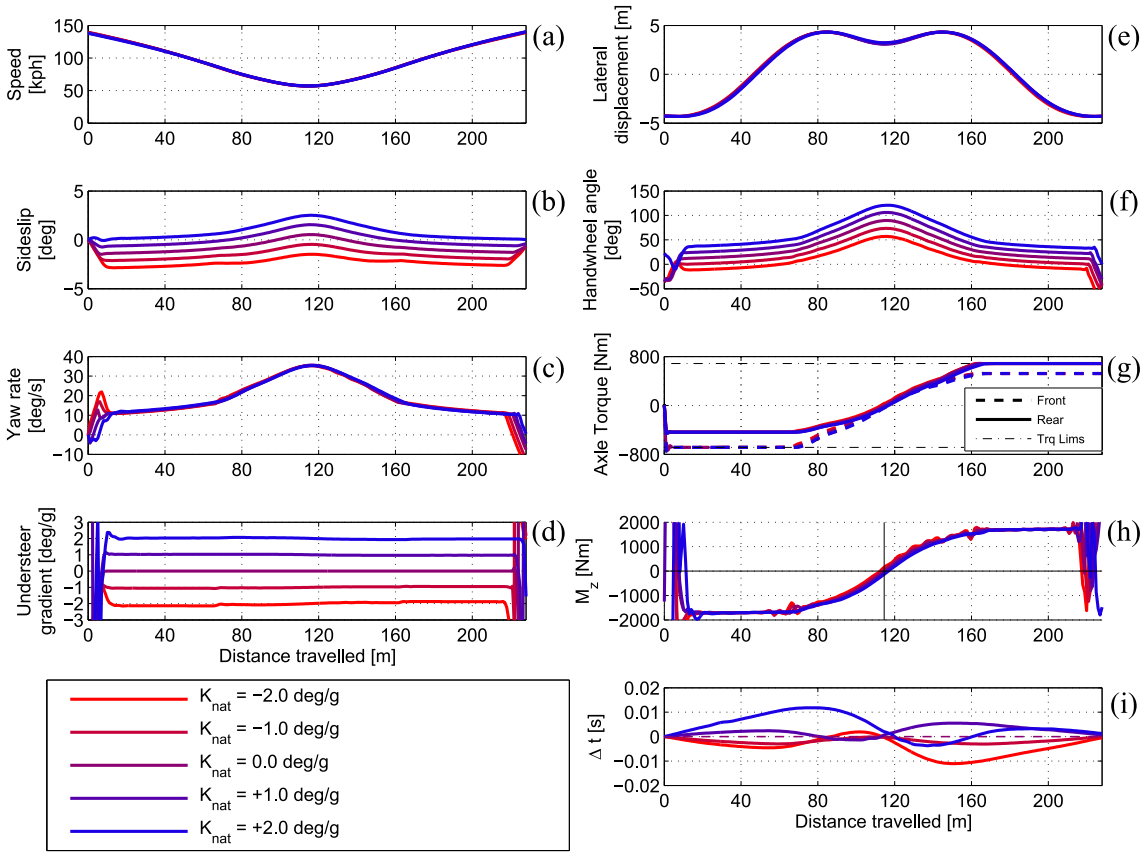

Figure 4.8: Effect of varying passive understeer gradient (defined by steady-state cornering stiffness) on torque vectoring-controlled vehicle: states and controls

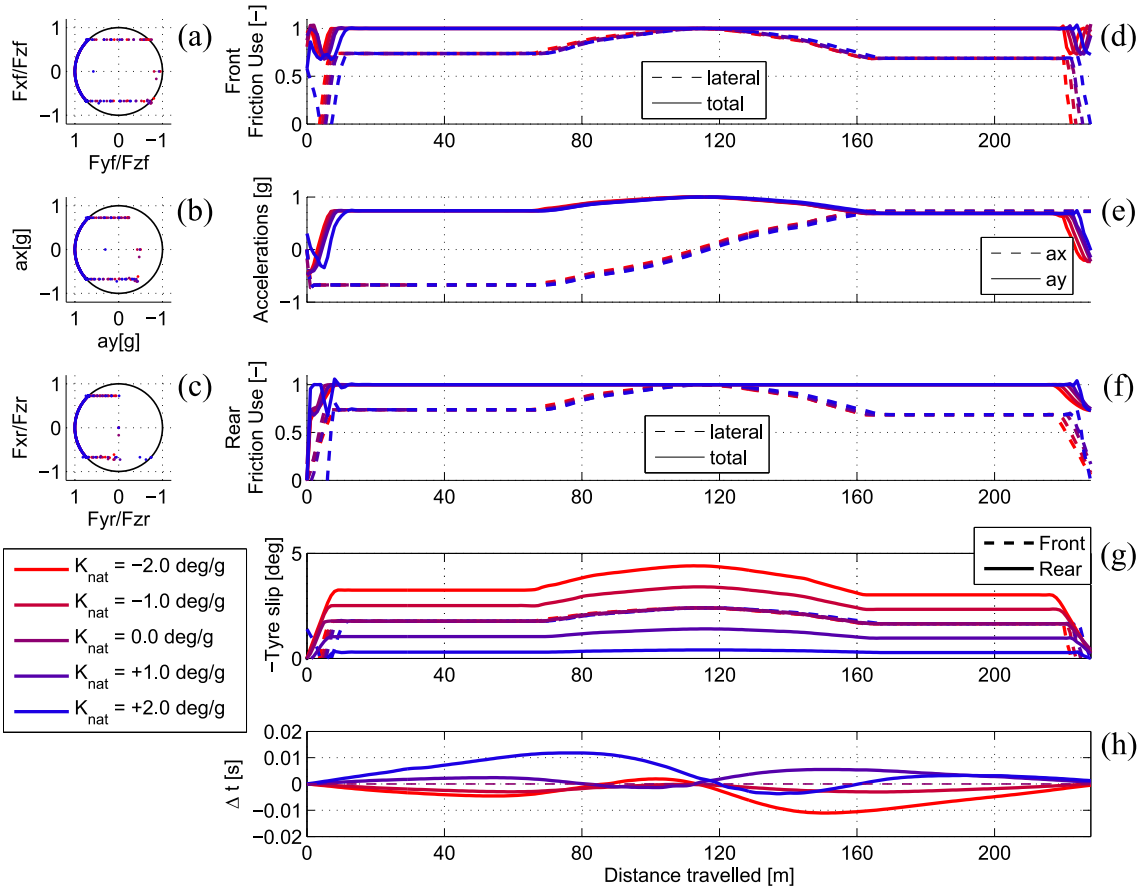

Figure 4.9: Effect of varying passive understeer gradient (defined by steady-state cornering stiffness) on torque vectoring-controlled vehicle: friction utilisation

4.5 Results: Closed-loop control

The second objective of this study is to evaluate the relative performance of the yaw rate reference on manoeuvre time by including the closed-loop TV feedback controller in the system dynamics. This section describes the inclusion of the closed-loop TV controller in the system dynamics to achieve this objective and compares results considering permutations in yaw rate reference.

For optimisation of the closed-loop control algorithm (§4.3.1), modifications are made to the open-loop control method optimal control formulation used in 4.4. Figure 4.1(b) shows the optimal control configuration including a simplified TV controller. The controller is composed of a yaw rate reference, which converts the driver steering angle input and vehicle speed into a reference yaw rate. Next, the controller takes the difference between the yaw rate reference and the vehicle yaw rate (yaw rate error) and applies a proportional gain to give one output: yaw moment demand, M_z. Finally, the control allocation determines the front/rear wheel torques, T_i, according to normal load. Recall (4.22) for the CA for the determination of front-rear torque distribution. The yaw moment term in (2.3) is now provided by the PID controller and not directly by the control variables, such that the control vector becomes:

$$\mathbf{u} = \{a_x, \dot{\delta}\}^T. \tag{4.38}$$

The yaw rate reference and PID controller are now incorporated into the mathematical definition of the objective function.

4.5.1 Mathematical definition of TV controller in system dynamics

The yaw rate reference, controller and CA are now incorporated into the mathematical definition of the system dynamics.

P controller

Feedback control is included in the form of a simple proportional-gain (P) controller:

$$M_z(s) = P\dot{\psi}_{err}(s), \tag{4.39}$$

where $\dot{\psi}_{err}$ is the yaw rate error.

To isolate the contribution of the yaw rate reference from the contribution of the performance of the system as a whole, it is important that the P controller is tuned in such a way as to deliver a consistent desired transient response. A parameter optimisation approach was used to find the P gain for a desired yaw response in the time domain. A single-track model was used as the plant, a step steer was applied with a constant forward speed and the yaw rate response simulated. The P gain was a decision variable chosen by Matlab function *fminsearchbnd* [113] such that the cost function minimised the root of the square of the yaw rate error between the desired yaw rate and actual yaw rate response. The desired transient yaw rate response, $\dot{\psi}_{ref}^{dyn}$, was generated as a first-order step response with 99% rise time, τ, of 0.2s chosen from experience in real-world data, rising to the steady-state value, $\dot{\psi}_{ref}^{SS}$, calculated from the steady-state yaw rate reference. The desired transient yaw rate response was:

$$\dot{\psi}_{ref}^{dyn} = \dot{\psi}_{ref}^{SS}(1 - e^{\frac{-t}{\tau}}) \tag{4.40}$$

This choice accords with Wong ([6], pp359) "*The optimum transient response of a vehicle is that which has the fastest response with a minimum of oscillation in the process of approaching the steady-state motion.*" The tuning process described was repeated for a range of speeds, and the mean value taken for the P gain, $P = 100\text{kNm/rads}^{-1}$ (to 1 significant figure).

4.5.2 Effect of target understeer gradient

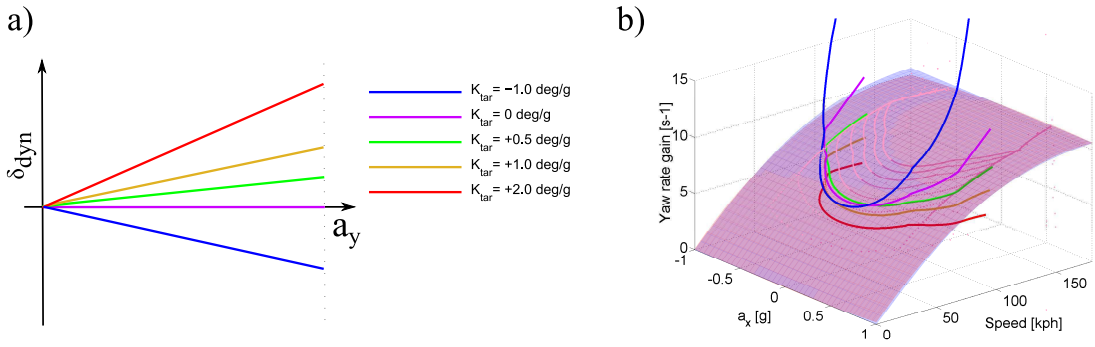

Figure 4.10: (a) Yaw rate reference 'handling diagram' form (b) Yaw rate gain plots as a function of vehicle speed for K_{tar}

It has been observed that the optimally-controlled open-loop *control method* (TV) can reduce manoeuvre time by 0.374s over the TV-inactive vehicle with equal front:rear torque distribution for a U-turn manoeuvre with $R = 35$m. Now, incorporating the feedback controller into the optimal control system dynamics, the effect of yaw rate reference will be evaluated.

The standard steady-state single-track yaw rate reference is of particular interest since it is the common reference adopted by the literature. It is defined [6]:

$$\dot{\psi}_{ref}^{SS} = \frac{V}{K_{tar}V^2 + L}\delta, \tag{4.41}$$

Set-up	K_{tar} (°/g)	dev. from K_{pas}^{SS} (°/g)	Time (s)	Δt_f [a] (s)	Δt_f [b] (s)
OL	n/a	n/a	8.827	+0.000	-0.018
CL	2.0	+1.5	9.763	+0.937	+0.919
CL	1.5	+1.0	9.469	+0.642	+0.624
CL	1.0	+0.5	9.160	+0.333	+0.315
CL*	+0.5	+0.0	8.845	+0.018	+0.000
CL	0.0	-0.5	9.197	+0.371	+0.353
CL	-0.5	-1.0	9.547	+0.720	+0.703
CL	-1.0	-1.5	9.883	+1.056	+1.039
CL	-1.5	-2.0	10.207	+1.380	+1.362

Table 4.4: Effect of yaw rate target (TV), Baseline $K_{pas}^{SS} = 0.5°$/g
[a]Time difference with respect to open-loop baseline.
[b]Time difference with respect to $K_{tar*} = K_{pas}^{SS} = +0.5°$/g.

This is parameterised by the target understeer gradient, K_{tar}. The selection method of K_{tar} in the literature is heuristic, depending on preference for stability or agility. In the following, optimisations with $K_{tar} = \{-1.5, 1.0, 0.0, +0.5, +1.0, +1.5, +2.0\}°$/g (as shown in Figure 4.10) are performed. These optimisations will reveal: a) how close the causal *closed-loop control algorithm* can approach the a-causal baseline *open-loop control method*; b) the influence of target understeer gradient on manoeuvre time. The optimal reference, K_{tar*}, is the linear reference with target equal to the natural balance $K_{tar} = K_{nat}^{SS} = 0.5$deg/g. Optimisations for a U-turn manoeuvre with $R = 35$m were run for each yaw rate reference. In Table 4.4, maneouvre times and final time differences, Δt_f, to open-loop baseline (penultimate column) and Δt_f to K_{tar*} (ultimate column) are set out, and visualised in Figure 4.11. The closed-loop (CL) controller including K_{tar*} as the yaw rate reference is able to complete the manoeuvre only 0.017s (3s.f.) slower than the open-loop baseline, pointing to a good choice of CA and a well-tuned PID controller. Inspection of the final time differences with respect to K_{tar*} (final column) reveals

a clear trend of time loss in proportion to how far K_{tar} departs from K_{nat}^{SS}, with maximum time loss occurring at extreme understeer $K_{tar} = +2.0$deg/g and extreme oversteer targets $K_{tar} = -1.5$deg/g ($+0.919$s and $+1.362$s respectively). The mean rate of time loss is 0.65s/deg/g as K_{tar} moves away from K_{tar*}, which equates to 7.3% of the K_{tar*} manoeuvre time. This is a clear demonstration not only that the optimal yaw rate reference should follow the natural steady-state behaviour of the TV-inactive vehicle but, significantly, that selection of a sub-optimal yaw rate reference has a highly negative effect on manoeuvre time and therefore the tuning of the reference is crucial.

Remark 2 *It is noteworthy that since the TV-inactive vehicle is* 0.357*s slower than* K_{tar*}*, only CL set-ups with* K_{tar} *within* $\sim 0.5^{\circ}$*/g of* K_{nat}^{SS} *will bring any benefit when the TV controller is active; anything else will make the TV perform worse than with TV inactive.*

Figure 4.12 overlays states, controls and calculated quantities for a small subset of the closed-loop optimisations: K_{tar} ± 0.5 and ± 1.5deg/g away from K_{nat}^{SS} in both more understeering and more oversteering directions. In Figure 4.12(h), K_{tar*} ($K_{tar} = 0.5$deg/g) yaw moment transitions from stabilising under braking to destabilising under acceleration to overcome load transfer effects, as in section 4.4.1. Two exceptions are the most extreme targets. For -1.0deg/g, yaw moment is in fact destabilising under braking and for $+2.0$deg/g, stabilising under acceleration. Figures 4.13(d), (f) and Figure 4.13(g) plots front and rear friction utilisation and tyre lateral slip respectively. For -1.0deg/g, under braking, rear friction utilisation is maximal. Thus the only way to increase oversteer is by decreasing the front slip angles, by reducing front lateral force. If front lateral force is reduced, then a positive, destabilising, yaw moment is required to compensate and maintain dynamic equilibrium. The same phenomenon explains the corresponding scenario under acceleration for the $+2.0$deg/g target.

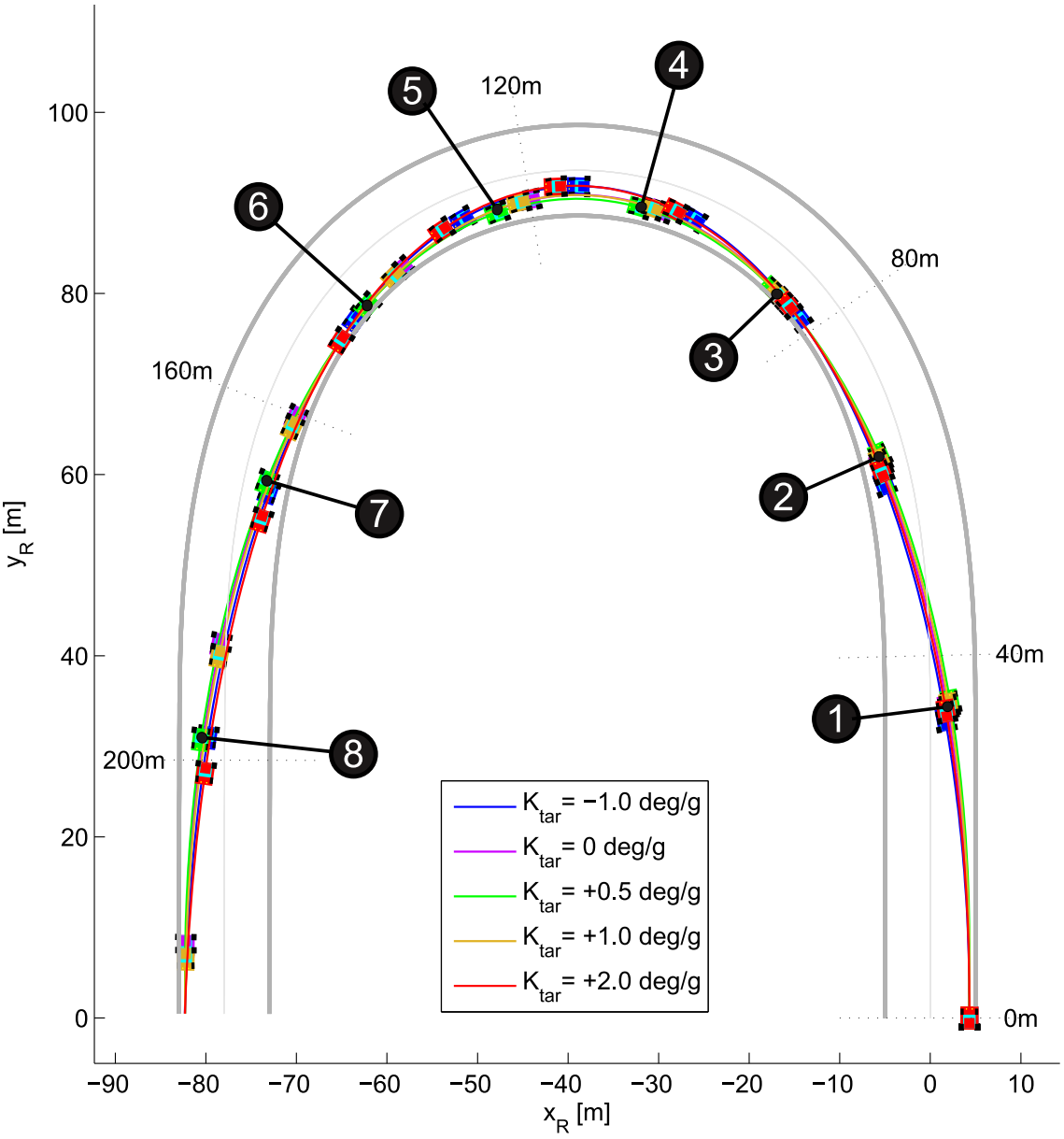

Figure 4.11: Comparison of closed-loop torque vectoring for oversteering to understeering K_{tar} gradients: controlled path trajectory comparison with vehicle snapshots drawn for every second (numbered circles)

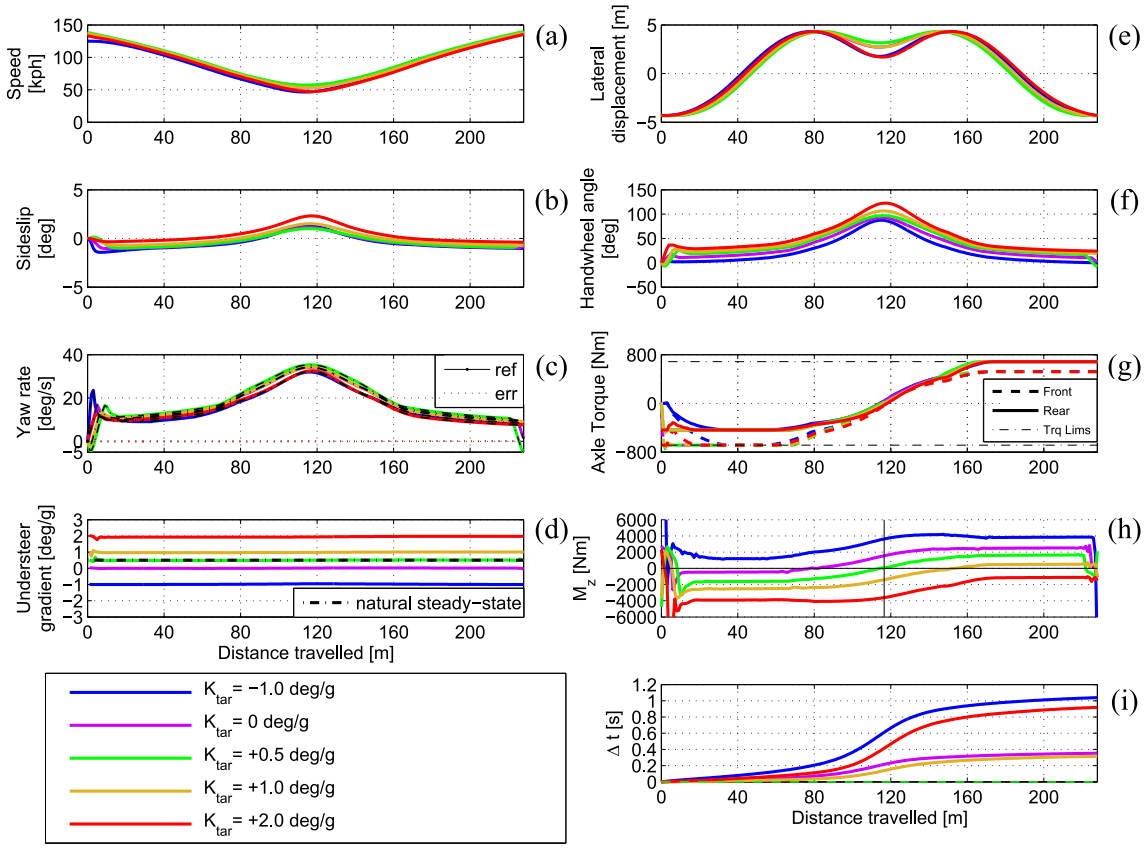

Figure 4.12: Comparison of closed-loop torque vectoring for oversteering to understeering K_{tar} gradients: states and controls

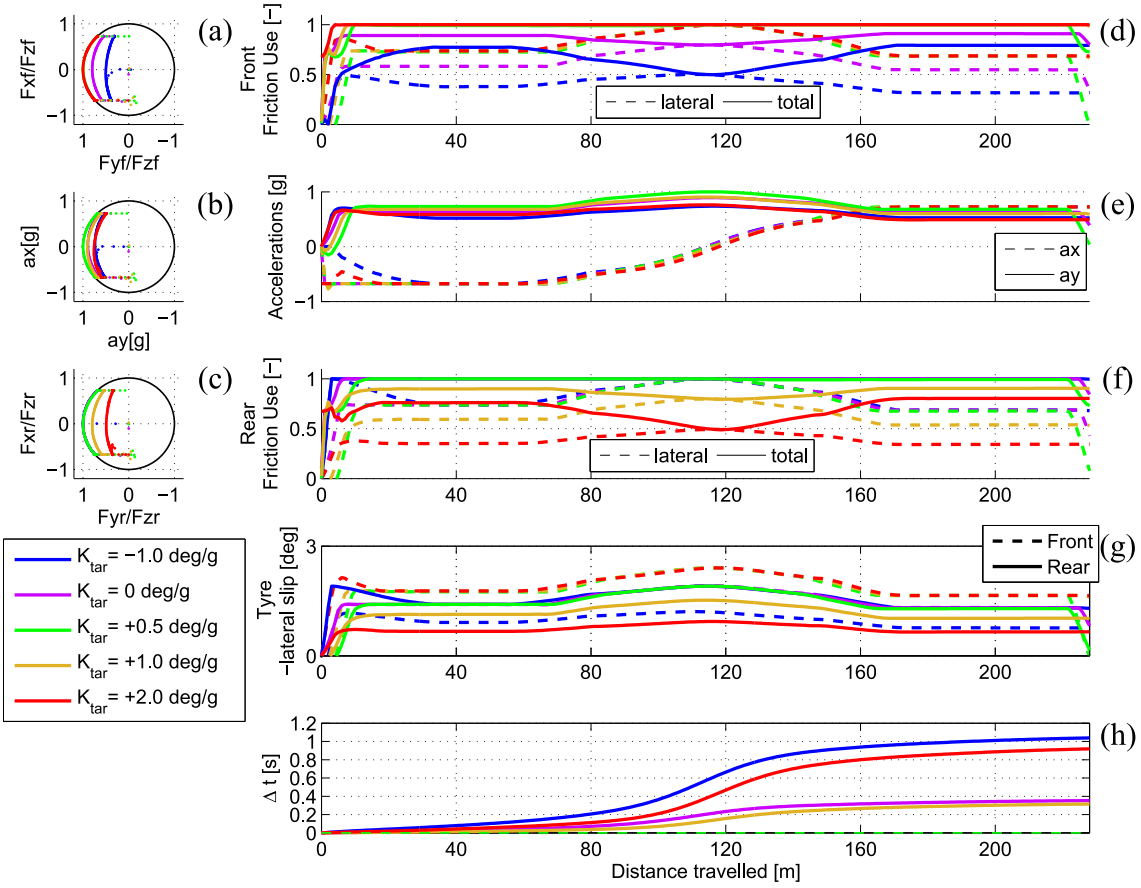

Figure 4.13: Comparison of closed-loop torque vectoring for oversteering to understeering K_{tar} gradients: friction utilisation

Figure 4.12(h) shows that the greater the target away from the natural, the greater the maximum magnitude of yaw moment required to follow the reference. In addition, it can be seen that the point at which yaw moment transitions from its lower value to upper value shifts to earlier in the manoeuvre for oversteer target and later for more understeering target.

$K_{tar*} = K^{SS}_{pas} = +0.5°$/g achieves highest minimum speed by some margin (Fig. 4.12(a)), which corresponds with the greatest proportion of time loss occurring for $s \in [90, 140]$m, at which point the difference in yaw rate is greatest.

With reference to Figures 4.12(c) and 4.12(i), it is clear that manoeuvre time reduces with increasing maximum yaw rate. $K_{tar*} = K^{SS}_{pas} = +0.5°$/g achieves highest maximum yaw rate and corresponding lowest manoeuvre time. This is slightly counter-intuitive as one might expect the most extreme oversteer target (-1.0deg/g) to have the greatest yaw rate. In actual fact, the yaw rate reference is derived from yaw rate gain (6.1), which the optimisation achieves through a combination of yaw rate and steering angle application. In Figure 4.12(f), the steering angle applied is highest for understeer reference and lowest for oversteer reference. Yaw rate gain combines yaw rate and steering angle and is plotted as a function of speed and longitudinal acceleration in Figure 4.4(b). The K_{tar*} trace (green) sits on the K^{SS}_{nat} surface; neutral steer (purple) adopts a straight line; oversteer -1.0deg/g (blue) tends towards infinity as it approaches its critical speed. Optimisation seeks to minimise manoeuvre time and is able to do so most effectively (with greatest yaw rate) when following K_{tar*}.

Analysis of friction utilisation affords some insight into the reasons for the superiority of K_{tar*}. For the oversteer cases, friction is saturated at the rear axle at all times, and vice versa for understeer. For vehicle handling with TV-inactive, a shift towards oversteer under braking and understeer during acceleration occurs due to load transfer. For oversteer targets, the rear tyre friction is fully utilised under braking, whereas only 80% of

front potential is used, (50% lateral contribution). Illustrated in Figures 4.13(a) and (c), longitudinal force is restricted because of torque/power limits, but lateral does not take up the extra capacity, sitting away from the circumference of the friction circle because an increase in lateral force would require an increase in tyre slip angle at the front and therefore result in a more understeering behaviour away from the oversteer reference, which is prohibited by the PID controller. Staying with the braking phase and looking at the $+2.0$deg/g target (red), the opposite situation is true. Here front friction is fully utilised (again, longitudinal force saturated by torque/power limits), which requires a greater front slip angle than the understeer case. The rear friction is under-utilised since, although the cornering stiffness is reduced because of load transfer, any greater lateral force would require a greater lateral slip angle at the rear, which would force the handling balance away from the target and is therefore not permitted by the optimisation.

During the acceleration phase ($s > 120m$), a similar pattern is observed. Weight transfer now gives a greater total force capacity on the rear axle, the rear slip angle can be lower to produce the same lateral force, and correspondingly, the front slip angle must reduce in order to maintain the target handling balance and hence is only able to use a lower proportion of the friction capability. The total friction capability, then, is limited both by the requirement for a front slip angle lower than the rear and torque/power limits constraining longitudinal force.

The most time is lost for all sub-optimal references during steady-state cornering where $s \in [90, 140]$m. This is due to a reduction in total friction utilisation at the unsaturated tyre. Taking $K = -1.0$deg/g case as an example, in Figure 4.13(d) the front friction utilisation drops from 80% under maximum braking to a 50% minimum at the apex, at which point lateral friction utilisation increases. Total utilisation decreases since longitudinal acceleration reduces to zero. But in order to achieve the reference balance, the front lateral force cannot be increased since that would increase the slip angle and

hence alter the balance too far towards understeer.

The total friction capability and therefore performance, then, is limited by K_{tar}, which requires a certain difference between front and rear slip angles which in turn dictates the permissible lateral force at front or rear. Only by following K_{tar*} ($K_{tar} = 0.5$deg/g) can friction be fully utilised and manoeuvre time minimised.

4.6 Conclusions

Torque vectoring (TV) has a powerful ability to actively modify vehicle handling of electric vehicles. Torque vectoring control systems require a yaw rate reference, usually set using a subjective, heuristic method. In contrast, an optimal yaw rate reference, K_{tar*}, was found in this chapter. The results of open-loop optimal control problems for minimising manoeuvre time found K_{tar*} to be identical to the steady-state natural single-track expression for yaw rate gain (with TV inactive). K_{tar*} was able to make full use of overall friction capacity such that longitudinal load transfer effects were negated and a U-turn manoeuvre navigated significantly faster than the vehicle with TV inactive. Longitudinal load transfer negation was demonstrated for a range of passive handling characteristics.

Setting yaw rate reference away from natural understeer gradient demonstrated a marked negative effect on manoeuvre time, even under-performing the vehicle with TV inactive in extreme cases. By full utilisation of available friction at all times by maximising front and rear lateral forces, K_{tar*} achieved the greatest minimum speed and maximum yaw rate.

Chapter 5

Time-optimal handling: 7DOF Vehicle model

5.1 Introduction

In this section, an identical methodology is followed to chapter 4, but with the employment of the 7DOF vehicle model. Some practical modifications are also made to the optimal control formulation to improve tractability.

5.2 Control configurations

To meet the objectives of generating baseline optimal trajectories, assessing passive charactistics on controlled behaviour, and to evaluate the effect of modifying the yaw rate reference of the TV controller, once again two OCP formulations are required. Figure 5.1(a) shows the open-loop *control method* [29, 30] from which the maximum perfor-

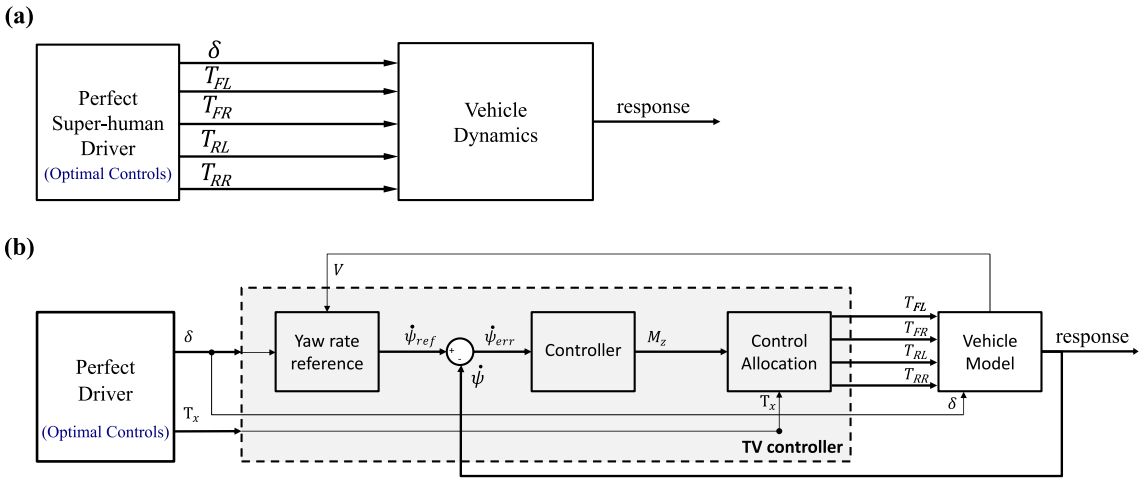

Figure 5.1: In the open-loop OCP formulation (a), the control inputs are steering rate and 4 torques. In the closed-loop OCP (b), the control inputs to be optimised are steering rate and torque demand. The 4 wheel torques are determined by the closed-loop TV controller which follows a yaw rate reference corresponding to the desired modified handling behaviour.

mance potential of the vehicle with TV may be ascertained– by determining the optimal control inputs that must be applied to the vehicle *directly*. This formulation is used to generate the baseline optimal trajectories for TV in §5.3.1, and to analyse the effect of passive handling balance on controlled response in §5.3.2. In contrast to §4.12, the optimal control problem now has control over 4 individual wheel torques.

Figure 5.1(b) shows the closed-loop *control algorithm* formulation [29, 30]. Perfect open-loop control is a-causal and hence only of theoretical interest; a causal active yaw control system is required to determine the torques applied at each wheel to follow the desired high-level motion objectives– in this case yaw rate, $\dot{\psi}$, and total longitudinal torque demand, T_x. The specific component of interest for this research is the yaw rate reference and by incorporating a closed-loop controller into the system dynamics of the OCP, the performance of the reference may be evaluated (§5.4). To evaluate the reference, a 'perfect' driver is once again required but merely a 'human' one, with authority over only longitudinal torque demand and steering (equation 5.3), not individual wheel torques which

are now outputs of the control allocation.

5.2.1 Mathematical Formulation

The 7DOF vehicle model introduced in §2.3 is employed in this analysis. The state and control vectors for the vehicle model configurations are:

$$\mathbf{x}(s) = \{V(s), \beta(s), \dot{\psi}(s), \omega_{ij}(s), x_R(s), y_R(s), \theta_R(s), s_n(s), \chi(s), \delta(s), t(s)\}^T, \quad (5.1)$$

$$\mathbf{u}(s) = \{T_{FL}(s), T_{FR}(s), T_{RL}(s), T_{RR}(s), \dot{\delta}(s)\}^T, \quad (5.2)$$

where T_{ij} are the individual wheel torques, $\dot{\delta}$ is steering rate. Time elapsed, t, is included as a state to allow analysis as a function of time to be performed. For the *closed-loop control method* (TV), the control vector includes only overall torque demand, T_x (as illustrated in Figure 5.1(b)):

$$\mathbf{u}(s) = \{T_x(s), \dot{\delta}(s)\}^T. \quad (5.3)$$

As for the 3DOF analysis in chapter 4, the equations are transformed into the distance base using curvilinear coordinates.

The cost function seeks to minimise time, but in contrast to §4.3.2, boundary constraints are included implicitly in the cost instead. The cost function is composed primarily of the Lagrange integral term to minimise time to complete the manoeuvre. In contrast to §4.3.2, a Mayer term is introduced to ensure straight-line running conditions at the start of the manoeuvre. Including the initial conditions in the cost function is more tractable for the solver than imposing a hard constraint (given the increased size of the system),

and is equivalent with carefully-chosen weightings[1]. The cost function is:

$$J(s) = W_0\phi[\mathbf{x}(s_0, s_f)] + \int_{s_0}^{s_f} \frac{1}{\dot{s}}\, ds, \qquad \text{where} \tag{5.4}$$

$$\phi[\mathbf{x}(s_0, s_f)] = \frac{\beta_0^2}{\bar{\beta}^2} + \frac{\dot{\psi}_0^2}{\bar{\dot{\psi}}^2} + \frac{\delta_0^2}{\bar{\delta}^2} + \frac{\chi_0^2}{\bar{\chi}^2}, \tag{5.5}$$

where β_0, $\dot{\psi}_0$, δ_0 and χ_0 are initial sideslip, yaw rate, steer angle and relative yaw angle values respectively. '$\bar{\mathbf{x}}$' are normalisation factors for the equivalent states. W_0 is the relative weighting of the Mayer term for the initial conditions. The full set of boundary conditions are tabulated in Table 5.1.

For optimisation considering the vehicle with TV inactive, a static torque distribution is enforced by including an additional term into the Lagrange integral expression. Again, considering torque limits in the cost function is more tractable than setting torque limits as a hard constraint:

$$J(s) = \tag{5.6}$$
$$W_0\phi[\mathbf{x}] + \int_{s_0}^{s_f} \left(\frac{\dot{s}^{-1}}{\bar{t}} + W_T \frac{(T_{FL}-T_{FR})^2+(T_{RL}-T_{RR})^2+(T_{FL}(1-\gamma)-\gamma T_{RL})^2}{\bar{T}^2} \right) ds,$$

where $\bar{t}$ and $\bar{T}$ are time- and torque-normalisation factors respectively, W_T is the relative weighting on the torque terms and γ is the proportion of total torque applied at the front axle.

Constraints are once again imposed on steering rate. The maximum torque,T_{max}, of each individual motor (rather than axle) is constrained:

$$|T_{ij}| \leq T_{max}. \tag{5.7}$$

[1]The NLP solver used is SNOPT [104]. In chapter 7, IPOPT is introduced that is able to handle boundary conditions and constraints more easily

Boundary Conditions		
$\mathbf{x}$	$\mathbf{x}_0$	$\mathbf{x}_f$
s	0	s_f
V	free[b]	free
ψ	0	free
ω_{ij}	free	free
s_n	free	free
χ	0	free
x_R	free	free
y_R	free	free
θ_R	$\frac{\pi}{2}$	free
δ	0	free
t	0	free

Table 5.1: Boundary conditions

Power is not constrained to ease the computation for this more difficult problem. This is justified since, for the 3DOF model, the power constrains were inactive; rather constant torque constraints were shown to limit performance at high speed.

5.3 Results: Open-loop control method

In this section, the absolute potential of the TV system is determined. This is the *open-loop control method* described in §5.2 (and shown in Fig. 5.1(a)). This will allow the torque vectoring performance to be compared against the vehicle with TV inactive in §5.3.1. It will also allow analysis of what effect the passive, steady-state understeer gradient has on the controlled response in §5.3.2.

A U-turn manoeuvre (Figure 5.2) with $R = 35$m is navigated. In general terms, the vehicle enters the manoeuvre on the right at high speed in a straight line, exerting maximum braking torque. As the speed reduces and the road curvature increases, braking is reduced, steering is gradually applied until the maximum curvature point is reached

and the vehicle has moved to the inside road boundary. After this midpoint (where lateral acceleration is maximal), torque is gradually applied, steering is reduced to zero as high-speed, straight-line running is approached and the vehicle returns to the outside road boundary.

5.3.1 Torque Vectoring active vs. inactive

The optimal control problems for TV-active and TV-inactive set-ups are presented for comparison in this section. The *TV* set-up is formulated as in §5.2.1, with cost function (5.4). The vehicle with TV inactive (hereafter, *NoTV*) is compared by setting the static drive torque distribution to produce 4WD, ($\gamma_{drive} = 0.6$). Braking distribution is $\gamma_{brake} = 0.7$. These distributions require cost function (5.6). The effect of FWD or RWD distributions are then assessed.

Finally, the impact of TV with dynamic load transfer (LT) removed (i.e. normal loads become simply a function of static weight distribution) is examined (hereafter *TV no LT*) and TV without torque limits (hereafter *TV no trq lim*).

Thus three open-loop control method optimisations are now presented for comparison. With torque vectoring capability, the manoeuvre time of 8.502s is -0.380s (to 3 significant figures) faster than *NoTV*. This is a significant benefit for just one corner and when extrapolated over a whole lap of 10-15 turns, would give a benefit of the order of $\sim 3-4$s, which is considerable in the racing context. *TV no LT* is -0.038s faster than *TV*: In this analysis, two plots will be examined.

First, Figure 5.3 overlays states, controls and calculated quantities for all optimisations. The steady-state understeer gradient calculated at every instant, K_{inst}^{SS} (recall (4.30))is plotted in Figure 5.3(d). Further insight is drawn from plots of friction utilisation, as shown in Figure 5.4, for each tyre separately. Friction utilisation is defined as

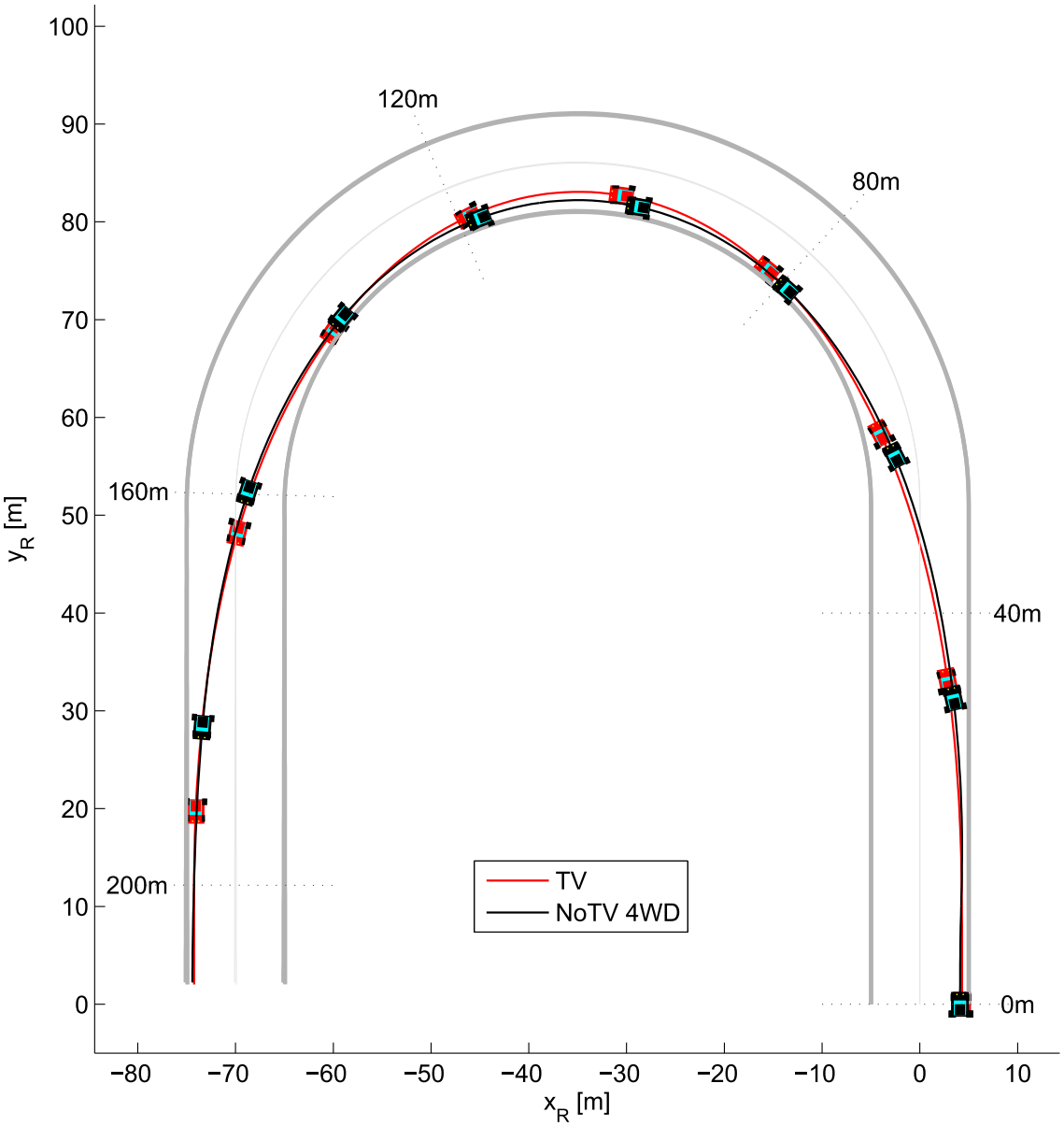

Figure 5.2: Path trajectory comparison of TV inactive (70:30 front:rear static brake torque distribution, 60:40 propulsive torque distribution) with optimal TV. Vehicle position is plotted every second.

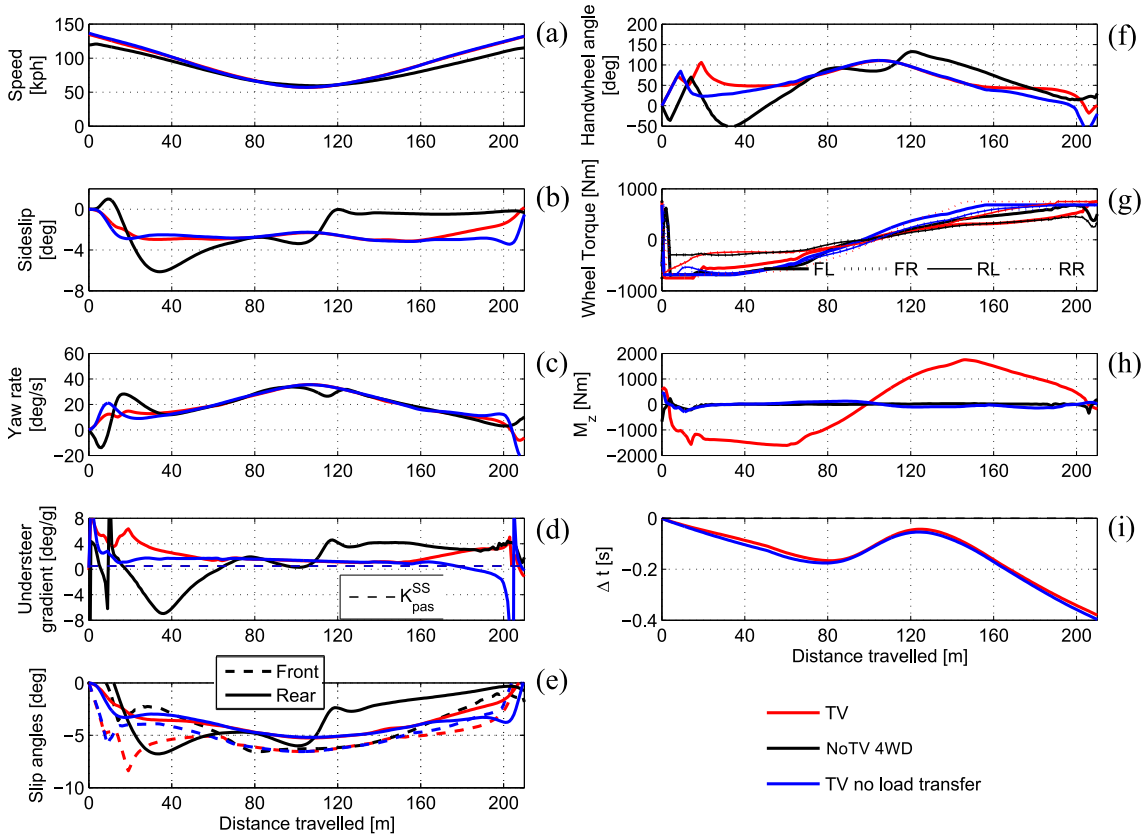

Figure 5.3: States and controls comparison of TV inactive (70:30 front:rear static brake torque distribution, 60:40 propulsive torque distribution) with optimal TV.

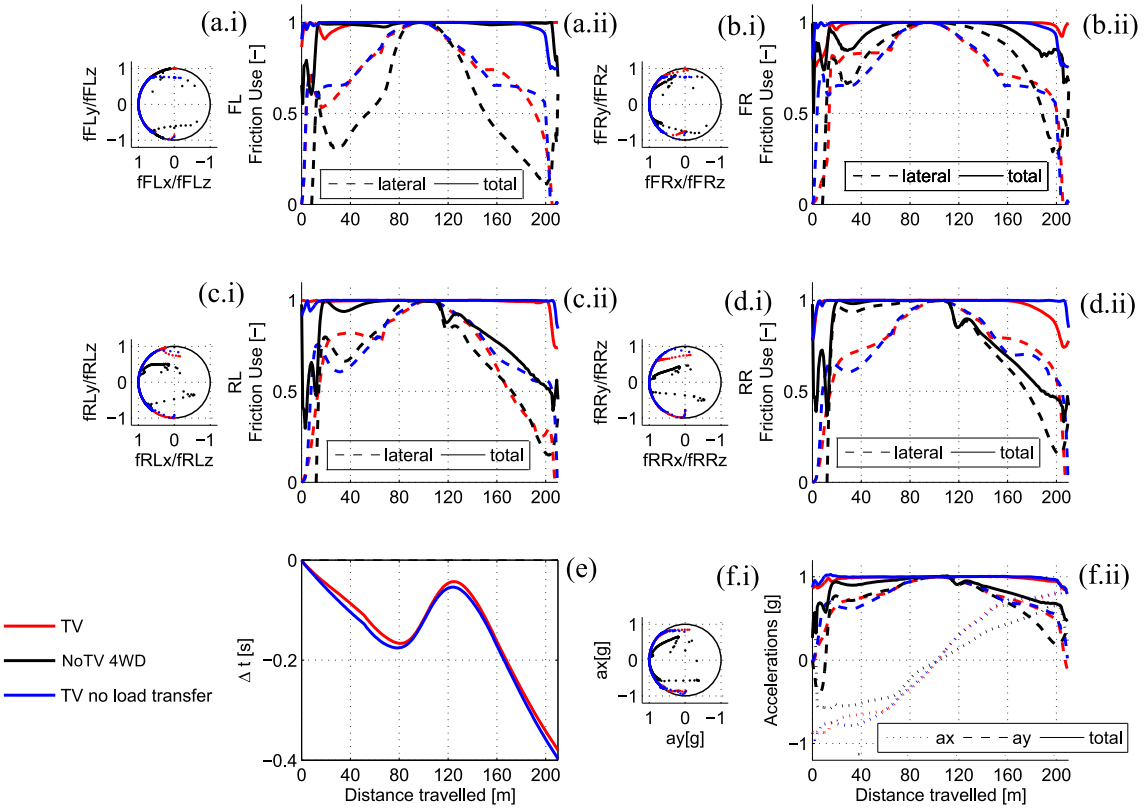

Figure 5.4: Friction utilisation comparison of TV inactive (70:30 front:rear static brake torque distribution, 60:40 propulsive torque distribution) with optimal TV.

the lateral, longitudinal or resultant force divided by the total force available on the wheel:

$$\mu_{ijk} = \frac{F_{ijk}}{\mu_{max} F_{ijz}}, \tag{5.8}$$

where $i \in [F,R]$; $j \in [L,R]$; $k \in [x,y]$ and μ_{max} is the tyre-road friction coefficient.

Subfigures enumerated with (i) show friction utilisation on the friction circle; subfigures enumerated with (ii) show friction utilisation as a function of distance travelled (lateral and total). Accelerations at the centre of gravity (CM) are shown in subfigures (f.i) and (f.ii) in a similar manner (lateral, longitudinal and total).

Looking first of all at the vector velocity and acceleration traces, with reference to Figure 5.3(a) and 5.4(f), it is clear that *TV* is able to sustain a greater magnitude of total longitudinal acceleration and hence can both start and exit the manoeuvre at higher speeds than *NoTV*.

There is an interesting difference in path trajectory at the midpoint (Fig. 5.2): the vehicle with TV inactive takes a tighter line, hugging the inside edge of the track for $80 < s < 130$m, whilst *TV* takes more of a 'double apex', reaching a point of maximum path curvature ($\max(\kappa_{path})$, at point of minimum speed, V_{min}) at $s = 0.5 s_f$. *TV* has a lower V_{min}, since in effect its maximum path curvature is greater than for the TV inactive paths: $V_{min} \approx \sqrt{\frac{a_{centripetal}}{\max(\kappa_{path})}}$. The *NoTV* vehicle is able to maintain 3km/h higher speed over $90 < s < 120$m and thus gain time back during this portion of the manoeuvre.

TV uses all friction available on each wheel through most of the manoeuvre. When torques are saturated by motor limits, a small reduction in friction utilisation is observed at the front tyres during high-speed deceleration ($0 < s < 40$m) and on the rear tyres at high-speed acceleration ($180 < s < 210$m). The torque limits reduce the amount of torque vectoring that can be applied at high speed (Figure 5.3(h)) and, therefore, greater handwheel angle (Figure 5.3(f)) is required to compensate for the reduced influence on

the lateral dynamics that are possible from the both the left-right torque difference and the coupling effect of longitudinal forces on lateral via the friction circle. The handwheel angle increases the understeer gradient during these periods (Figure 5.3(d)).

Understeer gradient for *TV* is highly understeering during turn entry (where yaw moment is stabilising), maintains a near-constant value for most of the turn before increasing understeer once again as torques reach their limits. *NoTV* exhibits high levels of oversteer for turn-entry during the pendulum turn, progressing to mild understeer at the apex, with significant levels of understeer during the second half of the manoeuvre under acceleration. Oversteer during turn entry is due to use of the pendulum-turn technique (yawing out of the turn before yawing into the turn).

Friction usage for *NoTV* is maximal for FL for the duration of the manoeuvre. Front-right friction is ~ 0.8 during high speed portions. Under braking, rear tyres usage is near-unity but under acceleration, front tyre use reduces to only ~ 0.5 at the end of the manoeuvre. This is due to a torque distribution that favours the less-loaded front tyres, despite the rearward load transfer that occurs during acceleration.

Figure 5.3(d) shows that *TV* is able to 'flatten' the understeer gradient characteristic substantially when compared with *NoTV*, through applying a stabilising yaw moment under braking and a destabilising yaw moment under acceleration. This is attributed to compensation for load transfer effects. Inspection of Figure 5.3(h) shows that magnitude of yaw moment is proportional to a_x. This trend of direct yaw control effecting a stabilising yaw moment under deceleration and a destabilising yaw moment under acceleration is confirmed by findings for a similar electric vehicle topology analysed in [45], and a brake torque vectoring differential study for a RWD conventionally-powered touring car in research by Tremlett et. al. [64, 78, 111] and Kaspar et. al. [112]. De Novellis et. al. [36] describe a similar finding for this yaw moment trend when a yaw rate reference independent of longitudinal acceleration is used. Indeed, the β-method described in the seminal

work of Shibahata et. al. [16] showed that direct yaw control can overcome load transfer effects, considering a 6DOF vehicle model with roll and pitch DOFs and nonlinear tyres.

By removing load transfer effects, further insights may be gained. For *TV no LT* (normal loads are equal to their static values according to weight distribution), almost no yaw moment is required to match the handwheel, sideslip, yaw rate and understeer gradient profiles as *TV*, and friction usage is near-maximal (where the vehicle is not torque-limited). This gives further credence to the theory that TV improves performance by making use of tyre force coupling effects: controlling longitudinal forces such that lateral forces are reduced/increased on each corner for a greater resultant force, and hence a greater total acceleration than would otherwise be possible.

TV inactive: 4WD vs FWD vs RWD

The effect of drive/brake distribution for TV inactive is now investigated, with three vehicle topologies with TV inactive compared by varying the static drive torque distribution to produce 4WD, FWD and RWD ($\gamma_{drive} = 0.6$, $\gamma_{drive} = 0.99$ and $\gamma_{drive} = 0.01$). Braking distribution is $\gamma_{brake} = 0.7$. These are shortened to *NoTV 4WD*, *NoTV FWD* and *NoTV RWD* respectively in the following.

NoTV FWD and *NoTV RWD* compare less favourably than *NoTV 4WD* against *TV*; 0.615s and 0.443s and 0.362s slower than TV, respectively. Looking first of all at the vector velocity and acceleration traces, with reference to Figure 5.6(a), final speeds for the TV inactive set-ups reduce from *4WD*, to *RWD*, to *FWD*, while apex speeds are similar.

NoTV set-ups exhibit the same handwheel angle, sideslip and understeer gradient profiles during braking, since they have the same braking torque distribution. A pendulum-turn technique is used during initial turn in. Under acceleration, with different torque distributions, *NoTV RWD* exhibits the lowest steering angle and greatest sideslip. *NoTV*

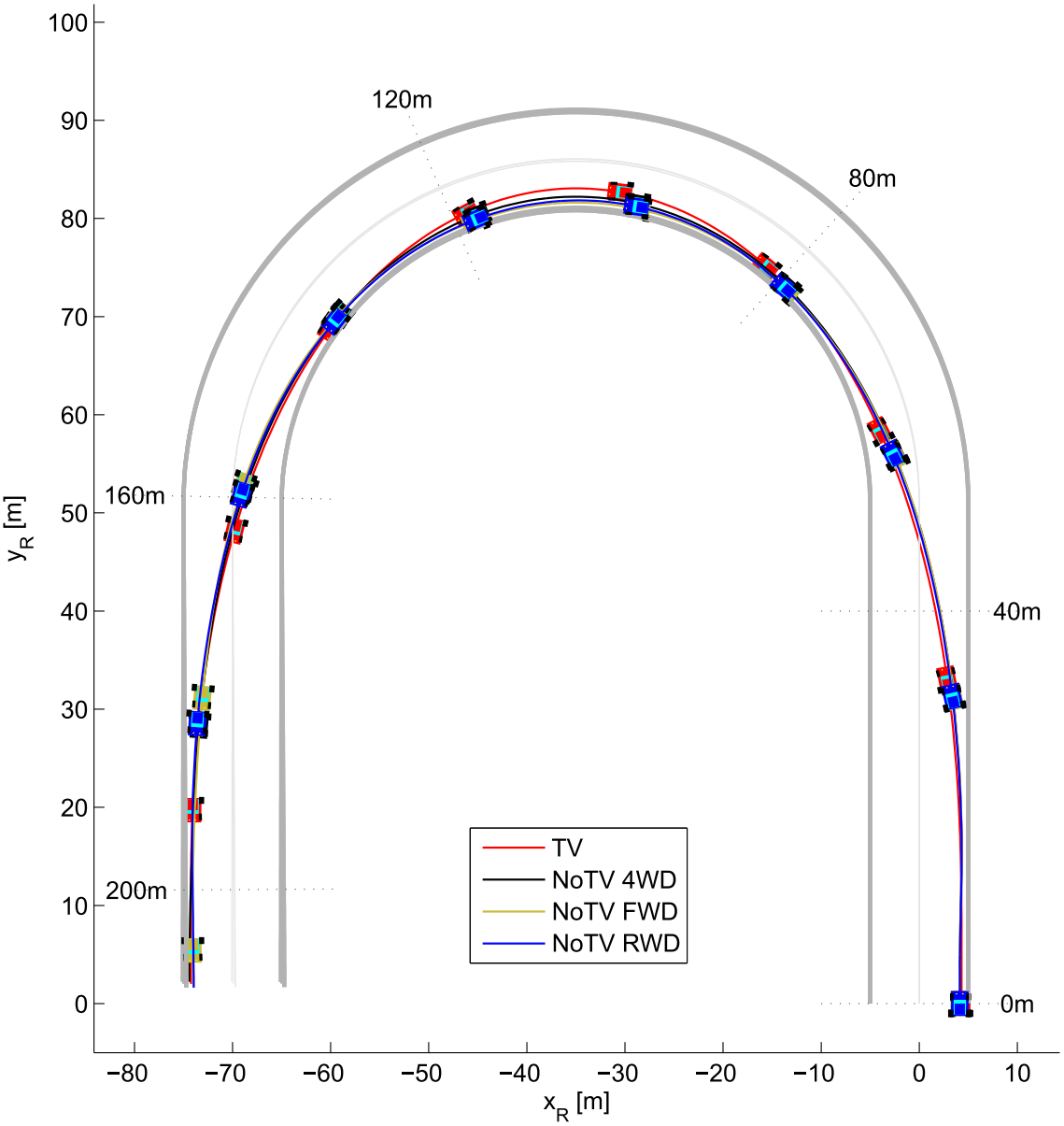

Figure 5.5: Path trajectories comparison of TV with TV-inactive with torque distributions of 4WD (60:40), FWD and RWD.

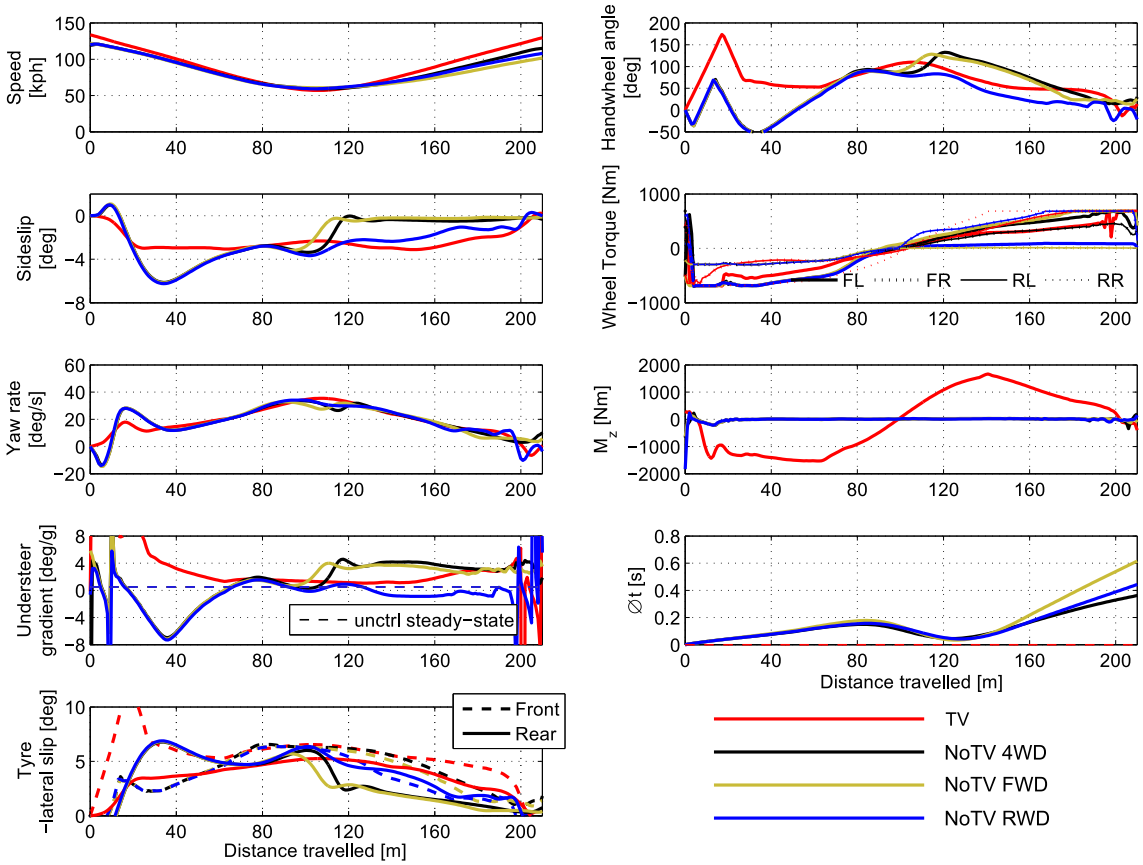

Figure 5.6: States and controls comparison of TV with TV-inactive with torque distributions of 4WD (60:40), FWD and RWD

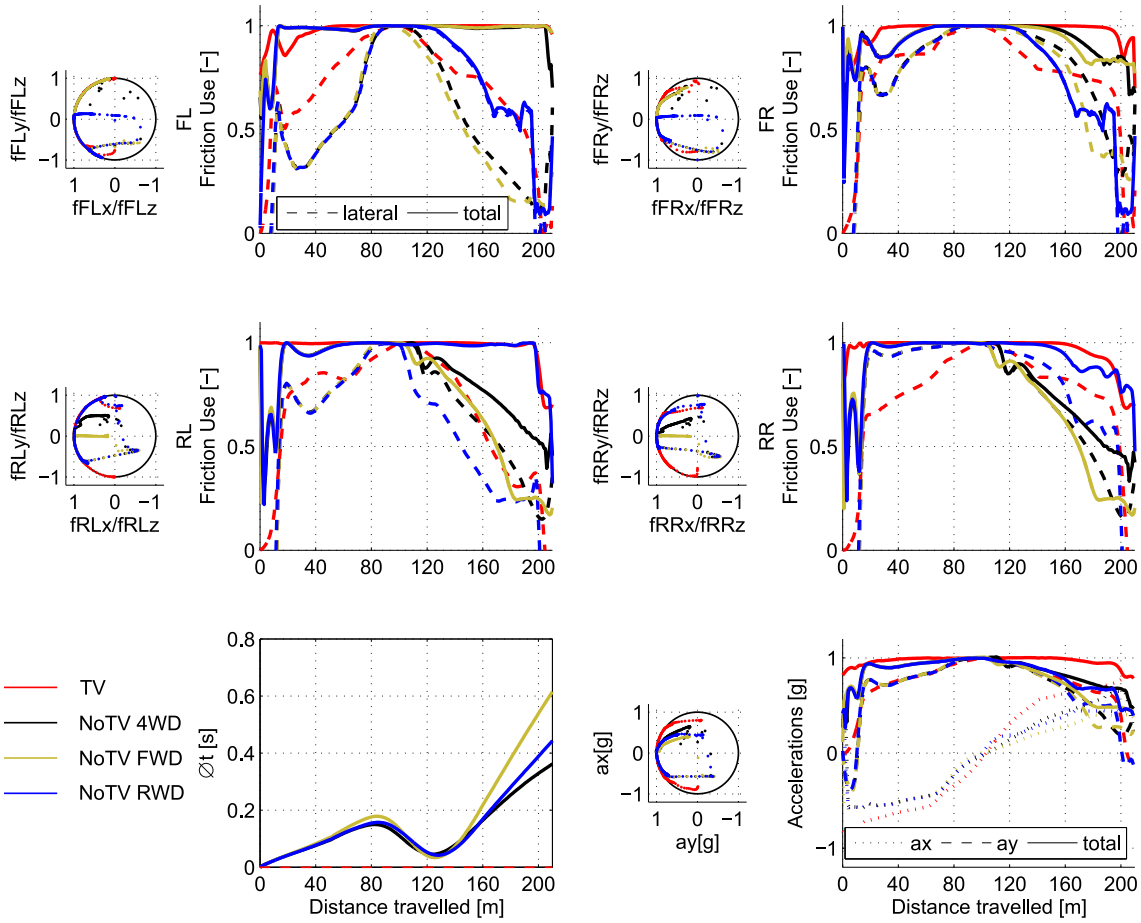

Figure 5.7: Friction utilisation comparison of TV with TV-inactive with torque distributions of 4WD (60:40), FWD and RWD

4WD and *NoTV FWD* show very similar handwheel angle and sideslip profiles.

Figure 5.7 shows friction usage. The plots reveal that, during the second half of the manoeuvre, FWD and 4WD use more front friction potential than RWD, while RWD uses a greater proportion of the rear friction potential.

Effect of load transfer and motor torque

To facilitate analysis of underlying mechanisms, a further TV optimisations were run in addition to the set-up in the previous section. TV with no torque constraints (shortened to *TV no trq lim*) and TV with dynamic load transfer removed (*TV no LT*, re-presented from earlier in this section by means of comparison). States, controls and calculated quantities are shown in Figure 5.8. *TV no trq lim* is -0.044s faster than **TV**. This is a relatively small difference, as only a small amount of time is spent where torques are limited. This is a similar degree faster than *TV* as *TV no LT*.

TV no trq lim uses all friction available on each corner throughout the manoeuvre. When torque limits are imposed (*TV*), a small reduction in friction utilisation is observed at the front tyres during high-speed deceleration ($s \in [0, 40]$m) and on all corners at high-speed acceleration ($s \in [180, 210]$m). The constraints on torque reduce the amount of yaw moment that can be applied at high speed (Figure 5.8(h)) and therefore, greater steering input is required during these periods to help mitigate this effect. This has a strong effect on understeer gradient (Figure 5.8(d)), exhibiting strong understeer corresponding to the reduced yaw moment magnitude and increased steering. *TV no trq lims* and *TV no LT* show a similar understeer gradient profile, which remains fairly constant through most of the manoeuvre, which is higher than the steady-state understeer gradient of the passive vehicle. Further analysis in chapter 6 suggests reasons for this.

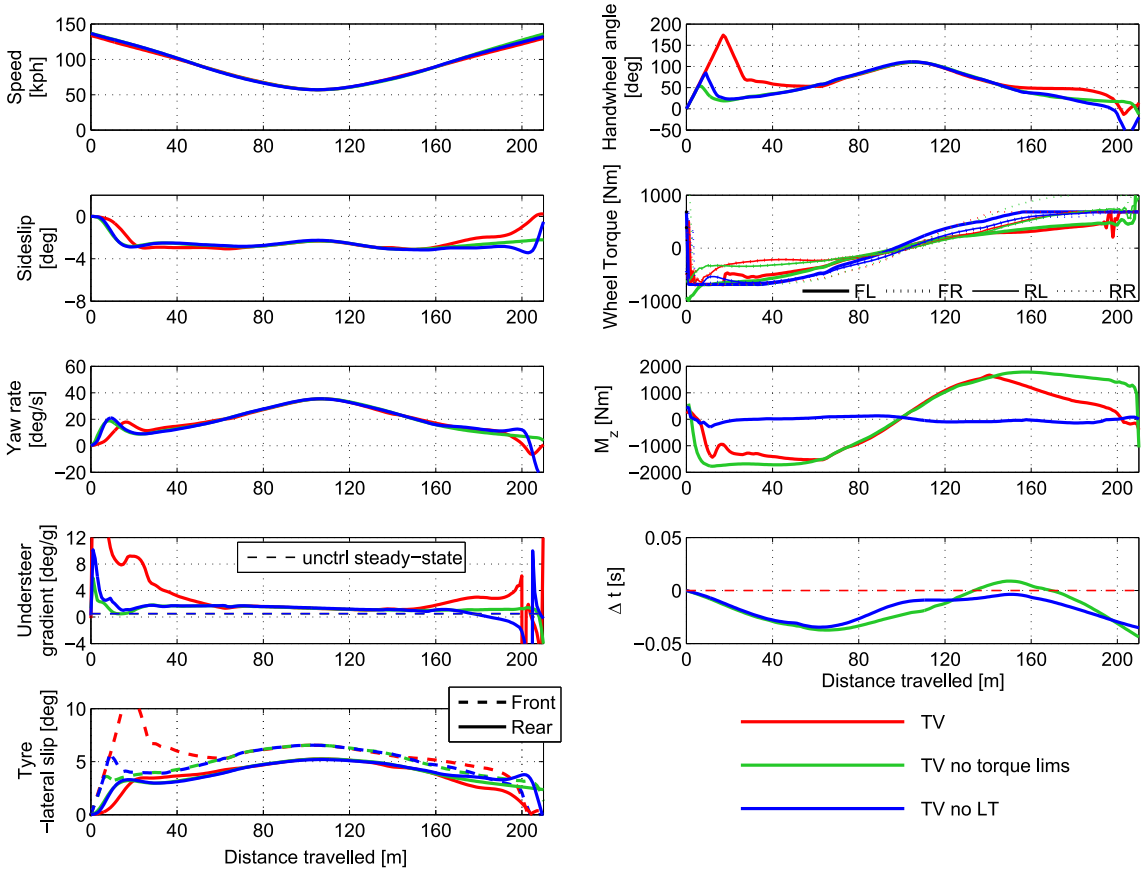

Figure 5.8: Comparison of TV, TV with no motor torque limits, TV with no load transfer: states and controls

5.3.2 Effect of passive handling characteristic

It has been demonstrated that *TV* is -0.380s faster than *NoTV*, for a passive steady-state understeer gradient $K^{SS}_{pas} = 0.5°/\text{g}$.

Since TV extends the performance envelope of the vehicle by the correct distribution of tyre forces, the pertinent question is whether there is a certain K^{SS}_{pas} for which tyre force distribution by TV gives the greatest performance envelope and therefore delivers a faster manoeuvre time. To answer this question, optimal control problems (with TV active) are formulated and solved for a range of passive understeer characteristics. This is achieved by modifying tyre parameters.

In chapter 4, considering the same method with the 3DOF vehicle model, the instantaneous understeer gradient followed the passive value very closely.

In the present study, optimisations were run for TV for $K^{SS}_{pas} = \{-1, -0.5, 0, 0.5, 1\}$ by altering front and rear tyre stiffness parameters, B_F and B_R, according to Table 4.2. The range was restricted compared to section §4.4.3 since the more extreme values proved intractable by the optimal control solver. The manouevre time for all optimisations is 8.52s (to two decimal places). This clearly demonstrates that the controlled performance is insensitive to the passive characteristic of the vehicle for these modest perturbations from neutral steer, as was found for the 3DOF model results.

Figure 5.9 shows states, controls and calculated quantities for the range of passive handling balances. Figure 5.9(d) shows that K^{SS}_{inst} follows K^{SS}_{pas} fairly closely for neutral steer for $60 < s < 140$m where torques are below their limit value. There is some variation with acceleration and associated normal load (as was found in [62]). Similar profiles of understeer gradient with distance travelled are observed for all permutations: slightly greater understeer effect for $0 < s < 100$m during braking and slight reduction on understeer effect under acceleration for $100 < s < 200$m during acceleration. (This is

the opposite trend to that experienced by the vehicle with TV inactive). For variation in K_{pas}^{SS}, it is clear that the further from neutral steer, the greater the instantaneous understeer gradient deviates from the passive value. For example, where $K_{pas}^{SS} = 1°$/g (red), K_{inst}^{SS} is around $\sim 3°$/g.

Where wheel torques are saturated, the understeer gradient is dramatically increased due to the greater contribution of steering required to generate the lateral forces, since torque vectoring is no longer able to assist to the same degree in the optimal redistribution of tyre forces.

Remark 3 *Wheel torques (and consequently M_z) show little variation. This is an important result since it demonstrates that the control yaw moment (vehicle authority) is predominantly used to counteract load transfer effects. The main differentiator between the optimisation controls is the handwheel angle, which is increased in proportion with passive understeer gradient. Correspondingly, for sideslip angle, there is a clear trend of increasing tail-out sideslip as K_{pas}^{SS} progresses from $+1.0$ to $-1.0°/g$ (Fig. 5.9(c)). Steering angle (driver control authority), is used to generate front lateral force and hence the angle required depends on the understeer gradient.*

Figure 5.10 shows friction utilisation and CM vehicle accelerations. Total friction usage for each tyre is similar in all cases (Fig. 5.10(a-d)). Friction use on the front tyres during $0 < s < 40$m shows a reduction from the maximum, corresponding to the curtailment of torque vectoring ability by actuator limitations. The same is true for the rear-right tyre when $160 < s < 210$m.

Time deltas relative to neutral steer (Figure 5.9(i)) show interesting symmetry about the point $s = 0.5s_f$, but no consistent trends as a function of understeer gradient. The

final time deltas are of small enough magnitude to be inconclusive, possibly as a result of optimisation peculiarities rather than the fundamental system dynamics.

In summary, for the 7DOF, as for the 3DOF model in chapter 4, manoeuvre time for the controlled vehicle is insensitive to the passive vehicle understeer characteristic for this manoeuvre. For the 3DOF model, the understeer gradient of the TV vehicle follows the passive closely; for the 7DOF model, the understeer gradient of the TV vehicle deviates increasingly from the passive value the further away from neutral steer. In addition, the 7DOF understeer gradient is not constant for the manoeuvre but shows a small variation towards greater understeer during deceleration and vice versa for acceleration, and a significant increase where torque vectoring is limited by motor constraints.

It must be reiterated that the open-loop set-up with T_{ij} directly applied is unrealisable in the real world for reasons noted in §5.2; nonetheless it demonstrates the required open-loop optimal controls to achieve optimality in terms of time minimisation. The next section will evaluate how close the closed-loop performance can approach the baseline open-loop result and what effect the yaw rate reference has on manoeuvre time.

5.4 Results: Closed-loop control

The second objective of this study is to evaluate the relative performance of the yaw rate reference on manoeuvre time by including the closed-loop TV feedback controller in the system dynamics. This section describes the inclusion of the closed-loop TV controller in the system dynamics to achieve this objective and compares results considering permutations in yaw rate reference.

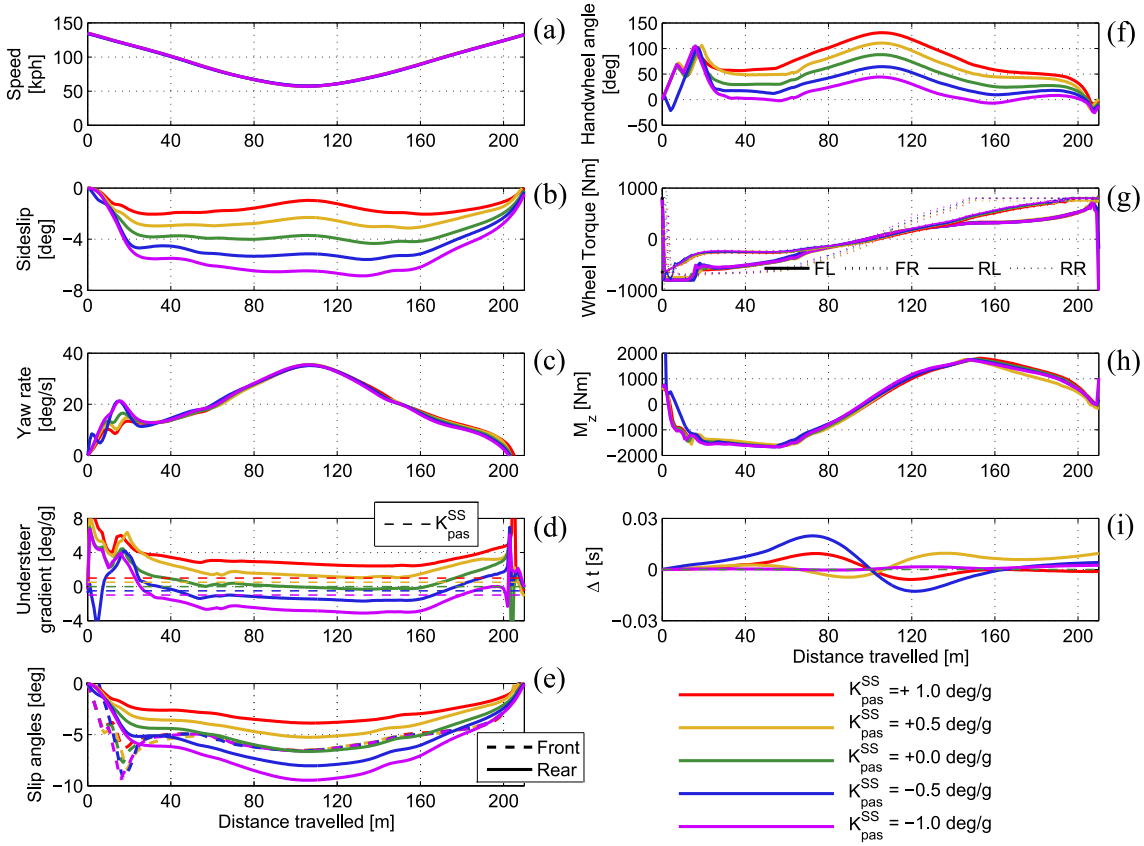

Figure 5.9: Effect of varying passive understeer gradient (defined by steady-state cornering stiffness) on vehicle with torque vectoring: states and controls

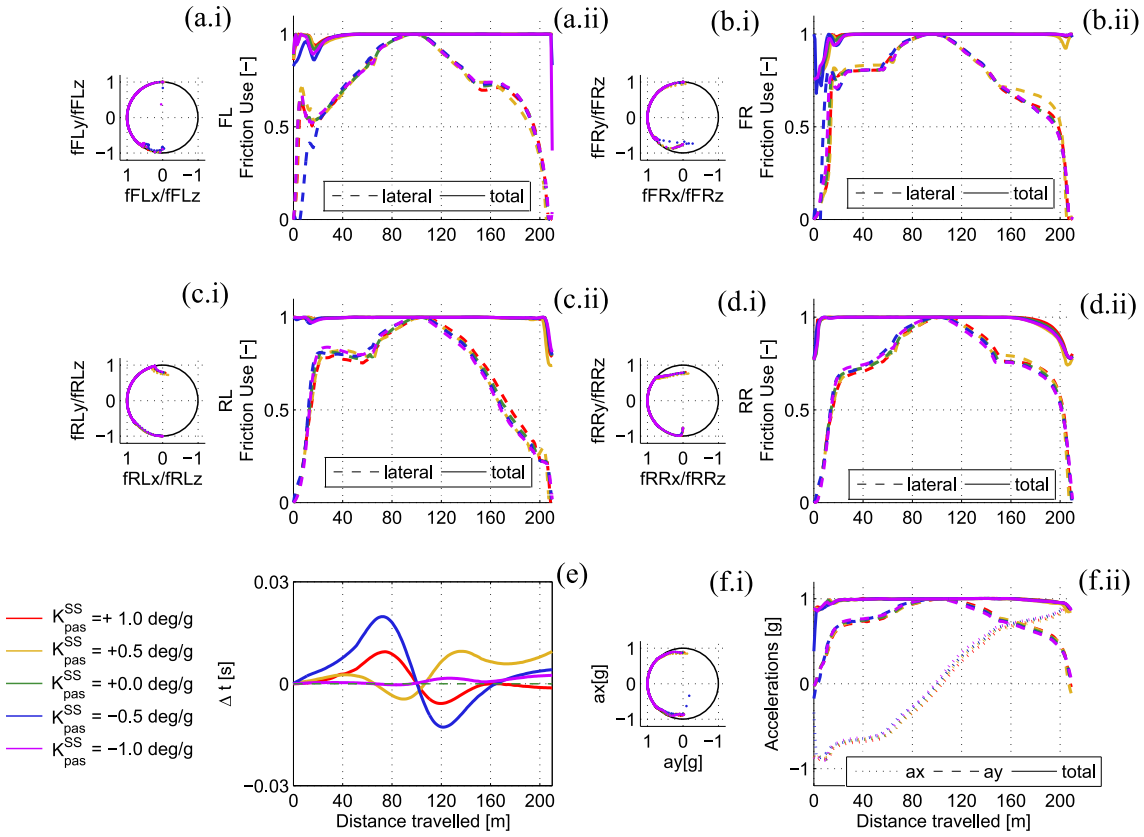

Figure 5.10: Effect of varying passive understeer gradient (defined by steady-state cornering stiffness) on torque vectoring-controlled vehicle: friction utilisation

5.4.1 Mathematical definition of TV controller in system dynamics

For optimisation of the closed-loop control algorithm (§5.2), modifications are made to the open-loop control method optimal control formulation used in §5.3. Figure 5.1(b) shows the optimal control configuration which including a simplified TV controller. The controller is identical to the one described in §4.5.1. with the exception of the control allocation.

Control Allocation

The requested yaw moment, M_z, is generated by the combination of wheel torques via the control allocation. After the overall difference in torque between the left and right tracks is calculated, the approach distributes torques front-rear by allocating wheel torques in proportion to the normal load on the axle, since this was found to be the optimal distribution in the literature for minimum-time manoeuvring [45, 59] and in general permits a higher cornering force [16]. The following approach is simplified from [93].

First, torque limits are calculated for left and right tracks: the minimum of motor limits and adhesion limits. The achievable overall longitudinal torque, T_x, is converted to longitudinal force, F_x, by division by the tyre radius. The torque that must be supplied by each track are given by the following equations:

$$T_L = \frac{r}{w}\left(\frac{w}{2}F_x - M_z\right), \tag{5.9}$$

$$T_R = \frac{r}{w}\left(\frac{w}{2}F_x + M_z\right), \tag{5.10}$$

$$\tag{5.11}$$

where T_L and T_R are the longitudinal torques to be supplied by the left and right tracks of the vehicle, respectively and w is the track width. The track torques are split front-rear

according to the proportion of normal load on each wheel:

$$T_{FL} = T_L \frac{f_{FLz}}{(f_{FLz}+f_{RLz})}, \qquad T_{FR} = T_R \frac{f_{FRz}}{(f_{FRz}+f_{RRz})}, \tag{5.12}$$

$$T_{RL} = T_L \frac{f_{RLz}}{(f_{FLz}+f_{RLz})}, \qquad T_{RR} = T_R \frac{f_{RRz}}{(f_{FRz}+f_{RRz})}. \tag{5.13}$$

$$\tag{5.14}$$

Thus, the overall torque demand, T_x, from the driver, and the yaw moment demand from the P-controller, M_z, are converted into the torques at each wheel, while considering motor and friction limits.

5.4.2 Effect of target understeer gradient

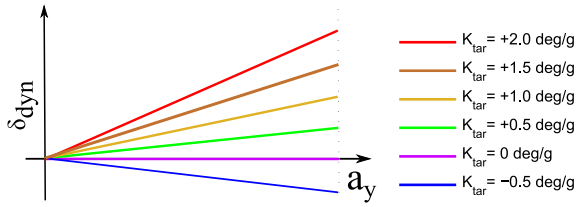

Figure 5.11: The steady-state single-track yaw rate references parameterised by target understeer gradient, K_{tar}, expressed in 'handling diagram' form; dynamic steering angle against lateral acceleration.

It has been observed that the optimally-controlled open-loop *control method* (TV) can reduce manoeuvre time by -0.380s over the vehicle with TV inactive for a U-turn manoeuvre with radius $R = 35$m. Now, incorporating the feedback controller into the optimal control system dynamics, the effect of yaw rate reference will be evaluated.

The standard steady-state single-track yaw rate reference is adopted once again (4.41), parameterised by the target understeer gradient, K_{tar}. The selection method of K_{tar} in the literature is heuristic, depending on preference for stability or agility. In the following,

Set-up	K_{tar} (°/g)	dev. from K_{pas}^{SS} (°/g)	Time (s)	Δt_f [a] (s)	Δt_f [b] (s)
OL	n/a	n/a	8.502	+0.000	-0.017
CL	2.0	+1.5	8.522	+0.019	+0.003
CL	1.5	+1.0	8.517	+0.015	-0.002
CL	1.0	+0.5	8.518	+0.016	-0.001
CL	+0.5	+0.0	8.519	+0.017	+0.000
CL	0.0	-0.5	8.523	+0.021	+0.005
CL	-0.5	-0.7	8.529	+0.027	+0.010

Table 5.2: Effect of yaw rate target (TV), Baseline $K_{pas}^{SS} = 0.5°$/g
[a]Time difference with respect to open-loop baseline.
[b]Time difference with respect to $K_{tar} = K_{pas}^{SS} = +0.5°$/g.

optimisations with $K_{tar} = \{-0.5, 0.0, +0.5, +1.0, +1.5, +2.0\}°$/g are performed. These optimisations will reveal: a) how close the causal *closed-loop control algorithm* can approach the a-causal baseline *open-loop control method*; b) the influence of target understeer gradient on manoeuvre time. Optimisations for a U-turn manoeuvre with $R = 35$m were run for each yaw rate reference. In Table 5.2, manoeuvre times and final time differences, Δt_f, relative to the open-loop (OL) baseline ($K_{pas}^{SS} = +0.5°$/g, penultimate column) and Δt_f to $K_{tar} = +0.5°$/g (ultimate column) are set out. The closed-loop (CL) controller with $K_{tar} = +0.5°$/g is able to complete the manoeuvre only $+0.017$s slower than the open-loop baseline. In the racing context, this could result in around $+0.2$s per 10-15 turn lap. The performance deficit of the closed-loop result to the baseline is 4% of the performance difference between *TV* and *NoTV*, so a large proportion of the potential is realised.

The second purpose of this section was to evaluate the influence of target understeer gradient on performance using the single-track reference. Manoeuvre times for the single-track reference lie within 0.012s of each other, with a standard deviation of 0.004s. This is a very small variation, which cannot be reliably attributed to the system dynamics alone;

discretisation and the particular numerical accuracies of the optimisation algorithm will have a bearing. Nevertheless, a physical explanation arising from the nonlinear tyre characteristics is given in §6.3. Thus, the data suggest that minimum-time manoeuvring with TV is largely insensitive to target understeer gradient. Analysis of the vehicle behaviour

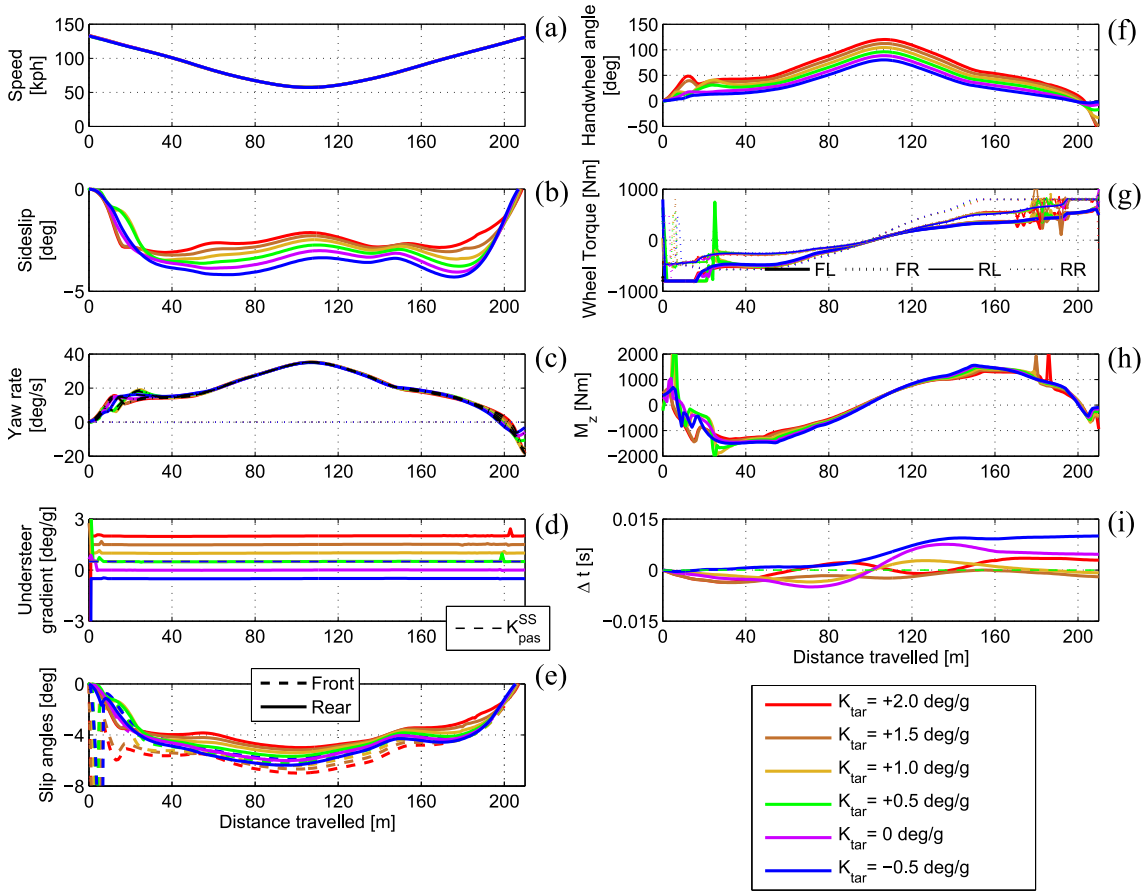

Figure 5.12: Comparison of closed-loop torque vectoring performance for a range of oversteering to understeering target gradients, K_{tar}: states and controls.

over the course of the manoeuvre yields further insight. Figure 5.12 overlays states, controls and calculated quantities for the closed-loop optimisations: $K_{tar} = \{-0.5, 0, 0.5, 1.0, 2.0\}^\circ$/g. Figure 5.12(a) shows a common speed trace for all cases. Of key interest is the yaw rate and understeer gradient, since these are the object of control and the high-level means by which to control it, respectively. Yaw rate (Figure 5.12(c)) follows the refer-

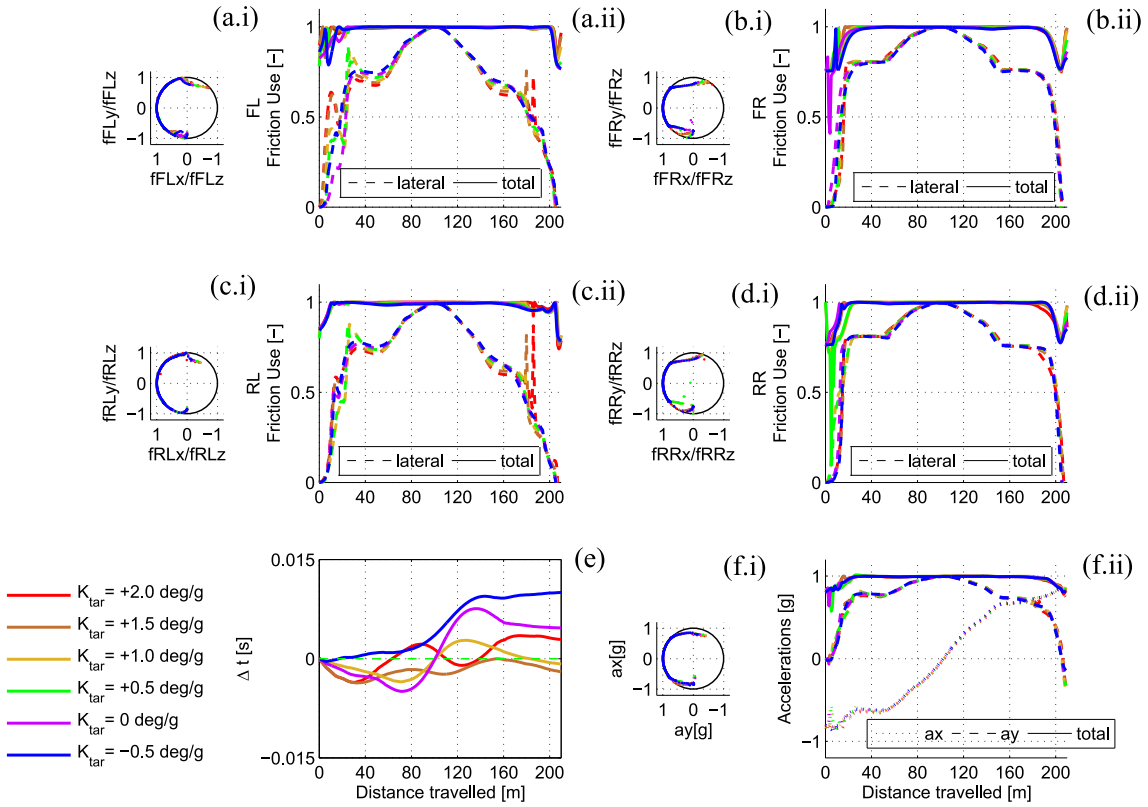

Figure 5.13: Comparison of closed-loop torque vectoring performance for a range of oversteering to understeering target gradients, K_{tar}: friction utilisation

ence closely and, in so doing, achieves the target understeer gradient (Figure 5.12(d)) in all cases.

Sideslip (Figure 5.12(b)) is tail-out for all simulations, with increasing magnitude as understeer gradient reduces. The difference in sideslip between most extreme targets ($K_{tar} = 2°$/g and $K_{tar} = -0.5°$/g) has a maximum over the course of the manoeuvre of 2.5°. The maximum difference between optimisations of handwheel angle is 40°, which is a significant difference in workload for the driver.

The most noteworthy feature of these results is that a very similar yaw rate is achieved for each understeer target. There is, therefore, a general yaw rate profile for this particular K_{pas}^{SS}, that minimises manoeuvre time, to within a very small tolerance—yet it is achieved through a variety of combinations of target understeer gradients and driver control inputs. According to equation (4.41), the only means to achieve the same yaw rate profile is by modification of the steering angle, as L and K_{tar} are constant and V is to be maximised at all times and does not vary according to target. Figure 5.12(f) shows that handwheel angle is increased in inverse proportion to K_{tar}, with greatest steering angles required for $K_{tar} = 2°$/g. Note that the ability to follow this yaw rate profile is dependent on the 'perfect' driver (which the optimal control represents) maximising the potential of the controlled-vehicle set-up.

The yaw moment provided by the torque difference between left and right tracks shows a similar trend for all targets: stabilising effect under braking and destabilising under acceleration. A greater magnitude of yaw moment (and therefore torque difference across tracks) is required as understeer target decreases, observable in the regions $20 < s < 60$m and $120 < s < 180$m.

Further insight is drawn from plots of friction utilisation, as shown in Figure 5.13. The immediate observation is that, with the exception of the initial and final 10m and 20m respectively where torque is limited, friction utilisation is maximal for every tyre,

for every understeer target. Maximum total friction use is key to maximum performance. This is a combination of the effects of torque vectoring and driver control inputs.

The steady-state single-track reference is a very simple expression, parameterised simply by the length of the vehicle in addition to the understeer target. This simplicity is undoubtedly a key reason for its widespread adoption in the literature.

Results of the open-loop control method optimisations in §5.3 demonstrated that torque vectoring seeks to neutralise the negative effects of weight transfer on total cornering force. It achieves this using two mechanisms: directly by generating a yaw moment from the left-right torque difference; indirectly by longitudinal forces influencing the cornering stiffness and therefore lateral forces -and the associated yaw moments generated- through coupling effects. The steady-state single track reference in effect commands not only no lateral load transfer (since there is no track width) but also no longitudinal load transfer (since it does not consider longitudinal dynamics). Thus, its inherent characteristics match the characteristics observed in the optimal baseline open-loop results, and this is why it delivers a very high level of performance even in the 7DOF model.

In this section, it has been demonstrated that in spite of the simplicity of the single-track yaw rate reference, a high level of performance is still achieved. This level of performance is not affected by the choice of target understeer gradient, opening up the possibility of selecting the target based on driver preference– without loss of performance.

5.5 Conclusions

This chapter has studied the effect of handling characteristics, passively and actively modified, of torque-vectored vehicles for minimum-time manoeuvring, using a 7DOF vehicle model with nonlinear tyres and lateral load transfer. Optimal control techniques were used

to generate open-loop control trajectories for a U-turn manoeuvre for an electric vehicle with 4 independent motors. Results confirmed that TV is able to compensate for adverse load transfer effects encountered under acceleration, braking and high lateral accelerations. The effect of altering the passive handling of the vehicle was studied, concluding that while the passive characteristics of the vehicle had negligible effect on the minimum-time performance of the TV-controlled vehicle, notable differences in the steering input and sideslip response were observed.

An optimal control framework that incorporated a TV controller in the system dynamics was then used to evaluate the ability of the controller to realise the baseline potential when following a yaw rate reference. The standard steady-state single-track model reference was shown to come close to the baseline performance. Finally, a major finding is that manoeuvre time for the reference-following TV vehicle is largely insensitive to target understeer gradient, opening up the possibility of subjective target selection without compromising performance.

Chapter 6

Time-optimal handling: Further modelling analysis

6.1 Introduction

Chapters 4 and 5 exposed key similarities and differences between the 3DOF and 7DOF vehicle models. Both models demonstrated that torque vectoring could deliver a very similar manoeuvre time, irrespective of the passive handling balance. However, it was shown that the 3DOF model manouvrer time is highly sensitive to targer understeer gradient, whilst the 7DOF model is largely insensitive.

In this chapter, the mechanisms and modelling assumptions that give rise to these similarities and differences are explored in more detail, by both assessing the generalised dynamics behaviour and investigating specific scenarios.

First, generalised time-optimal yaw rate gain surfaces are generated for both vehicle models, including an assessment of the impact of motor limits on the results. Secondly,

open-loop manoeuvres are performed to assess the effect of modelling assumptions on friction usage, as a proxy for minimum-time manoeuvring.

6.2 Time-optimal yaw rate gain surfaces

Three-dimensional time-optimal yaw rate gain surfaces as a function of longitudinal acceleration and vehicle speed are generated for both vehicle models. Surfaces that demonstrate the effects of limiting motor torque (and therefore realisable yaw moment) are also generated.

The surfaces are generated from optimisation results. OCPs described in chapters 4 and 5 are re-run for the same U-turn manoeuvre, for additional turn radii of $R \in [10{:}10{:}80]$m.

Yaw rate gain is calculated simply by the division of yaw rate by steering angle for all data points of the simulations ($\frac{\dot{\psi}}{\delta}$). In the following analyses, the steady-state analytical definition for yaw rate gain is used by means of comparison [6]:

$$\frac{\dot{\psi}}{\delta} = \frac{V}{K_{nat}^{SS} V^2 + L}, \tag{6.1}$$

Note that the passive understeer gradient, K_{nat}^{SS}, is used to parametrise the equation.

6.2.1 3DOF with/without Mz constraints

In Figure 6.1, yaw rate gain surfaces are plotted for the 3DOF vehicle model simulation results, continuing from chapter 4. Individual data points from simulation are plotted over the analytical mesh surface defined by (6.1). Figure 6.1(a) shows the *TV* result, while Figure 6.1(b) shows the result with TV inactive. Figure 6.1(a) shows clearly that

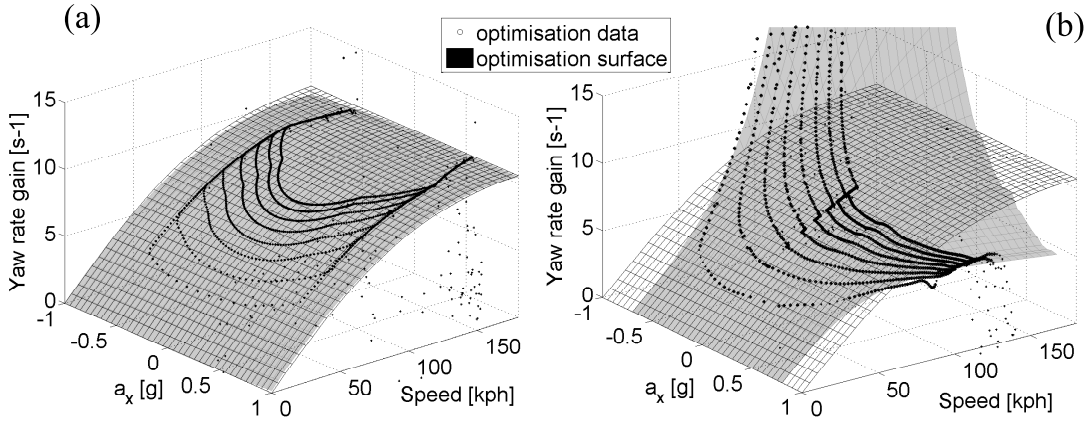

Figure 6.1: Yaw rate gain surfaces as a function of speed and longitudinal acceleration dynamic OCP results (grey surface) overlaid on steady-state analytic (mesh) for (a) TV and (b) TV inactive.

the TV-controlled vehicle data points lie on the passive surface. Conversely, the TV inactive optimisation surface shows that under braking, yaw rate gain exceeds the natural characteristic, tending to a greater oversteer behaviour with increasing magnitude of deceleration. It is also seen that yaw rate gain increases with speed under braking, tending to infinity at critical speed. While under longitudinal acceleration, the yaw rate gain response is lower than the passive response, leading to an increase in understeer. Where a_x=0m/s^2, the numerical fit from OCPs intersects the analytical solution. Figure 6.1(a) generalises the specific solution for *TV*: that for all dynamic manoeuvres in this range, *TV* is able to negate load transfer effects such that the yaw rate gain response is identical to the steady-state response.

The surfaces in Figure 6.1 do not consider constraints on the feasible yaw moment by considering motor torque limits. It was seen in §4.4.2 that enforcing yaw moment constraints inhibits torque vectoring effectiveness at high speeds. The surfaces considering yaw moment constraints is shown in Figure 6.2 in green, in addition to *NoTV* and *TV* without yaw moment constraints (3 projections are shown to give a clearer picture).

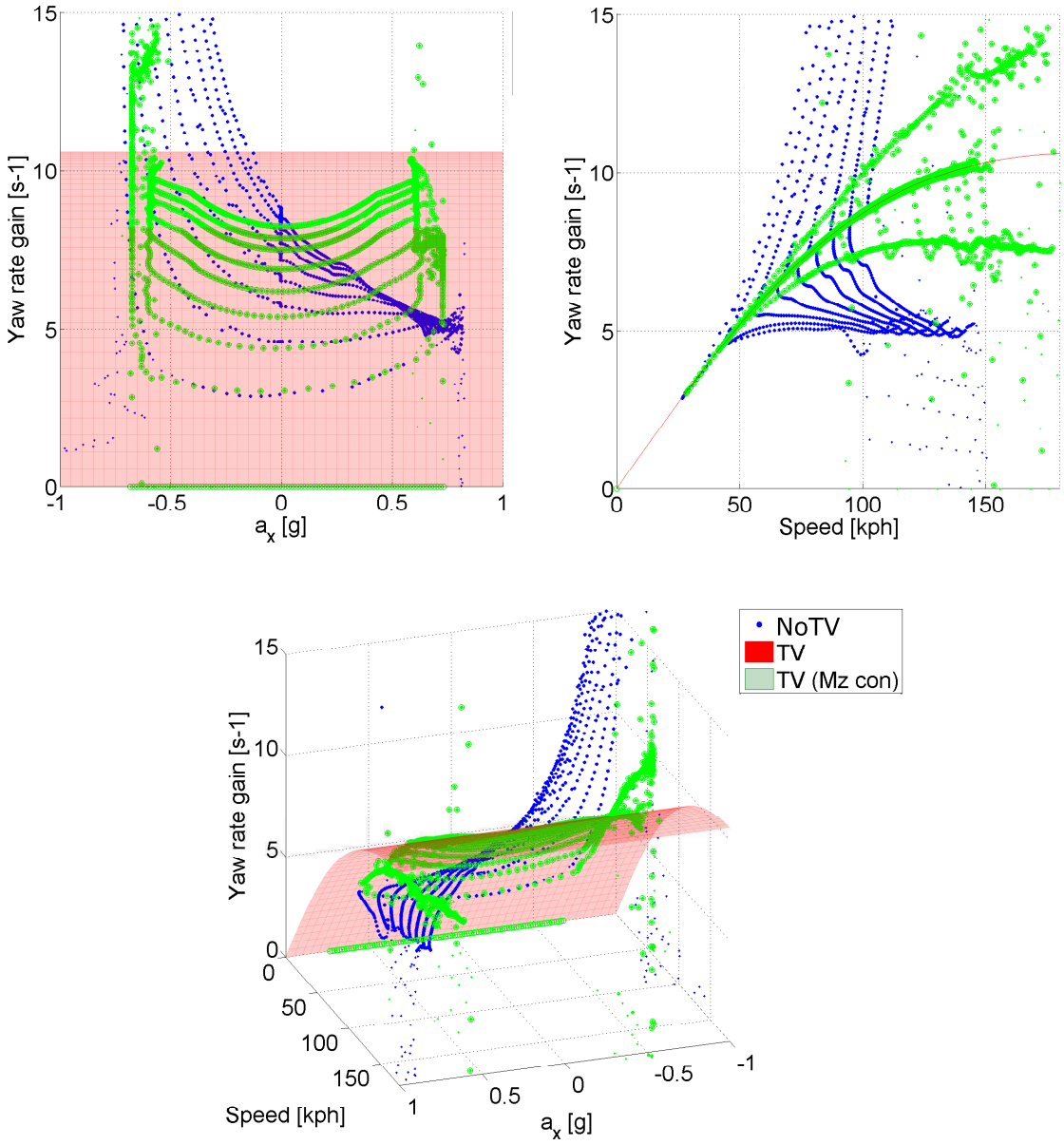

Figure 6.2: Yaw rate gain surfaces as a function of speed and longitudinal acceleration dynamic OCP results for *TV-inactive* (blue points), *TV* (red surface) and *TV con* (green points)

It is clear that with yaw moment constraints, the vehicle behaviour is no longer able to attain the unconstrained response in all conditions. The ability of the TV system at high longitudinal accelerations to counteract load transfer effects is reduced and therefore the yaw rate gain falls where $a_x > 0.6$g (due to an increased steering angle for the same yaw rate) and increases where $a_x < 0.6$g (due to an reduced steering angle for the same yaw rate).

6.2.2 7DOF with/without torque constraints

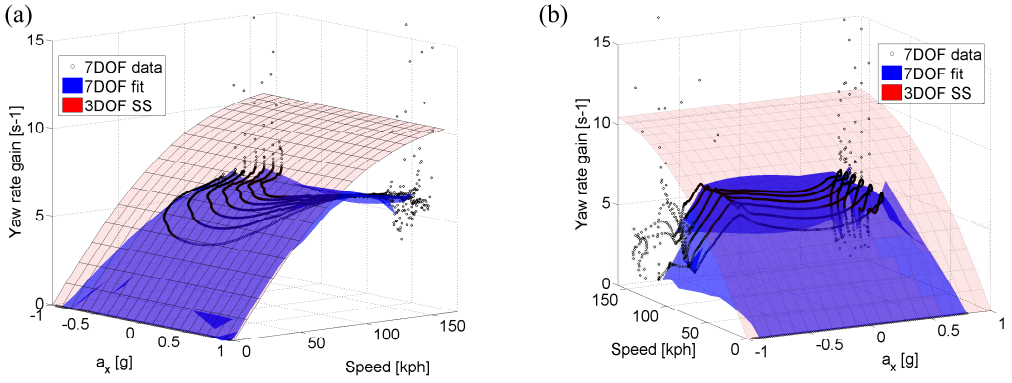

Figure 6.3: Yaw rate gain as a function of speed and longitudinal acceleration for 7DOF model optimisations (a) unlimited motor torque (b) considering motor torque limits. 7DOF model dynamic OCP results (data points) are overlaid by a simple, minimum-curvature fit to a coarse grid (blue surface). The analytically-calculated 3DOF model steady-state yaw rate gain is included for comparison (red surface). Straightline running initial conditions were not enforced in order to focus on the dominant shapes by excluding highly transient data.

Yaw rate gain surfaces were generated for the 7DOF vehicle model, using the results form optimal control manoeuvres in chapter 5. Figure 6.3 shows a surface yaw rate gain as a function of speed and longitudinal acceleration for 7DOF model optimisations (a) unlimited motor torque (b) considering motor torque limits. The data points are the results from optimisations, whilst the mesh surface is the steady-state single-track analytical

expression (6.1).

Figure 6.3(a) generalises the specific solution for *TV* from §5.3.1: that for all dynamic manoeuvres in this range, *TV* is able to a great extent to negate load transfer effects such that the yaw rate gain response shows little variation with longitudinal acceleration. It further demonstrates the observation that the understeer characteristic is greater for the 7DOF model than the steady-state single-track (3DOF) model (lower yaw rate gain). A likely explanation for this is that the tyre model cornering stiffnesses are only equivalent at zero slip angle only ($\eta_i = B_i CD$), and not considering combined slip. At non-zero slip angles, the difference between front and rear cornering stiffnesses for the nonlinear tyre model are not the same as for the linear model. Hence, from Figure 6.3, it can be concluded that since the nonlinear tyre yaw rate gain surface has a lower degree of average yaw rate gain, that the front cornering stiffness is lower relative to the rear cornering stiffness than for the linear tyre and hence there is a greater degree of understeer in dynamic conditions. This also explains why the dynamic understeer gradient shown in Figure 5.8(d) and Figure 5.9(d) do not follow the passive steady-state values, while in Figure 4.4(d) and Figure 4.8(d), the linear tyre model do.

Figure 6.3(b) shows that imposing motor torque limits of 750Nm (and hence the feasible TV yaw moment) reduces the ability of the TV system to counteract load transfer effects at high longitudinal accelerations and therefore the yaw rate gain falls dramatically where $|a_x| > 0.6$g (due to an increased steering angle for the same yaw rate). The key difference between the 3DOF and 7DOF vehicle models when considering realistic yaw moments is under braking. For 3DOF, this yaw rate gain was higher when yaw moment is limited, while for 7DOF it is reduced.

6.3 Vehicle Model comparison: open loop manoeuvre

Chapters 4 and 5 present results from an identical methodology for 3DOF and 7DOF vehicle models. For closed-loop control manoeuvring, it was found that for the 3DOF model, manoeuvre time was minimised by setting $K_{tar} = K_{pas}^{SS}$ and significant degradation in time was found when K_{tar} deviated from K_{pas}^{SS}; while the 7DOF vehicle was largely insensitive to target understeer gradient.

This section investigates what mechanisms caused these contradictory results between models. In order to isolate the contribution of the controlled vehicle from the driver action, open-loop manoeuvres were conducted in Matlab with these vehicle models. Since limit operation was of interest, a steady-turn skidpad manoeuvre was chosen, with the vehicle subject to constant longitudinal acceleration to deliver a combined cornering condition. Simulations were conducted with a starting speed of 1kph, handwheel angle of 60° and a longitudinal acceleration of 0.2g. With TV active, the following range of target understeer gradients were run for each vehicle model: $K_{tar} = \{0.5, K_{pas}^{SS}, +1.5\}^\circ$/g, i.e. 1°/g either side of the passive understeer gradient. Tyre friction utilisation was taken as a metric to demonstrate which model could extract the most performance from the vehicle, and therefore by proxy, would reduce manoeuvre time when run in a closed-loop manoeuvre

There are three principal differences between the 3DOF and 7DOF models: tyre model (linear coupled-at-limit vs. nonlinear combined-slip-coupled); lateral load transfer (none vs. quasi-static); torque vectoring yaw moment generation mechanism (external yaw moment approximation vs. left-right track torque difference). The results of investigating each follow.

6.3.1 Effect of tyre model

The modelling effect that delivered the greatest influence on the results was the tyre model. Recall that the 3DOF vehicle model used a linear tyre model, with a friction circle constraint reducing the lateral force when the combined tyre friction reaches the combined limit. The 7DOF model utilised a combined-slip Pacejka model, such that there was a persistent coupling between tyre forces. To isolate the effect of the tyre models, simulations were run for the 3DOF linear model and then with the 3DOF model fitted with the nonlinear tyre model used by the 7DOF model previously.

In Figures 6.4, 6.5, and 6.6, total friction usage is plotted as a function of manoeuvre time, in addition to understeer gradient and slip angles. Slip ratios are also included for the nonlinear models. In each, the top left (a.i) shows the time-histories of the 3DOF linear and (a.ii) shows the 3DOF nonlinear time-histories. As speed and lateral acceleration increase over the duration of the manoeuvre, the tyre slips increase and hence the tyre friction utilisation accordingly. The values of slip angle and slip ratio when the first axle reaches peak friction are plotted. Tyre curves corresponding to these values of slip ratio are plotted as a function of slip angle and the operating points denoted by markers in Figures 6.4, 6.5, and 6.6(b).

In Figure 6.4, where $K_{tar} = K_{pas}^{SS}$, friction utilisation is maximal for 3DOF linear, the difference in slip angles means that front and rear axles reach peak friction simultaneously. The nonlinear tyres are also close to maximal.

In Figure 6.5, where $K_{tar} = 1.5°/\text{g}$, the rear tyre operates at lower friction levels, reducing performance. Notice that the nonlinear tyre curve differs from Figure 6.4 due to the presence of longitudinal slip. Nevertheless, tyre friction is close to maximal, as the gradient of the slope still tends to zero as the peak is approached.

In Figure 6.6, where $K_{tar} = -0.5°/\text{g}$, the rear tyre reaches peak friction first. A similar

effect to Figure 6.5 is shown for the linear tyre. Whilst the slope of the nonlinear tyre curve as the peak is approached is greater than the previous examples, the reduction in tyre friction is small compared to the linear reduction in tyre friction.

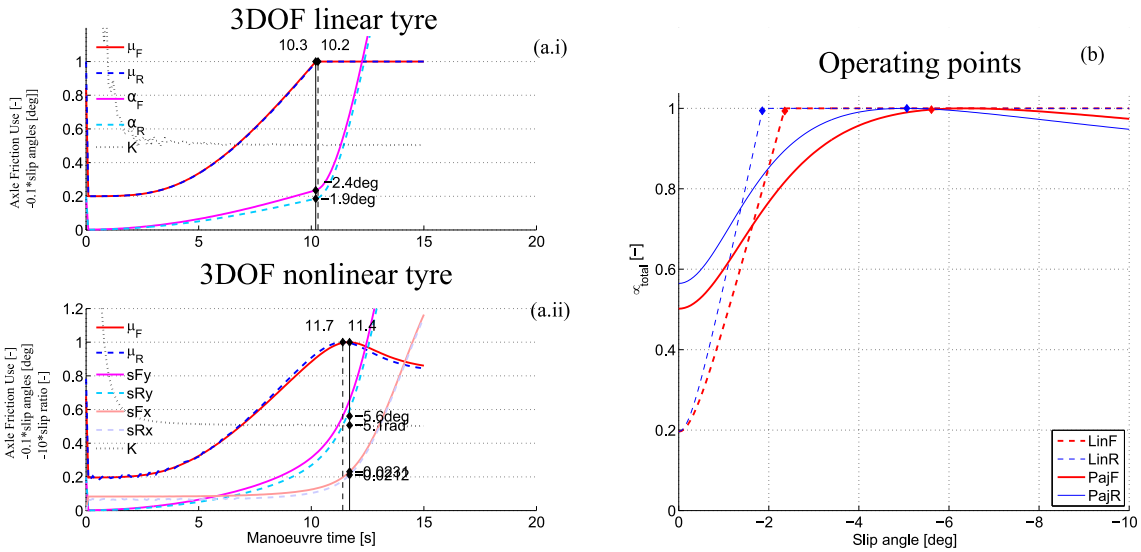

Figure 6.4: $K_{tar} = K_{pas}^{SS} = 0.5°/g$ Comparison of friction utilisation against manoeuvre time for: (a.i) 3DOF with linear tyres; (a.ii) 3DOF with nonlinear tyres; (b) Tyre friction plots as a function of slip angle, with operating points corresponding to front friction peak values highlighted by markers

General explanation of the effect of tyre nonlinearity The open loop manoeuvre results point clearly to the nonlinearity of the tyre model. By examining the tyre curves for pure lateral motion, and leveraging the steady-state definition of understeer gradient, a simple, general explanation can be given for the behaviour seen in the open-loop manoeuvre. For simplicity, Figure 6.7 plots lateral friction against slip angle, assuming pure steady state cornering with zero longitudinal acceleration. Linear and nonlinear tyre models are shown for front and rear tyres. Rear stiffness is greater than front to give $K_{pas}^{SS} = 0.5°/g$. The tyre models are equivalent at zero slip only ($\eta_i = B_i CD$) and hence the nonlinear tyre lags the linear at higher values of slip, and reaches its peak at a higher slip angle.

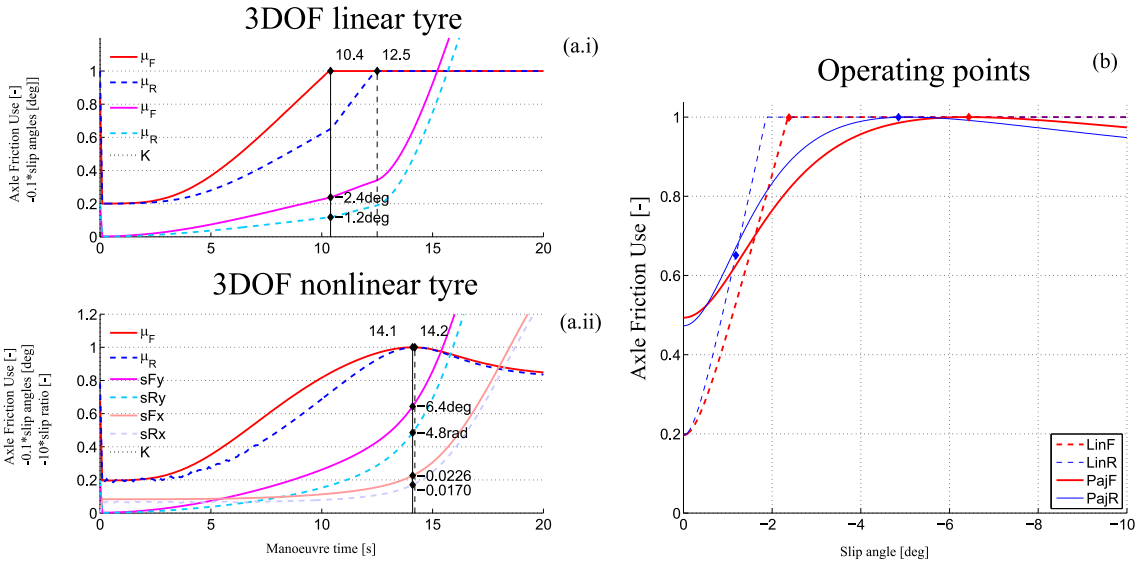

Figure 6.5: $K_{tar} = 1.5°/g$ Comparison of friction utilisation against manoeuvre time for: (a.i) 3DOF with linear tyres; (a.ii) 3DOF with nonlinear tyres; (b) Tyre friction plots as a function of slip angle, with operating points corresponding to front friction peak values from highlighted by markers

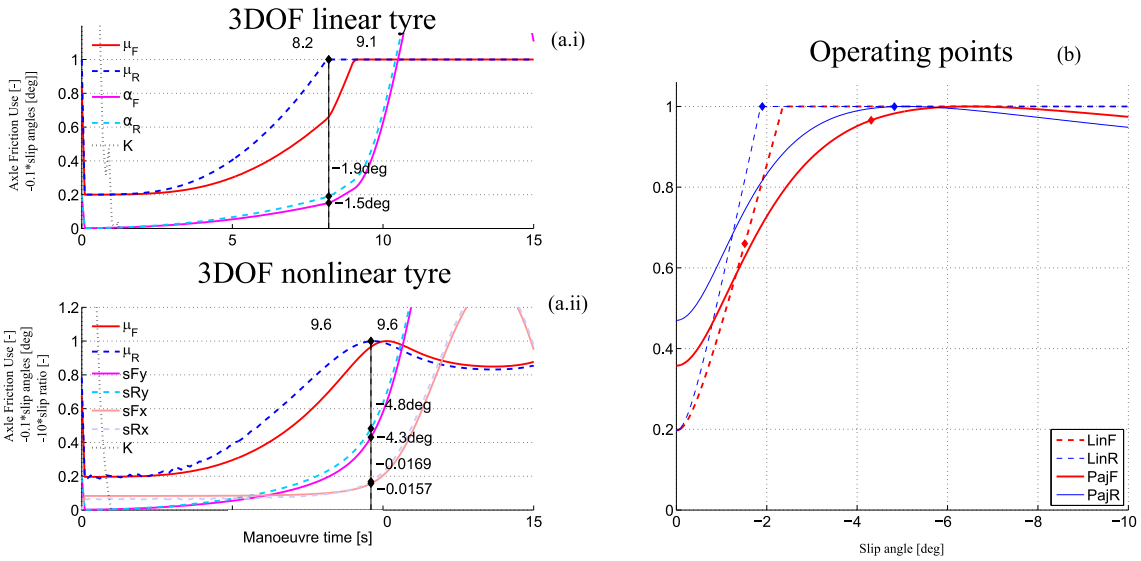

Figure 6.6: $K_{tar} = -0.5°/g$ Comparison of friction utilisation against manoeuvre time for: (a.i) 3DOF with linear tyres; (a.ii) 3DOF with nonlinear tyres; (b) Tyre friction plots as a function of slip angle, with operating points corresponding to front friction peak values from highlighted by markers

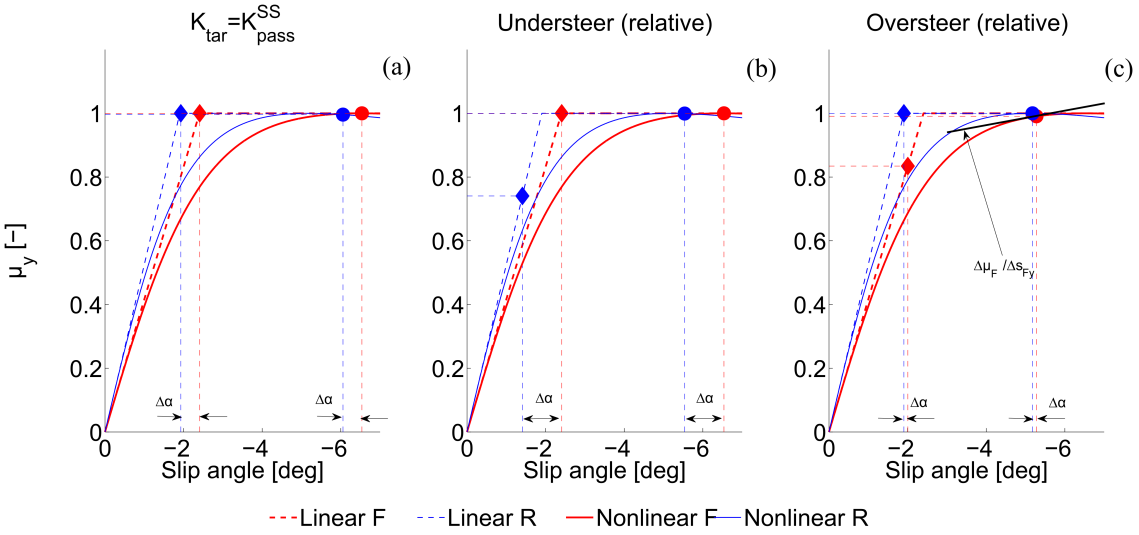

Figure 6.7: Linear and nonlinear lateral tyre friction curves for steady-state cornering as a function of slip angle. Operating points shown following target understeer gradients (a) where $K_{tar} = K_{pas}^{SS}$, (b) relative understeer with respect to K_{pas}^{SS}, and (c) relative oversteer with respect to K_{pas}^{SS}.

To acheive a target understeer gradient at a given lateral acceleration, a difference in slip angles, $\Delta\alpha$, is required, since understeer gradient is related to slip angles from the definition [6] (note that this is equivalent to equation (4.30)):

$$K_{SS} = (|\alpha_f| - |\alpha_r|)/a_y = \Delta\alpha/a_y. \tag{6.2}$$

To demonstrate and explain the difference between the tyre models, reference are made to the three cases of $K_{tar} = K_{pas}^{SS}$, as well as understeer and oversteer targets in Figure 6.7(a), (b) and (c) respectively.

- **Target=Passive.** $K_{tar} = K_{pas}^{SS}$ (Figure 6.7(a)). As steady-state velocity is increased, lateral acceleration and slip angles increase. The peak tyre friction is approached at front and rear simultaneously for the linear tyre, since $\Delta\alpha$ to respect the K_{tar} matches that for K_{pas}^{SS}. Total tyre friction is $\sum\mu = 2$. For the nonlinear tyre, the

cornering stiffness is not identical front and rear, at high slip angles, so peak tyre friction is reached at front slightly before rear, but still offering near-maximal total friction ($\sum \mu_{nonlinear} \sim 2$).

- **Relative understeer:** $K_{tar} > K_{pas}^{SS}$(Figure 6.7(b)). In this case, the front tyres peak first: a greater $\Delta\alpha$ is required than for K_{pas}^{SS}, and hence for the linear case, the rear tyres cannot deliver maximum friction utilisation ($\sum \mu \sim 1.75$). For the nonlinear tyres, the same $\Delta\alpha$ is required, yet $\sum \mu_{nonlinear} \sim 2$. As slip angle increases and the peak of the $\mu-$slip curve is approached, the gradient of the curve for the linear tyre remains high, whereas in the nonlinear case the gradient approaches zero.

- **Relative oversteer:** $K_{tar} < K_{pas}^{SS}$(Figure 6.7(c)). This is a similar situation to relative understeer, except that the rear tyres saturate first. $\Delta\alpha$ is much smaller than for K_{pas}^{SS} (and is still positive, since in absolute terms, the target is still mildly understeering). For the linear case, the front tyres cannot deliver maximum friction utilisation ($\sum \mu \sim 1.82$). Again, the $\Delta\mu/\Delta\alpha$ gradient at the peak of the nonlinear tyres is close to zero for the rear tyre. However, the front tyre is operating further from the peak that in (a) and (b) and hence the the $\Delta\mu_F/\Delta s_{Fy}$ gradient is slightly increased — yet the total tyre friction generated is still close to maximal.

Therefore, at any target where $K_{tar} \neq K_{pas}^{SS}$, tyre friction levels for linear are non-maximum (decreasing as the difference between the target and the passive increases) whereas the nonlinear tyre model is always close to maximal, since even with a large difference in slip angles (front-rear), the reduction in tyre friction will be very small. Tyre force coupling of the nonlinear tyres below the limit further improves the overall friction level, as at high slip ratios, the $\Delta\mu/\Delta\alpha$ angle gradients are even closer to zero as the peak is approached. Further investigation revealed that lateral load transfer contributes a minor influence but the control allocation distributing torque according to normal load ensures

that tyre cornering stiffnesses are equalised as far as possible between all four tyres.

Remark 4 *Clearly, if a sufficiently large* $\Delta\alpha$ *was imposed by the TV controller, nonlinear tyres would result in loss of* $\sum \mu_{nonlinear}$. *However, for the range of* K_{tar} *considered in this paper (resulting in large variation in maximum steering angle) the optimal performance is practically insensitive to* K_{tar}.

6.3.2 Effect of lateral load transfer

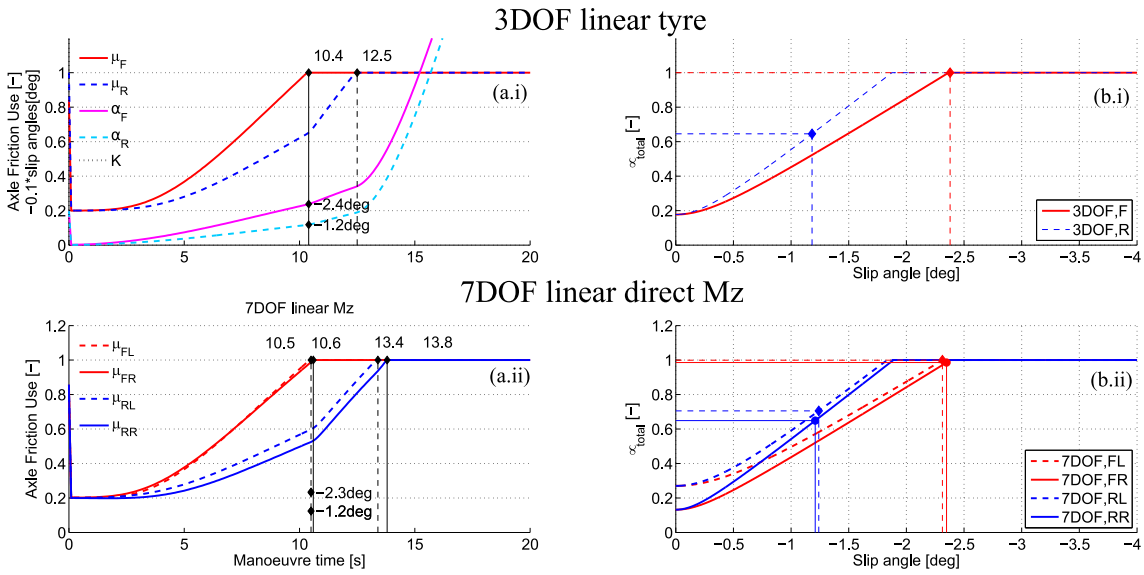

Figure 6.8: $K_{tar} = 1.5°$/g. Comparison of friction utilisation against manoeuvre time for: (a.i) 3DOF with linear tyres; (a.ii) 7DOF with linear tyres; (b.i) Tyre friction plots as a function of slip angle (3DOF); (b.ii) Tyre friction plots as a function of slip angle (7DOF). Operating points corresponding to front friction peak values (3DOF) and FL (7DOF)

Figure 6.8 shows the effects of lateral load transfer (LLT) on tyre friction utilisation by comparison of the 3DOF model and 7DOF model. As shown in the previous section, linear tyres do not allow simultaneous operation at the peak for front and rear for the

3DOF model if the target is not equal to the passive understeer gradient. This holds true also for the 7DOF model fitted with linear tyres (yaw moment is generated by M_z term in the yaw acceleration equation to ensure LLT is the only variable). Other targets show a similar effect. The FL tyre reaches peak friction level first, so all other friction levels are calculated at the operating points when FL reaches peak. On the right hand track (greater loading), the cornering stiffnesses are greater relative to the inner left track. Therefore, when the $\Delta\alpha$ concept is invoked, it can be seen that the loaded track generates overall slightly less friction than the inner track. Thus, LLT when considering linear tyres gives a negative effect. However, the difference is not as marked as when comparing linear and nonlinear tyres (not shown) for the same reason of the reduced slope near the peak (see Fig. 6.7(c)).

6.3.3 Effect of TV mechanism

The yaw moment term, M_z, in the single-track yaw dynamics equation (2.3) was introduced with the objective of emulating the left-right torque vectoring capability of the vehicle. The contributions to the total yaw moment applied to the vehicle from lateral and longitudinal forces and direct yaw moment assuming small-angle approximations, are:

$$M_z^{lat} = F_{yf}\ell_f - F_{yr}\ell_r \tag{6.3}$$

$$M_z^{long} = 0 \tag{6.4}$$

$$M_z^{tot} = M_z^{lat} + M_z \tag{6.5}$$

For a double-track, four-wheel model, the yaw moment contributions, assuming small-angle approximations are:

$$M_{z,4WM}^{lat} = (F_{yfl}+F_{yfr})\ell_f-(F_{yrl}+F_{yrr})\ell_r \tag{6.6}$$

$$M_{z,4WM}^{long} = \frac{w}{2}\left(-F_{xfl}+F_{xfr}-F_{xrl}+F_{xrr}\right) \tag{6.7}$$

$$M_{z,4WM}^{tot} = M_{z,4WM}^{lat}+M_{z,4WM}^{long} \tag{6.8}$$

where w is the vehicle track width. Since there is a coupling between lateral and longitudinal forces for the nonlinear tyre model (a coupling is only included on the limit of the friction circle for the linear tyres for the single-track model), it is not possible to directly compare the two models. In general, however, it can be observed that M_z for the single track model is equivalent to the yaw moments that arise from the longitudinal force components of the 4WM with a lever arm of half the track width:

$$M_z \simeq M_{z,4WM}^{long} = \frac{w}{2}\left(-F_{xfl}+F_{xfr}-F_{xrl}+F_{xrr}\right). \tag{6.9}$$

To compare the modelling effects on performance of generating the torque vectoring yaw moment via a direct term (as in the 3DOF model) and the longitudinal force difference between tracks (7DOF model), a new model was required. To keep the tyre model and lateral load transfer consistent between models, the 7DOF nonlinear tyre model was developed to include a direct yaw moment term in the yaw acceleration equation. The value of this was calculated from the P controller in exactly the same manner to the 7DOF model used in chapter 5. The control allocation distributed torques front-rear according to normal load for left and right tracks independently, as presented before, however, the torque difference between tracks was set to zero, such that controlled torque vectoring

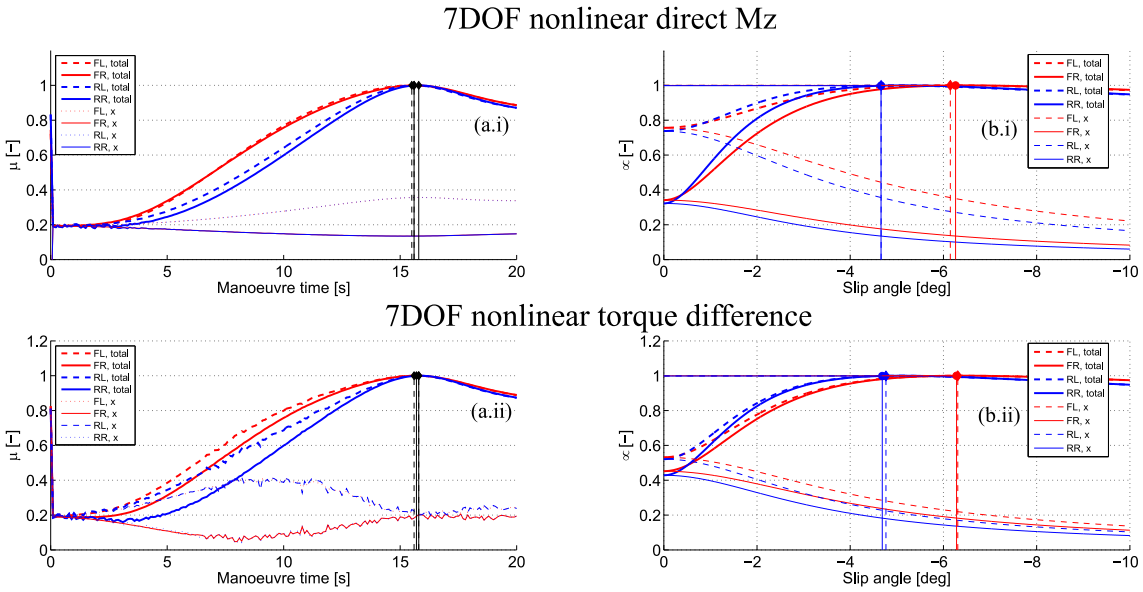

Figure 6.9: $K_{tar} = 1.5°/g$ Comparison of friction utilisation against manoeuvre time for 7DOF nonlinear tyres with yaw moment generation mechanism: (a.i) direct yaw moment; (a.ii) yaw moment from torque differential; (b.i) and (b.ii) Tyre friction plots as a function of slip angle, with marked operating points corresponding to operating points denoted in left figures.

yaw moment was generated solely from the direct term. Note that the since a contribution to yaw moment is still generated from unbalanced tyre forces that arise from load transferl

In Figure 6.9, 7DOF with direct yaw moment are plotted in (a.i, b.i), 7DOF with realistic torque difference in (b.i, b.ii). Plots (a) show time histories of the same open-loop manoeuvre described in previous subsections. Peak friction points are depicted with circles. The lateral and longitudinal slips and normal loads where the FL tyre saturates are used to construct the tyre force curves in the plots on the right hand plot. By varying lateral slip angle, while maintaining the same normal force as the peak and respecting the combined slip equations, the friction utilisation curves are completed.

In Figure 6.9(a.i) and (a.ii), it can be seen that the peak tyre forces are achieved at identical times, despite different tyre force histories up to the peak. In Figure 6.9(a.i) it can be seen that the longitudinal μ values are equal for FL and RL; FR and RR, since

friction is proportional to normal load on each track. Since overall torque demand is split 50/50 between tracks, as the degree of lateral load transfer to the right track increases with lateral acceleration (as time passes), a greater proportion of longitudinal friction is used by left tyres and lesser proportion by right tyres.

Conversely, Figure 6.9(a.ii) shows longitudinal μ difference between tracks increase, then decrease to almost zero at the peak.

Inspection of Figs. 6.9(b.i) and (b.ii) shows that despite differences in the overall friction utilisation curves below the peak, peak friction is still found at the same slip angles. Since the slip angle-friction utilisation slopes are almost identical at the peak, the overall friction utilisation is essentially identical for both yaw moment generation mechanisms. However, it is important to note that is the tyres were operating at lower slip angles, the difference in the slip angle-friction utilisation slopes, would differentiate the performance of the TV generation mechanism. Hence, for limit operation, the conclusion is that TV mechanism is unimportant.

6.4 Conclusions

Generalised yaw rate gain surfaces were generated by further OCPs run for different radii U-turns. The 3DOF model was able to entirely compensate for load transfer effects and deliver TV-controlled performance equal to the steady-state yaw rate gain surface. For open-loop control in nonlinear optimal control, yaw rate gain is insensitive to longitudinal acceleration. When considering yaw moment constraints related to torque limits of the motors, the ability of TV to counteract load transfer effects is reduced at high longitudinal accelerations.

Similarly, the 7DOF model was able to negate load transfer effects to a large extent,

with the yaw rate gain surface largely insensitive to longitudinal acceleration, except at high longitudinal accelerations when considering feasible limits on motor torques. Difference in effective tyre cornering stiffness leads to lower values of yaw rate gain for the 7DOF model.

The three key differences between the models was investigated in open-loop constant steer, steady longitudinal acceleration open-loop manoeuvres. The effect of using the nonlinear, combined-slip tyre model was found to be the most influential, since near the peak friction, the gradient of the slip-friction curve is near-zero, and hence even large differences in slip angle between front and rear tyres results in only small reduction in total-vehicle friction utilisation. Lateral load transfer when considering linear tyres delivers a reduction in performance on the greater-loaded tyres because the cornering stiffness is increased (and hence slip-friction slope), and hence a change in slip angle operation delivers a greater reduction in friction. For the nonlinear tyres, lateral load transfer again has a negative effect, but the effect is negligible, owing to the near-zero slope near peak friction levels. Finally, the effect of the TV mechanism was investigated, concluding that the mechanism does not make a difference to overall friction levels at the limit, despite different longitudinal friction distributions. It is noted that this conclusion is unlikely to hold for non-peak operation.

It was shown that when the models are run with target understeer gradient equal to the passive value, the difference between the models is minimised; the greater the difference between the target and the passive, the greater the difference between the models.

It is clear that a nonlinear tyre model is an essential component to model torque vectoring.

Part III

Optimal Agile Manoeuvring

Chapter 7

Optimality of Agile manoeuvring handling characteristics

This chapter continues the investigation into optimal handling characteristics for torque vectoring vehicles by using numerical optimal control methods to explore the operation of the vehicle in agile manoeuvring scenarios.

7.1 Introduction

'Agility' is a concept which, for most, may seem intuitive, evoking mental pictures, perhaps, of a cheetah hunting down its prey, or a rally car winding its way around a twisty, narrow road high up in the mountains above Monte Carlo. Any attempts to define the common elements of these scenes, either qualitatively or quantitatively is not trivial. A starting point could be 'a rapid change in direction (to avoid obstacles) whilst maintaining momentum in the desired direction of travel'.

Agility is an attribute that is highly desirable for passenger vehicles, especially for OEMs that are trying to achieve a sporty 'DNA', (e.g. Jaguar Land Rover) and, in the case of active chassis control, a driver-selectable 'sporty' mode. Agility does, however, have a more critical significance, as in the case of active chassis control. In active safety systems, for example, the ability to avoid collisions by virtue of enhanced vehicle dynamic performance is a prized objective. Furthermore, for emergency response vehicles, an agile vehicle could mean the difference between life and death for road traffic accident victims.

It is clear, therefore, that agility is a highly desirable vehicle dynamics attribute which has a variety of applications. In this chapter, the aim is to investigate how torque vectoring can be deployed to increase the agility of the baseline vehicle used throughout this thesis.

The objectives are four-fold:

1. define quantitative measure(s) of agility: agility metrics;
2. determine the optimal controls required for agile manoeuvring for the vehilces with TV active and TV inactive;
3. assess the effect on TV agility of constraints on longitudinal slip ;
4. assess the sensitivity of yaw inertia on TV agility.

A secondary line of investigation will offer a critique on the metrics used in the literature to quantify agility, and additional metrics proposed in this chapter, and will give recommendations for the context in which each may be considered most relevant.

7.2 Review of agile manoeuvring

Unfortunately a standard definition of agility has not been agreed in the vehicle dynamics context. In the body of vehicle dynamics literature, there have been attempts to qualify

and quantify agility, as well as using this information to attempt to improve agility. Manoeuvring, and associated levels of agility can be classified broadly into two categories: low-sideslip and high-sideslip. Low sideslip manoevring includes both everyday passenger driving at low lateral accelerations within the linear range of the tyres, and circuit racing, where expert drivers control the vehicle at high accelerations near the peak friction limits of the tyres. High-sideslip manoeuvring, on the other hand, is achieved by highly-skilled expert rally drivers operating the vehicle in an extreme manner, typically with high frequency steering inputs. For low-sidesip manoeuvring, agility vs. stability is a frequent binary employed in the literature, referring usually to the handling balance of the vehicle; agility is linked with oversteer, and stability with understeer [45]. De Novellis et. al. [36], for instance, choose a yaw rate reference to produce a more agile response by reducing understeer with respect to the passive vehicle. This simple definition implies that agility increases with a decrease in degree of understeer.

Tremlett et. al. [111] represent stability via 'frozen-time' eigenvalue analysis and investigate agility by generating a 'yaw rate bandwidth' metric. The yaw rate bandwith metric quantifies 'directional authority', with a higher metric indicating greater agility of the open-loop response of the vehicle. The metric is defined as the frequency at which the yaw rate gain, normalised by a nominal yaw rate gain for the case where acceleration is zero, reaches a value of $1/\sqrt{2}$. The metric is calculated for a range of linearised operating points over the GG diagram at different speeds, and lateral- and longitudinal accelerations for a touring car with an LSD. The results reflected the subjective response of racing drivers: the vehicle is unstable yet agile under heavy braking and at the lateral acceleration limit. The drawback for this metric is that is requires the model to be linearised.

Cossalter et. al. [105] employ a two-point boundary optimal control problem with the cost function to force a motorcycle to travel between two points while maximising

'manoeuvrability'. 'Manoeuvrability' is defined as: '[the ability] to complete complex manoeuvres fast'. This is an intuitive definition, hingeing on the key words 'complex' and 'fast', since this implies a need for adequate handling capabilities and significant transient components to the manoeuvre. Manoeuvrability is claimed to be an intrinsic property of the vehicle, as opposed to 'handling' which involves driver skill level. Optimal control is used to deliver an ideal, perfect driver, in the same manner as chapters 4 and 5. The cost function is used to mathematically define the manoeuvrability. Minimum-time of manoeuvre was desired for a small section of a race circuit, consisting of two corners, as this would show the ability of the vehicle to be 'able to complete complex manoeuvres fast'. An equivalent cost function was used to make the OCP more tractable: maximise distance travelled for a set manoeuvre time. Whilst simply using manouevre distance to compare manoevurability has the advantage of simplicity, it does not capture quantitatively *how* this is achieved in terms of states and controls.

Yamakado et. al. [109] claim to improve agility *and* stability by the regulation of longitudinal acceleration. Their control law uses lateral jerk information to determine the longitudinal acceleration demand to improve comfort over a U-turn bend. Their strategy attempts to compensate for longitudinal load-transfer-induced oversteer (and hence, stability) under braking by increasing the rear tyre cornering stiffness by reducing the deceleration demand. Correspondingly, under acceleration, the demand is reduced, giving a relative increase in the front tyre cornering stiffness, and a reduction in understeer, and therefore 'agility'. Their notion of agility, therefore, is defined by an unspecificied degree of understeer.

In a simliar vein, Siampis et. al. [34], use the concept of velocity regulation to mitigate terminal understeer for a vehicle with rear-axle torque vectoring manoeuvring around a U-turn with curvature increasing to the apex. Whilst no explicit mention is made of agility, this technique increases stability, and the ability of the vehicle to follow an intended path.

The preceding studies share the characteristic of operating at low-sideslip angles, with fairly slowly-varying lateral dynamics. Expert rally drivers have shown, however, that operating at high-sideslip angles allow the car to be turned rapidly in a small space. Shibahata [16] showed that this is possible due to a reduction in stablising yaw moment available at high sideslip angles.

A series of studies using numerical optimal control have attempted to emulate the behaviour of expert rally drivers, who are able to control the vehicle in the highly-nonlinear range of the tyres, in order to perform manoeuvres such as the 'pendulum' turn.

Velenis, Tsiotras & Lu [65] build on their earlier work [80] to reproduce rally trail-braking techniques (simultaneous use of brake and steering) collected from experimental data using numerical optimisation techniques. They observed control input patterns and a low-order single-track model enriched with front and rear torque inputs and Pacejka tyres. A baseline simulation with minimum time objective over a 90°-turn on a low-friction surface ($\mu = 0.5$) was run. A final x_R position 30m beyond the corner was set as a final condition. Repeating this with a final x_R position on the exit of the curvature resulted in a significantly higher maximum sideslip angle; boundary conditions therefore have a strong bearing on the trajectory. Results were validated using a high-fidelity CarSim model.

Tavernini et. al. [66] investigated the optimality of limit handling techniques through the use of nonlinear optimal control for a tight hairpin bend. Low-slip cornering on dry and wet paved road and high-slip on dirt and gravel were investigated, as well as the effect of transmission layout (FWD, RWD and AWD). A single-track vehicle model enriched with Pacejka nonlinear tyres with longitudinal and lateral coupling were used. A quasi-static approximation of the longitudinal load transfer were used, with suspension dynamics emulated by a simple first-order delay on the normal loads. Lateral and longitudinal tyre force relaxation effects were modelled by the application of first-order delays

on the tyre forces, with the tyre forces were included as states in the optimisation problem to facilitate this. Wheel spin dynamics were also included. Constraints were imposed on the steering bandwidth (to model a perfect human driver), torque demand bandwidth and total engine power.

Initial conditions enforced straight-line running and an initial speed of 55kph, starting in the centre of the road, with a free final lateral position. Straight line running was also enforced at the end of the manoeuvre. The objective function sought to minimise time of travel.

By changing tyre characteristics, adjusting the peak friction and slip at which peak friction is reached, dry paved, wet paved, gravel and dirt surfaces were mimicked. A pendulum turn effect was found for the high-grip paved tyre, with differences in line observed between the FWD, RWD and AWD vehicles. Both this and the low-grip paved tyre gave a similar effect - with low-sideslip observed. For the gravel and dirt tyres, where peak friction occurs at high slip, high-sideslip is observed. The key finding is that the value of slip at which peak tyre force is generated is the central factor in the drifting characteristic, *not* the peak friction itself.

Later work by the same authors investigated, using a similar method, the handbrake turn manoeuvre, including handbrake torque as an additional control input [82]. Here, numerical optimal control results are validated against professional rally driver data. It was found that a cost function that minimised time for the first half of a hairpin manoeuvre and minimised lateral deviation from the inside of the track from the apex to the end of the course was required to recreate the high-sideslip aggressive manoeuvre, the vehicle using the 'pendulum' technique consistently across a range of sensitivity analyses including tyre curve, inertia values and CM location. The important result is that a very tight path was made possible in addition to a 180° turn with the correct control inputs and cost function.

The numerical optimisation studies of [65, 66, 82] successfully mimicked expert rally

driver manoeuvring, demonstrating the optimal controls required to operate the vehicle in such conditions. Other studies have analysed extreme manoeuvres from a dynamic stability perspective. Edelmann & Plöch [114] investigated the stability of a powerslide manoeuvre for a conventional vehicle by linearisation of a nonlinear four-wheel model at trim operating points and performed root locus analyses, concluding that the powerslide is an open-loop unstable manoeuvre that needs to be stabilised by the driver.

Yi et. al. [115] studied dynamic stability and agility of a vehicle during a pendulum manoeuvre, comparing professional and typical human drivers. Stability analysis was conducted via a two-track vehicle model with rear sideslip angle as a state, constructing yaw rate-rear sideslip angle phase-plane portraits. Previous work [116] had concluded that yaw rate-sideslip portraits delivered more conservative stability boundaries. A high-fidelity CarSim vehicle model was used to re-create the pendulum turn manoeuvre from logged data in [65], giving similar results. Analysis of the yaw rate-rear slip angle trajectories in conjunction with the phase-plane stability analyses showed that the expert driver operates the vehicle in the open-loop unstable condition. The simulation was re-run with constraints on longitudinal acceleration to mimic a driver of average skill. In contrast to the expert driver, the vehicle remained in the stable region, operated the vehicle at significantly lower sideslip angle. Metrics for agility were devised based on lateral jerk and lateral acceleration information, and these demonstrated the expert driver trajectories were of higher agility.

[117] built on the work of Yi et. al. [115] of expert driver-inspired operation of the vehicle outside the open-loop stable region. They calculated, for simplified dynamics, the phase-plane portrait for no control input β vs $\dot{\psi}$, with the saddle points demarking the open loop stable operating rectangle. Then, using LQR, the closed-loop phase plane portrait was calculated, considering steering feedback, delivering a closed-loop envelope with vertices at the new saddle points. It was shown that an autonomous radio-controlled

vehicle was able to follow an expert human-generated path and velocity profile using MPC, with the closed-loop β -$\dot{\psi}$ phase plane envelope. The lateral jerk metrics compared well with the human's result. In comparison, the MPC constrained to the open-loop stable region could not reach the same level of performance.

To summarise the literature on the study of agility, the following main points can be made:

- There is no agreed standard definition of agility. However, each study refers, directly or by implication, to the ease of changing vehicle posture, and the ability to effect this change quickly. Studies of expert drivers conducting extreme manoeuvres such as drifting and pendulum turn demonstrate that agility requires the operation of the vehicle at high-sideslip angles and lateral slip angles where the vehicle is open-loop unstable. The driver is required to stabilise the vehicle.

- For most studies, conventional vehicles are investigated with control inputs limited to the driver steering and throttle/brake action. Yamakado [109], in contrast, offers an actively-controlled strategy for agile manoeuvring, but this is within the normal, low-sideslip condition that passenger vehicle drivers are comfortable with. Li et. al. [116] develop a high-agility controller for a conventional vehicle but this is manoeuvre-specific.

- For low-sideslip manoeuvring, the approach for increasing agility consists of setting a yaw rate target to reduce the understeer gradient or specify an oversteer target.

- For high-sideslip manoeuvring, numerical optimal control has successfully been used to mimic the expert driver manoeuvres, given appropriate choice of tyre model, cost functions and boundary conditions. Quantitative phase-plane analysis concluded that the vehicle must be operated in open-loop unstable configuration to

achieve the desired motion.

- Metrics for capturing agility based on lateral jerk and lateral acceleration information have successfully differentiated between average and expert driver operation, and open-loop stable and closed-loop stable operation.

- There is no work established in the literature that investigates agile maneouvring for vehicles equipped with torque vectoring capability for aggressive manoeuvring.

In the following, general insight into extreme manoeuvring using TV is sought by making use of nonlinear optimal control and the same highly-overactuated vehicle under consideration in previous chapters. By leveraging the powerful agility metric concepts proposed in [115], analysis is performed comparing both the agility of TV against the vehicle with TV inactive, and the performance of various TV configurations.

7.3 Agility Definition

The concept of agility was borrowed from aerospace and defined 'by the physical properties of the vehicle which relate to its ability to change, rapidly and precisely, its motion path or heading axis and to its ease of completing that change' [115]. Manoeuvre agility is a combination of vehicle manoeuvrablilty and controllability (7.1). The former being the 'ability to change the magnitude and direction of the velocity vector'; the latter being the 'ability to change the manoeuvre state through rotation about the centre of gravity by a change of control power' [115]. Agility is thus a function of the driver and vehicle performance (driver skill level is kept constant in the following by limiting the steering rate).

$$\text{Manoeuvre Agility} = \text{Vehicle manoeuvrability} + \text{Vehicle controllability}. \tag{7.1}$$

Four agility metrics are defined based on lateral jerk (the time derivative of lateral acceleration) and lateral acceleration; an instantaneous and a total-manoeuvre variation for each, expressed as a function of distance travelled along the vehicle CM trajectory (N.B. *not* the road centreline). In the literature review of the previous section, it became clear that defining agility is a challenging task. The definitions adopted in this chapter will be those from Yi et. al. [115], as they were developed by both analysis of a real-world rally driving manoeuvre and through strong mathematical analysis. In addition, further metrics inspired by the approach in [115] are introduced.

Metrics are a useful way to distill meaningful information from complex data, but it must be borne in mind that the entire trajectory is the best measure, as Dixon [23] points out. Therefore, the relative merits of each metric will also be assessed for their ability to discern agile behaviour.

Lateral Motion Metrics [115] defines the following measures of agility. A transient lateral jerk metric is defined in equation 7.2. In essence, it simply captures the rate of change of lateral acceleration. For zero sideslip, the agility is approximately proportional to the rate of change of the trajectory curvature [115], hence Yamakado et. al. [118] describe lateral jerk as a measure of the yaw acceleration of a vehicle, for low-sideslip manoeuvring.

Lateral jerk is defined:

$$J_y = \dot{a}_y - a_x\dot{\psi} \tag{7.2}$$

$$= \ddot{V}_x + \dot{V}_y\dot{\psi} + V_y\ddot{\psi} + (\ddot{V}_x - V_y\dot{\psi})\dot{\psi}, \tag{7.3}$$

where J_y is the lateral jerk, $\dot{a}_y$, $\dot{V}_x$, $\dot{V}_y$ are the time derivatives of lateral acceleration, longitudinal speed and lateral speed respectively, and $\ddot{V}_x$ and $\ddot{V}_y$ are the second time derivatives

of longitudinal speed and lateral speed respectively.

A total-manoeuvre lateral jerk metric may be defined as the sum of the distance history of the lateral jerk normalised by the manoeuvre distance:

$$A_{Js} = \frac{1}{s_t} \int_0^{s_t} |J_y(s_t)| ds_t \tag{7.4}$$

where A_{Js_t} is the total-manoeuvre lateral jerk metric. A normalised lateral acceleration is defined in the equation 7.5. It quantifies the relative utilisation of the full lateral capability at any given instant.

$$A_A(s_t) = \frac{|a_y|}{g\mu_{y,max}}, \tag{7.5}$$

where $A_A(s_t)$ is the transient relative lateral acceleration metric, $\mu_{y,max}$ is the tyre-road friction coefficient in the lateral direction. $A_A(s_t)$ quantifies the relative utilisation of the full lateral capability. And a total-manoeuvre relative lateral acceleration metric is given as:

$$A_{As_t} = \frac{1}{s_t} \int_0^{s_t} A_A(s_t) ds_t, \tag{7.6}$$

where A_{As_t} is the total-manoeuvre relative lateral acceleration metric.

Rotational Motion Metrics In addition to lateral motion, new metrics are proposed of yaw rate and yaw acceleration, in a similar formulation to Yi et. al. [115]. A total-manoeuvre yaw rate metric is given as:

$$A_{\dot{\psi}s_t} = \frac{1}{s_t} \int_0^{s_t} |\dot{\psi}(s_t)| ds_t. \tag{7.7}$$

A total-manoeuvre yaw acceleration metric is given as:

$$A_{\ddot{\psi}s_t} = \frac{1}{s_t}\int_0^{s_t} |\ddot{\psi}(s_t)| ds_t. \tag{7.8}$$

Progression Metrics Total manoeuvre time and distance values serve as metrics for agility, as shown in [105]. In the following section, this is extended to analyse phases of the total manoeuvre, giving two time 'progression' metrics:

$$A_t = \max(t), \tag{7.9}$$

$$A_{t,k} = \frac{t_{kf} - t_{k0}}{A_t}, \tag{7.10}$$

where A_t is the total-manoeuvre time, $A_{t,k}$ is the time in phase k of the manoeuvre, and t_{kf} and t_{k0} are the final and initial times of the phase. In the same way, two progression metrics in terms of distance are:

$$A_s = \max(s_t), \tag{7.11}$$

$$A_{s,k} = \frac{s_{kf} - s_{k0}}{A_s}, \tag{7.12}$$

where A_s is the total-manoeuvre distance travelled by the vehicle CM, $A_{s,k}$ is the distance travelled in phase k of the manoeuvre, and s_{kf} and s_{k0} are the final and initial distance values of the phase.

7.4 Agile Manoeuvre Scenario

In this section, the vehicle model, manoeuvre definition and optimal control problem are set up to deliver the results in the following section.

7.4.1 Aggressive Turn-around Definition

Levin et. al. [119] investigate the optimal control inputs and corresponding vehicle state trajectories for minimising the space required to perform an aggressive turn-around manoeuvre (ATA) for a fixed-wing unmanned aerial vehicle (UAV). The motivation was to allow the UAV to maneouvre out of tight spaces in which it may unintentionally find itself. For a rally car, [82] it was found that a minimisation of the lateral position from the inside road boundary gave a (subjectively, qualitatively) more agile manoeuvre.

The ATA manoeuvre is adopted in the following studies, with some variations. The objective of the ATA is to change the acceleration vector by 180° in as small a space in the $x_R - y_R$ plane as possible, returning to the starting point such that speed is equal to the start value. The objective is to minimise manoeuvre time. The manoeuvre definition is shown in Figure 7.1.

7.4.2 Vehicle modifications

For this study, an extension to the 7DOF model in chapter 5 is used. An increased understanding of optimal control algorithms over the course of the research programme has allowed increased modelling complexity to be used while still obtaining solutions to OCPs in a reasonable time frame: aerodynamic drag is now included in addition to tyre force

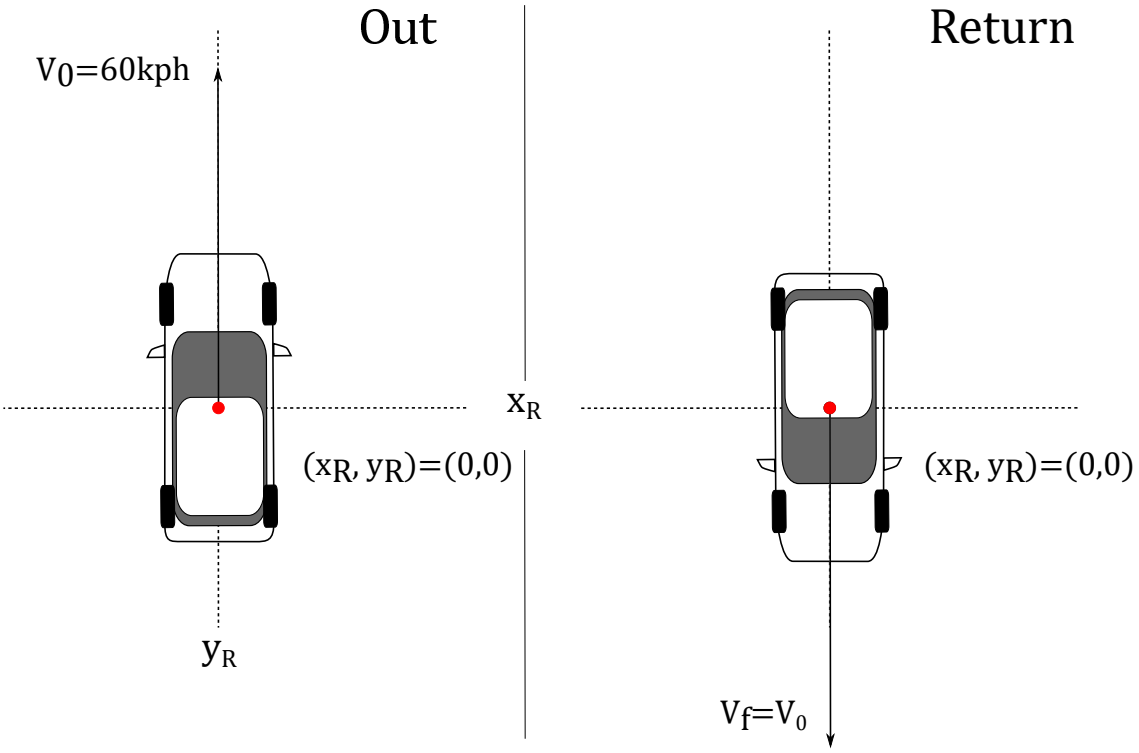

Figure 7.1: Manoeuvre definition

dynamics. The equations of motion for the 7DOF vehicle model (Fig. 2.2) are:

$$\begin{aligned}
\dot{V} &= \frac{1}{m}\left[(f_{FLx}+f_{FRx})\cos(\delta-\beta)-(f_{FLy}+f_{FRy})\sin(\delta-\beta)\right. && (7.13)\\
&+ \left.(f_{RLx}+f_{RRx})\cos\beta+(f_{RLy}+f_{RRy})\sin\beta+f_{aerox}cos^3\beta\right], \\
\dot{\beta} &= \frac{1}{mV}\left[(f_{FLx}+f_{FRx})\sin(\delta-\beta)+(f_{FLy}+f_{FRy})\cos(\delta-\beta)\right. && (7.14)\\
&- \left.(f_{RLx}+f_{RRx})\sin\beta+(f_{RLy}+f_{RRy})\cos\beta-f_{aerox}\sin\beta\cos^2\beta\right]-\dot{\psi}, \\
\ddot{\psi} &= \frac{1}{I_z}\left[\ell_F\left\{(f_{FLy}+f_{FRy})\cos\delta+(f_{FLx}+f_{FRx})\sin\delta\right\}-\ell_R\,(f_{RLy}+f_{RRy})\right. && (7.15)\\
&+ t_w/2\,(f_{FLy}\sin\delta-f_{FLx}\cos\delta-f_{RLx}) \\
&+ \left.t_w/2\,(f_{FRx}\cos\delta-f_{FRy}\sin\delta+f_{RRx})\right], \\
& && (7.16)
\end{aligned}$$

where: m is the vehicle mass; I_z is the moment of inertia about the vertical axis; V is the vehicle velocity at the center of mass (CM); β is the vehicle sideslip angle at the CM; $\dot{\psi}$ is the yaw-rate. the steering angle is, δ. Tyre forces are denoted by f_{ijk}. The parameters ℓ_F, ℓ_R determine the location of the CM with respect to the center of each wheel; t_w is the track width.

Aerodynamic drag has been included, since these effects are commonplace in similar studies [64, 66, 76, 82]. Aerodynamic drag force is included considering a simple cross-sectional area representation [66]:

$$f_{aerox} = 0.5\rho_{air}C_dA_{xz}V^2, \tag{7.17}$$

where ρ_{air} is the air density, C_d is the aerodynamic drag coefficient and A_{xz} is the vehicle cross-sectional area in the $x-z$ plane.

Tyre force lag effects are introduced on the relatively slow-varying dynamics of lateral loads and normal loads to give a more realistic representation of handling ability. Including derivative information also assists the NLP solver, as analytical derivative information is provided to the solver and results in a more tractable problem. Including tyre force dynamics is more important in this manoeuvre than the U-turn in part II because of the highly transient nature of the ATA.

Tyre relaxation effects are included for the lateral tyre forces by including a first-order delay on the Magic Formula expression:

$$\dot{f}_{ijy} = \left(f_{ijy}^{MF} - f_{ijy}\right) \frac{V_{ijx}}{\sigma}, \tag{7.18}$$

where f_{ijy}^{MF} is the Magic Formula value for the lateral tyre force and σ is the tyre relaxation length. Suspension dynamics are simply represented by incorporating a first-order lag on the normal tyre forces, considering a 'suspension time constant':

$$\dot{f}_{ijz} = \left(f_{ijz}^{MF} - f_{ijz}\right) \frac{1}{t_z}, \tag{7.19}$$

where f_{ijz}^{MF} is the Magic Formula value for the normal tyre load and t_z is the effective suspension time constant.

Wheel dynamics are included by:

$$\dot{\omega}_{ij} = \frac{1}{I_w} \left(T_{ij} - f_{ijx} r\right), \tag{7.20}$$

where the moment of inertia of each wheel about its axis of rotation is I_w; the wheel radius is r; the wheel angular speeds are ω_{ij}; the drive/brake torque applied on each wheel is T_{ij}.

7.4.3 Optimal Control Formulations

Nonlinear optimal control is once again employed to simulate the optimal behaviour of the driver-vehicle system. Wheel torque rates are used as inputs rather than wheel torques, simplifying the inclusion of rate limits. The state and control vectors follow as:

$$\mathbf{x}(t) = \{V, \beta, \dot{\psi}, \omega_{ij}, f_{ijz}, f_{ijy}, x, y, \psi_{CM}, T_{ij}, \delta, s\}^T, \tag{7.21}$$

$$\mathbf{u}(t) = \{\dot{T}_{ij}, \dot{\delta}\}^T, \tag{7.22}$$

where $\dot{T}_{ij}$ are the individual wheel torque rates. Including wheel rotational dynamics, torque rate inputs (and therefore torques as states), lateral force and normal force lags thus adds 16 states to the state vector used in chapter 5 Curvilinear coordinates are, however, no longer required as states; the net effect is therefore 13 extra states.

The CM position coordinate equations of motion are:

$$\dot{x} = V_x \cos\psi - V_y \sin\psi \tag{7.23}$$

$$\dot{y} = V_x \sin\psi + V_y \cos\psi \tag{7.24}$$

The objective function seeks to minimise the total time of the manoeuvre:

$$J(t) = \int_{t_0}^{t_f} dt. \tag{7.25}$$

Using a combination of state bounding and equality and inequality constraints on non-state quantities, the problem is fully formulated. State constraints are placed on the steer-

ing rate and torque rates (if applied in the cost function).

$$|\dot{T}_{ij}| \leq \dot{T}_{max} \tag{7.26}$$

$$|\dot{\delta}| \leq \dot{\delta}_{max} \tag{7.27}$$

where $\dot{T}_{max} = 7500\text{Nms}^{-1}$ [38], and $\dot{\delta}_{max} = 1Hz$.

Equality path constraints are applied to simulate the vehicle with TV inactive: torque difference between front wheels; torque difference between rear wheels; torque difference between front and rear axles:

$$T_{FL} - T_{FR} = 0 \tag{7.28}$$

$$T_{RL} - T_{RR} = 0 \tag{7.29}$$

$$\frac{T_{FL}}{T_{FL} + T_{RL}} - \gamma = 0 \tag{7.30}$$

where $\gamma = \gamma_{drive} = 0.5$ during acceleration and $\gamma = \gamma_{brake} = 0.7$ during deceleration. Where (7.30) is undefined, the constraint is deactivated since this only occurs when there is no torque at the front or the rear. Boundary conditions are set out in Table 7.31. Entry 'free' denotes a freedom within state/constraint bounds. Specific state bounds are imposed on the individual torques:

$$|T_{ij}| \leq T_{max}, \tag{7.31}$$

$$y_R \leq y_{R,max}, \tag{7.32}$$

where $T_{max} = 685\text{Nm}$ and $y_{R,max} = 40\text{m}$. The latter state bound is inactive but reduces the search space and hence hastens the calculation of a solution. Since there is no road

Boundary Conditions		
$\mathbf{x}$	$\mathbf{x}_0$	$\mathbf{x}_f$
t	0	free
V	60kph	60kph
$\dot{\psi}$	0	0
ω_{ij}	V_{ijx}/r	free
f_{ijy}	0	free
f_{ijz}	f_{ijz0}	free
x	0	0
y	0	0
ψ	$\frac{\pi}{2}$	$\frac{3\pi}{2}$
T_{ij}	0	free
δ	0	0
s	0	free

Table 7.1: Aggressive Turn-Around problem

boundary, no constraint is required. A dynamic initial guess was used to initialise the solution of the optimal control problem and an interior-point solver was used. More information on these is included in Appendix A.4 and A.5, respectively.

7.5 Agile manoeuvre results

In contrast to the track-bound U-turn manoeuvre in chapters 4 and 5, the formulation in this section is designed to generate a highly agile manoeuvre. It is demanding since a complete change in direction, return to initial posture and starting point are required as quickly as possible. The predicted optimal solution will aim to reduce travel distance and maximise speed simultaneously.

7.5.1 Results: TV active vs TV inactive

Optimisations were run for a vehicle with and without TV active, with the state and control vectors and constraints described in §7.4.3.

Yaw moment that is controlled by torque vectoring, $M_{z,long}$, arises from the longitudinal tyre forces resolved in the body-frame multiplied by half the track width as the lever arm (6.6). The yaw moment definition used includes trigonometric functions as the small angle approximations no longer hold at high lateral slip angles. The magnitude of the yaw moment is controlled indirectly by the front steering angle and the coupling of the lateral and longitudinal tyre forces, while magnitude of the longitudinal tyre force components are controlled by individual wheel torques, subject to the wheel dynamics equations. It is useful to determine when the TV yaw moment acts in either a stabilising manner, acting to reduce the yaw acceleration, or in a destabilising, acting to increase yaw acceleration. Let the definition of destabilising yaw moment be:

$$M_{z,destab.} := \text{sgn}(\ddot{\psi}) = \text{sgn}(M_z), \tag{7.33}$$

where $\ddot{\psi}$ is the yaw acceleration, and sgn is the signum function.

Path radius is calculated considering the centripetal and tangential accelerations acting at the centre of mass, transformed to the body-frame accelerations:

$$R = \frac{V^2}{a_y \cos\beta - a_x \sin\beta} \tag{7.34}$$

Maneouvre overview Figures 7.2 and 7.3 plot the results, with agility metrics plotted in Figure 7.4 tabulated in Table B.1 in Appendix B. The independent axis is the manoeuvre time normalised by the final time: $\tilde{t}$. In the following, *TV* refers to the vehicle with

torque vectoring; *NoTV* refers to the vehicle with TV inactive. It is clear from the trajectory plot in Figure 7.2(a), that the total manoeuvre distance is significantly higher for *NoTV* (25% further). It must however be remembered when observing that while, for example, phase E state and control plots give similar state profiles, they are achieved over different distances. Although the greater distance permits a lower path curvature for much of the manoeuvre (not shown in Figure 7.2(d)), and hence a higher speed (governed by the centripetal motion equations), *NoTV* is still 17% slower than *TV*. Recall, however, that the minimum speeds are similar.

Sideslip peak is $\sim 30\%$ greater for *TV*. For both configurations, little lateral friction is used in the second half of the manoeuvre; predominantly longitudinal friction is used to accelerate the vehicle in a straight line to the final position.

Manoeuvre composition detail The manoeuvre can be broken down into five distinct phases (denoted by letters A-E, Figure 7.2): A. Turn-in preparation phase; B. Braking turn-in phase; C. Maximum rotation phase; D. Acceleration turn-out phase; E. Attitude restoration phase.

A. Turn-in preparation phase.

This phase serves a similar purpose to a rally-driving pendulum turn, yawing in the opposite direction of the main cornering direction of the manoeuvre to overcome yaw inertia, before returning instantaneously to zero yaw rate at the end of the phase.

- **TV** The vehicle is braking from 60kph. Initially the car steers and yaws to the right, while $M_{z,long}$ acts in a stabilising manner, which permits a greater lateral acceleration at a lower speed. Lateral jerk exhibits a large spike, correspondingly. Right-hand steer is then reduced to zero and left steering begins while simultaneously the yaw moment becomes destabilising to increase yaw acceleration. Yaw

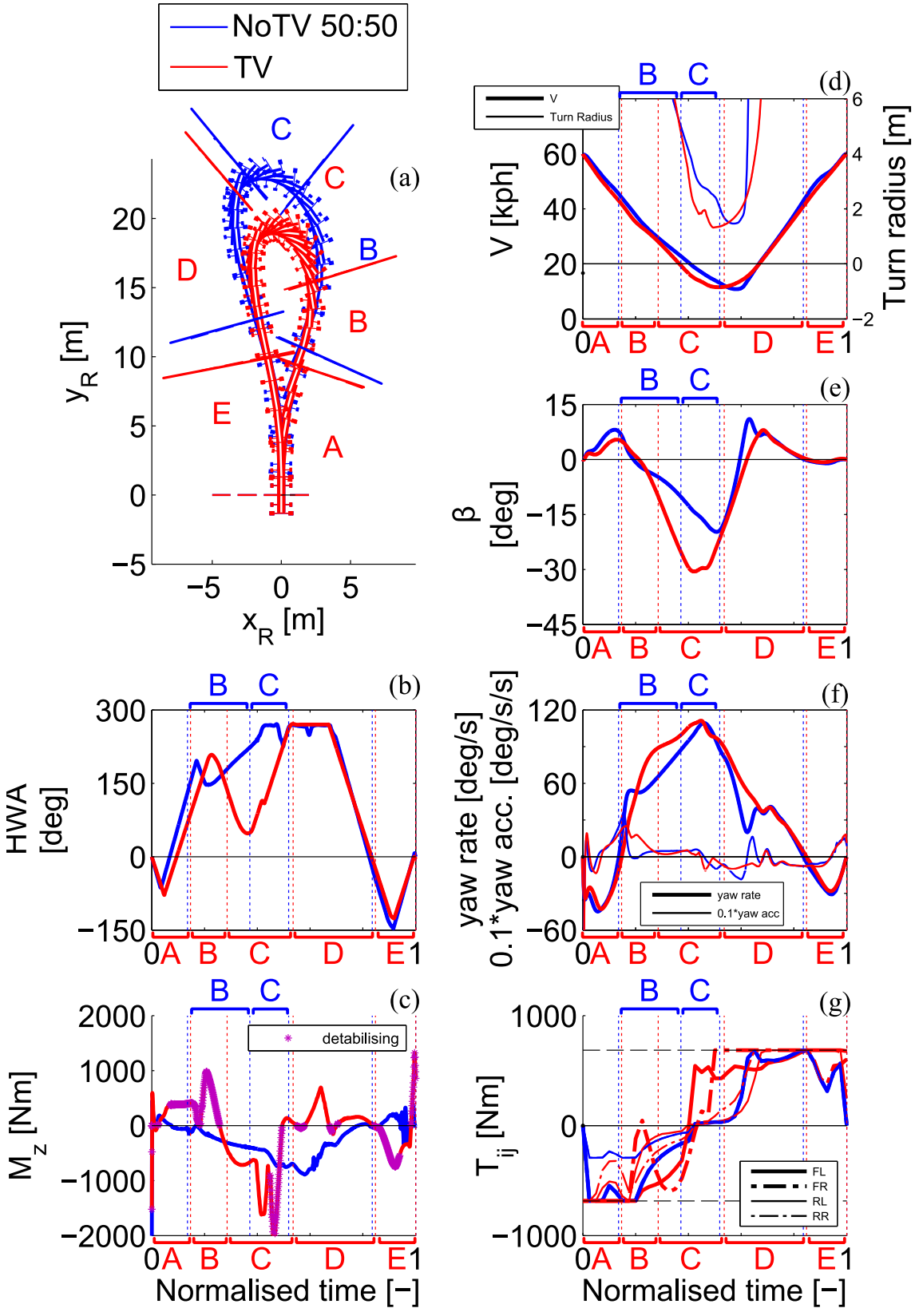

Figure 7.2: NoTV 50:50 vs TV: state and control trajectories

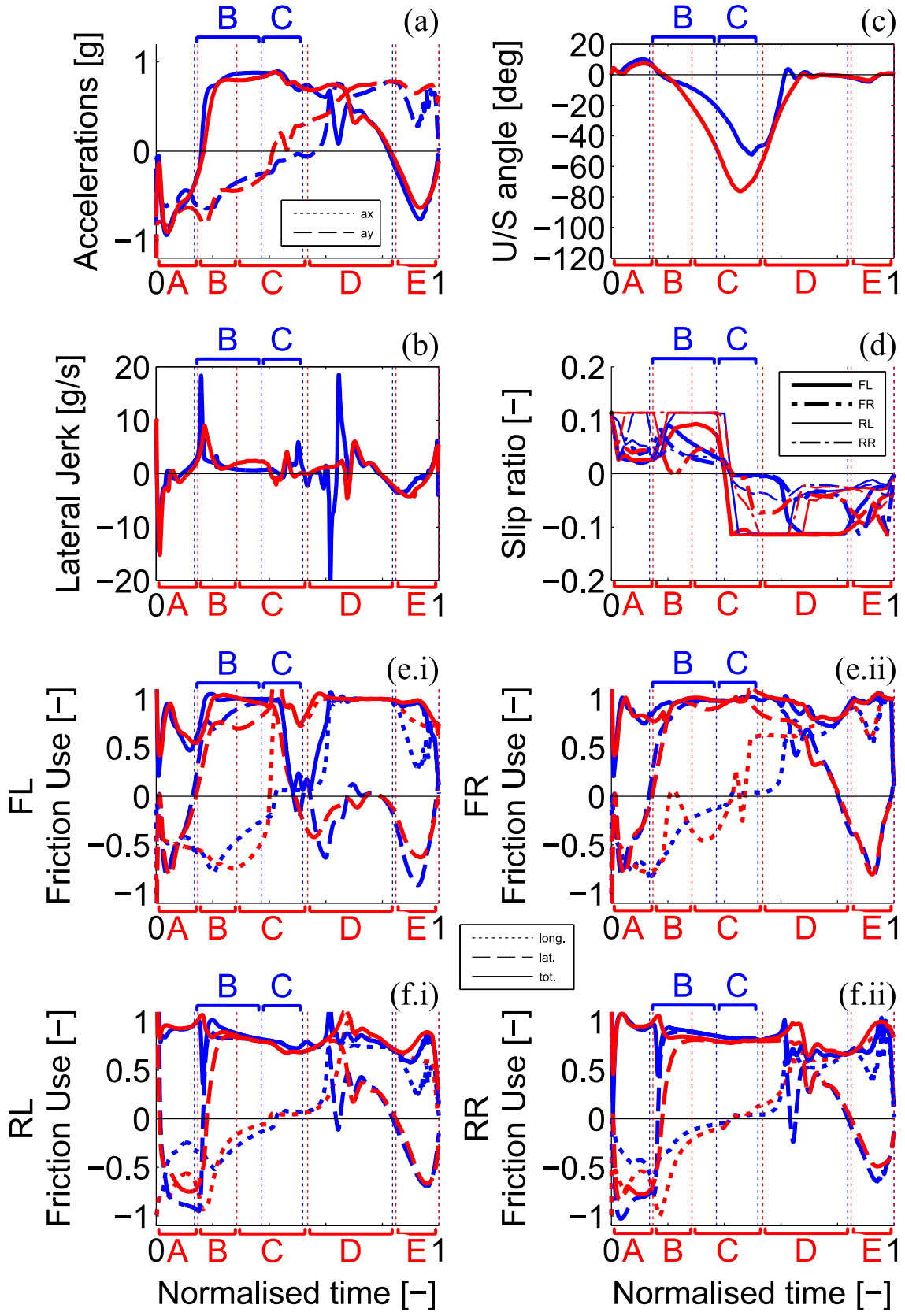

Figure 7.3: NoTV 50:50 vs TV: acceleration and friction trajectories

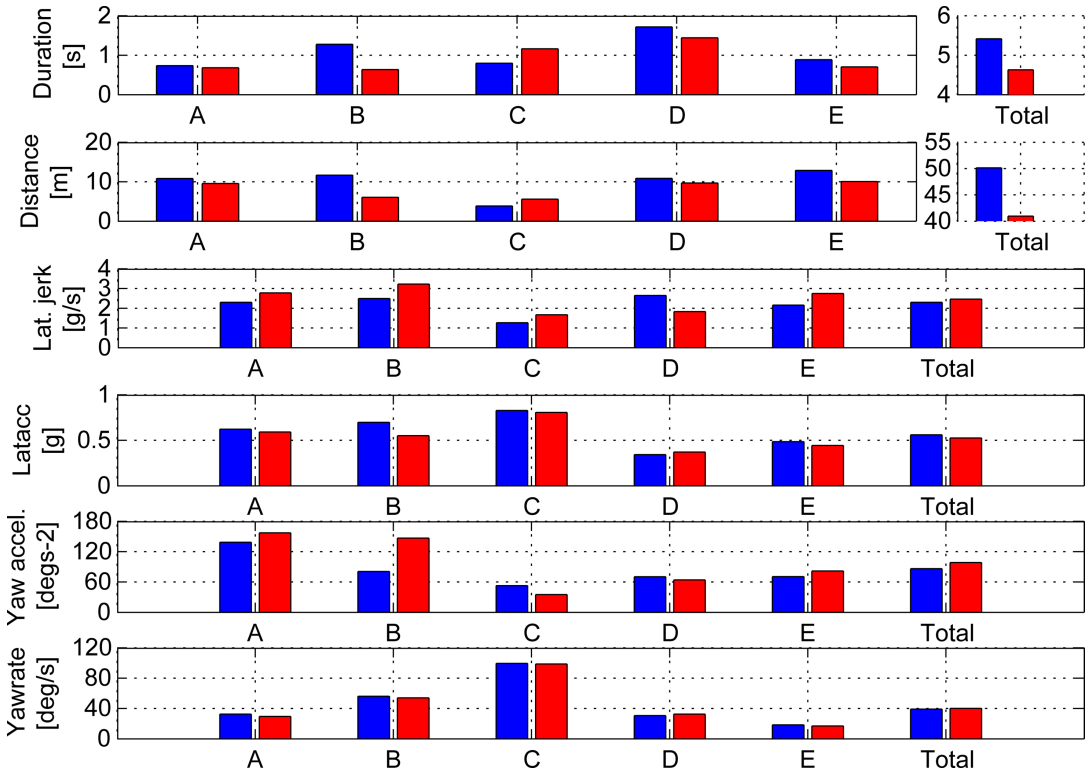

Figure 7.4: NoTV 50:50 vs TV: agility metrics

rate magnitude reduces from its maximum negative value, while sideslip increases in nose-out nature before reducing to zero at the end of the phase.

- **NoTV** Aside from TV yaw moment, the control and response are similar to TV.

- **Comparison** The similarity of this phase is reflected in the metrics, with similar time and distance. The steer angle rate for *TV* is lower than *NoTV*, and the speed slightly lower. Lateral jerk is marginally higher for *TV*, while *NoTV* generates slightly higher lateral acceleration. *TV* exhibits greater yaw acceleration and slightly lower yaw rate. During this phase, both vehicles are understeering, *TV* to a lesser degree. *TV* yaw acceleration peaks have a greater magnitude than *NoTV*; lateral jerk likewise ([115] notes that for low-sideslip angles, lateral jerk and yaw acceleration can be considered equivalent).

B. Braking turn-in phase.

This phase initiates the change of direction in the main cornering direction while braking. Let it be defined as the segment from zero yaw rate to where yaw rate reaches 80% of its peak value ($0 < |\dot{\psi}| < 0.8|\dot{\psi}_{peak}|$).

- **TV** Handwheel angle is now increasing while $M_{z,long}$ is destabilising such that yaw acceleration reaches a manoeuvre maximum. Subsequently, handwheel angle is 'backed-off' to reduce front lateral force (this effect is more pronounced on front left lateral force than front right, perhaps due to lateral load transfer). $M_{z,long}$ becomes stabilising and yaw acceleration reduces. At this point sideslip rate is constant, to a point of peak tail-out sideslip magnitude at the end of the phase. The vehicle is highly oversteering at this point.
- **NoTV** Phase B is significantly longer, proportionally, for *NoTV* than *TV*, encompassing slightly different controls. HWA for *NoTV* reaches a first peak value just after yaw rate has started increasing from zero, as braking torques reduce from their maximum. HWA then 'backs-off' by $\sim 50^{\circ}$ before rising again. The yaw rate rises steadily from a stationary point, sideslip increasing steadily in a tail-out manner.
- **Comparison** There are significant differences in the *TV* and *NoTV* responses during phase B. Notably, the length of the phase is proportionally longer in terms of time for *NoTV*, since the yaw acceleration is much lower, reflected in the phase metrics. Lateral jerk is also higher for TV, despite a lower peak value. Lateral acceleration is significantly higher for *NoTV* because of the higher speeds and similar initial path curvature. Yaw rate metrics are similar, despite dissimilar profiles: *NoTV* starts the phase higher but grows slowly; *TV* starts lower but grows at a greater rate. The visible difference is that *TV* sideslip peak is 30% greater than *NoTV*.

C. Maximum rotation phase.

This phase is characterised by the proximity of the yaw rate to the peak ($|\dot{\psi}| > 0.8|\dot{\psi}_{peak}|$) and corresponds to the point of highest path curvature and minimum speed.

- **TV** HWA is increasing to its limit value and $M_{z,long}$ becomes destabilising once again. Longitudinal acceleration is near-zero. There exists a very small stabilising yaw moment that arrests the reducing yaw rate at $\tilde{t} \sim 0.5$.

  During the second part of phase C, the vehicle is accelerating, with handwheel angle saturated at its maximum value, coinciding with a spike of stabilising $M_{z,long}$, which continues to reduce sideslip magnitude and yaw rate. The minimum turn radius is ~ 1.5m.

- **NoTV** HWA rises to its limit value, and longitudinal acceleration is near-zero. Halfway through the phase, total front-left friction use drops from near-full to near-zero, occurring at the same point as a spike in lateral jerk as the sign of yaw acceleration changes sign. Front-right remains close to full and rear tyre friction use is ~ 0.75. The low level of front-left friction arises from a low combined slip, itself a function of wheel velocity components.

- **Comparison** Phase C is significantly shorter for *NoTV* than *TV*, spending far less time proportionately at near-peak yaw rate, reaching the peak at a greater rate, but dropping away from the peak at a comparable but lower rate than *TV*. *NoTV* exhibits a lesser degree of oversteer and sideslip angle than *TV*. Interestingly, while both have a near-identical minimum path radius, *NoTV* drops initially to ~ 3m during phase C before dropping again to the minimum, which actually occurs at the beginning of phase D. *NoTV* is travelling at a higher velocity during phase C than *TV*, permitted by the higher turn radius. The lateral jerk metric is higher for *TV*, but lateral acceleration is lower. Yaw acceleration is significantly higher for *NoTV*, which reflects the rate at which that the peak yaw rate is approached. The yaw rate

metrics are identical, because of the phase definition.

D. Acceleration turn-out phase.

During phase D, the vehicle is accelerating and yaw rate reducing as it returns towards the starting position

- **TV** Handwheel angle begins the phase at its limit value, before reducing at a constant rate to zero. $M_{z,long}$ acts very briefly in a mildly destabilising manner, before a peak of stabilising action. A slight destabilising action accompanies the moment at which HWA starts to reduce, before once again acting in a mildly stabilising manner.

  During this phase, speed is increasing. Yaw rate reduces at a greater rate than it built up to the peak. There is a small arrest in yaw rate reduction that corresponds to a tiny moment of destabilising $M_{z,long}$ at $\tilde{t} \sim 0.7$.

  Lateral acceleration reduces significantly over the second half of phase D as low-sideslip, high longitudinal acceleration begins to dominate. The friction utilisation plots show that, whilst utilisation is not maximal, friction is predominantly applied in a longitudinal direction.

- **NoTV** The HWA inputs are very similar for phase D, starting at peak saturated value, before rapid reduction to zero, while longitudinal acceleration grows. Velocity increases accordingly, while sideslip drops to zero in a similar manner to TV. The yaw rate drops from a high rate. There is an oscillation in the yaw rate for the middle third of phase D, corresponding to a high wheel torque rate application that influences the lateral dynamics; the lateral jerk exhibits two opposite-sign, high magnitude spikes in quick succession at this point.

- **Comparison** Looking at the metrics in Table B.1, Figure 7.4, similar time-proportions of the manoeuvre are spent in phase D. Lateral jerk is significantly higher for *NoTV*

because of the peaks resulting from acceleration fluctuation as wheel torques are applied. Lateral acceleration metrics are comparable. Yaw acceleration is greater for *NoTV*, although yaw rates are similar, owing to the yaw rate oscillations mentioned previously.

E. Attitude restoration phase

Phase E is concerned with rightward steering and torque modulation to achieve straight line running with zero sideslip and yaw rate by the end of the manouevre, and a return to the initial speed of 60kph.

- **TV** HWA changes sign, assisted by destabilising $M_{z,long}$ to help overcome the yaw inertia in order to return the vehicle to zero sideslip condition and the straight-ahead. Longitudinal acceleration is high as the speed returns to its initial value. The final transient $M_{z,long}$ spike is required to obtain perfect straight-line attitude required by the OCP boundary conditions.
- **NoTV** Rightward steering is applied. Wheel torques are modulated to obtain the correct final posture.
- **Comparison** The peak negative HWA is slightly greater for *NoTV*, and the steering rate to achieve it, since no active yaw moment is available to assist. Sideslip and yaw rate responses are very similar, although the resulting lateral acceleration is slightly greater for *NoTV* but lower lateral jerk and yaw acceleration metrics that *TV*. *NoTV* requires 20% more distance to complete this phase of the manoeuvre.

The phases may be summarised briefly as follows:

A: Turn-in preparation phase. Rightward steer and braking. *TV* is assisted by destabilising yaw moment.

B: Braking turn-in phase. Leftward steer applied, increasing yaw rate and sideslip.

Steering is backed off part way through the phase. *TV* phase is substantially shorter than *NoTV*.

C: Maximum rotation phase. Yaw rate is close to peak. For *TV*, yaw moment is destabilising, steering is at maximum limit. *NoTV* spends less time in phase C.

D: Acceleration turn-out phase. Steering reduces, yaw moment is applied stabilising and destabilising at different points, mildy, with longitudinal acceleration dominating over lateral. Similar phase trajectories for both configurations

E:Attitude restoration phase. Steering and significant yaw moment help attitude for *TV*, while *NoTV* relies on wheel torque modulation and consequently takes 20% longer to complete the manoeuvre.

Overall, a significant reduction in x_R-y_R space is possible with *TV* (20% longitudinal, 25% lateral), with the total manoeuvre path 20m shorter. This is achieved by $\sim$ 30% greater sideslip angles, resulting in higher total manoeuvre lateral jerk and yaw acceleration metrics for *TV*. The lateral acceleration metric is greater for *NoTV* due to greater path curvature hence a greater minimum speed is possible.

For both vehicles, the manoeuvres are asymmetric. Rotation is biased to the first half of the manoeuvre, while in the return second half, longitudinal acceleration dominates as the vehicle attitude is orientated to the straight-ahead. *TV* uses greater longitudinal slip ratios (rear) to reduce the effective cornering stiffness of the tyres, increasing rear slip angles and increasing the oversteer characteristic required for faster rotation. *TV* yaw moment ensures the initial and final stages can be executed more rapidly to overcome the vehicle's yaw inertia. At the same time, *TV* in general requires a reduced level of HWA.

7.5.2 Results: TV longitudinal slip limits

The previous results demonstrated high-sideslip cornering, despite limiting longitudinal slip ratio to the value at which peak friction is achieved.

In this section, the *TV* optimisation was re-run with the longitudinal slip limit raised to 2 and 4 times the slip ratio at peak friction. The purpose of this is to assess the sensitivity of *TV* agility to the longitudinal slip limit - since through tyre force coupling, longitudinal slip influences cornering stiffness.

Figures 7.5 and 7.6 plot overlays of the optimisations and a metric comparison is given in Figure 7.7 and data in Table B.2 in Appendix B.

Overview Some clear general impressions can be gleaned by a quick glance at Figures 7.5 and 7.6. First of all, the trajectory path shape is similar, as are the HWA traces, and therefore the manoeuvre can be broken down into the same phases as *TV* in the previous section.

Whilst the results are very similar, the following differences are observed as the longitudinal slip limit is increased:

- less space is taken by the manoeuvre in the x_R-y_R plane;
- the minimum radius reduces;
- the length of the manoeuvre reduces;
- steering effort is reduces;
- tail-out sideslip increases and a greater magnitude of understeer angle (oversteering) is observed.

A phase-by-phase analysis draws out more detail:

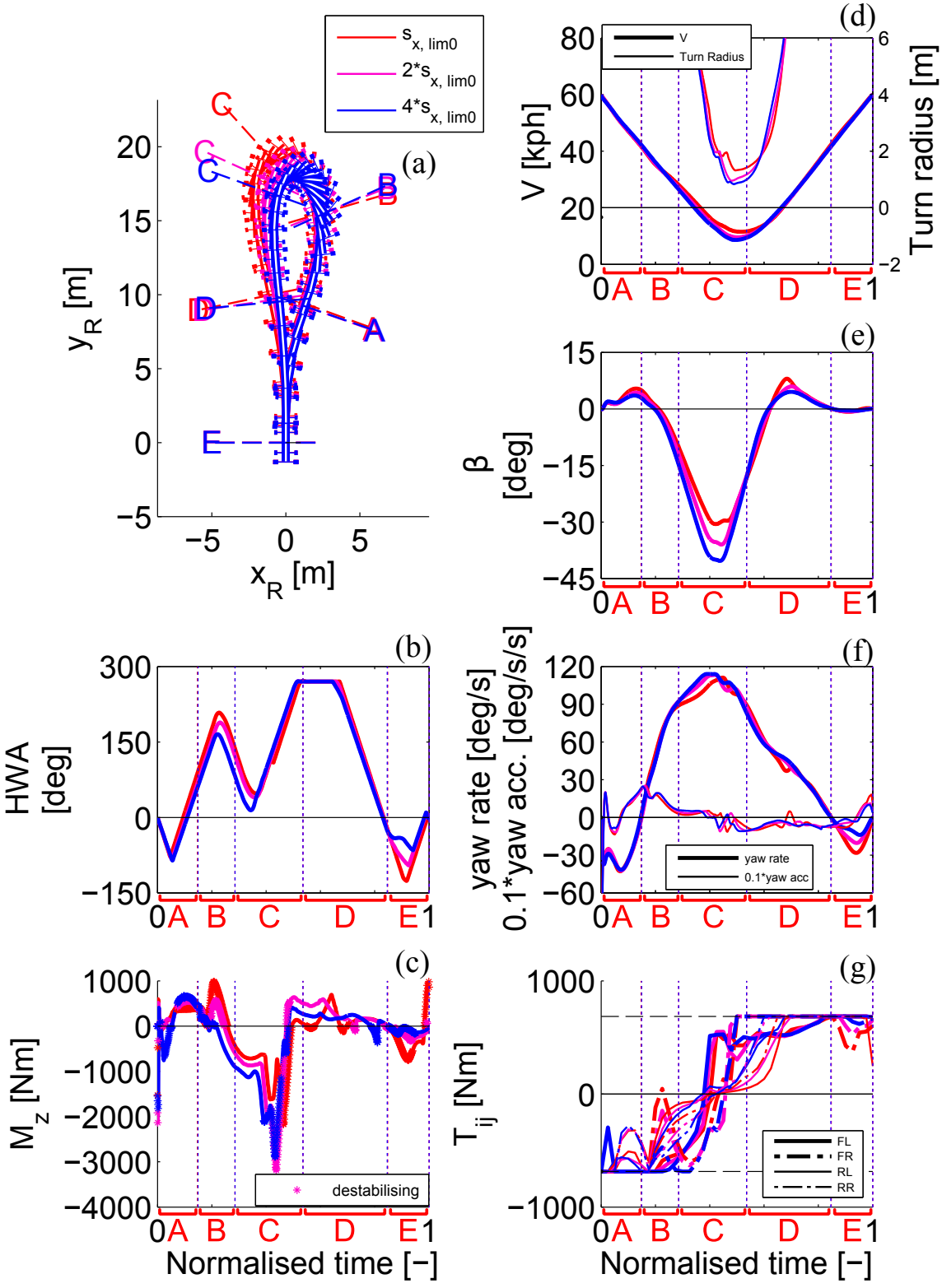

Figure 7.5: TV slip constraint compare: state and control trajectories

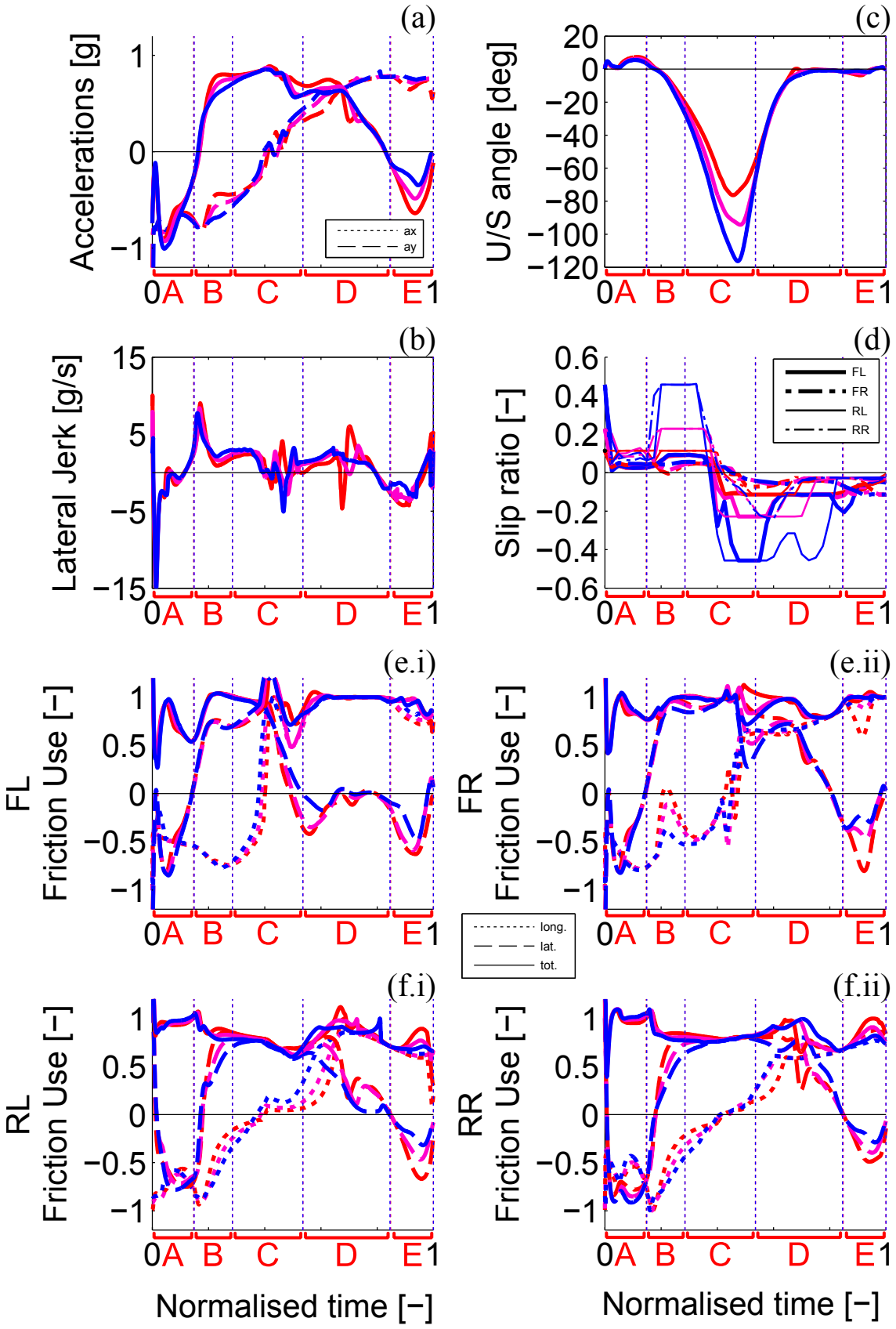

Figure 7.6: TV slip constraint compare: acceleration and friction trajectories

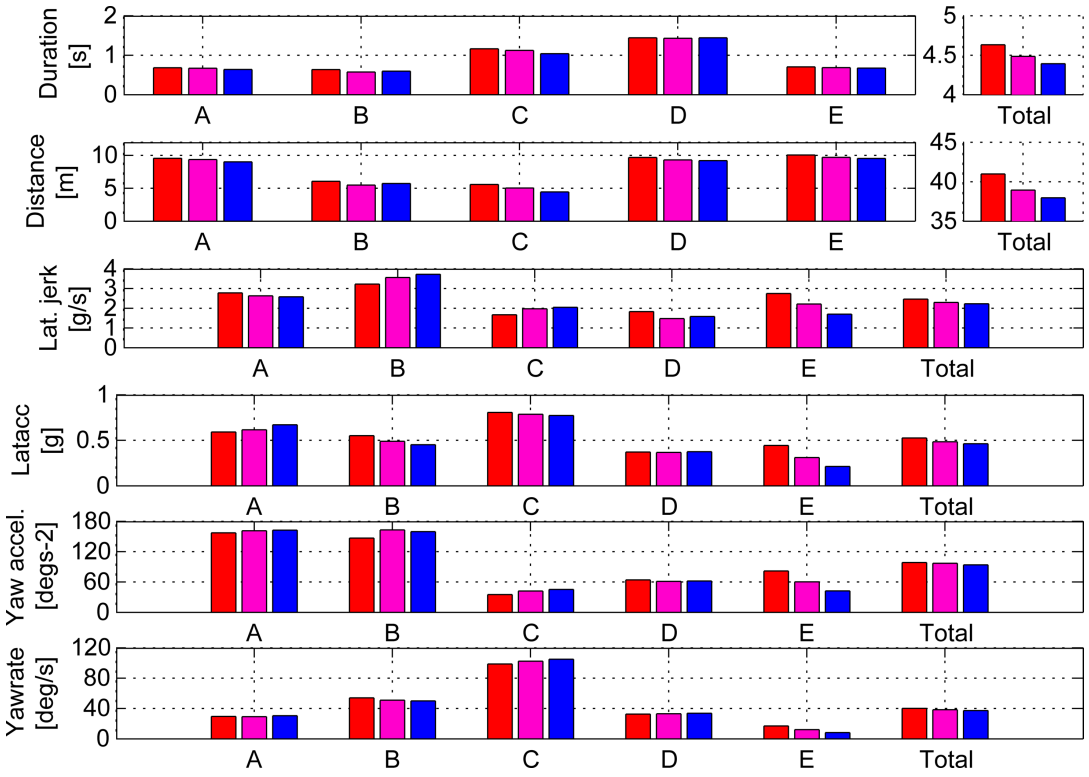

Figure 7.7: TV slip constraint compare: agility metrics

A: Turn-in preparation phase. Clockwise steering is applied proportionally later in the manoeuvre as slip limit increases, while the magnitude of destabilising yaw moment increases too. The lateral jerk metric reduces with longitudinal slip limit increase, while lateral acceleration and yaw accelerations increase marginally. Yaw rate exhibits little differentiation.

B: Braking turn-in phase. Peak HWA reduces, as well as destabilising yaw moment magnitude as slip limit increases. $4s_{x,lim0}$ uses limit longitudinal slip at the rears, reducing rear cornering stiffness and hence reduced HWA and yaw moment required to deliver yaw acceleration. In the metrics, lateral jerk increases, while lateral acceleration and yaw rate reduces with slip limit increase.

C: Maximum rotation phase. Initially, as HWA is reducing, less steering effort is required as slip limit increases, but thereafter the trajectories are similar, although $4s_{x,lim0}$

increases again earliest of the configurations. The minimum turn radius decreases with slip limit, although $2s_{x,lim0}$ and $4s_{x,lim0}$ are very similar. In the metrics, lateral jerk and yaw rate increases, while lateral acceleration and yaw acceleration decrease as slip limit is increased.

D: Acceleration turn-out phase. Again, HWA is similar, but reduces earliest for $4s_{x,lim0}$. Yaw moment is largely stabilising, but the trajectories show some variation in application. Nose-out sideslip is lowest for $4s_{x,lim0}$ and turn radius increases earlier. For the metrics, lateral jerk decreases with slip limit, while lateral acceleration increases. Yaw acceleration and yaw rate are similar.

E: Attitude restoration phase. HWA effort reduces; significantly lower angle is required and destabilising yaw moment is lower in magnitude as slip limit increases. This is because the vehicle posture is already much closer to the required final conditions from the straighter exit of phase D.

In conclusion, increasing the longitudinal slip limit reduces the space required for the ATA, increases the curvature and reduces the steering effort required. In some parts of the manoeuvre, reduced TV yaw moment is required, and; in others, more. The coupling between longitudinal and lateral forces means that, in the crucial phase B (Braking, turn-in) and early phase C (Maximum rotation), the rear tyre cornering stiffness reduces as longitudinal slip limit is increased. The reduced cornering stiffness results in lower steering effort and reduced destabilising yaw moment. In consequence, lateral jerk and yaw acceleration metrics, in addition to yaw rate increase with slip limit in phase C.

7.5.3 Results: TV yaw inertia sensitivity

The previous results demonstrated high-sideslip cornering, with decreasing manoeuvre space as longitudinal slip limit was raised.

In this section, the TV optimisation was re-run with yaw inertia set to half and 1.5 times the nominal value, hereafter $0.5I_{z,nom}$ and $1.5I_{z,nom}$, respectively. The purpose of this was to assess the sensitivity of the agility to inertia properties.

Figures 7.8 and 7.9 plot overlays of both the optimisations and a metric comparison is shown in bar form in Figure 7.10 and numerically in Table B.3 in Appendix B.

Overview Once again, some clear general impressions can be gleaned by a short glance at Figure 7.5 and 7.6, and since the trajectory path and HWA traces show only small variation the manoeuvre can be broken down into the same phases as TV in §7.5.1.

Whilst the results are very similar, the following differences are observed as the yaw inertia is increased:

- greater space is taken by the manoeuvre in the x_R-y_R plane;
- the minimum radius increases marginally;
- the length of the manoeuvre increases;
- steering effort increases, more for $I_{z,nom}$ and $1.5I_{z,nom}$;
- yaw moment magnitude increases;
- lateral jerk reduces signficantly;
- sideslip magnitude and oversteer reduces.

Further, phase C and D time proportions are the same for $I_{z,nom}$ and $1.5I_{z,nom}$ but time spent in C is markedly lower for $0.5I_{z,nom}$.

A phase-by-phase analysis draws out more detail:

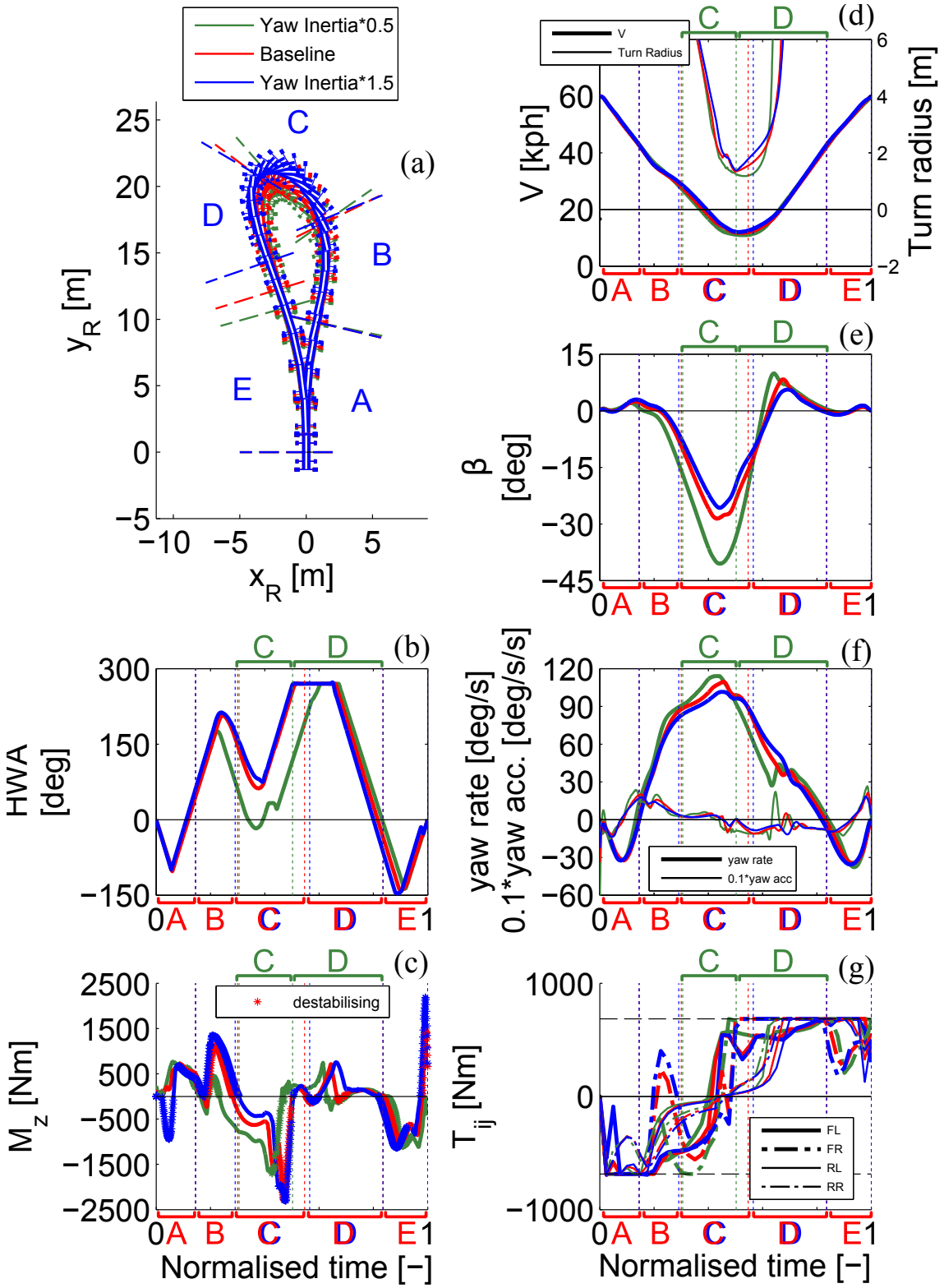

Figure 7.8: TV yaw inertia sensitivity: state and control trajectories

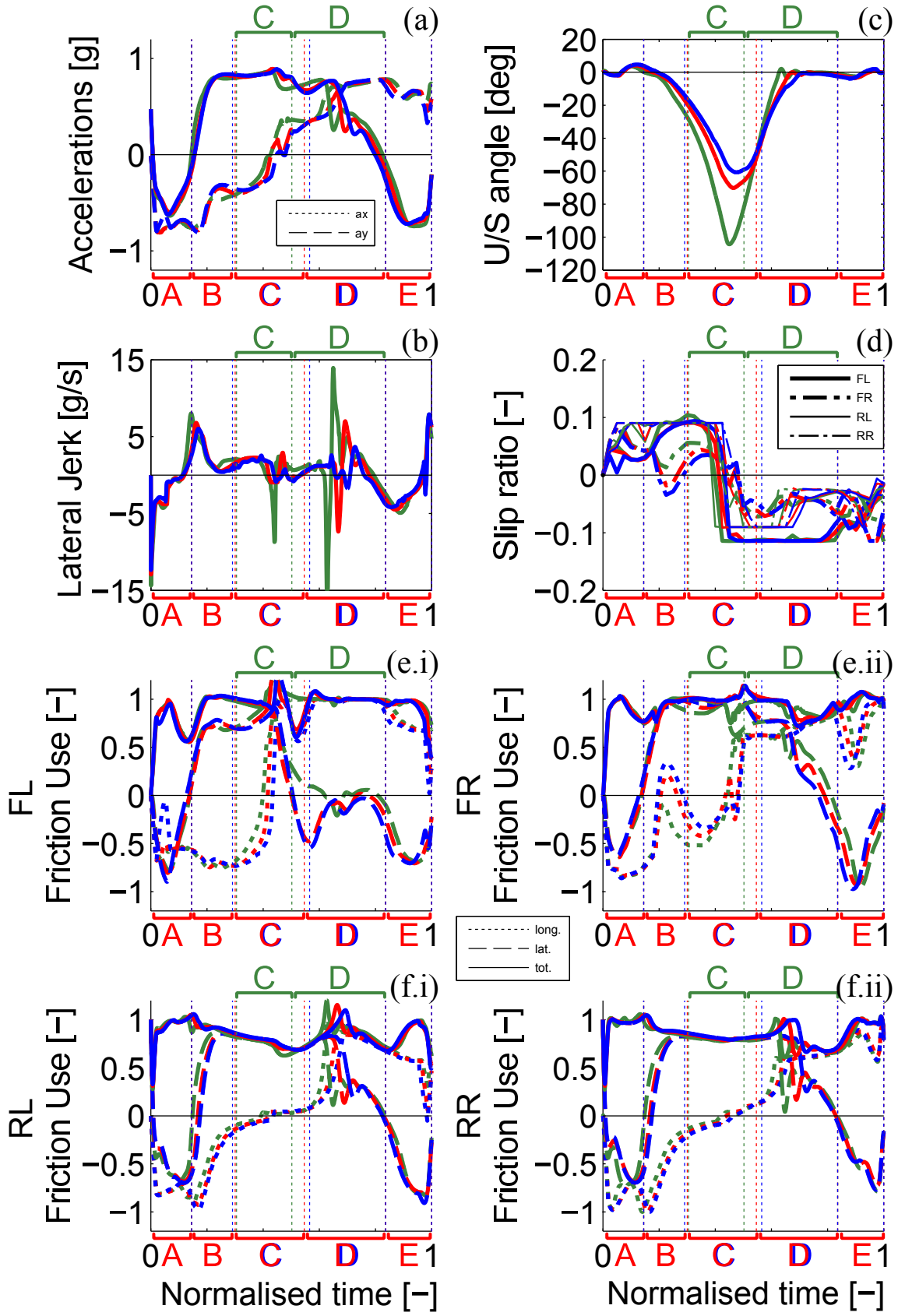

Figure 7.9: TV yaw inertia sensitivity: acceleration and friction trajectories

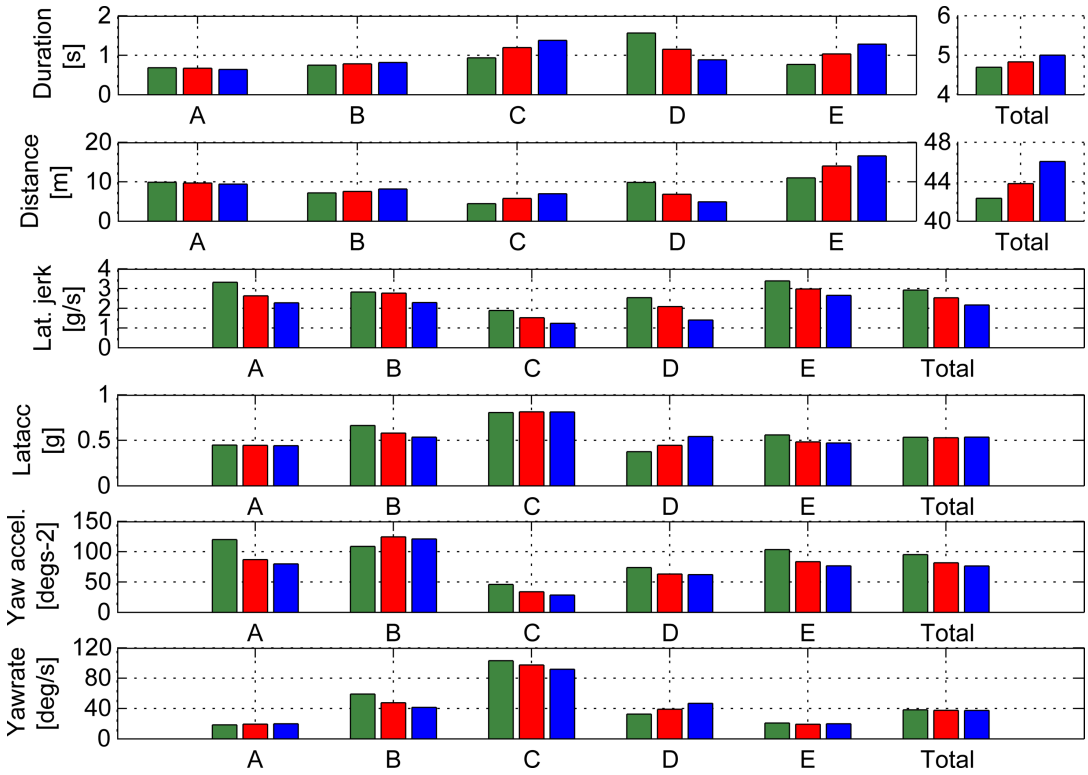

Figure 7.10: TV yaw inertia sensitivity: agility metrics

A: Turn-in preparation phase. $1.5I_{z,nom}$ requires slightly earlier HWA application but the biggest difference in controls is the requirement for large destabilising yaw moment immediately to overcome greater inertia. In the metrics, as inertia increases, time spent is similar, distance reduces, lateral jerk and yaw acceleration reduces, while yaw rate and lateral accelerations are similar.

B: Braking turn-in phase. The HWA 'backs off' for $0.5I_{z,nom}$ earlier: less steering effort is required. Yaw moment is destabilising but much smaller in magnitudie for $0.5I_{z,nom}$, becoming stabilising as HWA backs off. Yaw rate and tail-out sideslip magnitudes are greater for $0.5I_{z,nom}$

C: Maximum rotation phase. The phase is shortest for $0.5I_{z,nom}$, since the yaw rate remains above 0.8 of the peak for a shorter time. HWA required is much lower for $0.5I_{z,nom}$ and briefly countersteers. Similar yaw moment patterns are exhibited but again, where

destabilising, the magnitude is lower for smaller yaw inertia. For the metrics, as yaw inertia increases, duration and distance increases, while lateral jerk, yaw acceleration and yaw rate reduce. Lateral accelerations are similar.

D: Acceleration turn-out phase. Greater proportion is spent in phase D for $0.5I_{z,nom}$, since yaw rate reduces faster. HWA application is similar for $I_{z,nom}$ and $1.5I_{z,nom}$ but for $0.5I_{z,nom}$, is still increasing at beginning. HWA is at its limit for a much reduced perod of time. The yaw moment pattern is similar but there is a delay in application as yaw inertia increases. Metrics show for increasing yaw inertia, time and distance decrease, lateral jerk and yaw acceleration decrease; lateral acceleration and yaw rate increase.

E: Attitude restoration phase. HWA is applied to a similar degree and shape but earlier as inertia increases. Yaw moment is also deployed earlier. The control and phase traces are similar for each configuration, as the vehicles exit phase D with similar attitudes. Thus the metrics for lateral acceleration and yaw rate are, therefore, similar, but lateral jerk and yaw acceleration reduce with increased yaw inertia. Time and distance increase.

The time difference for the total manoeuvre is -2% and $+4\%$ of $I_{z,nom}$ time ($-0.2s/+$ 0.3s) for $0.5I_{z,nom}$ and $1.5I_{z,nom}$, respectively. Total manoeuvre distance differences are -0.5 and 2m, respectively. As yaw inertia is increased, lateral jerk and yaw acceleration reduce, while lateral acceleration and yaw rate are similar.

In conclusion, reducing yaw inertia results in lower manoeuvre time and distance, and smaller steering and yaw moment inputs are required. Phases C and D phase proportions are different for $0.5I_{z,nom}$: C is much smaller because yaw acceleration is greater and hence less time is spent with yaw rate greater than 0.8 of peak yaw rate. Over the manouevre, a lower yaw inertia increases agility according to the lateral jerk and yaw acceleration metrics, while yaw rate and lateral acceleration are identical. On an intuitive basis, it can be argued that the acceleration metrics are most representative of capturing

agility in this scenario.

7.6 Metric critique

Agility metrics were adopted from [115] and further metrics proposed in this chapter.

In the opinion of the author, it was found that for all the metrics, the trends shown in the numbers reflected the subjective intuition. For example for the TV vehicle, the manoeuvre occupied less space, took less time and travel distance. Total manoeuvre metrics of yaw rate, yaw acceleration and lateral jerk metrics were all greater for TV than the vehicle with TV inactive. For some of the phases, the vehicle with TV inactive gave greater metrics, but the reasons behind these cases have been pointed out. For example, the yaw acceleration in phase C is greater for TV inactive than TV due to the fact that the TV vehicle builds yaw rate at a proportionally earlier point in the manoeuvre.

The lateral acceleration metric did not show increase with an increase in intuited agility. In contrast, the lateral acceleration metric was greater for TV inactive, implying intuitively that this is not a good overall measure for agility.

For the sensitivity study of slip ratio limit, it was seen that in the crucial phase C (corresponding to maximum rotation), lateral jerk, yaw acceleration and yaw rate increase with slip ratio limit, pointing to greater agility during the rotation phase, while lateral acceleration decreased.

On the basis of lateral acceleration metric following the reverse trend of the other agility metrics and conflicting with intuition, it is proposed that it should not be used to judge agility.

7.7 Conclusions

In this chapter, an agile turn-around manoeuvre was solved using numerical optimisation methods to find the optimal controls for minimising time, subject, in particular, to boundary constraints that ensured the vehicle must start and end at the same point in space.

It was found that torque vectoring allows a substantially reduced space in the x_R-y_R plane than the area required for the vehicle with TV inactive. This was achieved by operating the vehicle at greater sideslip angles, resulting in higher lateral jerk and yaw acceleration agility metrics for torque vectoring. Lateral acceleration metric was greater for TV inactive, implying intuitively that this is not a good overall measure for agility.

For both trajectories, rotation is biased towards the first half of the manouevre, while the return portion involves predominantly longitudinal acceleration. Handwheel effort is similar for both TV active and TV inactive (with one exception); this implies that a control law could be developed that would allow an average driver to perform this aggressive manoeuvre with assistance from TV. Destabilsing yaw moment assisted the TV vehicle to overcome inertial effects to help build yaw acceleration, while stabilising yaw moment is used to help maintain stability.

The trajectories were split into 5 distinct phases, for which the agility metrics were calculated for each. This approach is important, since TV and TV inactive configurations use dissimilar yaw rate and lateral acceleration trajectories to complete the manoeuvre. For example, yaw acceleration metric is greater for TV in phase B, but lower in phase C, although the total manoeuvre metric favours TV; this reflects that TV initiates rotation earlier in the manoeuvre.

For the TV configuration, a study of the effect of longitudinal slip ratio limit was

conducted. It was found that increasing the limit reduced the space in the x_R-y_R plane, increased the manoeuvre curvature and reduced the required steering effort. For the total-manoeuvre metrics, all reduced with increased slip ratio limit. This is counter-intuitive. However, through an analysis of the crucial phase C (corresponding to maximum rotation) it was seen that lateral jerk, yaw acceleration and yaw rate increase with slip ratio limit, pointing to greater agility during the rotation phase.

A further study of yaw inertia sensitivity was conducted for the TV configuration, perturbing the yaw inertia by 50% above and below the nominal value. The influence on manoeuvre time and distance was minimal. Total-manoeuvre agility metrics of lateral jerk, yaw acceleration and yaw rate increase as inertia is reduced, while lateral acceleration metrics are invariant.

To summarise, the key conclusions are:

- TV dramatically increases agility over the vehicle with TV inactive;
- it is important to consider phases of the manoeuvre when analysing the agility metrics;
- increasing the longitudinal slip limit increases agility for TV;
- decreasing yaw inertia increases agility for TV;
- intuitively, lateral jerk, yaw acceleration and yaw rate metrics capture agility whereas lateral acceleration does not.

Chapter 8

Conclusions

The fundamental aim of this thesis was to investigate the optimal handling characteristics of an electric vehicle with torque vectoring ability by virtue of four independent motors.

The objectives pursued in reaching this aim were to: i) develop and test a TV control system through the full design and test process; ii) investigate the optimal handling characteristics while manoeuvring in minimum time, with a particular emphasis on sensitivity of manoeuvre time to yaw rate reference; iii) investigate the effect of vehicle model fidelity on minimum-time manoeuvring results; iv) investigate the optimal controls to conduct highly agile manoeuvres with torque vectoring.

This chapter presents a brief summary of the work undertaken in each chapter of the thesis and highlights the key findings in relation to the objectives. Areas for future work are also suggested.

8.1 Torque Vectoring Control System development

In the past decade, an increasing number of studies have developed torque vectoring control systems, with the majority of them adopting similar hierarchical layouts comprising controller reference (typically yaw rate), controller and control allocation.

As a basis for the investigation of optimal handling characteristics of an electric vehicle with torque vectoring, a TV control system for active control of yaw dynamics was developed in chapter 3. A model-based design process was adopted, culminating in real-time SiL testing and real-world vehicle testing.

A hierarchical TV control system was developed in Matlab/Simulink in co-simulation with IPG CarMaker, consisting of Reference Generator, PID controller and Control Allocation. Step-steer and steady-turn open-loop manoeuvres were simulated to assess the effect of yaw rate reference and controller tuning on steady-state and transient handling responses. Practical considerations for real-time implementation were tested using simulated CAN delays and sensor noise. After development in the desktop environment, tests were conducted in real-time using Cranfield University's SiL rig. Vehicle tests were carried out on the Delta Motorsport E4 coupe, equipped with 4 inboard electric motors at Jaguar Land Rover's test track in Gaydon, Warwickshire. Step-steer and steady-turn manoeuvres were completed for a range of yaw rate references for both understeer and oversteer targets.

The key findings were that the torque vectoring control system was able to:

- successfully modify the handling characteristic to target understeer gradients significantly far from the TV inactive behaviour in both understeer and oversteer directions;

- follow the reference in both steady-state and transient manoeuvres with an acceptable transient response and steady-state tracking;
- to be incorporated successfully into a real-time environment and to demonstrate robust operation in the presence of sensor noise and delays using measured signals over a CAN system.

8.2 Time optimal handling

A survey of the literature identified that whilst many studies had worked on optimising controller and control allocation aspects of active torque vectoring control systems, little work had been undertaken in assessing or improving the yaw rate reference. The yaw rate reference had been selected subjectively, and its contribution to overall vehicle system performance had not been investigated where closed-loop manoeuvring was concerned. In addition, optimal control studies for minimum-time manoeuvring had focussed on open-loop control, with an absence of closed-loop feedback control for active systems.

In chapters 4 and 5, investigating the optimal handling characteristics at the limit of performance was addressed by using numerical optimisation techniques to generate minimum-time manoeuvres. Three objectives were pursued: i) to determine the effect of a vehicle with torque vectoring compared to a vehicle with TV inactive; ii) to investigate the effect of variation of the passive handling characteristic (in terms of understeer gradient of the vehicle with TV inactive) when TV is active; iii) to investigate the effect of the target understeer gradient on the performance of the actively-controlled vehicle. Nonlinear numerical optimisation was used to determine the optimal controls to operate the vehicle to minimise time taken to navigate a U-turn manoeuvre.

The work was divided into two chapters pursing identical objectives but using the

3DOF single-track and 7DOF double-track vehicle models (4 and 5, respectively). Chapter 6 compared the results from both vehicle models and conducted open-loop manouevre simulations to understand the difference between the models.

8.2.1 3DOF vehicle model

Firstly, control inputs of steering rate, longitudinal acceleration demand and a direct-yaw moment term (to emulate torque vectoring) were used to generate open-loop control baselines with and without torque vectoring. The vehicle model consisted of a single track, linear tyres and included longitudinal load transfer. Tyre friction was coupled at the limit by a friction circle and longitudinal tyre forces were distributed front-rear in proportion to the normal load. Wheel dynamics were neglected. The manoeuvre baselines for the vehicle with TV active and TV inactive were compared. Imposing realistic limits on yaw moment was also shown. Secondly, the effect of modifying the passive handling characteristic on the TV vehicle manoeuvre time and trajectories was investigated.

The final investigation reformulated the optimal control problem to incorporate the closed-loop TV controller developed in chapter 3 in the system dynamics such that the effect of variation in target understeer gradient (which parametrised the yaw rate reference) on manoeuvre time could be investigated. The control inputs were reduced to steering rate and longitudinal acceleration, with yaw moment being determined by a P-controller acting on the yaw rate error.

The key findings are as follows:

- The baseline torque vectoring vehicle was 0.374s faster than the vehicle with TV inactive over the U-turn by making full use of friction availability at front and rear at all times. This was achieved by compensating for longitudinal load transfer ef-

fects. Constraining yaw moment to realistic values only restricted this effect at high longitudinal accelerations.

- Modifying the passive handling characteristic showed no effect on manoeuvre time when torque vectoring was active.
- For the closed-loop control formulation, modifying the yaw rate reference away from the passive characteristic of the vehicle exhibited a severely negative effect on manoeuvre time. The time-optimal reference was equal to the passive characteristic, for which the vehicle achieved greatest minimum speed and maximum yaw rate, as well as full friction utilisation.

8.2.2 7DOF vehicle model

The methodology applied to the previous chapter was also employed here, using a more complex vehicle mode. The 7DOF vehicle model used adopted nonlinear tyres, coupled through the combined slip model. Longitudinal and lateral load transfers were included, as well as wheel dynamics for the four wheels. The open-loop control configuration required steering rate and individual wheel torques as inputs. For the optimal control problems including the TV controller in the system dynamics, the control inputs reduced to steering rate and total torque demand only; the control allocation determined the torque distribution according to the yaw moment demand from the P-controller.

The key findings are as follows:

- The open-loop baseline torque vectoring optimisation was 0.380s faster than the vehicle with TV inactive. Torque vectoring compensates for adverse lateral and longitudinal load transfer effects. Limiting wheel torques to realistic values reduced

torque vectoring capability only at high longitudinal accelerations.

- For the closed-loop TV controller in the system dynamics, the standard single-track yaw rate reference parameterised by target understeer gradient delievered a very similar manouevre time to the open-loop baseline. This is because the reference effectively commands no load transfer, the negative consequences of which the torque-vectored vehicle is able to compensate for.

- The most significant finding was that manoeuvre time was largely insensitive to the target understeer gradient. The important deduction is that the yaw rate reference may be chosen according to the subjective requirements of the driver without compromising absolute performance.

8.2.3 Modelling effects

The optimisations, including the TV controller in the system dynamics delivered contradictory results between the vehicle models. Chapter 6 set out to investigate the differences in detail and to conclude which effects had a bearing on the results.

Firstly, yaw rate gain surfaces as a function of speed and longitudinal acceleration were generated from open-loop numerical optimisation results for a range of U-turn radii for both 3DOF (with and without yaw moment constraints) and 7DOF vehicle models (with and without torque constraints). It was shown that the 3DOF model was able to entirely compensate for longitudinal load transfer effects and deliver an identical response to the steady-state yaw bicycle model yaw rate gain. Applying realistic torque limits modified the surface at high longitudinal accelerations.

Similarly, the 7DOF model was able to negate load transfer effects to a large extent. The yaw rate gain, however, reduced relative to the 3DOF at high speeds, due to the fact

that the tyre model cornering stiffnesses are only equivalent at zero slip.

Questions were raised from the contradictory results in chapters 4 and 5, resulting from differences in the vehicle model. Further investigations to identify and explain these differences were undertaken by using open-loop manoeuvres to eliminate the driver effect on results for a fair comparison. Since this meant minimum-time manoeuvring was no longer possible, tyre friction utilisation was taken as a proxy metric. Constant-steer simulations under constant acceleration were performed with both vehicle models with closed-loop TV control for three different target understeer gradients.

Three principle differences between the vehicle models were investigated: tyre model; lateral load transfer; torque vectoring yaw moment generation mechanism.

The key findings were that:

- The main difference between vehicle models was found to be tyre nonlinearity; for the nonlinear tyre near peak tyre friction, only a small reduction in friction occurs even with large deviation from the slip value at which peak friction is generated. For the linear tyre, however, the friction-slip gradient is steeper and hence a greater reduction in friction is observed.
- Lateral load transfer had a larger negative effect when considering the linear tyres but only a small effect when considering nonlinear tyres.
- The torque vectoring yaw moment generation mechanism (via individual wheel torques or external yaw moment term) had little impact on performance.
- The difference between the models was minimised when target understeer gradient was set equal to the passive characteristic because this is the optimal setting for the linear tyre.

8.3 Agility optimal handling

The precise meaning of the term ‘agility’ is elusive and, in the literature studied, its definition was ambiguous. A number of vehicle dynamic studies that seek to mimic expert driving manoeuvres at high sideslip angles have been performed using numerical optimisation techniques for optimal control for conventionally-powered vehicles. A recent study had defined agility in terms of a number of metrics.

The work in the chapter brought together numerical optimisation techniques and the agility metrics to investigate the optimal handling of torque vectoring vehicles for agiliy. Firstly, vehicles with and without torque vectoring were compared for an agile turn-around manoeuvre, which requires the vehicle to return to its starting position and straight-ahead posture at the same speed but in the opposite direction. The objective function for the optimal control sought to minimise manoeuvre time.

- TV dramatically increased agility over the vehicle with TV inactive;
- it was important to consider phases of the manoeuvre when analysing the agility metrics;
- increasing the longitudinal slip limit increased agility for TV;
- decreasing yaw inertia increased agility for TV;
- intuitively, lateral jerk, yaw acceleration and yaw rate metrics captured agility whereas lateral acceleration did not.

8.4 Contribution

The work presented in this thesis has made a contribution to the knowledge in the vehicle dynamics and control discipline in the following four areas.

Firstly, the work in chapters 4 and 5 incorporated a closed-loop yaw rate controller as part of the system dynamics of an optimal control problem that was solved using nonlinear numerical optimisation techniques. To the knowledge of the author, this has not been undertaken in the field of road vehicle dynamics, although after developing the technique independently, it was found that a similar approach has been attempted recently for aerial vehicles [119].

The second contribution, is the objective assessment of the effect of the yaw rate reference on any quantifiable objective for a closed-loop manouevre. The evaluation of yaw rate reference on the closed-loop manoeuvring behaviour of the actively-controlled vehicle, has, up to this point, been conducted subjectively. Fair objective comparisons up to this point have only been conducted using typical open-loop manoeuvres such as the step-steer and skid-pad tests. Studies, in general, have focussed on the active system as a whole, and especially on the controller and control allocation of typical systems. The purpose of incorporating the closed-loop yaw rate controller in the system dynamics of the optimal control problem was to isolate the effect of the yaw rate reference on the closed-loop manoeuvring performance of the vehicle. Thus, the sensitivity of manoeuvre time on the yaw rate reference was determined in chapters 4 and 5 for different vehicle models. The optimal control technique was essential for 'driving' the vehicle at the limit of performance.

The third contribution of this thesis work is the assessment of the level of vehicle model modelling realism required to capture the key phenomena that torque vectoring depends upon. Chapters 4 and 5 assessed the effect of yaw rate reference on manouevre time for a 3DOF single-track model with linear tyres and a 7DOF two-track vehicle model

with nonlinear tyres. The results were contradictory, which prompted further analysis to understand where the differences originated.

In the literature, the optimality of expert driving techniques of conventionally-powered vehicles have been assessed using optimal control methods. There have also been attempts to quantify the agility of such techniques and manoeuvres. The fourth contribution of this thesis combined both optimal control techniques and quantitative metrics to investigate the agility of vehicles with torque vectoring in extreme (high-sideslip) manoeuvring. A subjective and objective analysis of the suitability of the agility metrics was also performed in this context. To the author's knowledge, torque vectoring in high-sideslip manoeuvres using optimal control has not been attempted before.

8.4.1 Publications

Smith E, Velenis E, Tavernini D, Cao D,. Effect of handling characteristics on minimum time cornering with torque vectoring. Vehicle System Dynamics (in publication)

Smith E, Velenis E, Cao D, Tavernini D. Evaluation of optimal yaw rate reference for electric vehicle torque vectoring. In: Advanced Vehicle Control: Proceedings of the 13th International Symposium on Advanced Vehicle Control (AVEC16), September 13-16, 2016, Munich, Germany; Dec. CRC Press/Balkema; 2016. p. 619624; Available from: http://dx.doi.org/10.1201/9781315265285-98.

Smith E, Tavernini D, Claret C, Velenis E, Cao D. Optimal yaw-rate target for electric vehicle torque vectoring system. In: The Dynamics of Vehicles on Roads and Tracks: Proceedings of the 24th Symposium of the International Association for Vehicle System

Dynamics (IAVSD 2015), Graz, Austria, 17-21 August 2015. CRC Press; 2016. p. 107.

8.5 Future Work

Recommendations for extending the work in this thesis are as follows:

- Since the vehicle model comparison points to nonlinear tyres being the dominant characteristic for accurately capturing torque vectoring effects, while lateral load transfer and yaw moment generation being secondary, a single-track vehicle model with nonlinear tyres should be used to rerun the optimisation methodology in chapters 4 and 5.
- It was concluded in chapter 5 that the target understeer gradient has almost zero effect on laptime. The near-identical laptimes are achieved by operating the vehicle using different levels of steering angle and resulting degrees of sideslip. It would be interesting to apply the eigenvalue and yaw rate response analysis in [111] to the TV vehicles following different yaw rate references to make a prediction as to which reference would be most desirable to a racing driver. Circuit testing could be used to investigate the correlation between theory and practice.
- Further investigation of the optimal agility manoeuvres in chapter 7 could be undertaken with the objective of developing a closed-loop controller to replicate the optimal manoeuvre in a high-fidelity simulation environment. This could take the form of an MPC controller with carefully chosen yaw rate or lateral jerk references.

Appendix A

Practical considerations for numerical optimal control

A.1 Example Code

Examples of the Matlab code used to solve the optimal control problems in this thesis will be made available at an online repository by searching for this thesis. Search for gitlab.com username @ednevsmith.

A.2 Introduction

The second part collates practical notes on using GPOPS-II to solve optimal control problems that the author has developed during the course of the doctoral research. It is intended to help short cut the learning process for future students and form a 'body of knowledge' for Cranfield University's Advanced Vehicle Engineering Centre; a great deal

of time was spent learning how to use numerical optimal control and it is hoped that this will save time of researchers new to the field.

Particular thanks is extended to Davide Tavernini, who was helpful in setting up the first example problems for the author to build upon, and to Anthony Tremlett and Efstathios Siampis for their help in the learning process.

A.3 Work flow

The following process should be followed:

1. Generate vehicle equations of motion and simulate using ODE45 or similar in Matlab to eliminate errors before progressing to GPOPS-II. Ensure that the scaling procedure gives correct results. These results can be used as the initial guess to the problem.

2. Make a new folder for each optimal control problem to run.

3. Ensure the state bounds and constraints make sense

4. Run ADIgator separately to GPOPS to ensure that derivative files can be produced without error - this way returns error messages to the command window

5. Conduct a test run in GPOPS, with the mesh iteration count set to 2. Even if the problem has difficulty solving, it will still give you a result to plot and give insight as to what may be causing problems.

6. If constraints are causing difficulties, it can help to relax these, run the relaxed problem and then use that as the initial guess to the more constrained problem.

7. For some problems, a kinematic initial guess is sufficient, for others the dynamic guess if better. The dynamic guess is not guaranteed to be superior, because it may lead to a local minimum that does not give sensible results.

8. Write some code to make an automatic copy of all the files used to run the optimal control problem and save these with the results file. This is a simple way to be able to check exactly the configuration used.

A.4 Initial Guess

An initial guess is required by GPOPS-II. In Part II, this was provided in the form of kinematic equations; subsequent optimisations used the initial optimisation results as the initial guess. Sometimes, an initial guess considering dynamics has been used for some of the optimisations by solving a simulation for the dynamic vehicle model in §7.4.2 using ODE45 in Matlab.

Steering rate control inputs are determined by a simple proportional controller acting on the error between the yaw rate and kinematic yaw rate, based on a curvature nominal path for a U-turn of 10m radius:

$$\dot{\delta} = P_{\dot{\psi}}(V\kappa_{ref} - \dot{\psi}), \tag{A.1}$$

where κ_{ref} is the reference path curvature and $P_{\dot{\psi}}$ is the proportional gain.

Torque rate inputs are determined by an additional simple proportional controller acting on the error between the vehicle speed and a speed reference:

$$\dot{T}_{ij} = P_{\dot{T}_{ij}}(V_{ref} - V), \tag{A.2}$$

where $P_{\dot{T}_{ij}}$ is the proportional gain. In order to deliver a feasible manoeuvre, (V_{ref} is set to a nominal value of 35kph for zero-curvature path reference and according to 75% of the maximum steady-state cornering speed for the constant-curvature section of the U-turn reference:

$$V_{ref} = 0.75\sqrt{\frac{\mu_{max} g}{|\kappa_{ref}|}}. \tag{A.3}$$

The parameters chosen to construct the dynamic initial guess are far from the optimal solution. However, the main purpose of the initial guess is to give a feasible starting point from which the OCP algorithm can calculate the search direction to proceed towards the minimum of the objective function. The dynamic initial guess fulfills the criteria of being feasible and sufficiently close to the solution that the OCP solver finds an optimal solution that makes intuitive sense (the existence of multiple local minimisers is possible) and ensures the starting point is tractable.

A.5 NLP solver

In chapters 4 and 5, the NLP solver SNOPT [104] was used.

After further research, it was decided that IPOPT [120] would be tried for the simulations in this section. Contemporary studies [63, 74, 79] use this interior-point barrier method to solve the discretised subproblem. Using IPOPT significantly improved the rate of convergence with active constraints, in particular those required to ensure the fixed torque distribution of the vehicle with TV inactive.

A.6 Calculation of derivatives

GPOPS-II does is able to use finite-differencing methods to calulate derivatives. However, supplying derivative information approximately halves the computation time, in the authors' experience. *ADIgator* [121] is available to download online and uses the operator-overloading to produce derivative functions based on the system equations coded into the Matlab files used by GPOPS. It is very simple to use but has certain limitations. It can cope with certain switching functions, but all operations coded into the Matlab script must be array-wise. i.e. one cannot use only subsets of variable arrays. For this reason, only proportional control could be used in chapters 4 and 5. Integral and derivative errors could not be calculated cumulatively along the time history.

It is also important to eliminate discontinuities. Discontinous operations such as *min*, *max*, *sign* and *abs* should be replaced by close approximations that are continuously differentiable [74].

Calculating derivatives symbolically is certainly worth investigation, for the increased speed of execution [81]. Francesco Biral at the University of Trento can be contacted for obtaining a license for PINS and Xoptima software (indirect optimisation approach).

A.7 Scaling scheme

Scaling the vehicle dynamics approximately halved the solution time of the optimal control problem compared to the automatic scaling algorithm provided by GPOPS. It is highly recommended to implement this for nonlinear optimal control but also MPC.

A scaling scheme has been applied in the same manner as [74], achieved by applying scaling factors to all physical quantities, based on three fundamental quantities of length, mass and time. For example: let mass scaling factor $\tilde{m} = m^{-1}$, then scaled mass becomes

$m\tilde{m} = 1$; let length scaling factor $\tilde{L} = L^{-1}$, then scaled wheelbase becomes $L\tilde{L} = 1$; let time scaling factor $\tilde{t} = \sqrt{(L/g)}$, then scaled time becomes $t\tilde{t}$. Velocity is scaled by a combination of length and time scaling factors, according to its units, and becomes $V\tilde{L}\tilde{t}^{-1}$. The conditioned dual problem is solved and then unscaled to give results in the original domain.

To apply this scaling, make sure all inputs to the GPOPS solver are scaled. To view the results, simply multiply by the inverse of the scaling factors. This technique is simple but it is easy to make errors but just one unscaled equation is not acceptable.

A.8 Computation time

Optimisations were performed on a desktop PC with 8GB RAM and an Intel Core^{TM} i7-3370 CPU at 3.40GHz delivering a computation time between 3 and 60 minutes depending on the particular OCP setup. It is difficult to be precise because of the variation in procedure between different problems. Some required a great deal of manipulation of constraints and boundaries to eventually iterate to the desired result.

A.9 Concluding Advice

A great deal of time and effort is required to set up the optimal control problems. The greatest proportion of time should be spent on ensuring that the the problem is formulated sensibly. It is also helpful to build up experience from very simple problems, collating a mental library of how to solve common problems.

Appendix B

Agility Metrics

The data used to produce the bar plots in chapter 7 are included in full below.

- **TV active vs. TV inactive**:Table B.1 contains the data plotted in Figure 7.10.
- **Effect of slip limits**: Table B.2 contains the data plotted in Figure 7.7.
- **Yaw inertia sensitivity**: Table B.3 contains the data plotted in Figure 7.10.

Phase	Config.	Duration (s)	$\frac{\text{phase}}{\text{Total}}$ (-)	distance (m)	Lat. jerk (g/s)	Lat. acc. g	yaw acc. ($^\circ s^{-2}$)	yaw rate ($^\circ s^{-1}$)
A	NoTV	0.7	0.14	10	2.3	0.62	138	33
	TV	0.7	0.15	10	2.8	0.59	157	30
B	NoTV	1.3	0.24	11	2.5	0.70	80	56
	TV	0.6	0.14	6	3.2	0.55	147	54
C	Unctrl	0.8	0.15	4	1.3	0.83	52	99
	TV	1.2	0.25	6	1.7	0.81	35	99
D	NoTV	1.7	0.32	11	2.6	0.34	70	30
	TV	1.4	0.31	10	1.8	0.37	64	33
E	NoTV	0.9	0.16	12	2.2	0.48	71	18
	TV	0.7	0.15	10	2.7	0.44	82	17
Total	NoTV	5.4	1.00	50	2.3	0.56	86	39
	TV	4.6	1.00	41	2.5	0.53	98	40

Table B.1: Min time Agility metrics: NoTV vs TV

Phase	Config.	Duration (s)	$\frac{\text{phase}}{\text{Total}}$ (-)	distance (m)	Lat. jerk (g/s)	Lat. acc. g	yaw acc. ($^\circ s^{-2}$)	yaw rate ($^\circ s^{-1}$)
A	$s_{x,lim0}$	0.7	0.15	9.6	2.8	0.59	157	30
	$2s_{x,lim0}$	0.7	0.15	9.4	2.6	0.62	161	29
	$4s_{x,lim0}$	0.6	0.15	9.0	2.6	0.67	162	31
B	$s_{x,lim0}$	0.7	0.14	6.1	3.2	0.55	147	54
	$2s_{x,lim0}$	0.7	0.13	5.5	3.6	0.49	163	51
	$4s_{x,lim0}$	0.6	0.14	6.7	3.7	0.45	159	50
C	$s_{x,lim0}$	1.2	0.25	5.6	1.7	0.81	35	99
	$2s_{x,lim0}$	1.1	0.25	5.0	2.0	0.79	42	102
	$4s_{x,lim0}$	1.0	0.24	4.4	2.0	0.77	45	105
D	$s_{x,lim0}$	1.4	0.31	9.7	1.8	0.37	64	33
	$2s_{x,lim0}$	1.4	0.32	9.3	1.5	0.36	61	33
	$4s_{x,lim0}$	1.4	0.33	9.2	1.6	0.38	62	34
E	$s_{x,lim0}$	0.7	0.15	10.1	2.7	0.44	82	17
	$2s_{x,lim0}$	0.7	0.15	9.7	2.2	0.31	60	12
	$4s_{x,lim0}$	0.7	0.15	9.5	1.7	0.21	43	8
Total	$s_{x,lim0}$	4.6	1.00	40.9	2.5	0.53	98	40
	$2s_{x,lim0}$	4.5	1.00	38.9	2.3	0.48	97	38
	$4s_{x,lim0}$	4.4	1.00	38.0	2.2	0.46	94	37

Table B.2: Min time Agility metrics: TV slip limit compare

Phase	Config.	Duration (s)	$\frac{\text{phase}}{\text{Total}}$ (-)	distance (m)	Lat. jerk (g/s)	Lat. acc. g	yaw acc. ($^\circ s^{-2}$)	yaw rate ($^\circ s^{-1}$)
A	$0.5I_{z,nom}$	0.7	0.15	9.9	3.3	0.45	120	19
	$I_{z,nom}$	0.7	0.14	9.7	2.6	0.45	87	19
	$1.5I_{z,nom}$	0.6	0.13	9.4	2.3	0.44	80	20
B	$0.5I_{z,nom}$	0.7	0.16	7.2	2.8	0.66	108	59
	$I_{z,nom}$	0.8	0.16	7.5	2.8	0.58	124	48
	$1.5I_{z,nom}$	0.8	0.16	8.2	2.3	0.53	121	42
C	$0.5I_{z,nom}$	0.9	0.20	4.5	1.9	0.80	46	103
	$I_{z,nom}$	1.2	0.25	5.8	1.5	0.80	34	97
	$1.5I_{z,nom}$	1.4	0.28	7.0	1.2	0.81	29	92
D	$0.5I_{z,nom}$	1.5	0.33	9.8	2.5	0.38	74	33
	$I_{z,nom}$	1.2	0.24	6.8	2.1	0.44	63	39
	$1.5I_{z,nom}$	0.9	0.18	4.9	1.4	0.54	62	47
E	$0.5I_{z,nom}$	0.8	0.16	11.0	3.4	0.56	103	21
	$I_{z,nom}$	1.0	0.21	14.0	3.0	0.48	84	19
	$1.5I_{z,nom}$	1.3	0.25	16.5	2.7	0.47	77	20
Total	$0.5I_{z,nom}$	4.7	1.00	42.3	2.9	0.53	95	38
	$I_{z,nom}$	4.8	1.00	43.8	2.5	0.52	82	38
	$1.5I_{z,nom}$	5.0	1.00	46.0	2.2	0.54	76	38

Table B.3: Min time Agility metrics: Yaw inertia sensitivity

References

[1] Metz L. What constitutes good handling? SAE Technical Paper; 2004.

[2] Van Zanten AT. Bosch ESP Systems: 5 Years of Experience. Warrendale, PA: SAE International; 2000. SAE Technical Paper 2000-01-1633; Available from: http://papers.sae.org/2000-01-1633/.

[3] FIA. FIA Formula-e championship. http://www.fiaformulae.com/en/championship/overview/.; accessed: 2017-08-05.

[4] Beckwith J. Mercedes to race in Formula-e from 2019. https://www.autocar.co.uk/car-news/motorsport-formula-e/mercedes-race-formula-e-2019. ; accessed: 2017-08-05.

[5] Current-e. Artificial intelligence meets human ingenuity. http://current-e.com/features/artificial-intelligence-meets-human-ingenuity/. ; accessed: 2017-08-05.

[6] Wong JY. Theory of ground vehicles. John Wiley & Sons; 2001.

[7] Jazar RN. Vehicle dynamics theory and application. Riverdale, NY: Springer Science+ Business Media; 2008.

[8] Milliken WF, Milliken DL. Race car vehicle dynamics. Vol. 400. Society of Automotive Engineers Warrendale; 1995.

[9] Sharp R. Vehicle dynamics and the judgment of quality. Pauwelussen, JP, Swets & Zeitlinger Publishers, Lisse, the Netherlands. 1999;:87–96.

[10] Crolla DA, Cao D. The impact of hybrid and electric powertrains on vehicle dynamics, control systems and energy regeneration. Vehicle System Dynamics. 2012 Jan;50(sup1):95–109; Available from: http://www.tandfonline.com/doi/abs/10.1080/00423114.2012.676651.

[11] Rauh J. Virtual development of ride and handling characteristics for advanced passenger cars. Vehicle System Dynamics. 2003;40(1-3):135–155.

[12] Crolla D. Vehicle dynamics, control and suspensions. Lecture notes. Cranfield University. 2004.

[13] Bucchi F, Frendo F. A new formulation of the understeer coefficient to relate yaw torque and vehicle handling. Vehicle System Dynamics. 2016 Jun; 54(6):831–847; Available from: http://www.tandfonline.com/doi/full/10.1080/00423114.2016.1167225.

[14] Bedner E, Fulk D, Hac A. Exploring the trade-off of handling stability and responsiveness with advanced control systems. SAE Papers. 2007;:01–0812Available from: http://pt.delphi.com/pdf/techpapers/2007-01-0812.pdf.

[15] Wu X, Farhad M, Wong JM. Design and tuning of chassis characteristics to achieve desirable vehicle transient handling performance. International Journal of Vehicle Performance. 2013;1(1):5–27.

[16] Shibahata Y, Shimada K, Tomari T. Improvement of vehicle maneuverability by direct yaw moment control. Vehicle System Dynamics. 1993;22(5-6):465–481.

[17] Inagaki S, Kushiro I, Yamamoto M. Analysis on vehicle stability in critical cornering using phase-plane method. JSAE Review. 1995;2(16):216.

[18] Mimuro T, Ohsaki M, Yasunaga H, Satoh K. Four parameter evaluation method of lateral transient response. SAE Technical Paper; 1990.

[19] Manning W, Crolla D. A review of yaw rate and sideslip controllers for passenger vehicles. Transactions of the Institute of Measurement and Control. 2007; 29(2):117–135.

[20] Chen D. Subjective and objective vehicle handling behaviour. PhD thesis. University of Leeds; 1997.

[21] Dang J, Chen H, Gao B, Li Q, Li M, Watanabe T, Hayama R, Lou L, Nakano S. Optimal design of on-center steering force characteristic based on correlations between subjective and objective evaluations. SAE International Journal of Passenger Cars-Mechanical Systems. 2014;7(2014-01-0137):992–1001.

[22] Nybacka M, He X, Su Z, Drugge L, Bakker E. Links between subjective assessments and objective metrics for steering, and evaluation of driver ratings. Vehicle System Dynamics. 2014;52(sup1):31–50.

[23] Dixon PJ. The influence of the sideslip target on the performances of vehicles with actively controlled handling. PhD thesis. Loughborough University, 2004.

[24] Mirzaei M. A new strategy for minimum usage of external yaw moment in vehicle dynamic control system. Transportation Research Part C: Emerging Technologies. 2010;18(2):213–224.

[25] Rubin D, Arogeti SA. Vehicle yaw stability control using active limited-slip differential via model predictive control methods. Vehicle System Dynamics. 2015 Jun;:1–16Available from: http://www.tandfonline.com/doi/full/10.1080/00423114.2015.1046461.

[26] Piyabongkarn D, Lew JY, Rajamani R, Grogg JA, Yuan Q. On the use of torque-biasing systems for electronic stability control: limitations and possibilities. IEEE Transactions on Control Systems Technology. 2007;15(3):581–589.

[27] Piyabongkarn D, Lew JY, Rajamani R, Grogg JA. Active driveline torque-management systems. IEEE Control Systems. 2010;30(4):86–102.

[28] De Novellis L, Sorniotti A, Gruber P, Shead L, Ivanov V, Hoepping K. Torque vectoring for electric vehicles with individually controlled motors: state-of-the-art and future developments. In: 26th Electric Vehicle Symposium 2012; 2012.

[29] Horiuchi S. Evaluation of chassis control method through optimisation-based controllability region computation. Vehicle System Dynamics. 2012;50(sup1):19–31.

[30] Horiuchi S. Evaluation of chassis control algorithms using controllability region analysis. In: The Dynamics of Vehicles on Roads and Tracks: Proceedings of the 24th Symposium of the International Association for Vehicle System Dynamics (IAVSD 2015), Graz, Austria, 17-21 August 2015. CRC Press; 2016. p. 35.

[31] Vignati M, Sabbioni E, Tarsitano D, Cheli F. Electric powertrain layouts analysis for controlling vehicle lateral dynamics with torque vectoring. In: Electrical and Electronic Technologies for Automotive, 2017 International Conference of. IEEE; 2017. p. 1–5.

[32] De Novellis L, Sorniotti A, Gruber P. Design and comparison of the handling performance of different electric vehicle layouts. Proceedings of the Institution of Mechanical Engineers, Part D: Journal of Automobile Engineering. 2014;228(2):218–232.

[33] de Castro R, Tanelli M, Araújo RE, Savaresi SM. Design of safety-oriented control allocation strategies for overactuated electric vehicles. Vehicle System Dynamics. 2014;52(8):1017–1046.

[34] Siampis E, Velenis E, Longo S. Rear wheel torque vectoring model predictive control with velocity regulation for electric vehicles. Vehicle System Dynamics. 2015; (ahead-of-print):1–25.

[35] Bächle T, Graichen K, Buchholz M, Dietmayer K. Vehicle dynamics control in challenging driving situations using nonlinear model predictive control allocation. In: 2014 IEEE Conference on Control Applications (CCA). IEEE; 2014. p. 346–351.

[36] De Novellis L, Sorniotti A, Gruber P. Wheel torque distribution criteria for electric vehicles with torque-vectoring differentials. IEEE transactions on vehicular technology. 2014;63(4):1593–1602.

[37] Wang J, Longoria RG. Coordinated and reconfigurable vehicle dynamics control. IEEE Transactions on Control Systems Technology. 2009;17(3):723–732.

[38] Basrah MS, Siampis E, Velenis E, Cao D, Longo S. Wheel slip control with torque blending using linear and nonlinear model predictive control. Vehicle System Dynamics. 2017;:1–21.

[39] Bünte T, Kaspar S, Hohmann S, Brembeck J. Inverse model based torque vectoring control for a rear wheel driven battery electric vehicle. In: IFAC World Congress; 2014. Available from: http://user.das.ufsc.br/~trofino/pub/IFAC%202014/media/files/0802.pdf.

[40] De Novellis L, Sorniotti A, Gruber P, Orus J, Rodriguez Fortun JM, Theunissen J, De Smet J. Direct yaw moment control actuated through electric drivetrains and friction brakes: Theoretical design and experimental assessment. Mechatronics. 2015 Mar;26:1–15; Available from: http://linkinghub.elsevier.com/retrieve/pii/S0957415814002104.

[41] De Novellis L, Sorniotti A, Gruber P, Pennycott A. Comparison of feedback control techniques for torque-vectoring control of fully electric vehicles. IEEE Transactions on Vehicular Technology. 2014;63(8):3612–3623.

[42] Pinto L, Aldworth S, Watkinson M, Jeary P, Franco-Jorge M. Advanced yaw motion control of a hybrid vehicle using twin rear electric motors. Advanced Vehicle Control. 2010;:640–645.

[43] Kaiser G, Liu Q, Hoffmann C, Korte M, Werner H. Torque vectoring for an electric vehicle using an LPV drive controller and a torque and slip limiter. In: Decision and Control (CDC), 2012 IEEE 51st Annual Conference on. IEEE; 2012. p. 5016–5021; Available from: http://ieeexplore.ieee.org/xpls/abs_all.jsp?arnumber=6426553.

[44] De Novellis L, Sorniotti A, Gruber P, Pennycott A. Comparison of feedback control techniques for torque-vectoring control of fully electric vehicles. IEEE Transactions on Vehicular Technology. 2014;63(8):3612–3623.

[45] de Castro R, Tanelli M, Araujo RE, Savaresi SM. Minimum-time manoeuvring in electric vehicles with four wheel-individual-motors. Vehicle System Dynamics. 2014 Jun;52(6):824–846; Available from: `http://www.tandfonline.com/doi/abs/10.1080/00423114.2014.902973`.

[46] De Novellis L, Sorniotti A, Gruber P. Optimal wheel torque distribution for a four-wheel-drive fully electric vehicle. SAE International Journal of Passenger Cars-Mechanical Systems. 2013;6(2013-01-0673):128–136.

[47] Yu Z, Leng B, Xiong L, Feng Y. Vehicle stability self-tuning control strategy based on joint criterion. In: 24th International Symposium on Dynamics of Vehicles on Road and Tracks of the International Association for Vehicle System Dynamics (IAVSD). VSD; 2015.

[48] Gruber P, Sorniotti A, Lenzo B, De Filippis G, Fallah S. Energy efficient torque vectoring control. In: Advanced Vehicle Control: Proceedings of the 13th International Symposium on Advanced Vehicle Control (AVEC'16), September 13-16, 2016, Munich, Germany. CRC Press; 2016. p. 17.

[49] Sawase K, Ushiroda Y, Inoue K. Effect of the right-and-left torque vectoring system in various types of drivetrain. SAE Technical Paper; 2007.

[50] Crolla D, Chen D, Whitehead J, Alstead C. Vehicle handling assessment using a combined subjective-objective approach. SAE Technical Paper; 1998.

[51] Hancock M, Williams R, Fina E, Best MC. Yaw motion control via active differentials. Transactions of the Institute of Measurement and Control. 2007;29(2):137–157.

[52] Tchamna R, Youn I. Yaw rate and side-slip control considering vehicle longitudinal dynamics. International Journal of Automotive Technology. 2013 Feb;14(1):53–60; Available from: http://link.springer.com/10.1007/s12239-013-0007-1.

[53] Rajamani R. Vehicle Dynamics and Control. Mechanical Engineering Series; Boston, MA: Springer US; 2012; Available from: http://link.springer.com/10.1007/978-1-4614-1433-9.

[54] Ni J, Hu J. Handling performance control for hybrid 8-wheel-drive vehicle and simulation verification. Vehicle System Dynamics. 2016;:1–22.

[55] Emìrler MT, Kahraman K, Şentürk M, Acar OU, Aksun Güvenç B, Güvenç L, Efendìoglu B. Lateral stability control of fully electric vehicles. International Journal of Automotive Technology. 2015 Apr;16(2):317–328; Available from: http://link.springer.com/10.1007/s12239-015-0034-1.

[56] Canale M, Fagiano L, Milanese M, Borodani P. Robust vehicle yaw control using an active differential and IMC techniques. Control Engineering Practice. 2007 Aug;15(8):923–941; Available from: http://linkinghub.elsevier.com/retrieve/pii/S0967066106002267.

[57] Polesel M, Shyrokau B, Tanelli M, Savitski D, Ivanov V, Ferrara A. Hierarchical control of overactuated vehicles via sliding mode techniques. In: Decision and Control (CDC), 2014 IEEE 53rd Annual Conference on. IEEE; 2014. p. 4095–4100; Available from: http://ieeexplore.ieee.org/xpls/abs_all.jsp?arnumber=7040026.

[58] Naraghi M, Roshanbin A, Tavasoli A. Vehicle stability enhancement an adaptive optimal approach to the distribution of tyre forces. Proceedings of the Institution

of Mechanical Engineers, Part D: Journal of Automobile Engineering. 2010 Apr; 224(4):443–453; Available from: http://pid.sagepub.com/lookup/doi/10.1243/09544070JAUTO1332.

[59] Pennycott A, De Novellis L, Sorniotti A, Gruber P. The Application of Control and Wheel Torque Allocation Techniques to Driving Modes for Fully Electric Vehicles. Warrendale, PA: SAE International; 2014. Report No.: 2014-01-0085; Available from: http://www.sae.org/technical/papers/2014-01-0085.

[60] Wheals JC, Baker H, Ramsey K, Turner W. Torque vectoring AWD driveline: Design, simulation, capabilities and control. 2004; sAE Technical Paper 2004-01-0863.

[61] Mokhiamar O, Abe M. How the four wheels should share forces in an optimum cooperative chassis control. Control Engineering Practice. 2006 Mar;14(3):295–304.

[62] Smith E, Tavernini D, Claret C, Velenis E, Cao D. Optimal yaw rate target for electric vehicle torque vectoring system. In: 24th International Symposium on Dynamics of Vehicles on Road and Tracks of the International Association for Vehicle System Dynamics (IAVSD). VSD; 2015.

[63] Perantoni G, Limebeer DJ. Optimal control for a formula one car with variable parameters. Vehicle System Dynamics. 2014;52(5):653–678.

[64] Tremlett A, Massaro M, Purdy D, Velenis E, Assadian F, Moore A, Halley M. Optimal control of motorsport differentials. Vehicle System Dynamics. 2015; 53(12):1772–1794.

[65] Velenis E, Tsiotras P, Lu J. Optimality properties and driver input parameterization for trail-braking cornering. European Journal of Control. 2008;14(4):308–320.

[66] Tavernini D, Massaro M, Velenis E, Katzourakis DI, Lot R. Minimum time cornering: the effect of road surface and car transmission layout. Vehicle System Dynamics. 2013 Oct;51(10):1533–1547; Available from: http://www.tandfonline.com/doi/abs/10.1080/00423114.2013.813557.

[67] Sharp R, Peng H. Vehicle dynamics applications of optimal control theory. Vehicle System Dynamics. 2011;49(7):1073–1111.

[68] Pennycott A, De Novellis L, Sabbatini A, Gruber P, Sorniotti A. Reducing the motor power losses of a four-wheel drive, fully electric vehicle via wheel torque allocation. Proceedings of the Institution of Mechanical Engineers, Part D: Journal of Automobile Engineering. 2014;:0954407013516106.

[69] Brayshaw D. Use of numerical optimisation to determine on-limit handling behaviour of race cars.. 2004;.

[70] Timings JP, Cole DJ. Minimum maneuver time calculation using convex optimization. Journal of Dynamic Systems, Measurement, and Control. 2013; 135(3):031015.

[71] Hendrikx J, Meijlink T, Kriens R. Application of optimal control theory to inverse simulation of car handling. Vehicle System Dynamics. 1996;26(6):449–461.

[72] Casanova D. On minimum time vehicle manoeuvring: The theoretical optimal lap. 2000;.

[73] Casanova D, Sharp R, Symonds P. Minimum time manoeuvring: The significance of yaw inertia. Vehicle system dynamics. 2000;34(2):77–115.

[74] Limebeer D, Perantoni G. Optimal control of a formula one car on a three-dimensional trackpart 2: Optimal control. Journal of Dynamic Systems, Measurement, and Control. 2015;137(5):051019.

[75] Tremlett A, Limebeer D. Optimal tyre usage for a formula one car. Vehicle System Dynamics. 2016;54(10):1448–1473.

[76] Lot R, Dal Bianco N. Lap time optimisation of a racing go-kart. Vehicle System Dynamics. 2016;54(2):210–230.

[77] Lot R, Dal Bianco N, Matthys K. Lap time simulation and design optimisation of a brushed dc electric motorcycle for the isle of man tt zero challenge. Vehicle System Dynamics. 2017;.

[78] Tremlett A, Assadian F, Purdy D, Vaughan N, Moore A, Halley M. The control authority of passive and active torque vectoring differentials for motorsport applications. In: Proceedings of the FISITA 2012 World Automotive Congress. Springer; 2013. p. 335–347.

[79] Limebeer DJ, Perantoni G, Rao AV. Optimal control of formula one car energy recovery systems. International Journal of Control. 2014;87(10):2065–2080.

[80] Velenis E, Tsiotras P. Minimum time vs maximum exit velocity path optimization during cornering. In: 2005 IEEE international symposium on industrial electronics; 2005. p. 355–360.

[81] Lot R, Da Lio M. A symbolic approach for automatic generation of the equations of motion of multibody systems. Multibody System Dynamics. 2004;12(2):147–172.

[82] Tavernini D, Velenis E, Lot R, Massaro M. The optimality of the handbrake cornering technique. Journal of Dynamic Systems, Measurement, and Control. 2014; 136(4):041019.

[83] Lot R, Dal Bianco N. The significance of high-order dynamics in lap time simulations. In: 24th International Symposium on Dynamics of Vehicles on Road and Tracks of the International Association for Vehicle System Dynamics (IAVSD). VSD; 2015.

[84] Bakker E, Nyborg L, Pacejka HB. Tyre modelling for use in vehicle dynamics studies. SAE Technical Paper; 1987.

[85] Ewin N. Traction Control for electric vehicles with independently driven wheels [dissertation]. Oxford University; 2016; Available from: https://ora.ox.ac.uk/objects/uuid:dfc99786-fe17-4225-bd91-3ab83416981f.

[86] Siampis E. Optimal torque vectoring control strategies for stabilisation of electric vehicles at the limits of handling [dissertation]. Cranfield University; 2016; Available from: https://dspace.lib.cranfield.ac.uk/handle/1826/11777.

[87] Velenis E, Katzourakis D, Frazzoli E, Tsiotras P, Happee R. Steady-state drifting stabilization of rwd vehicles. Control Engineering Practice. 2011;19(11):1363–1376.

[88] Autonomie. Model-based design approach. http://www.autonomie.net/projects/model_based_design_10.html; accessed: 2015-09-04.

[89] Soltani A. Low cost integration of Electric Power-Assisted Steering (EPAS) with Enhanced Stability Program (ESP) [dissertation]. Cranfield University;

2014; Available from: https://dspace.lib.cranfield.ac.uk/handle/1826/8829.

[90] Paul D, Velenis E, Cao D, Dobo T. Optimal mu-estimation-based regenerative braking strategy for an awd hev. IEEE Transactions on Transportation Electrification. 2017;3(1):249–258.

[91] MathWorks. PID Controller, Discrete PID Controller. 2015; Available from: http://uk.mathworks.com/help/simulink/slref/pidcontroller.html.

[92] Franklin GF, Powell JD, Emami-Naeini A. Feedback control of dynamics systems. Pearson Education, London; 2006.

[93] Claret C. Torque vectoring control for electric and brake-by-wire vehicles: Masters thesis. Cranfield University; 2014.

[94] BS ISO 4138:2012 Passenger cars -Steady-state circular driving behaviour - Open-loop test methods. British Standards Institution, London; 2012.

[95] Nocedal J, Wright S. Numerical optimization. Springer Science & Business Media; 2006.

[96] Betts JT. Practical methods for optimal control and estimation using nonlinear programming. Vol. 19. Siam; 2001.

[97] Diehl M, Gros S. Numerical optimisation of dynamic systems. http://www.syscop.de/files/2015ws/noc-dae/00-book.pdf. 2016.

[98] Limebeer DJ, Rao AV. Faster, higher, and greener: vehicular optimal control. IEEE Control Systems. 2015;35(2):36–56.

[99] Massaro M, Dal Bianco . Direct and indirect methods for minimum lap time optimal control problems. Cambridge Vehicle Dynamics Conference, March 21, 2017, Cambridge, UK.

[100] Patterson MA, Rao AV. Gpops- ii: A matlab software for solving multiple-phase optimal control problems using hp–adaptive gaussian quadrature collocation methods and sparse nonlinear programming. ACM Transactions on Mathematical Software. 2013;39(3):1–41.

[101] Biegler LT, Zavala VM. Large-scale nonlinear programming using ipopt: An integrating framework for enterprise-wide dynamic optimization. Computers & Chemical Engineering. 2009;33(3):575–582.

[102] Bertolazzi E, Biral F, Da Lio M. Symbolic–numeric indirect method for solving optimal control problems for large multibody systems. Multibody System Dynamics. 2005;13(2):233–252.

[103] Leyffer S, Mahajan A. Nonlinear constrained optimization: methods and software. Argonee National Laboratory, Argonne, Illinois. 2010;60439.

[104] Gill PE, Murray W, Saunders MA. Snopt: An sqp algorithm for large-scale constrained optimization. SIAM journal on optimization. 2002;12(4):979–1006.

[105] Cossalter V, Da Lio M, Lot R, Fabbri L. A general method for the evaluation of vehicle manoeuvrability with special emphasis on motorcycles. Vehicle system dynamics. 1999;31(2):113–135.

[106] Yuhara N, Tajima J. Advanced steering system adaptable to lateral control task and driver's intention. Vehicle System Dynamics. 2001;36(2-3):119–158.

[107] Massaro M, Cole D. Neuromuscular-steering dynamics: Motorcycle riders vs. car drivers. In: ASME 2012 5th Annual Dynamic Systems and Control Conference joint with the JSME 2012 11th Motion and Vibration Conference. American Society of Mechanical Engineers; 2012. p. 217–224.

[108] Lot R, Biral F. A curvilinear abscissa approach for the lap time optimization of racing vehicles. IFAC Proceedings Volumes. 2014;47(3):7559–7565.

[109] Yamakado M, Nagatsuka K, Takahashi J. A yaw-moment control method based on a vehicle's lateral jerk information. Vehicle System Dynamics. 2014;52(10):1233–1253.

[110] Kasius R. Racing driver preference u/s -o/s in a hairpin. private communication. 2015 August.

[111] Tremlett A, Assadian F, Purdy D, Vaughan N, Moore A, Halley M. Quasi-steady-state linearisation of the racing vehicle acceleration envelope: a limited slip differential example. Vehicle System Dynamics. 2014;52(11):1416–1442.

[112] Kaspar S, Pruckner A, Stroph R, Hohmann S. Potential of vehicle dynamics via single wheel drive for installation space optimized electric vehicles. In: Aachener Kolloquium Fahrzeug-und Motorentechnik, Aachen; 2012.

[113] Senn M. fminsearchbnd, fminsearchcon - File Exchange - MATLAB Central. 2012 (accessed January 25, 2017); Available from: `http://uk.mathworks.com/matlabcentral/fileexchange/8277-fminsearchbnd--fminsearchcon`.

[114] Edelmann J, Plöchl M. Handling characteristics and stability of the steady-state powerslide motion of an automobile. Regular and Chaotic Dynamics. 2009; 14(6):682–692.

[115] Yi J, Li J, Lu J, Liu Z. On the stability and agility of aggressive vehicle maneuvers: a pendulum-turn maneuver example. Control Systems Technology, IEEE Transactions on. 2012;20(3):663–676.

[116] Li J, Yi J. Vehicle motion stability with two vehicle dynamics models. In: ASME 2011 Dynamic Systems and Control Conference and Bath/ASME Symposium on Fluid Power and Motion Control. American Society of Mechanical Engineers; 2011. p. 893–900.

[117] Arab A, Yu K, Yi J, Liu Y. Motion control of autonomous aggressive vehicle maneuvers. In: Advanced Intelligent Mechatronics (AIM), 2016 IEEE International Conference on. IEEE; 2016. p. 1663–1668.

[118] Yamakado M, Abe M, Kano Y. Fundamental study on ideal longitudinal control for improved dynamical handling characteristics. In: 24th International Symposium on Dynamics of Vehicles on Road and Tracks of the International Association for Vehicle System Dynamics (IAVSD). VSD; 2015.

[119] Levin JM, Nahon M, Paranjape AA. Aggressive turn-around manoeuvres with an agile fixed-wing uav. IFAC-PapersOnLine. 2016;49(17):242–247.

[120] Wächter A, Biegler LT. On the implementation of an interior-point filter line-search algorithm for large-scale nonlinear programming. Mathematical programming. 2006;106(1):25–57.

[121] Weinstein MJ, Rao AV. A source transformation via operator overloading method for the automatic differentiation of mathematical functions in matlab. ACM Transactions on Mathematical Software (TOMS). 2016;42(2):11.